

**STRUCTURAL SCAFFOLD-FREE COOPERATIVE ROBOTIC FABRICATION**

Edvard P.G. Bruun

A DISSERTATION

PRESENTED TO THE FACULTY

OF PRINCETON UNIVERSITY

IN CANDIDACY FOR THE DEGREE

OF DOCTOR OF PHILOSOPHY

RECOMMENDED FOR ACCEPTANCE BY

THE DEPARTMENT OF

CIVIL AND ENVIRONMENTAL ENGINEERING

Advisors: Sigrid Adriaenssens, Stefana Parascho

September 2024

© Copyright by Edvard P.G. Bruun, 2024.

All rights reserved.

## Abstract

Robotic automation has the potential to revolutionize the Architecture, Engineering, and Construction (AEC) industry by enabling novel construction processes for geometrically complex structures. Cooperative Robotic Fabrication (CRF) involves coordinating multiple robots to work together on construction tasks beyond the capabilities of individual robots. This dissertation explores the use of CRF methods for assembling, disassembling, and reusing discrete element structures. The key innovation lies in developing and physically demonstrating computational methods that enable teams of robotic arms to work together. These methods allow the robotic arms to precisely coordinate their actions to ensure structural stability is maintained during construction without needing external supports or scaffolding.

The dissertation begins with assembly-only applications and extends to more complex tasks involving structural disassembly and reuse. It starts with a bottom-up human-robot design framework where two cooperating robots help design branching spatial structures in pseudo real-time, using path-planning constraints in collaboration with human decision-making. Next, CRF is demonstrated for constructing spanning masonry structures. Here, the structure is modeled as a lumped spring system, and multiple robots are sequenced in either a sequential, cantilever, or optimized manner to ensure the stability of the central arch during construction without external scaffolding. Next, a resource-informed approach is demonstrated for designing space frame structures. This approach uses rigidity theory and Henneberg planar graph assembly steps to sequentially design and build rigid space frame structures that are specifically intended for scaffold-free assembly and disassembly using a CRF setup. Finally, CRF is applied to the scaffold-free disassembly and reuse of an existing structure, aligning with circular economy

principles by minimizing material waste and enabling reuse. A novel graph-based method utilizing the concept of structural support hierarchy is developed to isolate affected members within the structure. By unrolling the resulting subgraphs, this method generates sequences for removing members without compromising the integrity of the remaining structure.

This dissertation demonstrates that multiple robots working together can be utilized in previously unexplored construction scenarios, involving diverse materials, scales, and discrete element structural typologies. These practical demonstrations introduce novel cooperative robotic scaffold-free assembly, disassembly, and reuse methods to the AEC industry.

## Acknowledgments

This dissertation owes its completion to the invaluable advice, support, and guidance of a wide network of individuals.

First and foremost, I extend my deepest gratitude to Prof. Sigrid Adriaenssens, my advisor in the Civil and Environmental (CEE) Engineering department. Over the past five years, Prof. Adriaenssens has been instrumental in helping me navigate numerous academic challenges. I am particularly thankful for the trust and academic freedom she afforded me, enabling me to explore a broad range of novel and fascinating topics in the field of construction robotics. Her encouragement to publish early in my PhD, although daunting at the time, has proven invaluable, paving the way for a transition to a faculty position at Georgia Tech later this year. In such a competitive academic landscape, I am grateful for Prof. Adriaenssens' unwavering support and invaluable guidance throughout this process. Thank you also to the members of the Form Finding Lab and all the visiting researchers that worked with our group over the last few years.

Equally deserving of recognition is my co-advisor, Prof. Stefana Parascho, whose mentorship has been invaluable. Joining her research group in Princeton's School of Architecture (SoA) introduced me to the captivating field of digital fabrication and robotics. Despite my initial unfamiliarity with the field, Prof. Parascho patiently guided me through the fundamentals and provided invaluable research opportunities. Many of the ideas we explored together have culminated in the research forming the core of this dissertation.

I would also like to thank everybody I interacted with at the SoA's Embodied Computation Lab (ECL) where most of the physical robotic construction work featured in this dissertation took place. Amidst a global pandemic, the ECL was a true refuge. Tucked away in the forest at the

edge of campus, it was a place that I came to see as part research laboratory and part oasis. Some of the fondest memories from my PhD are from time spent working in the ECL. It is a beautiful place despite the chaos. In particular, I would like to thank Ian Ting, for the help on all the projects we worked together on, for all the conversations, and for all the smoke breaks. I would also like to thank Bill Tansley for his great attitude and willingness to help with anything.

I would also like to thank the many graduate student and postdoc friends I made along the way. There are too many to name all of you individually, but know that while the PhD can at times be a lonely endeavor, together you all made it significantly less lonely. Thank you to everyone I spent time with at the Ivy. Our post-pandemic time there were formative — a place to celebrate victories, mourn losses, compete in trivia (team name: Ivy Promises), or simply escape for a while. From my PhD cohort in CEE, I am happy to have made such lasting friendships: Sara, thank you for introducing me to Elena; Aaron, thank you for taking me to some beautiful places to go fishing. Thank you also to everybody on The Dammed, the CEE softball team. Playing in the summer league (and winning the C-league in 2023) was some of the most fun I had at Princeton.

I am deeply grateful to my parents for their steadfast encouragement and inspiration, serving as my unwavering role models in both life and academia. Their support and advice has been a source of strength throughout my academic journey. To my sister, I extend my gratitude for her example of balancing academic excellence with a fulfilling personal life. To Felix, thank you for being a constant source of joy.

And most importantly, I would like to thank Elena, my future wife, for supporting me. While I might be leaving Princeton with a PhD, you were by far the best thing that happened to me here. I am so excited about taking the next steps in life together!

To my family and friends

# Contents

Abstract	iii
Acknowledgments	v
Dedication	vii
1 Introduction	1
1.1 Background and Motivation . . . . .	2
1.2 Research Objectives . . . . .	5
1.3 Novelty and Significance of Research . . . . .	6
1.4 Dissertation Structure and Organization . . . . .	8
1.5 Prior Publications Contributing to this Dissertation . . . . .	9
2 Research Context and Literature Review on Structural Cooperative Robotic Fabrication	17
2.1 What is Cooperative Robotic Behaviour? . . . . .	18
2.2 Cooperative Robotics in the Built Environment . . . . .	20
2.3 Cooperative Robotics for a Circular Economy . . . . .	24
3 Human-Robot Collaboration for the Design and Construction of Unplanned Spatial Structures	39
3.1 Introduction . . . . .	41
3.2 State of the Art in the Robotic Context . . . . .	43
3.3 Methodology . . . . .	46
3.4 Final Structure . . . . .	54
3.5 Discussion . . . . .	56
3.6 Conclusion . . . . .	59

<b>4</b>	<b>Three Cooperative Robotic Fabrication Methods for the Scaffold-Free Construction of a Masonry Arch</b>	<b>65</b>
4.1	Introduction . . . . .	67
4.2	Review of Robotic Fabrication and Masonry Structures . . . . .	68
4.3	Methodology . . . . .	72
4.4	Central Arch Fabrication with Two Robots . . . . .	83
4.5	Central Arch Fabrication with Three Robots . . . . .	90
4.6	Conclusion . . . . .	97
<b>5</b>	<b>Cooperative Robotic Scaffold-Free (Dis)Assembly of Triangulated Space Frames Designed with Rigidity Theory</b>	<b>113</b>
5.1	Introduction . . . . .	115
5.2	Literature Review . . . . .	117
5.3	Graph Representation for Space Frame Structures . . . . .	121
5.4	Designing a Space Frame Structure for Cooperative Robotic Assembly . . . . .	127
5.5	Planning a Cooperative Robotic Disassembly Sequence . . . . .	136
5.6	Assembly and Disassembly Results and Discussion . . . . .	148
5.7	Conclusion . . . . .	154
<b>6</b>	<b>Cooperative Robotic Disassembly and Reuse of a Timber Frame Structure</b>	<b>167</b>
6.1	Introduction . . . . .	169
6.2	Literature Review . . . . .	170
6.3	Experimental Setup . . . . .	174
6.4	Workflow and Methods . . . . .	179
6.5	Results and Discussion . . . . .	193
6.6	Conclusion . . . . .	209
<b>7</b>	<b>Conclusions and Future Research</b>	<b>221</b>
7.1	Cooperative Robotic Fabrication for a Circular Economy . . . . .	222
7.2	Recommendations for Future Research . . . . .	229
7.3	General Conclusion . . . . .	237

Appendices	<b>241</b>
Appendix A Appendix for Chapter 4	<b>241</b>
A.1 2-Robot Fabrication Sequence Analysis Results . . . . .	242
A.2 Optimized Three Robot Method Analysis Results . . . . .	244
Appendix B Appendix for Chapter 5	<b>248</b>
B.1 Space Frame Arch Design and Assembly . . . . .	248
B.2 Axial Strain Energy in Disassembly . . . . .	251
Appendix C Appendix for Chapter 6	<b>255</b>
C.1 Code for Topological Support Hierarchy . . . . .	256
C.2 Fabrication Photos . . . . .	259

# List of Figures

1.1	Total urban and rural populations given UN estimates from 1900-2023 and projections to 2050 base on UN median fertility scenario (data from [2]) . . . . .	2
1.2	Construction industry's share of global energy use (left) and energy-related CO <sub>2</sub> emission (right) in 2020 (figure from [6]) . . . . .	3
1.3	The productivity growth of several industries in the United States measured as gross value added per hour worked compared to a baseline of 100 measured in 1947 (figure from [15]) . . . . .	4
1.4	Resource-informed design framework including implicit considerations for assembly and disassembly. . . . .	7
2.1	Cooperative robotic fabrication as situated in the overall robotic setup hierarchy (RF = robotic fabrication, MRF = multi-robotic fabrication, CRF = cooperative robotic fabrication, Co = collaborative). A setup is cooperative, if by the process of cooperation, a novel output is made possible (i.e., B), as opposed to a basic MRF process which only allows more of the same output to be created in parallel (i.e., A) . . . . .	19
3.1	A branching spatial structure assembled with two cooperating robotic arms. . . . .	40
3.2	Plan view of work domain. . . . .	47
3.3	Custom pneumatic grippers. . . . .	48
3.4	Custom setup components. . . . .	48
3.5	The RRT* algorithm used to plan different trajectories through the same domain space. . . . .	49

3.6	Example of the geometry generating procedure.	50
3.7	Flowchart for robotic path planning calculation loop.	52
3.8	Example of one full aggregation cycle (top = robot 1, bottom = robot 2).	53
3.9	Structure at the end of each aggregation cycle.	54
3.10	Final structure.	55
3.11	Example of inverse kinematics constraints during construction.	57
3.12	Hypothetical gradated constraint of domain space towards goal.	58
3.13	Examples of different domain space configurations for point generation.	59
4.1	A glass-brick masonry vault assembled with two cooperating robots.	66
4.2	The vault prototype assembled with two industrial robotic arms.	73
4.3	Geometry of the vault prototype and central arch (dimensions in mm).	73
4.4	Scaffolding in traditional two-sided masonry arch construction.	74
4.5	Representing a masonry structure with the double-cross model.	77
4.6	Deformed shape superimposed on the analytical representation of a generic masonry barrel vault load test.	79
4.7	Tuning the analytical to the initial experimental secant stiffness.	79
4.8	3DEC model where robotic support is modelled as a two-block interface restraint (A and B).	81
4.9	DE analysis of the partial arch.	82
4.10	Unidirectional construction sequences where two robots alternate the support of the partial arch and the placement of new bricks.	83
4.11	Twisting of the arch during construction with the sequential method.	86
4.12	Two robots build the central arch using the cantilever method.	88
4.13	Four-step fabrication loop.	95
4.14	An example four step loop in the 3-robot construction sequence.	96
5.1	A snapshot from the cooperative robotic assembly of a space frame arch structure.	114

5.2	Two trusses that both satisfy the planar Maxwell count condition but only the right is infinitesimally rigid. . . . .	120
5.3	Henneberg assembly steps for the construction of a graph with a generic rigid embedding in space ( $\mathbb{R}^3$ ) . . . . .	123
5.4	Rigidity graph (right) and rigid realization (left) of a minimally rigid tetrahedral cell ( $ V  = 4,  E  = 6$ ). . . . .	125
5.5	Stability graphs representing two different sets of support conditions on the same minimally rigid space frame structure. Condition 1 (left) is unstable since $ E  = 12 < 3 V  - 6$ , while condition 2 (right) is stable since $ E  = 15 \geq 3 V  - 6$ , a Henneberg assembly sequence exists, and the geometric constraints specified in Sections 5.3.2 and 5.3.3 are satisfied. Vertices/nodes in red are supported. . . . .	126
5.6	Cooperative robotic sequence to execute a 3-member rigidity-preserving Henneberg Type 1 step for members with concurrent lines of action at the added node. Stage B (left): $R1 = \text{Place}, R2 = \text{Support}$ ; Stage D (middle): $R1 = \text{Support}, R2 = \text{Place}$ ; Stage F (right): $R1 = \text{Place}, R2 = \text{Support}$ (adapted [15, fig. 3.19]) . .	128
5.7	The stability graphs at each of the 6 stages (A-F) for a Henneberg Type 1 step executed with two robots (R1 and R2) either supporting a member or retrieving the next member to add to the structure. Each edge highlighted in red represents three independent edges connecting a supported vertex in the structure to each of the three vertices representing the X, Y, Z translation constraints. . . . .	129
5.8	An assembly approach where a new node can connect to any three nodes results in a non-planar graph where a subgraph isomorphic to a tetrahedral rigid cell is not formed. . . . .	132
5.9	The sequential design of a structure and its realization in space (top) corresponds to the sequential addition of vertices to the existing graph (bottom), forming a topology that can be characterized as a series of nested tetrahedral cells preserving the property of planarity in the overall graph at each aggregation phase. . . . .	134
5.10	The planar graph (left) isomorphic to the designed space frame structure, represented as a linear partial order of rigid tetrahedral cells (right). . . . .	135

5.11	Renderings of the designed space frame arch structure showing the node numbers and start/end tetrahedral cells (red/blue). . . . .	136
5.12	Demonstration of a disassembly sequence where rigid cells are sequentially located, supported, isolated and then removed from a structure. . . . .	138
5.13	Isomorphic planar graph of a space frame arch structure indicating a potential support edge, $e_{support} = (11, 12)$ , used to initialize the rigid cell finding algorithm. .	140
5.14	The adjacent cell subgraph, $N'$ , is formed from the union of the reduced support neighborhood subgraphs, $N'_1$ and $N'_2$ . . . . .	142
5.15	Rigid tetrahedral cell subgraphs containing the supported member, $e_{support} = (11, 12)$ . These cells are computed from the addition of a single edge, $e_i \in E'_c$ , to the cell adjacency subgraph, and then removing vertices that are not 3-connected. .	143
5.16	Checking the viability of a rigid cell to support in relation to the location of the current cell being removed. $C_1$ is a valid cell to support, while $C_2$ and $C_3$ violate the adjacency criteria. . . . .	145
5.17	A typical structural node with connecting tabs (left). A robotic arm with pneumatic gripper placing and supporting a member in the structure (right). . . . .	148
5.18	Snapshots of the cooperative robotic assembly process for the space frame arch structure. Robotic support is shown on the structure and its isomorphic graph for a partially completed (top) and completed (bottom) 3-member Henneberg sequence.	149
5.19	The 17-noded space frame arch structure as the realization of a planar graph designed to have a rigidity-preserving (dis)assembly sequence. . . . .	150
6.1	An existing timber structure is disassembled and reassembled into a new configuration with a team of cooperating robots. . . . .	168
6.2	Layout of the three-robot cooperative fabrication cell with North defined towards the left. . . . .	175
6.3	The prototype timber structure. . . . .	176
6.4	Prototype structure shown as an assembly of five sub-structures with the members in each color-coded according to their type. . . . .	177

6.5	Computational workflow showing the interaction between the methods described in Section 6.4. . . . .	179
6.6	As-built point cloud of the prototype structure from combined individual captures transformed to the correct location in space with respect to the robotic cell (left). Point cloud density for a small region of the structure before (top-right) and after (bottom-right) down-sampling with low-definition settings. . . . .	181
6.7	Directed edges show that members B1, B2 are supported by members A1 and C1. These support members can also be shown subdivided into their constituent submembers that are connected with parallel and opposite edges to represent a fixed connection. . . . .	184
6.8	The global connection hierarchy in the timber prototype structure is represented as a multidirected graph with outgoing edges indicating the direction of support. The graph is organized into five regions, where the names and colors of the vertices are based on the convention introduced in Section 6.3.2. . . . .	185
6.9	Examples of active member subgraphs constructed using the algorithmic procedures described in Section 6.4.2. Vertices and edges are drawn to represent the different conditions as per the legend. . . . .	188
6.10	Example of a partial disassembly sequence (four steps) calculated from the subgraph for active members WP1_2 & WS3. After each step the subgraph is relabeled with new start nodes in green. . . . .	190
6.11	Left: Five pick locations (P1 - P5) on a member are manually initialized from the as-built point cloud of the structure. Middle: At each location three points are used to define a spatial plane for the robot to reach. Right: Inverse kinematic path planning checks reveal that only P3 is reachable by a robot without encountering collisions with the structure or other robots in the work cell. . . . .	191
6.12	Planning the removal of member SS1 . . . . .	194
6.13	Two new active member subgraphs generated from the inclusion of additional removal targets determined by the feasibility evaluation for the planned removal of SS1. . . . .	195

6.14	Phase 1 disassembly sequence.	196
6.15	Prototype structure at the end of the disassembly in Phase 1 (from [47]).	197
6.16	Planning the removal of the south wall as part of Phase 2 and resulting in a final structure that requires additional support.	200
6.17	Phase 2 disassembly sequence.	201
6.18	Phase 2 reassembly sequence.	202
6.19	Snapshots of Phase 2 disassembly.	202
6.20	The prototype structure at the end of the disassembly and reassembly in Phase 2.	203
6.21	The disassembly subgraph for the removal of the West wall and roof members.	205
6.22	Phase 3 disassembly and full reassembly (each member removed is reused).	206
6.23	The prototype structure at the end of the disassembly and reassembly in Phase 3.	207
6.24	Finite element analysis comparing the lateral stiffness of the original (top) to the reassembled (bottom) West wall.	208
7.1	Snapshots from the cooperative robotic fabrication of an unplanned structure	223
7.2	Scaffold-free cooperative robotic assembly of a masonry vault	224
7.3	Scaffold-free (dis)assembly of a spanning timber space frame arch structure	226
7.4	Snapshots from the different phases of the cooperative robotic disassembly and reassembly as part of the ZeroWaste project	228
7.5	Robotic setup used throughout dissertation research	234
7.6	Conceptual cooperative robotic gantry setup improving payload and reach.	236
C.1	Phase 1 fabrication photos	259
C.2	Phase 2 fabrication photos (disassembly)	260
C.3	Phase 2 fabrication photos (reassembly)	261
C.4	Phase 3 first half of disassembly/reassembly photos	262
C.5	Phase 3 second half of disassembly/reassembly photos	263

# List of Tables

4.1	Summary of structural parameters for full-scale masonry arch tests with published load-deflection data . . . . .	78
4.2	Initial experimental secant arch stiffness compared to calibrated element-spring model stiffness . . . . .	80
4.3	Average relative error in displacements across models between the proposed simplified model and DE analysis results. . . . .	83
4.4	Analysis results for the off-center support steps in the sequential method . . . . .	85
4.5	Comparison of cantilever to sequential method at critical steps . . . . .	87
4.6	Tensile forces in both 2-robot sequences (in N) . . . . .	89
4.7	Maximum forces supported by the robots . . . . .	90
4.8	Modifying the sequential method with an optimized third support . . . . .	93
4.9	3-robot cascading optimization . . . . .	94
4.10	Improvement to structural behavior with 3-robot optimized sequence . . . . .	97
5.1	The four disassembly phases planned for the arch structure designed in Section 5.4.5. . . . .	147
5.2	Documentation of the four phases of the rigidity-preserving disassembly sequence calculated and executed for the space frame arch structure. . . . .	152
5.3	The two members supported by either robot resulting in the minimum average axial strain energy ( $10^{-9} \text{ kN} \cdot \text{m}$ ) in each disassembly phase. . . . .	153
6.1	Members in the prototype structure . . . . .	178
6.2	Hyper-parameters and results for low-definition (LD) and high-definition (HD) down-sampling procedures . . . . .	182

A.1	Analysis results for the sequential method . . . . .	242
A.2	Analysis results for the cantilever method . . . . .	243
A.3	Analysis results for the three-robot sequence . . . . .	244
B.1	Vertex mapping to $\mathbb{R}^3$ and graph connectivity at each aggregation phase ( $G'$ ) following an iteration of the design process. . . . .	249
B.2	Cooperative robotic assembly sequence for the space frame arch. . . . .	250
B.3	Average axial strain energy ( $10^{-9} \text{ kN} \cdot \text{m}$ ) in disassembly phase 1. . . . .	252
B.4	Average axial strain energy ( $10^{-9} \text{ kN} \cdot \text{m}$ ) in disassembly phase 2. . . . .	253
B.5	Average axial strain energy ( $10^{-9} \text{ kN} \cdot \text{m}$ ) in disassembly phase 3. . . . .	254
B.6	Average axial strain energy ( $10^{-9} \text{ kN} \cdot \text{m}$ ) in disassembly phase 4. . . . .	254

# 1

## Introduction

## 1.1 Background and Motivation

Our world faces urgent societal challenges necessitating innovative solutions, including population growth, urbanization, low construction industry productivity, and escalating environmental impact in the building sector. The UN predicts the global population will reach 9.8 billion by 2050 [1], with global urbanization projected to increase from 56% in 2020 to 68% in 2050 [2]. This unprecedented urbanization trend becomes clear when viewed historically over the last several centuries, as depicted in Figure 1.1.

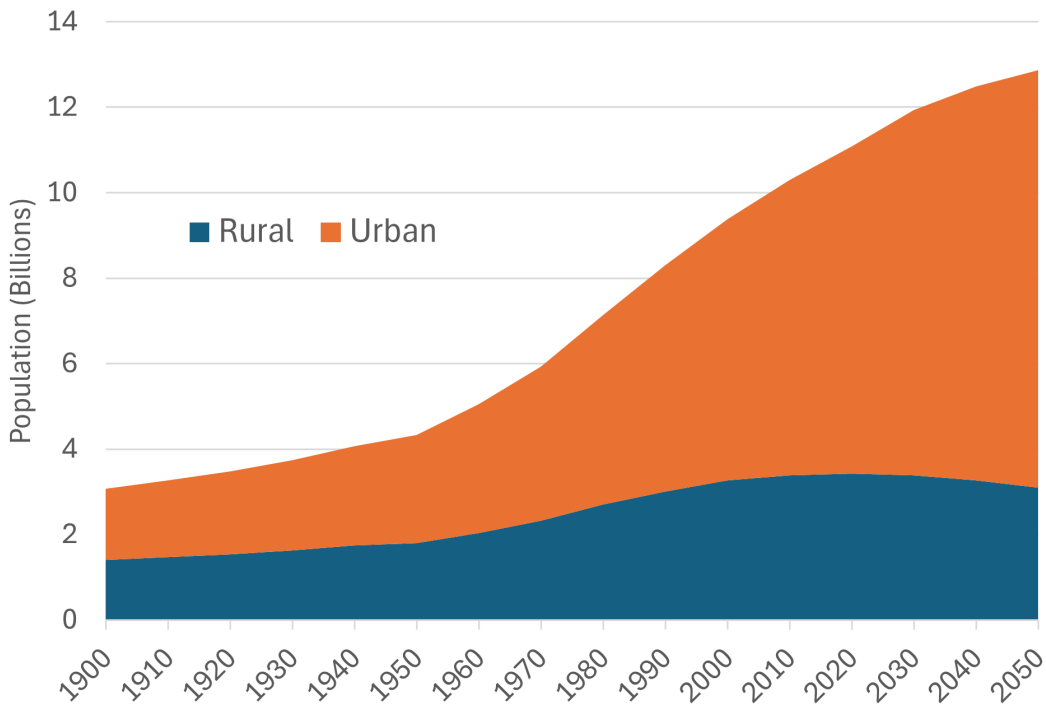


**Figure 1.1:** Total urban and rural populations given UN estimates from 1900-2023 and projections to 2050 base on UN median fertility scenario (data from [2])

Rapid population growth and urbanization are poised to drive increased demand for construction activities. However, the Architecture, Engineering, Construction (AEC) has a significant negative impact on the environment due to its material and energy-intensive manufacturing and construction processes [3], coupled with the high embodied carbon content of structural systems [4, 5]. For instance, buildings and construction activities contributed to 36% of global energy usage and 37% of global CO<sub>2</sub> emissions in 2020, as depicted in Figure 1.2 [6].

The environmental impact is further worsened by the increasing waste generated from con-

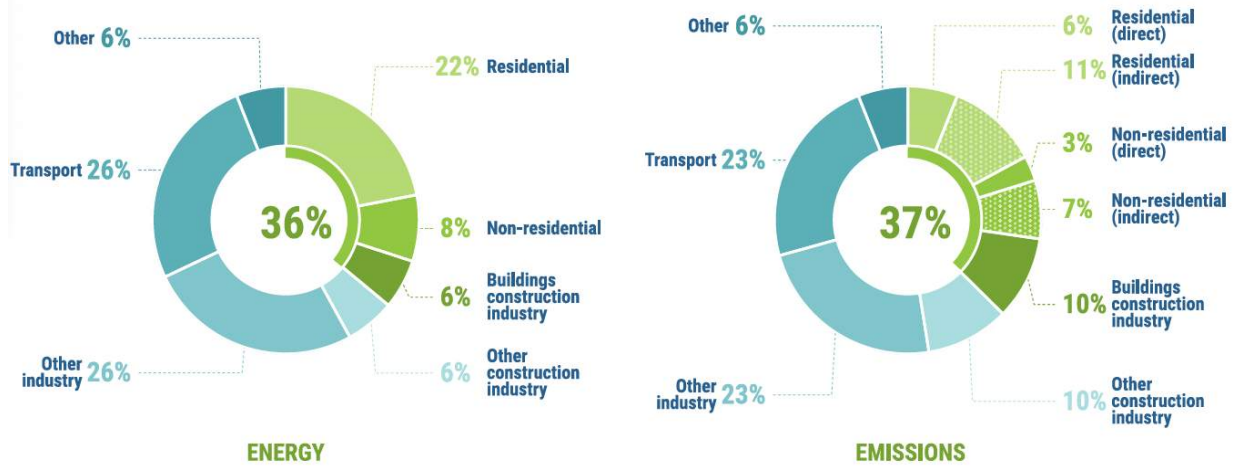


**Figure 1.2:** Construction industry's share of global energy use (left) and energy-related CO2 emission (right) in 2020 (figure from [6])

struction and demolition (C&D) processes [7, 8]. In the 1990s, C&D processes were estimated to contribute up to 30% of the total global waste [9, 10]. To illustrate this escalating issue, in the mid-1990s in the United States alone, C&D activities generated an estimated 100-135 million tons of waste, of which about 35-45% ended up in landfills [11, 12]. This C&D waste accounted for 29% of the total landfill volumes at that time [13]. However, by 2018, the volume of waste from C&D activities had skyrocketed to 600 million tons, with 144 million tons or 24% of this waste disposed of in landfills [14]. Consequently, approximately half of the landfill volumes in 2018 were attributed to C&D activities, while the remaining municipal solid waste contributed 146 million tons [14]. This trend is especially concerning when considering the significant construction needs of the upcoming century, where aging infrastructure must be replaced while accommodating the demands of a growing and rapidly urbanizing global population [2].

As a result, inefficiencies within the AEC industry not only impede its ability to meet increasing demands but also exacerbate environmental degradation through wasteful practices and resource-intensive methods. Technological advancements aimed at enhancing construction efficiency and material utilization can mitigate some of these environmental impacts. However, the challenge lies in the AEC industry's reluctance to embrace contemporary automation techniques and the productivity benefits they offer. For instance, while various industries have witnessed an uptick in labor productivity since the 1940s, the construction sector has experienced only minor improvements and actually a decline in productivity since 1968, as illustrated in Figure 1.3 [15].

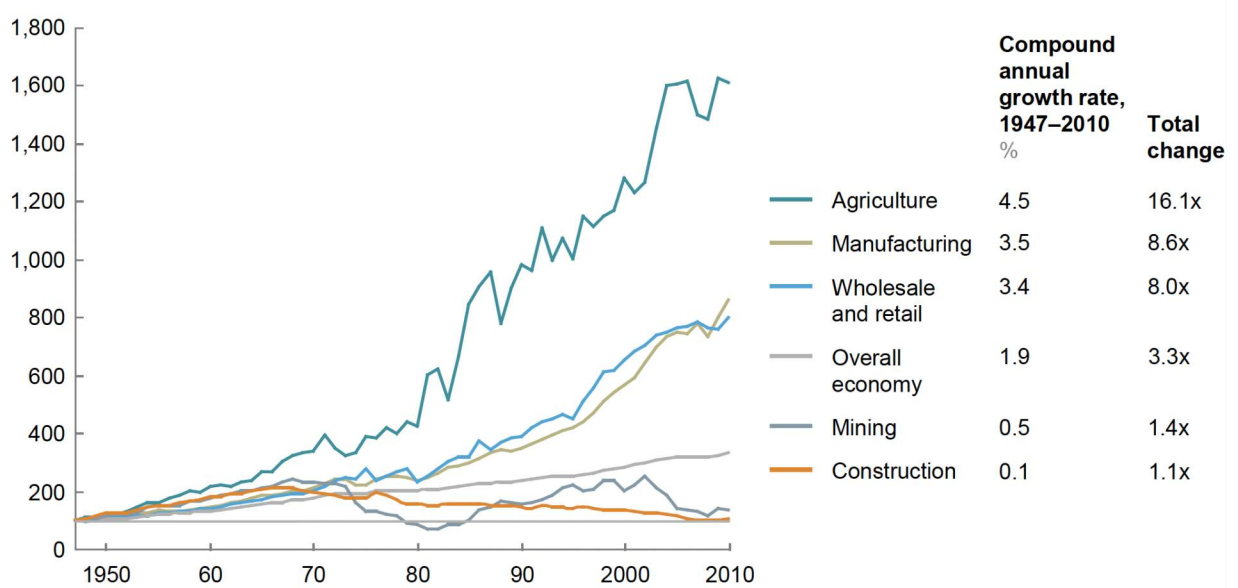


**Figure 1.3:** The productivity growth of several industries in the United States measured as gross value added per hour worked compared to a baseline of 100 measured in 1947 (figure from [15])

### 1.1.1 Broad Research Motivation stemming from Societal Challenges

The rapid increase in population growth and urbanization intensifies the need for construction activities, adding to the challenges already faced by the AEC industry, which struggles with stagnant productivity. This exacerbates environmental strain due to resource-intensive practices. While each challenge is significant on its own, their combined impact emphasizes the urgent requirement for changes in construction practices to promote sustainable development. It is crucial to adopt modern construction technologies that move away from wasteful and resource-intensive design approaches. Therefore, the broad motivation for this dissertation is to:

1. Demonstrate the use of novel technologies that can be used by the construction industry to meet the growing demands of urbanization and population growth.
2. Develop processes that enable the reduction of primary resource inputs to construction to minimize the environmental footprint of the building industry.

## 1.2 Research Objectives

The research goal of this dissertation, derived from the broad research motivations and the societal challenges outlined in [Section 1.1](#), is to demonstrate how robotic construction automation can be used to perform various construction tasks in such a way that makes external supports (such as scaffolding) unnecessary. Industrial robots are particularly applicable to construction of discrete element structures due to their application versatility [16] and spatial precision in picking and placing material [17]. They are experiencing growing adoption in both industry and academic contexts [18] and have already shown promise in tackling the AEC industry's lagging productivity and labor efficiency [19, 20].

This dissertation specifically explores the use of cooperative robotic fabrication (CRF) as a design approach and construction method. In CRF setups, individual robotic agents are sequenced to work together, improving productivity by allowing for the automation of a wider range of construction tasks, including intricate pick-and-place processes. Furthermore, the dissertation showcases how CRF can advance the adoption of sustainable circular models in building design and construction. This is achieved by minimizing primary resource consumption during construction and facilitating disassembly and reuse processes. A thorough literature review of CRF can be found in [Chapter 2](#), which provides information about CRF in this specific research context.

The dissertation focuses on the practical application of CRF as demonstrated in physical construction scenarios. The body of the dissertation is organized as a series of research chapters demonstrating increasingly intricate uses of CRF methodologies across various construction contexts, involving different materials, and structural typologies. Across all research, the central theme is utilizing CRF setups to execute construction tasks without the need for additional external temporary support materials, essentially maintaining stability without relying on formwork or scaffolding during any stage of construction. Multiple robots are strategically coordinated to collaborate in adding or removing structural elements while providing necessary support to the temporary structure independently. In each research project, this type of cooperative robotic sequencing is leveraged, where a team of two or more robots execute multiple tasks simultaneously, or perform complimentary passive/active functions, in coordinated manner to achieve scaffold-free behavior. The research presented in this dissertation starts with assembly-

only applications, but increase in complexity to include applications of disassembly as well. By integrating disassembly into the design and fabrication process, opportunities for future structural reconfiguration and reuse within a circular economy framework are explored and demonstrated.

The overall goal of demonstrating CRF's potential to improve construction productivity through automation while highlighting applications for it to be used for material reduction and circular models of construction, is achieved through the following specific research objectives:

1. Develop a structurally-informed support-place sequencing method for cooperative robotic construction processes that allows for the scaffold-free (de)construction of spanning (i.e., arches, vaults, frames etc.) as opposed to vertical or layer-based structures.
2. Demonstrate CRF in increasingly complex applications for different structural typologies and material systems:
  - (a) small-scale test of human-robot collaborative assembly
  - (b) assembly of masonry vaults and arches
  - (c) (dis)assembly of space frames designed for reversibility
  - (d) dis-and-reassembly of existing timber stick frames
3. Establish future research directions and applications of the developed CRF method

### 1.3 Novelty and Significance of Research

While the use of robots and construction automation gained prominence initially in the 1970s with single-task robots used for the prefabrication of modular homes in Japan [21–24], it was only in the last two decades that the Digital Fabrication (DFab) movement in construction began to gain significant attention [25]. As part of this movement researchers have aimed to expand the geometric design possibilities and productivity in construction through the utilization of robots for bespoke structures [26, 27].

Despite the strides made in the DFab movement, robotic fabrication's application to discrete element structures remains predominantly focused on vertical layer-based construction [28–34]. This dissertation represents a significant departure from this convention by presenting the first

examples of assembling various types of spanning structures, rather than vertical or layer-based ones, at the architectural pavilion scale, without the need for external scaffolding or support. Additionally, this research broadens the scope of CRF methods by successfully applying them to scaffold-free disassembly and reassembly for the first time. These advancements build on the first demonstrated examples of scaffold-free cooperative robotic assembly, for vertical steel spatial structures, in the PhD work of Parascho [35].

In addition, this dissertation explores CRF for the first time through the lens of resource-informed design. Resource-informed design integrates considerations of assembly and disassembly processes directly into the design of structures, as illustrated in a simple design loop in [Figure 1.4](#). Addressing waste begins at the design phase, where strategic planning can significantly reduce material usage and waste generation throughout the project life cycle. Research indicates that a notable portion of construction waste stems from inadequate waste reduction measures early in the design stages, particularly in planning for building decommissioning [36]. Resource-informed design involves developing connections between the structure and fabrication setups to maximize cooperative potential, thereby optimizing efficiency and reducing resource inputs during fabrication. This approach aims to minimize the use of structural materials, temporary scaffolding, and manual labor while facilitating the reuse of materials, thus promoting sustainability and moving away from single-use construction practices. Overall, resource-informed design seeks to create structures that are not only functional and aesthetically pleasing but also efficient, sustainable, and adaptable throughout their life cycle.

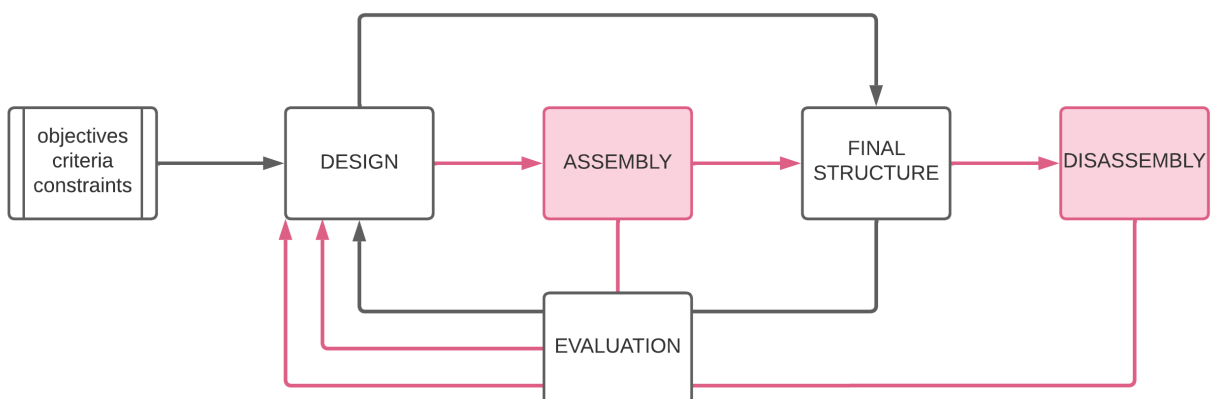


**Figure 1.4:** Resource-informed design framework including implicit considerations for assembly and disassembly.

## 1.4 Dissertation Structure and Organization

Through a series of independent research projects, this dissertation develops and demonstrates the application of CRF for scaffold-free construction. Given the diversity of structural and material types, and construction scopes explored, a project-specific literature review is provided at the beginning of each chapter. The organization of this dissertation is as follows:

[Chapter 2](#) functions as a general literature review and introduces CRF as a technology and reviews its previous applications across industries, with a focus on applications in the built environment. It explores the idea that CRF has the potential to achieve outcomes that align with certain aspects in the transition towards circular economic practices, as demonstrated in the research presented in the upcoming chapters.

[Chapter 3](#) introduces a novel bottom-up design framework where robots actively participate in the creative design process, detailing the cooperative aggregation of solid spherical units by two robotic arms to create a branching spatial structure assembled without requiring external scaffolding.

[Chapter 4](#) explores the use of multiple robots in cooperative assembly to construct complex spanning masonry structures without scaffolding, presenting and validating three fabrication approaches and demonstrating an optimized method for scaffold-free construction of a stable masonry arch.

[Chapter 5](#) presents a fabrication-informed design method for stable triangulated space frame structures, utilizing a graph theoretic framework to specifically design a rigidity-preserving spanning structure that can be assembled and disassembled without external scaffolding using two cooperating robots.

[Chapter 6](#) showcases how CRF enables the disassembly and reuse of existing timber buildings, demonstrating the development and use of the support hierarchy graph for planning different disassembly and reassembly sequences using up to 3 robots working together.

[Chapter 7](#) summarizes the body of the dissertation consisting of the four independent research projects and their contributions to advancing the various circular economy principles as outlined in Chapter 2, while discussing future directions for scaffold-free assembly and disassembly research utilizing CRF methods.

## 1.5 Prior Publications Contributing to this Dissertation

Except for this introductory chapter, all subsequent chapters in this dissertation comprise previously published peer-reviewed materials such as book chapters, journal papers, or conference papers. To maintain clarity of authorship, only publications where the author of this dissertation serves as the first and corresponding author are incorporated. These relevant publications are referenced at the outset of each chapter and are included with the publishers' consent. Additionally, the contributions of co-authors of these publications are recognized through a CRediT (Contributor Roles Taxonomy) author statement at the commencement of each chapter [37]. Minor adjustments from the original publication may have been made to align the content with the overall formatting requirements of this dissertation and to ensure stylistic coherence across chapters.

For a comprehensive compilation of all peer-reviewed publications pertaining to the dissertation's themes, authored or co-authored by the dissertation's author during the course of this degree, please refer below. This list encompasses co-authored works that, although not directly integrated into the body of this dissertation, bear significant relevance to its thematic focus and feature substantial contributions from the author.

### Book Chapters

1. **Bruun, E. P. G.**, Parascho, S., & Adriaenssens, S. (2024). Cooperative Robotic Fabrication for a Circular Economy. In A Circular Built Environment in the Digital Age (pp. 129–149). Springer Cham. [https://doi.org/10.1007/978-3-031-39675-5\\_8](https://doi.org/10.1007/978-3-031-39675-5_8)

### Peer-Reviewed Journal Papers

1. **Bruun, E. P. G.**, Adriaenssens, S., Besler, E., & Parascho, S. (2024). ZeroWaste: Disassembly and Reuse of a Timber Frame Structure using Cooperating Robots. *Construction Robotics*. (Accepted)
2. **Bruun, E. P. G.**, Oval, R., Al Asali, W., Gaspar, O., Paris, V., & Adriaenssens, S. (2024). Automating historical centering-minimizing masonry vaulting strategies: Applications to cooperative robotic construction. *Developments in the Built Environment*. (Under Review)
3. Oval, R., Paris, V., Pastrana, R., **Bruun, E. P. G.**, Gomis Aviño, S., Adriaenssens, S., &

- Al Asali, W. (2024). Digital guidework for augmented thin-tile vaulting construction. *Automation in Construction*. (Under Review)
4. Oval, R., Pastrana, R., **Bruun, E. P. G.**, Paris, V., Gomis Aviño, S., Adriaenssens, S., & Al Asali, W. (2024). An integrated digital design and construction approach for falsework-minimal masonry vaults. *Structures*, 63, 106428. <https://doi.org/10.1016/j.istruc.2024.106428>
  5. **Bruun, E. P. G.**, Adriaenssens, S., & Parascho, S. (2022). Structural rigidity theory applied to the scaffold-free (dis)assembly of space frames using cooperative robotics. *Automation in Construction*, 141, 104405. <https://doi.org/10.1016/j.autcon.2022.104405>
  6. **Bruun, E. P. G.**, Pastrana, R., Paris, V., Beghini, A., Pizzigoni, A., Parascho, S., & Adriaenssens, S. (2021). Three cooperative robotic fabrication methods for the scaffold-free construction of a masonry arch. *Automation in Construction*, 129, 103803. <https://doi.org/10.1016/j.autcon.2021.103803>
  7. **Bruun, E. P. G.**, Ting, I., Adriaenssens, S., & Parascho, S. (2020). Human–robot collaboration: A fabrication framework for the sequential design and construction of unplanned spatial structures. *Digital Creativity*, 31(4), 320–336. <https://doi.org/10.1080/14626268.2020.1845214>
  8. Parascho, S., Han, I. X., Walker, S., Beghini, A., **Bruun, E. P. G.**, & Adriaenssens, S. (2020). Robotic vault: A cooperative robotic assembly method for brick vault construction. *Construction Robotics*, 4(3), 117–126. <https://doi.org/10.1007/s41693-020-00041-w>

### Peer-Reviewed Conference Papers

1. **Bruun, E. P. G.**, Adriaenssens, S., Besler, E., & Parascho, S. (2022). ZeroWaste: Towards Computing Cooperative Robotic Sequences for the Disassembly and Reuse of Timber Frame Structures. *Proceedings of the 42nd Annual Conference of the Association for Computer Aided Design in Architecture*, 586–597. <http://arks.princeton.edu/ark:/88435/pr1wp9t657>
2. Paris, V., Lepore, N., **Bruun, E. P. G.**, Ruscica, G., Piccioni, M. D., Beghini, A., Parascho, S., & Adriaenssens, S. (2021). Robotic construction of a self-balancing glass masonry

- vault: DEM study of stability during construction stages. Proceedings of the IASS Annual Symposium 2020/2021, 314–325. <http://arks.princeton.edu/ark:/88435/pr12n4zh86>
3. Parascho, S., Han, I. X., Beghini, A., Miki, M., Walker, S., **Bruun, E. P. G.**, & Adriaenssens, S. (2021). LightVault: A design and robotic fabrication method for complex masonry structures. *Advances in Architectural Geometry* 2020, 350–375.  
<https://oar.princeton.edu/handle/88435/pr1s17ss>
  4. Han, I. X., **Bruun, E. P. G.**, Marsh, S., Adriaenssens, S., & Parascho, S. (2020). From concept to construction: A transferable design and robotic fabrication method for a building-scale vault. *Proceedings of the 40th Annual Conference of the Association for Computer Aided Design in Architecture*, 614–623.  
<https://doi.org/10.52842/conf.acadia.2020.1.614>

## References

- [1] United Nations, Department of Economic and Social Affairs, Population Division, World population prospects: Highlights, United Nations, 2019, ST/ESA/SER.A/423.
- [2] H. Ritchie, V. Samborska, M. Roser, Urbanization (2024).  
URL <https://ourworldindata.org/urbanization>
- [3] International Energy Agency, United Nations Environment Programme, 2018 Global Status Report: Towards a zero-emission, efficient and resilient buildings and construction sector, Tech. rep., Global Alliance for Buildings and Construction (2018).  
URL <https://wedocs.unep.org/20.500.11822/27140>
- [4] S. Kaethner, J. Burridge, Embodied CO<sub>2</sub> of structural frames, Structural Engineer 90 (5) (2012) 33–40.  
URL <https://www.istructe.org/sitefiles/handlers/DownloadFile.ashx?productId=1583>
- [5] D. Fang, N. Brown, C. De Wolf, C. Mueller, Reducing embodied carbon in structural systems: A review of early-stage design strategies, Journal of Building Engineering 76 (2023) 107054. doi:10.1016/j.jobe.2023.107054.
- [6] United Nations, Global Status Report for Buildings and Construction, Tech. rep., UN (2021).  
URL [https://globalabc.org/sites/default/files/2021-10/GABC\\_Buildings-GSR-2021\\_BOOK.pdf](https://globalabc.org/sites/default/files/2021-10/GABC_Buildings-GSR-2021_BOOK.pdf)
- [7] US EPA, Construction and Demolition Debris Generation in the United States, 2015, Tech. rep., Office of Resource Conservation and Recovery (Sep. 2018).  
URL <https://www.epa.gov/facts-and-figures-about-materials-waste-and-recycling/studies-summary-tables-and-data-related>
- [8] US EPA, Construction and Demolition Debris Management in the United States, 2015, Tech. rep., Office of Resource Conservation and Recovery (Mar. 2020).  
URL [https://www.epa.gov/sites/production/files/2020-03/documents/final\\_cd-eol-management\\_2015\\_508.pdf](https://www.epa.gov/sites/production/files/2020-03/documents/final_cd-eol-management_2015_508.pdf)

- [9] C. K. Purchase, D. M. A. Zulayq, B. T. O'Brien, M. J. Kowalewski, A. Berenjian, A. H. Tarighaleslami, M. Seifan, Circular Economy of Construction and Demolition Waste: A Literature Review on Lessons, Challenges, and Benefits, Materials 15 (1) (Jan. 2022). doi: 10.3390/ma15010076.
- [10] B. K. Fishbein, Building for the future: strategies to reduce construction and demolition waste in municipal projects, Vol. 5 of INFORM Special Report, INFORM, Inc., New York, 1998.
- [11] T. H. Mills, E. Showalter, D. Jarman, A cost-effective waste management plan, Cost Engineering 41 (3) (1999) 35–43.  
 URL <https://www.proquest.com/docview/220405711?pq-origsite=gscholar&fromopenvie w=true#>
- [12] US EPA, Characterization of building-related construction and demolition debris in the United States, Tech. Rep. EPA530-R-98-010, Municipal and Industrial Solid Waste Division (Jun. 1998).  
 URL <https://archive.epa.gov/epawaste/hazard/generation/web/pdf/cd-rpt.pdf>
- [13] W. Lu, H. Yuan, A framework for understanding waste management studies in construction, Waste Management 31 (6) (2011) 1252–1260. doi:10.1016/j.wasman.2011.01.018.
- [14] US EPA, Advancing Sustainable Materials Management: 2018 Fact Sheet, Tech. rep., Office of Resource Conservation and Recovery (Dec. 2020).  
 URL [https://www.epa.gov/sites/default/files/2021-01/documents/2018\\_ff\\_fact\\_sheet\\_dec\\_2020\\_fnl\\_508.pdf](https://www.epa.gov/sites/default/files/2021-01/documents/2018_ff_fact_sheet_dec_2020_fnl_508.pdf)
- [15] F. Barbosa, J. Woetzel, J. Mischke, M. Ribeirinho, M. Sridhar, M. Parsons, N. Bertram, S. Brown, Reinventing Construction: A Route to Higher Productivity, Tech. rep., McKinsey Global Institute (2017).  
 URL <https://www.mckinsey.com/business-functions/operations/our-insights/reinventing-construction-through-a-productivity-revolution>

- [16] G. Bravo-Palacios, A. D. Prete, P. M. Wensing, One robot for many tasks: Versatile co-design through stochastic programming, *IEEE Robotics and Automation Letters* 5 (2) (2020) 1680–1687. doi:10.1109/LRA.2020.2969948.
- [17] P. Eversmann, F. Gramazio, M. Kohler, Robotic prefabrication of timber structures: towards automated large-scale spatial assembly, *Construction Robotics* 1 (2017) 49–60. doi:10.1007/s41693-017-0006-2.
- [18] IFR, World robotics report (2018).  
 URL <https://ifr.org/ifr-press-releases/news/global-industrial-robot-sales-doubled-over-the-past-five-years>
- [19] B. García de Soto, I. Agustí-Juan, J. Hunhevicz, S. Joss, K. Graser, G. Habert, B. T. Adey, Productivity of digital fabrication in construction: Cost and time analysis of a robotically built wall, *Automation in Construction* 92 (2018) 297–311. doi:10.1016/j.autcon.2018.04.004.
- [20] V. R. P. Kumar, M. B. a. S. J. Raj, Robotics in construction industry, *Indian Journal of Science and Technology* 9 (23) (2016) 1–12. doi:10.17485/ijst/2016/v9i23/95974.
- [21] T. Bock, Construction robotics, *Autonomous Robots* 22 (3) (2007) 201–209. doi:10.1007/s10514-006-9008-5.
- [22] T. Bock, The future of construction automation: Technological disruption and the upcoming ubiquity of robotics, *Automation in Construction* 59 (2015) 113–121. doi:10.1016/j.autcon.2015.07.022.
- [23] T. Bock, T. Linner, Construction robots: Elementary technologies and single-task construction robots, Vol. 4, Cambridge University Press, 2016, ISBN: 978-1-316-78517-1.
- [24] J. S. Albus, Trip report: Japanese progress in robotics for construction, *Robotics* 2 (2) (1986) 103–112, publisher: North-Holland. doi:10.1016/0167-8493(86)90047-1.
- [25] F. Gramazio, M. Kohler, Digital materiality in architecture, 1st Edition, Lars Muller, Baden, 2008, ISBN: 978-3-03778-122-7.

- [26] F. Gramazio, M. Kohler (Eds.), Made by robots: Challenging architecture at a larger scale, 1st Edition, Academy Press, London, 2014, ISBN: 978-1-118-53548-6.
- [27] J. M. Davila Delgado, L. Oyedele, A. Ajayi, L. Akanbi, O. Akinade, M. Bilal, H. Owolabi, Robotics and automated systems in construction: Understanding industry-specific challenges for adoption, *Journal of Building Engineering* 26 (2019) 1–11. doi:10.1016/j.jobe.2019.100868.
- [28] R. Bärtschi, M. Knauss, T. Bonwetsch, F. Gramazio, M. Kohler, Wiggled brick bond, in: *Advances in Architectural Geometry* 2010, Springer, Wien/New York, 2010, pp. 137–147. doi:10.1007/978-3-7091-0309-8.
- [29] M. Kohler, F. Gramazio, J. Willmann, Gantenbein vineyard façade, in: *The Robotic Touch: How Robots Change Architecture*, The University of Chicago Press, Chicago, 2014, pp. 66–75, ISBN: 978-3-906027-37-1.
- [30] T. Bonwetsch, D. Kobel, F. Gramazio, M. Kohler, The informed wall: Applying additive digital fabrication techniques on architecture, in: *Proceedings of the 25th Annual Conference of the Association for Computer-Aided Design in Architecture*, 2006, pp. 489–495, ISBN: 978-0-9789463-0-2.
- [31] T. Bonwetsch, F. Gramazio, M. Kohler, Digitally fabricating non-standardised brick walls, in: *ManuBuild*, 2007, pp. 191–196, ISBN: 978-0-86017-710-4.
- [32] L. Piškorec, D. Jenny, S. Parascho, H. Mayer, F. Gramazio, M. Kohler, The brick labyrinth, in: *Robotic Fabrication in Architecture, Art and Design* 2018, Springer International Publishing, Zurich, 2018, pp. 489–500. doi:10.1007/978-3-319-92294-2\_37.
- [33] K. Dörfler, T. Sandy, M. Giftthaler, F. Gramazio, M. Kohler, J. Buchli, Mobile robotic brickwork: Automation of a discrete robotic fabrication process using an autonomous mobile robot, in: *Robotic Fabrication in Architecture, Art and Design* 2016, Springer International Publishing, Sydney, Australia, 2016, pp. 204–217. doi:10.1007/978-3-319-26378-6-15.

- [34] M. Gifthaler, T. Sandy, K. Dörfler, I. Brooks, M. Buckingham, G. Rey, M. Kohler, F. Gramazio, J. Buchli, Mobile robotic fabrication at 1:1 scale: The in situ fabricator, *Construction Robotics* 1 (1) (2017) 3–14. doi:10.1007/s41693-017-0003-5.
- [35] S. Parascho, Cooperative robotic assembly: Computational design and robotic fabrication of spatial metal structures, PhD Thesis, ETH, Zurich (2019).  
URL <https://doi.org/10.3929/ethz-b-000364322>
- [36] M. Osmani, J. Glass, A. Price, Architects' perspectives on construction waste reduction by design, *Waste Management* 28 (7) (2008) 1147–1158. doi:10.1016/j.wasman.2007.05.011.
- [37] L. Allen, A. O'Connell, V. Kiermer, How can we ensure visibility and diversity in research contributions? How the Contributor Role Taxonomy (CRediT) is helping the shift from authorship to contributorship, *Learned Publishing* 32 (1) (2019) 71–74. doi:10.1002/leap.1210.

# 2

## Research Context and Literature Review on Structural Cooperative Robotic Fabrication

This chapter is based on the following publication:

**Bruun, E. P. G.**, Parascho, S., & Adriaenssens, S. (2024). Cooperative Robotic Fabrication for a Circular Economy. In A Circular Built Environment in the Digital Age (pp. 129–149). Springer Cham. [https://doi.org/10.1007/978-3-031-39675-5\\_8](https://doi.org/10.1007/978-3-031-39675-5_8)

Contributor roles in publication:

- Bruun: Conceptualization, Methodology, Investigation, Writing (Original Draft), Writing (Review and Editing), Visualization
- Parascho & Adriaenssens: Writing (Review and Editing), Supervision, Funding Acquisition

## 2.1 What is Cooperative Robotic Behaviour?

Robotic fabrication (RF) refers to any fabrication process that is completed with some degree of automation. Cooperative Robotic Fabrication (CRF) is a subset of RF and can be thought of as any process where the robotic agents are specifically coordinated to accomplish tasks that would not be possible if the robots were working alone. Cao et al. state that “a multiple robot system displays cooperative behaviour if, due to [the mechanism of cooperation], there is an increase in the total utility of the system” [1, p.8]. Thus, cooperative robotic cells can fall under the category of either multi-arm individual robots, multiple single-arm robots, mechanical hands with independently controllable fingers, or a combination of these, working together in a synchronous fashion [2, 3].

A single robotic agent, regardless of physical or digital complexity, is naturally limited in the type and number of actions it can simultaneously execute. Only in multi-robotic fabrication (MRF), where multiple agents are placed together in a work cell, does it become possible to unlock the potential of collective behaviour to achieve more complex outputs. All MRF setups exhibit some form of collective behaviour, but while cooperative behaviour is subset of collective behaviour (i.e.,  $CRF \subseteq MRF$ ), the converse is not true (i.e.,  $MRF \not\subseteq CRF$ ). A CRF process entails further utility beyond the collective behaviour that comes from a basic implementation of MRF. This hierarchy is illustrated in [Figure 2.1](#), where the output of an MRF setup is defined as scaling linearly with the number of agents to produce more of the same output (i.e., several robots working in parallel), as opposed to a CRF process where the output is uniquely contingent on all the agents working together.

Another important distinction is between the terms cooperative and collaborative, which are commonly used interchangeably to describe multi-agent robotic processes in the literature. To avoid ambiguity, collaborative is within this dissertation only used for a process where robot(s) work together with, or alongside, human operators. Collaborative processes exist across the entire RF hierarchy illustrated in [Figure 2.1](#). For example, collaborative processes are possible with a human working with a single robot (Co-RF, as in [4]), with multiple robots in series on an assembly line (Co-MRF, as in [5]), or to complement the cooperative function of multiple robots (Co-CRF, as in [6]).

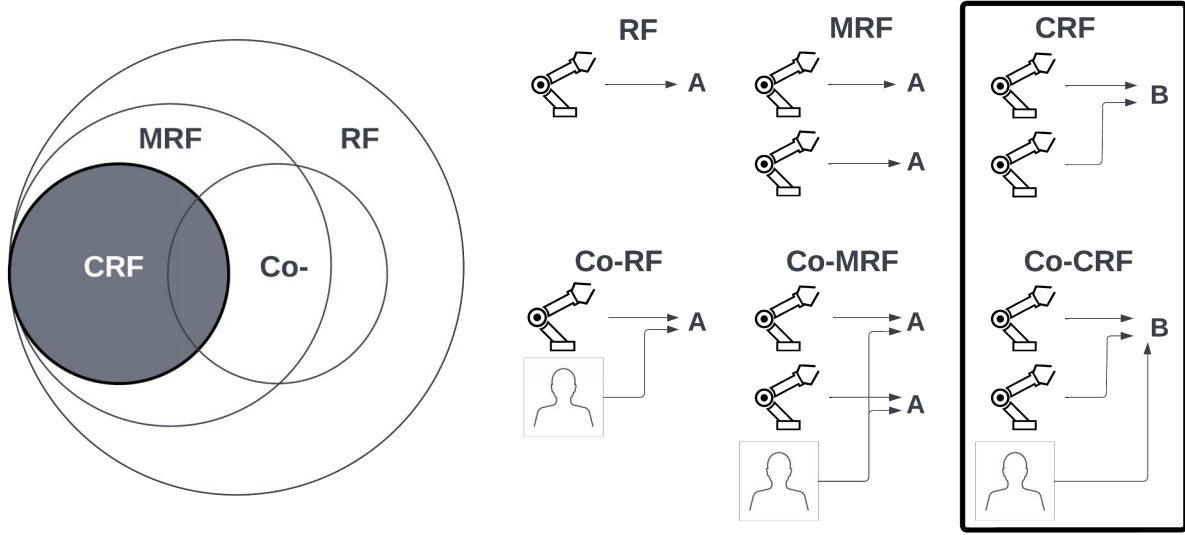


**Figure 2.1:** Cooperative robotic fabrication as situated in the overall robotic setup hierarchy  
 $(RF = \text{robotic fabrication}, MRF = \text{multi-robotic fabrication}, CRF = \text{cooperative robotic fabrication}, Co = \text{collaborative})$ . A setup is cooperative, if by the process of cooperation, a novel output is made possible (i.e., B), as opposed to a basic MRF process which only allows more of the same output to be created in parallel (i.e., A)

### 2.1.1 Broad Applications

Alongside applications in the built environment, which are specifically discussed in [Section 2.2](#), CRF is utilised in many industries when flexible manufacturing systems are necessary or where tasks occur in poorly structured environments [7]. In generic manufacturing applications, CRF processes have a conceptual advantage over single robot processes with their ability to distribute the work among several potentially smaller robots and thus better control the internal forces, torques and displacements associated with a payload [8]. In addition, CRF processes also allow for improved robustness against work interruptions through redundancy in the functions of the robots, improved flexibility through the ability to reconfigure a fabrication cell to fit different conditions, and improved task precision through the ability to dexterously grasp and then manipulate an object [8, 9]. Many generic tasks only become possible to automate when multiple robotic agents or manipulators are used cooperatively for: carrying heavy loads, moving voluminous objects, avoiding obstacles through complex movements, handling flexible objects with extra degrees of freedom, and assembling multiple components without using dedicated supporting fixtures or jigs [7, 10, 11]. Different industries use CRF workflows for various

industry-specific applications, for example:

1. The agricultural industry has seen major adoption of automation technologies in recent years [12], and specifically in cooperative robotic setups for foraging and picking tasks for various fruits and vegetables [13–16].
2. The automotive industry has a long history of being at the forefront of automation and is a leader in developing and utilizing both CRF and Co-CRF technologies [17] for tasks such as welding [18–20] and panel assembly [21].
3. The fibre composite manufacturing industry has been using cooperating robots for laying and smoothing sheets of material [22, 23] and in filament winding [24] for fabricating high-strength, geometrically complex components.
4. In heavy industry such as ship building and bridge construction, a dual-arm robot coupled with a hoist mechanism has been proposed to handle heavy work-pieces [25].
5. For generic industrial warehouse applications, cooperating mobile robots have long been used to move large and heavy objects [26, 27].

## 2.2 Cooperative Robotics in the Built Environment

The general use of robotics in the built environment is motivated by many of the same reasons as in the industries mentioned in [Section 2.1](#), specifically: high precision and task repeatability [28], improved productivity [29], improved site safety by reducing worker injuries [30], standardisation of product quality [31], and the ability to conduct work remotely to facilitate any necessary social distancing [28]. Typical applications fall under the categories of basic elementary operation such as materials handling, materials shaping, and material/structural joining [32]. One of the first recorded uses of robots in the construction industry was the Motor Mason automated bricklaying machine from the 1960s [33]. But it was not until the 1970s, in Japan, that robots in the construction industry saw serious exploration and use, specifically for the prefabrication of modular housing components [34]. In the 1980s more on-site robots appeared, followed by a proliferation of robots used for various specialised construction tasks over the next decades [35]. In

the mid-2000s, the large-scale application of robotics in the context of architectural and building design began with the growth of the Digital Fabrication (DFab) movement [36, 37]. This movement emphasised the design and construction of geometrically complex, efficient, and bespoke structures that were often only made possible, or sufficiently productive [38, 39], by combining novel digital technologies with more complex robotic setups.

A recent literature review on robots in the construction industry found that collaboration (used there to refer to both robot-robot and robot-human processes) is one of three major topics of recently published research [40]. CRF setups have been specifically demonstrated for automation, parallelisation, and scaling applied to rapid assembly of prefabrication, on-site additive manufacturing, and general task automation [41, 42], and for future building applications in challenging environments such as space construction [43].

In [Section 2.2.1](#), [Section 2.2.2](#), and [Section 2.2.3](#) CRF applications in the construction industry are summarized and organised according to the typical scale of their application (e.g., material, product, and building) and whether they originated from the general construction industry or from DFab research.

### 2.2.1 CRF at the Material Scale

CRF at the material scale is defined by small-scale processes that feature precise manipulation and subtractive/additive operations on single material units (e.g., a block of stone, a pipe, a structural member).

General construction applications include the use of dual-armed table-top sized robots, such as the IRB 14000 (YuMi) [44]. They are used, for example, for shaping materials and joining light building components such as small pipes [32]. But in general, such platforms suffer from limited payloads and are thus not capable of heavy lifting or manipulation of standard objects that are typical in most construction applications.

DFab applications include the use of CRF setups for cutting expanded polystyrene (EPS) foam blocks to create non-ruled and doubly curved surfaces. For example, custom concrete form-work was manufactured using a heated blade mounted on two robotic arms [45]. The relative displacement of the robot flanges was used to provide curvature to the blade, which shaped the

cut through the work piece as a third robot moved the foam block linearly through space. Another example used a heated wire instead, which two robots swept through a fixed foam block, using the resistance of the wire against the foam to create a non-standardised undulating surface profile for a series of wall panels [46]. In the tying of knots in cables, which is a material-scale task, the creation of loops and crossings cannot be performed by a single robot [47]. In a project on the aerial construction of tensile rope structures, the spatial manoeuvrability of multiple flying unmanned aerial vehicles (UAVs) was utilised to tie a knot using coordinated multi-robot flight trajectories, thus establishing a structural node in three-dimensional space [48, 49].

## 2.2.2 CRF at the Product Scale

CRF at the product scale is common in modular construction applications, building standalone components (i.e., walls, truss sections, shell panels), or transporting components as part of assembling a larger structure. In the context of prefabrication, CRF supports the goals of improving productivity, reducing labour, and maintaining a more predictable work environment [50].

General construction applications include the assembly of a box girder structure, which was performed with a team of mobile robots that cooperated to move separate panels, align the parts, and fasten them together [51]. In another mobile robot example, NASA's Jet Propulsion Laboratory (JPL) Robot Construction Crew, was used for picking and cooperatively transporting aluminium beams into an interlocking structure in the context of construction for space exploration applications [52, 53]. In another space-related application, tetrahedral truss structure modules for an astronomical telescope were built on a rotating platform as a second robot placed struts into accessible regions of the structure [54].

DFab applications include the construction of modular components for both wood and composite fibre structures. In one project, timber modules with non-planar geometries were constructed with two robotic arms used to place linear stud members while also supporting the corners of the structure in their unfinished state [55, 56]. In another research project, prefabricated cassettes for a segmented timber shell pavilion were assembled on a rotating central turntable where one robot manipulated the unfinished module in space while the other robot performed gluing, nailing, milling operations [57]. For composite fibre structures, a CRF process was used

in the construction of a modular fibre shell pavilion consisting of 36 geometrically varying panels [58]. Using the synchronised motion of two robots, a coreless filament was wound around an adaptable steel frame that defined the boundary polygon of each module [59, 60]. In another filament winding project, two robots exchanged a spool of filament allowing it to reach and wind around support points in space to create varying modules for a spanning space frame structure [61].

### 2.2.3 CRF at the Building Scale

CRF at the building scale is common for the in situ construction of large structures or for performing work in volumes beyond what is reachable by a single robot working alone. Processes at this scale emphasize the use of the robots to provide temporary support and guarantee stability for a structure as it is being built, or to expand the feasible work volume and reach of an RF setup.

General construction applications of CRF include an integrated construction robot platform featuring multiple robotic trolley hoists and mobile welding robots that are used to reach all areas of a steel structure as it is being constructed [62]. In one research project, the challenge of small payloads in aerial construction was overcome by the cooperative effort of multiple UAVs used to grasp, manipulate, and transport large structural elements into a structure on site [63]. Several examples exist for in situ construction for space-based structures and applications. The multi-limbed Hexbot robot was designed to assemble a telescope truss structure directly in space by carrying large components that required more than one arm to grasp. The robot used its multiple limbs to simultaneously walk on the structure, stay anchored, perform the gross movement of components, and connect them to the existing structure at the point of assembly [64]. In another related space construction project, the two-armed RoboSimian robot was used in a similar role as the Hexbot, for the manoeuvring and in-place assembly of a telescope truss structure [65].

DFab applications of CRF at the building scale have been demonstrated for various structural typologies and typically fall under two distinct categories of material systems: continuous (e.g., filaments or cables) or discrete (e.g., rods, studs, or bricks) elements. An example of a project where a continuous material system was combined with a CRF process was in the construction

of a large monocoque shell structure, where a UAV was used to pass a fibre spool between two static robotic arms placed at either end of the work volume. The filament was wound between the two robotic arms, expanding the feasible build volume by making it possible to build a structure within the interstitial space outside the reach of the two stationary robotic arms [66, 67]. In another aerial construction project, volumetric cable-structures were built in situ using two flying UAVs in a cooperative process of tying knots in space [68, 69]. In a final example of a continuous material system CRF process, multiple wall-climbing robots were used to pass filament between themselves, winding it around fixed anchor points to construct an in situ tensile structure [70].

CRF for discrete element assembly at the building scale was first developed for the assembly of geometrically differentiated metal space frame structures [71, 72]. This research focused on developing sequences and path-planning methods that allowed two robotic arms to provide temporary support to a structure while also adding elements to the structure, thus removing the need for external scaffolding in the assembly process. In another project where cooperating robots were used for temporary support, a branching arch structure was built out of foam blocks without requiring scaffolding by relying on two robots as simultaneous mobile temporary supports [73]. In the final example of a discrete element CRF process, a cooperative building-scale sequence was also demonstrated in the construction of a timber pergola roof structure, where one robot was used to support the member in space while the other performed an in situ drilling and fastening operation [74].

## 2.3 Cooperative Robotics for a Circular Economy

The architecture, engineering, and construction (AEC) industry is actively moving away from the traditional linear single-use material flow model. This transition is supported by the development of models to quantify environmental benefits of material circularity and explore reusing existing building stock, as evidenced in works like [75, 76]. Moreover, new frameworks have emerged to categorize circularity into principles concerning material and energy flows. An important framework is the *narrow, slow, close, and regenerate* framework outlined in [77, 78]. This framework serves as the foundation for recent literature, including [79], which explores

transitioning to a circular built environment using modern digital technologies. The same framework is used as a perspective for examining the research presented in the main body of this dissertation. It illustrates that CRF methods can generally facilitate a transition to a circular economy by addressing objectives aligned with the *narrow* ([section 2.3.1](#)), *slow* ([section 2.3.2](#)), and *close* ([section 2.3.3](#)) principles as summarized in the subsequent sections.

### 2.3.1 Narrow

With respect to the *narrow* principle, the following objectives are specifically applicable to CRF: (1) reducing primary resource inputs, (2) designing for structural performance, and (3) improving construction efficiency. First, primary resource inputs for constructing new structures can be reduced by leveraging the potential multi-functionality of a CRF setup. For example, while one robot places structural members during construction, other robots simultaneously provide temporary support to the structure in its unfinished state. All robots can then alternate their function throughout the fabrication process. Their function at each fabrication step, as either the active robotic agent (i.e., placing material) or the passive robotic agent (i.e., supporting the structure), is determined by the operator. A structure designed based on such an alternating “support-place” cooperative robotic sequence is considered fabrication informed as the fabrication process itself explicitly shapes its design. Using such an approach allows for the reduction, or complete removal, of temporary falsework, scaffolding, and supporting structure that would normally be required to build the structure using traditional construction methods, thereby reducing the primary resource inputs associated with constructing this temporary support structure. This cooperative approach is especially relevant for spanning discrete element structures (e.g., masonry vaults and space frame structures), which often require extensive temporary supporting structures as they are only self-stable at their completion or only at specific stages during the construction process. This type of cooperative sequencing is demonstrated in the research that is documented in the four chapters that comprise the body of this dissertation: [Chapter 3\[6\]](#), [Chapter 4 \[80, 81\]](#), [Chapter 5 \[82\]](#), and [Chapter 6 \[83, 84\]](#).

The second objective of the *narrow* principle applicable to CRF is based on how material usage in the structure itself can also be reduced by designing its form such that it maximizes struc-

tural performance. For example, form-found or topologically optimised structures are materially efficient by virtue of their shapes or connectivity being optimised for various loading conditions, but often result in geometrically complex structures that are challenging to construct with traditional methods. Applied to the prefabrication of structural modules, it is possible to realize complex geometries by relying on the spatial precision of a robot to place material accurately in 3D space. This capability is augmented in a CRF setup, which allows for the simultaneous cooperative manoeuvring and repositioning of structural modules that are under construction to facilitate accessibility.

The third objective recognises efficient but geometrically complex structures can be time-consuming and require several workers to construct [38, 39]. A CRF process can improve construction efficiency by taking on certain material handling and movement tasks to reduce the overall time and labour resources required.

### 2.3.2 Slow

With respect to the *slow* principle, the following objectives are specifically applicable to CRF: (1) design for reversibility, and (2) lifetime extension. Regarding the first objective, design for reversibility, CRF setups can be used for the disassembly of geometrically complex or spanning structures, which can thus be designed with explicit potential for reversibility from the outset. For example, the structure can be designed as an assembly of modules that can be more easily isolated and removed from the overall structure. To assist in this process, a CRF setup can be used with similar robotic task allocations as in assembly: the robots work cooperatively acting as temporary supports while simultaneously separating and removing self-rigid modules from the structure. The robots perform the physically demanding, and potentially dangerous, tasks of removing material while also indefinitely supporting and stabilizing the structure in its temporary state of disassembly. [Chapter 5](#) features a spanning space frame structure that is specifically designed so that it can be taken apart in a stability-preserving way when using a cooperative robotic sequence [82].

Regarding the second objective of the *slow* principle, CRF setups assisting in the task of disassembling a structure create an opportunity to start considering the use of automation for building

lifetime extension. If a structure is designed with modularity in mind, damaged components can be more quickly isolated, removed and eventually replaced without requiring large interruptions to the function of the structure (e.g., construction of temporary support or scaffolding).

### 2.3.3 Close

Regarding the *close* principle, the following activities are made possible through CRF: (1) tracking, documenting, and tracing building components, and (2) reuse and reassembly. First, accurate 3D models of a structure can be created and used to build a digital twin to document geometric location and placement accuracy of structural and non-structural components or to perform visual grading and inspection. CRF setups facilitate this process as the positional information that is inherent in a robotic platform can be used to accurately stitch together multiple 3D-image captures from different cameras and perspectives. This can create a complete digital model of an existing structure, which would not always be possible with a single robot due to obstructed perspectives. In terms of the second objective, when CRF is applied to disassembly, it also facilitates the reuse and reassembly of structural components while modifying a building or recuperating material that would normally be treated as construction waste. This approach is demonstrated in [Chapter 6 \[83, 84\]](#).

## References

- [1] Y. U. Cao, A. S. Fukunaga, A. Kahng, Cooperative Mobile Robotics: Antecedents and Directions, *Autonomous Robots* 4 (1) (1997) 7–27. doi:10.1023/A:1008855018923.
- [2] P. G. Ranky, Collaborative, synchronous robots serving machines and cells, *Industrial Robot: An International Journal* 30 (3) (2003) 213–217. doi:10.1108/01439910310473915.
- [3] G. Liu, J. Xu, X. Wang, Z. Li, On quality functions for grasp synthesis, fixture planning, and coordinated manipulation, *IEEE Transactions on Automation Science and Engineering* 1 (2) (2004) 146–162. doi:10.1109/TASE.2004.836760.
- [4] E. Asadi, B. Li, I.-M. Chen, Pictobot: A Cooperative Painting Robot for Interior Finishing of Industrial Developments, *IEEE Robotics & Automation Magazine* 25 (2) (2018) 82–94. doi:10.1109/MRA.2018.2816972.
- [5] C. Weckenborg, K. Kieckhäuser, C. Müller, M. Grunewald, T. S. Spengler, Balancing of assembly lines with collaborative robots, *Business Research* 13 (1) (2020) 93–132. doi:10.1007/s40685-019-0101-y.
- [6] E. P. G. Bruun, I. Ting, S. Adriaenssens, S. Parascho, Human–robot collaboration: A fabrication framework for the sequential design and construction of unplanned spatial structures, *Digital Creativity* 31 (4) (2020) 320–336. doi:10.1080/14626268.2020.1845214.
- [7] F. Caccavale, M. Uchiyama, Cooperative Manipulation, in: Springer Handbook of Robotics, Springer Handbooks, Springer International Publishing, Cham, 2016, pp. 989–1006.  
URL [https://doi.org/10.1007/978-3-319-32552-1\\_39](https://doi.org/10.1007/978-3-319-32552-1_39)
- [8] G. Montemayor, J. Wen, Decentralized Collaborative Load Transport by Multiple Robots, in: Proceedings of the 2005 IEEE International Conference on Robotics and Automation, 2005, pp. 372–377. doi:10.1109/ROBOT.2005.1570147.

- [9] J. Gudiño-Lau, M. A. Arteaga, Dynamic model and simulation of cooperative robots: a case study, *Robotica* 23 (5) (2005) 615–624. doi:10.1017/S0263574704001213.
- [10] Y. Gan, X. Dai, J. Li, Cooperative Path Planning and Constraints Analysis for Master-Slave Industrial Robots, *International Journal of Advanced Robotic Systems* 9 (3) (2012) 88. doi:10.5772/51374.
- [11] S. Li, Y. Zhang, Neural Networks for Cooperative Control of Multiple Robot Arms, SpringerBriefs in Applied Sciences and Technology, Springer Singapore, Singapore, 2018. URL <http://link.springer.com/10.1007/978-981-10-7037-2>
- [12] C. Lytridis, V. G. Kaburlasos, T. Pachidis, M. Manios, E. Vrochidou, T. Kalampokas, S. Chatzistamatis, An Overview of Cooperative Robotics in Agriculture, *Agronomy* 11 (9) (2021) 1818. doi:10.3390/agronomy11091818.
- [13] D. Sepulveda, R. Fernandez, E. Navas, M. Armada, P. Gonzalez-De-Santos, Robotic Aubergine Harvesting Using Dual-Arm Manipulation, *IEEE Access* 8 (2020) 121889–121904. doi:10.1109/ACCESS.2020.3006919.
- [14] H. Sarabu, K. Ahlin, A.-P. Hu, Graph-Based Cooperative Robot Path Planning in Agricultural Environments, in: 2019 IEEE/ASME International Conference on Advanced Intelligent Mechatronics, IEEE, Hong Kong, China, 2019, pp. 519–525. doi:10.1109/AIM.2019.8868747.
- [15] K. J. Ahlin, A.-P. Hu, N. Sadegh, Apple Picking Using Dual Robot Arms Operating Within an Unknown Tree, in: 2017 ASABE Annual International Meeting, American Society of Agricultural and Biological Engineers, Spokane, Washington, 2017, pp. 1–11. doi:10.13031/aim.201700471.
- [16] X. Ling, Y. Zhao, L. Gong, C. Liu, T. Wang, Dual-arm cooperation and implementing for robotic harvesting tomato using binocular vision, *Robotics and Autonomous Systems* 114 (2019) 134–143. doi:10.1016/j.robot.2019.01.019.
- [17] G. Michalos, S. Makris, N. Papakostas, D. Mourtzis, G. Chryssolouris, Automotive assembly technologies review: challenges and outlook for a flexible and adaptive approach,

CIRP Journal of Manufacturing Science and Technology 2 (2) (2010) 81–91. doi:  
10.1016/j.cirpj.2009.12.001.

- [18] S. Pellegrinelli, N. Pedrocchi, L. M. Tosatti, A. Fischer, T. Tolio, Multi-robot spot-welding cells for car-body assembly: Design and motion planning, *Robotics and Computer-Integrated Manufacturing* 44 (2017) 97–116. doi:10.1016/j.rcim.2016.08.006.
- [19] L. Wu, K. Cui, S. B. Chen, Redundancy coordination of multiple robotic devices for welding through genetic algorithm, *Robotica* 18 (6) (2000) 669–676. doi:10.1017/S0263574799001976.
- [20] N. Papakostas, G. Michalos, S. Makris, D. Zouzias, G. Chryssolouris, Industrial applications with cooperating robots for the flexible assembly, *International Journal of Computer Integrated Manufacturing* 24 (7) (2011) 650–660. doi:10.1080/0951192X.2011.570790.
- [21] C. Connolly, Motoman markets co-operative and humanoid industrial robots, *Industrial Robot: An International Journal* 36 (5) (2009) 417–420. doi:10.1108/01439910910980132.
- [22] M. Szcesny, F. Heieck, S. Carosella, P. Middendorf, H. Sehrs Schön, M. Schneiderbauer, The advanced ply placement process – an innovative direct 3D placement technology for plies and tapes, *Advanced Manufacturing: Polymer & Composites Science* 3 (1) (2017) 2–9. doi:10.1080/20550340.2017.1291398.
- [23] R. K. Malhan, A. M. Kabir, A. V. Shembekar, B. Shah, S. K. Gupta, T. Centea, Hybrid Cells for Multi-Layer Prepreg Composite Sheet Layup, in: 2018 IEEE 14th International Conference on Automation Science and Engineering, 2018, pp. 1466–1472. doi:10.1109/COASE.2018.8560586.
- [24] M. P. Sbanca, G. L. Mogan, Winding of Carbon Wire Composite Structures Using Two Cooperative Industrial Robots, *Applied Mechanics and Materials* 762 (2015) 291–298. doi:10.4028/www.scientific.net/AMM.762.291.
- [25] T. Shinohara, K. Miyawaki, K. Sunayama, Heavy material handling by cooperative robot control, *Advanced Robotics* 15 (3) (2001) 317–321. doi:10.1163/156855301300235841.

- [26] M. Mataric, M. Nilsson, K. Simsarin, Cooperative multi-robot box-pushing, in: Proceedings 1995 IEEE/RSJ International Conference on Intelligent Robots and Systems. Human Robot Interaction and Cooperative Robots, Vol. 3, 1995, pp. 556–561. doi:10.1109/IROS.1995.525940.
- [27] Y. Hirata, K. Kosuge, H. Asama, H. Kaetsu, K. Kawabata, Coordinated transportation of a single object by multiple mobile robots without position information of each robot, in: Proceedings of the 2000 IEEE/RSJ International Conference on Intelligent Robots and Systems, Vol. 3, 2000, pp. 2024–2029 vol.3. doi:10.1109/IROS.2000.895268.
- [28] X. Wang, C.-J. Liang, C. C. Menassa, V. R. Kamat, Interactive and Immersive Process-Level Digital Twin for Collaborative Human–Robot Construction Work, *Journal of Computing in Civil Engineering* 35 (6) (2021) 1–19. doi:10.1061/(ASCE)CP.1943-5487.000988.
- [29] X. Xu, B. Garcia de Soto, On-site Autonomous Construction Robots: A review of Research Areas, Technologies, and Suggestions for Advancement, in: 37th International Symposium on Automation and Robotics in Construction, Kitakyushu, Japan, 2020, pp. 385–392. doi:10.22260/ISARC2020/0055.
- [30] B. Chu, K. Jung, M.-T. Lim, D. Hong, Robot-based construction automation: An application to steel beam assembly (Part I), *Automation in Construction* 32 (2013) 46–61. doi:10.1016/j.autcon.2012.12.016.
- [31] S. Dritsas, G. S. Soh, Building robotics design for construction: Design considerations and principles for mobile systems, *Construction Robotics* 3 (1-4) (2019) 1–10. doi:10.1007/s41693-018-0010-1.
- [32] K. Afsari, Applications of Collaborative Industrial Robots in Building Construction, in: Proceedings of the 54th ASC Annual International Conference, Mississippi, 2018, pp. 472–479.
- [33] British Pathé, Mechanical bricklayer (1967).  
URL <https://www.youtube.com/watch?v=4MWald1Goqk>

- [34] T. Bock, T. Linner, Construction robots: Elementary technologies and single-task construction robots, Vol. 4, Cambridge University Press, 2016, ISBN: 978-1-316-78517-1.
- [35] T. Bock, Construction robotics, *Autonomous Robots* 22 (3) (2007) 201–209. doi:10.1007/s10514-006-9008-5.
- [36] F. Gramazio, M. Kohler, Digital materiality in architecture, 1st Edition, Lars Muller, Baden, 2008, ISBN: 978-3-03778-122-7.
- [37] T. Bonwetsch, D. Kobel, F. Gramazio, M. Kohler, The informed wall: Applying additive digital fabrication techniques on architecture, in: Proceedings of the 25th Annual Conference of the Association for Computer-Aided Design in Architecture, 2006, pp. 489–495, ISBN: 978-0-9789463-0-2.
- [38] B. García de Soto, I. Agustí-Juan, J. Hunhevicz, S. Joss, K. Graser, G. Habert, B. T. Adey, Productivity of digital fabrication in construction: Cost and time analysis of a robotically built wall, *Automation in Construction* 92 (2018) 297–311. doi:10.1016/j.autcon.2018.04.004.
- [39] J. M. Davila Delgado, L. Oyedele, A. Ajayi, L. Akanbi, O. Akinade, M. Bilal, H. Owolabi, Robotics and automated systems in construction: Understanding industry-specific challenges for adoption, *Journal of Building Engineering* 26 (2019) 1–11. doi:10.1016/j.jobe.2019.100868.
- [40] B. Xiao, C. Chen, X. Yin, Recent advancements of robotics in construction, *Automation in Construction* 144 (2022) 1–16. doi:10.1016/j.autcon.2022.104591.
- [41] K. H. Petersen, N. Napp, R. Stuart-Smith, D. Rus, M. Kovac, A review of collective robotic construction, *Science Robotics* 4 (28) (2019) 1–10. doi:10.1126/scirobotics.aau8479.
- [42] M. Kayser, L. Cai, S. Falcone, C. Bader, N. Inglessis, B. Darweesh, N. Oxman, FIBER-BOTS: an autonomous swarm-based robotic system for digital fabrication of fiber-based composites, *Construction Robotics* 2 (1-4) (2018) 67–79. doi:10.1007/s41693-018-0013-y.

- [43] Z. Xue, J. Liu, C. Wu, Y. Tong, Review of in-space assembly technologies, *Chinese Journal of Aeronautics* 34 (11) (2021) 21–47. doi:10.1016/j.cja.2020.09.043.
- [44] ABB, Product specification - IRB 14000, Tech. Rep. 3HAC052982-001, ABB (2015). URL <https://new.abb.com/products/robotics/collaborative-robots/yumi/irb-14000-yumi>
- [45] A. Søndergaard, J. Feringa, T. Nørbjerg, K. Steenstrup, D. Brander, J. Graversen, S. Markvorsen, A. Bærentzen, K. Petkov, J. Hattel, K. Clausen, K. Jensen, L. Knudsen, J. Kortbek, Robotic Hot-Blade Cutting, in: *Robotic Fabrication in Architecture, Art and Design 2016*, Springer International Publishing, Sydney, Australia, 2016, pp. 150–164. doi:10.1007/978-3-319-26378-6\_11.
- [46] R. Rust, D. Jenny, F. Gramazio, T. Kohler, Spatial wire cutting: cooperative robotic cutting of non-ruled surface geometries for bespoke building components, in: *Proceedings of the 21st International Conference of the Association for Computer-Aided Architectural Design Research in Asia*, Melbourne, 2016, pp. 529–538.
- [47] F. Augugliaro, E. Zarfati, A. Mirjan, R. D’Andrea, Knot-tying with flying machines for aerial construction, in: *2015 IEEE/RSJ International Conference on Intelligent Robots and Systems*, 2015, pp. 5917–5922. doi:10.1109/IROS.2015.7354218.
- [48] A. Mirjan, F. Gramazio, M. Kohler, F. Gramazio, M. Kohler, S. Langenberg, Building with Flying Robots, in: *Fabricate 2014: Negotiating Design & Making*, UCL Press, 2014, pp. 266–271. doi:10.2307/j.ctt1tp3c5w.36.
- [49] F. Augugliaro, A. Mirjan, F. Gramazio, M. Kohler, R. D’Andrea, Building tensile structures with flying machines, in: *2013 IEEE/RSJ International Conference on Intelligent Robots and Systems*, 2013, pp. 3487–3492. doi:10.1109/IROS.2013.6696853.
- [50] P. Vähä, T. Heikkilä, P. Kilpeläinen, M. Järvi vuoma, E. Gambao, Extending automation of building construction — Survey on potential sensor technologies and robotic applications, *Automation in Construction* 36 (2013) 168–178. doi:10.1016/j.autcon.2013.08.002.

- [51] M. Dogar, R. A. Knepper, A. Spielberg, C. Choi, H. I. Christensen, D. Rus, Multi-scale assembly with robot teams, *The International Journal of Robotics Research* 34 (13) (2015) 1645–1659. doi:10.1177/0278364915586606.
- [52] A. Stroupe, T. Huntsberger, A. Okon, H. Aghazarian, M. Robinson, Behavior-based multi-robot collaboration for autonomous construction tasks, in: 2005 IEEE/RSJ International Conference on Intelligent Robots and Systems, 2005, pp. 1495–1500. doi:10.1109/IROS.2005.1545269.
- [53] T. Huntsberger, A. Stroupe, B. Kennedy, System of systems for space construction, in: 2005 IEEE International Conference on Systems, Man and Cybernetics, Vol. 4, Waikoloa, Hawaii, 2005, pp. 3173–3178. doi:10.1109/ICSMC.2005.1571634.
- [54] W. Doggett, Robotic assembly of truss structures for space systems and future research plans, in: Proceedings of the 2002 IEEE Aerospace Conference, Vol. 7, IEEE, Big Sky, MT, USA, 2002, pp. 1–10. doi:10.1109/AERO.2002.1035335.
- [55] A. Thoma, A. Adel, M. Helmreich, T. Wehrle, F. Gramazio, M. Kohler, Robotic fabrication of bespoke timber frame modules, in: Robotic Fabrication in Architecture, Art and Design 2018, Springer International Publishing, Zurich, 2018, pp. 447–458. doi:10.1007/978-3-319-92294-2\_34.
- [56] A. Adel, A. Thoma, M. Helmreich, F. Gramazio, M. Kohler, Design of Robotically Fabricated Timber Frame Structures, in: Proceedings of the 38th Annual Conference of the Association for Computer Aided Design in Architecture, Mexico City, 2018, pp. 394–403.  
URL [http://papers.cumincad.org/cgi-bin/works/paper/acadia18\\_394](http://papers.cumincad.org/cgi-bin/works/paper/acadia18_394)
- [57] H. J. Wagner, M. Alvarez, O. Kyjanek, Z. Bhiri, M. Buck, A. Menges, Flexible and transportable robotic timber construction platform – TIM, *Automation in Construction* 120 (2020) 103400. doi:10.1016/j.autcon.2020.103400.
- [58] M. Doerstelmann, J. Knippers, A. Menges, S. Parascho, M. Prado, T. Schwinn, ICD/ITKE Research Pavilion 2013-14: Modular Coreless Filament Winding Based on Beetle Elytra, *Architectural Design* 85 (5) (2015) 54–59. doi:10.1002/ad.1954.

- [59] M. Prado, M. Dörstelmann, T. Schwinn, A. Menges, J. Knippers, Core-Less Filament Winding, in: Robotic Fabrication in Architecture, Art and Design 2014, Springer International Publishing, Ann Arbor, Michigan, 2014, pp. 275–289. doi:10.1007/978-3-319-04663-1\_19.
- [60] S. Parascho, J. Knippers, M. Dörstelmann, M. Prado, A. Menges, Modular Fibrous Morphologies: Computational Design, Simulation and Fabrication of Differentiated Fibre Composite Building Components, in: P. Block, J. Knippers, N. J. Mitra, W. Wang (Eds.), Advances in Architectural Geometry 2014, Springer International Publishing, Cham, 2015, pp. 29–45. doi:10.1007/978-3-319-11418-7\_3.
- [61] R. Duque Estrada, F. Kannenberg, H. J. Wagner, M. Yablonina, A. Menges, Spatial winding: cooperative heterogeneous multi-robot system for fibrous structures, Construction Robotics 4 (3) (2020) 205–215. doi:10.1007/s41693-020-00036-7.
- [62] K. Saidi, T. Bock, C. Georgoulas, Robotics in Construction, in: Springer Handbook of Robotics, Springer, Cham, Switzerland, 2016, pp. 1493–1520.  
URL [https://doi.org/10.1007/978-3-319-32552-1\\_57](https://doi.org/10.1007/978-3-319-32552-1_57)
- [63] D. Mellinger, M. Shomin, N. Michael, V. Kumar, Cooperative Grasping and Transport Using Multiple Quadrotors, in: Distributed Autonomous Robotic Systems, Vol. 83, Springer, Berlin, Heidelberg, 2013, pp. 545–558.  
URL [http://link.springer.com/10.1007/978-3-642-32723-0\\_39](http://link.springer.com/10.1007/978-3-642-32723-0_39)
- [64] N. Lee, P. Backes, J. Burdick, S. Pellegrino, C. Fuller, K. Hogstrom, B. Kennedy, J. Kim, R. Mukherjee, C. Seubert, Y.-H. Wu, Architecture for in-space robotic assembly of a modular space telescope, Journal of Astronomical Telescopes, Instruments, and Systems 2 (4) (2016) 1–15. doi:10.1117/1.JATIS.2.4.041207.
- [65] S. Karumanchi, K. Edelberg, J. Nash, C. Bergh, R. Smith, B. Emanuel, J. Carlton, J. Koehler, J. Kim, R. Mukherjee, B. Kennedy, P. Backes, Payload-centric autonomy for in-space robotic assembly of modular space structures, Journal of Field Robotics 35 (6) (2018) 1005–1021. doi:10.1002/rob.21792.

- [66] B. Felbrich, N. Frueh, M. Prado, S. Saffarian, J. Solly, L. Vasey, J. Knippers, A. Menges, Multi-machine fabrication: An integrative design process utilising an autonomous UAV and industrial robots for the fabrication of long span composite structures, in: Proceedings of the 37th Annual Conference of the Association for Computer Aided Design in Architecture, Cambridge, MA, 2017, pp. 248–259.
- [67] L. Vasey, B. Felbrich, M. Prado, B. Tahanzadeh, A. Menges, Physically distributed multi-robot coordination and collaboration in construction, *Construction Robotics* 4 (1) (2020) 3–18. doi:10.1007/s41693-020-00031-y.
- [68] A. Mirjan, F. Gramazio, M. Kohler, F. Augugliaro, R. D’Andrea, Architectural fabrication of tensile structures with flying machines, in: *Green Design, Materials and Manufacturing Processes*, 1st Edition, CRC Press, London, 2013, pp. 513–518.  
URL <https://doi.org/10.1201/b15002>
- [69] A. Mirjan, F. Augugliaro, R. D’Andrea, F. Gramazio, M. Kohler, Building a Bridge with Flying Robots, in: D. Reinhardt, R. Saunders, J. Burry (Eds.), *Robotic Fabrication in Architecture, Art and Design 2016*, Springer International Publishing, Sydney, Australia, 2016, pp. 34–47. doi:10.1007/978-3-319-26378-6\_3.
- [70] M. Yablonina, A. Menges, Distributed Fabrication: Cooperative Making with Larger Groups of Smaller Machines, *Architectural Design* 89 (2) (2019) 62–69. doi:10.1002/ad.2413.
- [71] S. Parascho, A. Gandia, A. Mirjan, F. Gramazio, M. Kohler, Cooperative fabrication of spatial metal structures, in: *Fabricate 2017: Rethinking Design and Construction*, UCL Press, London, 2017, pp. 24–29. doi:10.3929/ethz-b-000219566.
- [72] S. Parascho, T. Kohlhammer, S. Coros, F. Gramazio, M. Kohler, Computational design of robotically assembled spatial structures: A sequence based method for the generation and evaluation of structures fabricated with cooperating robots, in: *Advances in Architectural Geometry 2018*, Klein Publishing GmbH, Gothenburg, Sweden, 2018, pp. 112 – 139.  
URL <https://research.chalmers.se/en/publication/504188>

- [73] K. Wu, A. Kilian, Robotic equilibrium: Scaffold free arch assemblies, in: Proceedings of the 38th Annual Conference of the Association for Computer Aided Design in Architecture, Mexico City, 2018, pp. 342–349. doi:10.52842/conf.acadia.2018.342.
- [74] A. Thoma, D. Jenny, M. Helmreich, A. Gandia, F. Gramazio, M. Kohler, Cooperative Robotic Fabrication of Timber Dowel Assemblies, in: Research Culture in Architecture, De Gruyter, 2019, pp. 77–88.  
URL <https://doi.org/10.1515/9783035620238-008>
- [75] D. Cottafava, M. Ritzen, Circularity indicator for residential buildings: Addressing the gap between embodied impacts and design aspects, Resources, Conservation and Recycling 164 (Jan. 2021). doi:10.1016/j.resconrec.2020.105120.
- [76] L. Eberhardt, J. Rønholt, M. Birkved, H. Birgisdottir, Circular Economy potential within the building stock - Mapping the embodied greenhouse gas emissions of four Danish examples, Journal of Building Engineering 33 (2021) 101845. doi:10.1016/j.jobe.2020.101845.
- [77] J. Konietzko, N. Bocken, E. Hultink, Circular Ecosystem Innovation: An Initial Set Of Principles, Journal of Cleaner Production 253 (2020) 119942. doi:10.1016/j.jclepro.2019.119942.
- [78] S. Çetin, C. De Wolf, N. Bocken, Circular Digital Built Environment: An Emerging Framework, Sustainability 13 (11) (2021) 6348. doi:10.3390/su13116348.
- [79] C. De Wolf, S. Çetin, N. Bocken, A Circular Built Environment in the Digital Age, Circular Economy and Sustainability, Springer Cham, 2023. doi:10.1007/978-3-031-39675-5.
- [80] S. Parascho, I. X. Han, S. Walker, A. Beghini, E. P. G. Bruun, S. Adriaenssens, Robotic vault: A cooperative robotic assembly method for brick vault construction, Construction Robotics 4 (3) (2020) 117–126. doi:10.1007/s41693-020-00041-w.
- [81] E. P. G. Bruun, R. Pastrana, V. Paris, A. Beghini, A. Pizzigoni, S. Parascho, S. Adriaenssens, Three cooperative robotic fabrication methods for the scaffold-free construction of a masonry arch, Automation in Construction 129 (2021) 103803. doi:10.1016/j.autcon.2021.103803.

- [82] E. P. G. Bruun, S. Adriaenssens, S. Parascho, Structural rigidity theory applied to the scaffold-free (dis)assembly of space frames using cooperative robotics, *Automation in Construction* 141 (2022) 104405. doi:10.1016/j.autcon.2022.104405.
- [83] E. P. G. Bruun, S. Adriaenssens, E. Besler, S. Parascho, ZeroWaste: Towards Computing Cooperative Robotic Sequences for the Disassembly and Reuse of Timber Frame Structures, in: Proceedings of the 42nd Annual Conference of the Association for Computer Aided Design in Architecture, Philadelphia, USA, 2022, pp. 586–597.  
URL <http://arks.princeton.edu/ark:/88435/pr1wp9t657>
- [84] E. P. G. Bruun, S. Adriaenssens, E. Besler, S. Parascho, ZeroWaste: Disassembly and reuse of a timber frame structure using cooperating robots, *Construction Robotics*(Submitted) (2024).

# 3

## Human-Robot Collaboration for the Design and Construction of Unplanned Spatial Structures

This chapter is based on the following publication(s):

**Bruun, E. P. G.**, Ting, I., Adriaenssens, S., & Parascho, S. (2020). Human–robot collaboration: A fabrication framework for the sequential design and construction of unplanned spatial structures. *Digital Creativity*, 31(4), 320–336. <https://doi.org/10.1080/14626268.2020.1845214>

Contributor roles in publication:

- Bruun: Conceptualization, Methodology, Software, Validation, Investigation, Writing (Original Draft), Writing (Review and Editing), Visualization
- Ting: Conceptualization, Investigation, Writing (Original Draft), Writing (Review and Editing), Visualization
- Adriaenssens: Writing (Review and Editing), Supervision
- Parascho: Resources, Writing (Review and Editing), Supervision

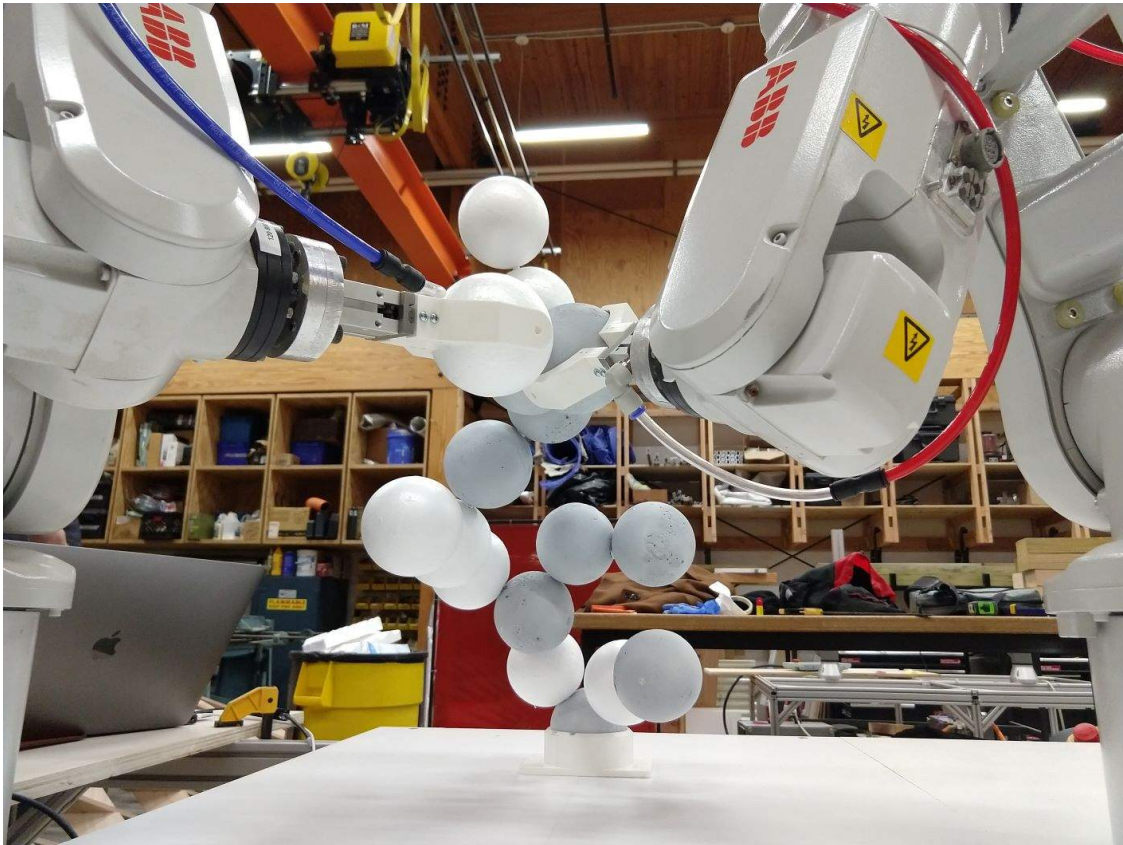


*Figure 3.1: A branching spatial structure assembled with two cooperating robotic arms.*

## Abstract

Robots in traditional fabrication applications act as passive participants in the process of creation — simply performing a set of predetermined actions to materialize a completed design. In this chapter, a novel bottom-up design framework is proposed in which robots are instead given the opportunity to participate centrally within a creative design process. This chapter describes how two table-top 6-axis industrial robotic arms were used to cooperatively aggregate a collection of solid spherical units. The branching spatial structure (shown in [fig. 3.1](#)) being constructed is unplanned at the outset of this process, and is instead designed in pseudo-realtime during construction. This “just-in-time design” approach relies on robotic input, in the form of path-planning constraints, in tandem with human evaluation and decision-making. The resulting structure emerges from a human-robot design collaboration (Co-CRF) operating within the specified physical domain.

## 3.1 Introduction

Robots are traditionally viewed as passive participants in the process of construction and creation: in this capacity they materialize a finished design through a set of pre-programmed actions (e.g. movements, material and tool manipulations). While useful in a highly controlled and repetitive industrial application, this approach does not allow the robot to contribute to the actual design of the finished structure in a meaningful way (i.e. acting as a creative agent). This project seeks to subvert the traditional fabrication paradigm in two ways: (1) utilizing a bottom-up approach to design a structure sequentially during construction, (2) creating a collaborative framework for the robots to participate centrally within the design process.

In this chapter, the results of a construction process for a branching three-dimensional structure assembled from the aggregation of solid spherical units are presented. A cooperative robotic assembly method, where two industrial robotic arms alternate between supporting and connecting new spheres to the existing structure is implemented. In the context of the proposed framework, the robots are thought of as both design agents and assembly instruments that facilitate the creation of a final structure. Rather than being pre-defined, the structure is designed and built incrementally on the basis of direct input from the robots, using their kinematic and path-planning constraints to generate a wide range of possible new additions to a structure. The human user is integrated into the geometry generation-aggregation process by being asked to evaluate the aesthetics of the proposed geometry in each new aggregation cycle, which sets up a collaborative dialogue between the human and robotic system. The design process can be thought of as completely decentralized as neither robot or human is aware of the final structure at the outset of the assembly process. The result is an unplanned stochastic topology and geometry where the placement of each new sphere is dictated by changes in both the physical and aesthetic criteria at each time-step.

### 3.1.1 Randomness in Design

The terms random and stochastic are used interchangeably in reference to generating an outcome that is not directly controlled or affected by a human user participating in the design process. Randomness in design can be thought of as an exploratory function, used to nonsubjectively

find a set of solutions that are feasible but not immediately apparent to a designer (i.e. unintuitive solutions that would not typically have been proposed) and thus to stimulate creativity. It is also be a way to sample a range of options from a broad design domain, where an exhaustive search of all design possibilities is computationally intractable.

The idea of using randomness in a design process is inspired by how randomness is used by evolutionary algorithms to create optimized solutions that are often not intuitive at the outset of the process. In the research presented in this chapter, the task is performed without an optimization target, as the goal is only to generate a feasible structure without being biased towards intuitively known solutions. Thus, randomness is used as an informed visualization process that helps represent a range of feasible designs for the structure on the basis of robotic constraints.

### 3.1.2 Bottom-up Design Methods

Bottom-up design describes a broad category of design methods which take as their starting point the definition of a clear set of their most basic units and actionable rules. These are combined and used systematically to create a more complex form or functional whole. Procedural design, where a sequence of instructions or procedures are used iteratively to generate form, is a subset of this category, as are computational techniques like evolutionary algorithms. These methodologies stand in contrast to top-down approaches, where the final form is the starting point which is then broken down to its constitutive components.

The proposed geometric aggregation strategy follows the bottom-up principle. The design formation process is viewed through the lens of architectural theorist Stan Allen's landmark essay "Field Conditions" [1, 2]. This theory describes the abstract formation of the whole: defined as a field condition or a spatial matrix "capable of unifying diverse elements" (Allen, 2013). This framework can also be applied to any bottom-up approach where emphasis is placed on the local connection between objects, rather than an overarching global scheme or "grand design". Allen's work, which comes from interest in emergent phenomena applied in the context of architecture and design, is also inspired by the more theoretical work on cellular automata: their classification [3] and their dynamics in creating complexity from simple rules [4].

## 3.2 State of the Art in the Robotic Context

The following section looks specifically at projects in the field of architectural fabrication that demonstrate robotic applications along the main themes of the current research: (1) cooperative robotic fabrication (CRF) setups used to assemble spatially complex structures, (2) robots used in stochastic processes, (3) human-robot collaboration frameworks. The section concludes with a summary of the conceptual framework represented by these projects and how the current chapter builds on the concepts described in the existing literature.

### 3.2.1 Cooperative Robotics and Complex Spatial Structures

Structures that are specifically designed for robotic construction are often simplified to follow an intuitive layer-based vertical aggregation strategy [5, 6]. But when using more than one robot in a CRF framework, the ability to alternate the functions of each robot opens up the design space to allow for much more spatial complexity in the type of structures that can be built without collapsing.

The assembly of spatial metal structures [7–9] and bespoke timber frame modules [10] are examples of recent robotic fabrication projects that demonstrated the potential of using cooperating robots to build non-planar geometries. All of these projects rely on two robotic arms working together to perform the aggregation process: performing tasks such as having one robotic arm to hold and support the structure while the other places a new member. Furthermore, these projects also required the careful coordination of the robots from the perspective of kinematic constraints in planning motion trajectories [11] to avoid collisions.

The simultaneous application of two robots allows one to be physically holding the assembly at all times, acting as a dynamic support structure. This allows for the exploration not only of more complex geometrical assemblies, but of a wider range of topological possibilities in the construction sequence. In addition to greater flexibility, cooperative robotic assembly eliminates the need for significant repetitive human intervention in the addition of structural supports outside the logic of modular structural aggregation. In the aforementioned projects the sequence of robots and their exact movements are pre-defined before construction, removing any exploratory possibilities associated with the construction process. In contrast, the research presented in this

chapter demonstrates the potential of cooperative assembly to explore the vast potential design space opened up by this fabrication method.

### **3.2.2 Stochastic Structural Aggregation**

The precise and algorithmic nature of robotic processes means that they are often not applied in random or chaotic application. But stochastic aggregation has been explored in a series of “granular matter” robotic fabrication projects [12, 13]. By aggregating numerous simple grains (i.e. small star-like components) researchers were able to achieve complex spatial forms on the global architectural scale. The general robotic placement of the grains was controlled (i.e. the location where the grains were chaotically scattered was planned), but the connection between individual components was completely random. Therefore, controlling the form of the individual grains was used as a means to program the overall structural behavior as a bottom-up design approach. These aggregated structures demonstrate how simple building blocks and randomness at the local scale (i.e. unit to unit connections) can be used to create a complex global form. The fabrication case study presented in this chapter seeks to emulate this type of bottom-up fabrication strategy using simple spherical units as components. But exploring a more controlled form of randomness, by placing each element individually, thereby allowing the stochastic process to shape the global rather than local form of the structure.

### **3.2.3 Collaborative Creation and Computational Creativity**

Computational creativity is defined as “a field of artificial intelligence focused on developing agents that generate creative products autonomously” [14], which is still a nascent topic in architectural fabrication. While the process of aggregation in this case study does not rely on artificial intelligence in an algorithmic sense, it is similar to recent work [15–17] by virtue of shifting away from the traditional process that “credits the human agent as the sole author and source of creativity” [18]. A suitable classification of the project would be that of collaborative creation, a broadly encompassing term which is defined as a human-machine interaction where “the human user is inspired by computational input, with optional suggestions or explicit changes to human creations acting as the stimulus for lateral thinking on the part of the designer” [19]. Bidgoli ex-

tends this idea directly to the field of architectural robotic fabrication with the theoretical concept of a “Design-Making” machine – a framework where suggestions are continually made by the Robot-Tool-Material (RTM) system for the user to evaluate [20].

### 3.2.4 Research Contribution

This case study seeks to extend the themes summarized in [Section 3.2.1](#), [Section 3.2.2](#), and [Section 3.2.3](#) in the following way:

- Use the logic of previous CRF projects that alternate support and placement functions ([section 3.2.1](#)), but extend the placement decision-making step through the pseudo-realtime interpretation of robotic kinematic and path-planning constraints.
- Use the exploratory nature of randomness in the process of structurally aggregating simple building blocks, but randomness on the global, rather than the local scale ([section 3.2.2](#)), to create an unplanned complex structure.
- Implement the theoretical construct of a “Design-Making” machine ([section 3.2.3](#)) in a collaborative creation framework by virtue of asking the human to evaluate options proposed by the robotic fabrication process. This fosters collaboration between the human and robot during the sequential process of designing and constructing an unplanned structure.

In summary, the novelty of the fabrication case study presented in this chapter lies in creating a framework that uses randomness as a means to generate potential design options. While the final aggregated structure is unpredictable, the process of assembly is governed by a simple rule-based process, which is described next in [Section 3.3](#), in combination with robotic feedback and human decision-making. This type of fabrication-informed sequential construction holds a major advantage over a traditional top-down process – it ensures every element in a structure can be successfully placed by the robot, and avoids having to do post-processing on a finished design to ensure placement feasibility. Finally, creativity is fostered as both the robot and the human are thought of as having some influence on the final design of the physical structure.

### 3.3 Methodology

The structure built as part of the case study presented in this chapter was being built using a cooperative robotic assembly strategy, where two industrial robotic arms alternate between supporting and connecting new spheres to the existing geometry. This assembly strategy was implemented to build a branching three-dimensional structure from solid expanded polystyrene (EPS) spheres. Since the purpose of this project was to explore a design process, rather than a material system, generic lightweight spherical units were chosen due to their aggregation flexibility – spheres are geometrically versatile as they have no aggregation constraints associate with directionality.

The structure had to be stable throughout all stages of construction, so the process of aggregation follows an alternating sequence; while one robot performs a pick-up and attachment sequence, the other holds the structure steady. The rest of the construction process was standardized as the pick-up actions occurred at a fixed location, and only the final sphere placement was calculated in each design cycle.

The overall aggregation is governed by the following set of local rules for each new solid sphere added to the structure:

1. Must be in contact with at least one other sphere.
2. New position must be reachable by the robot.
3. Must be placed in a way that avoids all obstacles.

The first rule describes the physical constraint associated with the material system: EPS spheres joined at a single point by means of a metal pin fastener. The second and third rules are associated with the constraints derived from inverse kinematic calculations performed by the robots during the path-planning process.

The following sections will explain how the actual process was executed, starting with an outline of the experimental setup ([section 3.3.1](#)), followed by a description of the three main steps that are repeated throughout the fabrication process: generating geometry ([section 3.3.2](#)), considering inverse kinematic and path-planning constraints ([section 3.3.3](#)), and robotic control ([section 3.3.4](#)).

### 3.3.1 Experimental Setup

The structure was built using two 6-axis IRB 120 robots (from ABB robotics) located 800mm apart on a work surface 620x1480mm ([fig. 3.2](#)) using commercially available 76.2mm (3in.) EPS spheres. The two robots are designated a common start location (based on a calibrated work object position), from which the actions for sphere pick-up and connection take place per aggregation cycle. The initial sphere of the total aggregation process is manually inserted into a fixed-base holder ([fig. 3.4c](#)) which is able to be placed anywhere within the working domain.

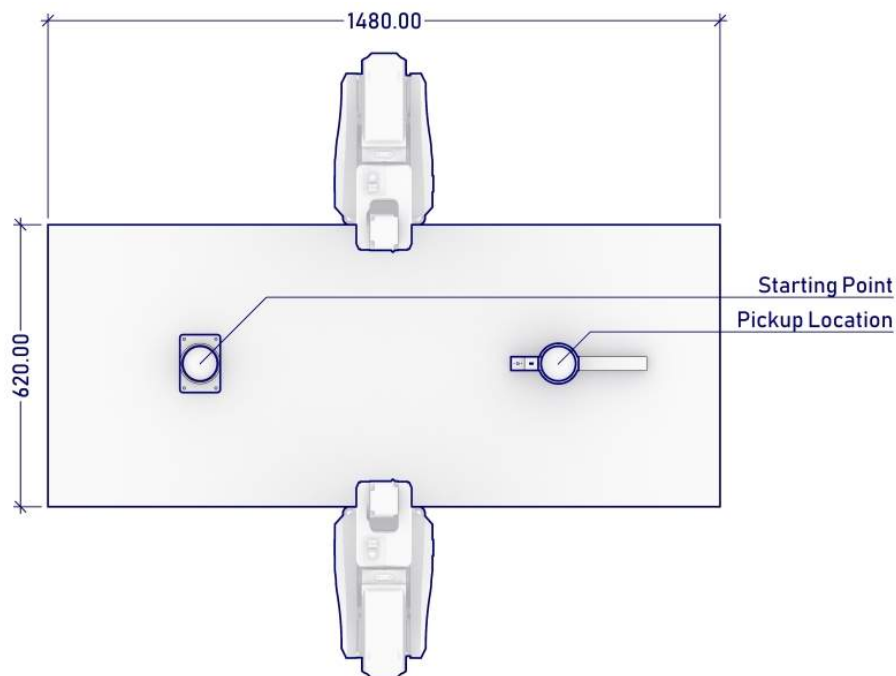


*Figure 3.2: Plan view of work domain.*

Individual spheres are held by the robots using a pneumatic gripper with custom jaws ([fig. 3.3](#)). In each new aggregation cycle, the respective robot starts the process by picking up a sphere from the pick-up holder ([fig. 3.4a](#)). The mechanical connection between spheres is achieved with the insertion of a double-pronged metal pin connector — after picking up the sphere, the robot presses the sphere onto the top half of a connector placed in the holder ([fig. 3.4b](#)). Upon extraction, the bottom half of the connector is revealed, and the sphere/connector assembly is guided by the robot to the correct spatial location. The new sphere is then pressed in to another sphere in the existing structure, connecting the two through a single pin connection.

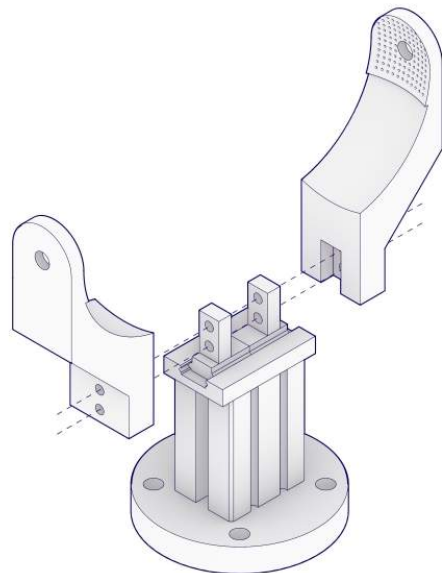
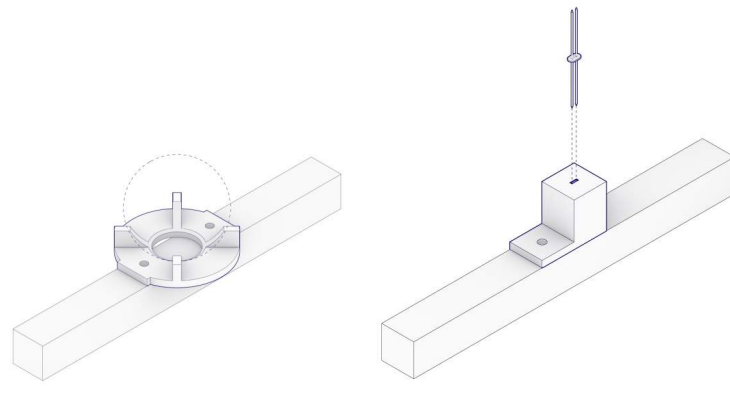


**Figure 3.3:** Custom pneumatic grippers.



(a) sphere pick-up holder      (b) pin connector holder



(c) fixed-base holder

**Figure 3.4:** Custom setup components.

### 3.3.2 Generating Stochastic Geometry

The process of generating new geometry is based on a random sampling approach inspired by the Rapidly-Exploring Random Tree (RRT) class of robotic motion planning algorithms [21]. These algorithms are used to randomly and incrementally explore a domain space to find a feasible trajectory, and are particularly successful since their sampling strategy biases them to search unexplored areas of a domain. Thus, the exploratory nature of an RRT sampling approach is perfectly suited to the goal proposed in this project: using randomness to explore a large physical design-space in the process of sequentially constructing an unplanned structure. Note that only the sampling strategy in this case study (i.e. generating potential positions for the next piece of a structure to aggregate at each time step) is borrowed from the RRT algorithm. Figure 3.5 shows examples of 2D patterns generated in a circular domain by an RRT\* algorithm [22]. The final tree structure and path is always different, and is unknown at the start of the process; the tree is grown by drawing a random sample in each iteration and connecting it to an existing branch. The final 3D form of the case study structure (see section 3.4) is visually reminiscent of this kind of branching output from an RRT algorithm as the solution path is expanded outward.

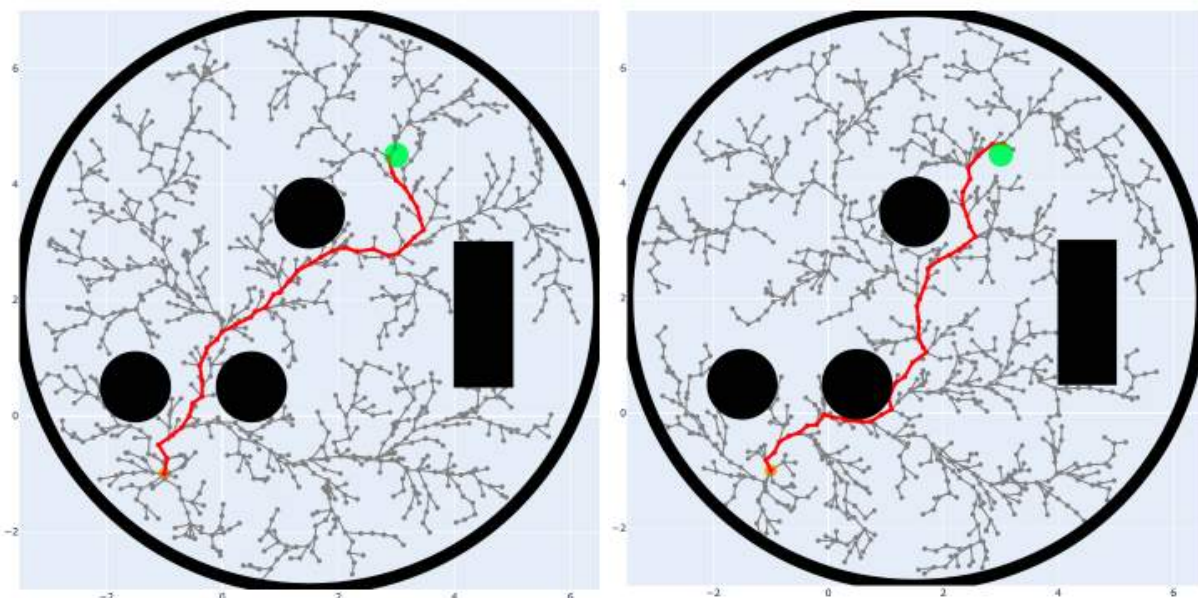


**Figure 3.5:** The RRT\* algorithm used to plan different trajectories through the same domain space.

The process by which new spheres in the structure are generated can be thought of as a 3D manifestation of an RRT sampling approach. The process is schematically shown in [Figure 3.6](#), which illustrates the following steps:

- Step 1. A random point is sampled from the physical domain.
- Step 2. The center of the closest sphere in the existing structure is located, and a vector is drawn between the random point and the center of this sphere.
- Step 3. The new sphere is located along this vector, tangent to the surface of the existing sphere.
- Step 4. The robot places the sphere following the approach vector calculated in Step 2.

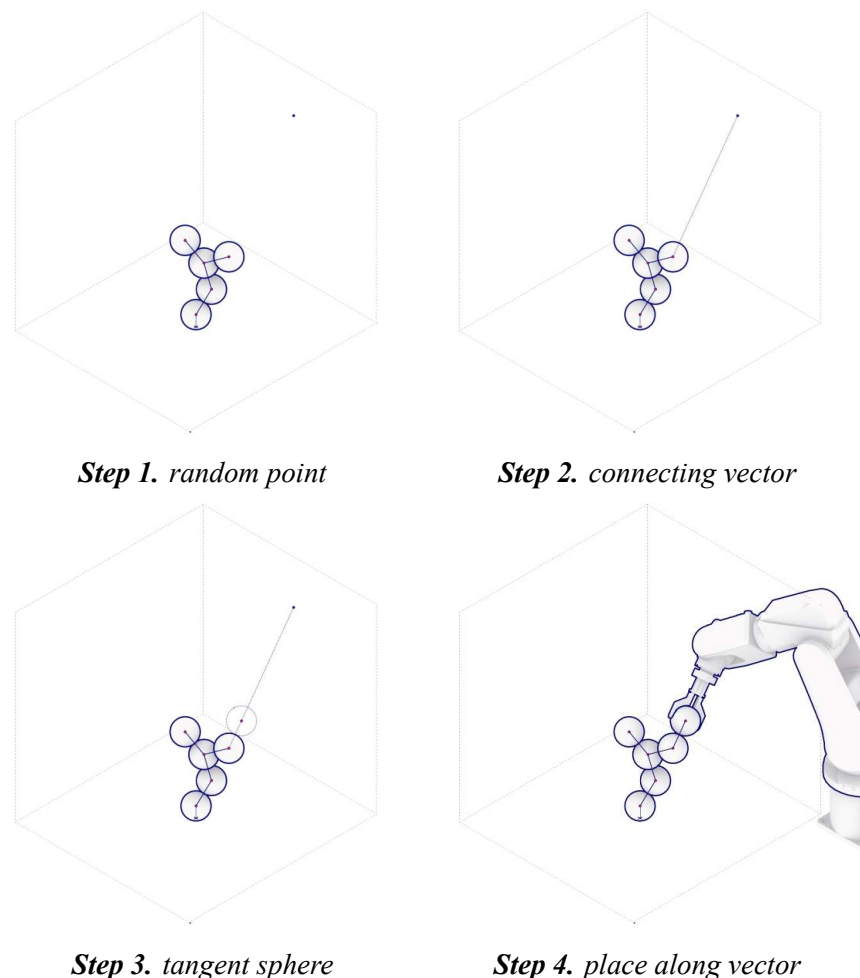


**Figure 3.6:** Example of the geometry generating procedure.

### 3.3.3 Inverse Kinematic and Path-Planning Constraints

A significant portion of the computation performed during the aggregation process occurs when determining whether the newly generated sphere is reachable, and can be placed without collision by the robotic arms. All geometric calculations (e.g. defining robotic frames/planes, transformations between coordinate systems) were done using the data structures available through the COMPAS framework [23], and the scene creation and inverse kinematic calculations was done through COMPAS Fab [24] by importing the Robot Operating System (ROS) back-end. A set of collision meshes, which represent the existing structure and the position of the other robot arm from the previous iteration, is added to the planning scene and included in the inverse kinematic calculation. If the calculation returns a PASS value, it means that the new sphere location is reachable by the robotic arm without colliding with any of the physical objects in the domain. In this way the robot itself, through its kinematic constraints, becomes an active participant in the creation of the structure as it dictates whether a newly generated random sphere is acceptable or not.

It is not the **calculation** of the next sphere that is considered “active participation”, but rather the **evaluation** of an input (i.e. suggested sphere) in relation to a physical state, leading to a **response**, that is considered creative participation from the perspective of the robot. In the case study presented in this chapter, the response is a simple binary (PASS/FAIL). But the distinction becomes more obvious if the framework is extended to trigger a more nuanced set of suggestions, which are perhaps based on previous history and additional sensor input. Therefore, the act of providing a response to stimuli, which is then used to stimulate a human decision, is defined as a creative input on the part of the robot.

The full computation loop is described in the flowchart shown in [Figure 3.7](#). Once a kinematically acceptable new sphere has been found, its position is assessed by the user for compliance with additional criteria. If deemed acceptable by both robot and human, the sphere is added to the model and the robot proceeds with the physical task of attaching the sphere to the existing structure ([Section 3.3.4](#)).

The human decision-making process in selecting a new sphere to aggregate was based on: (1) aesthetics, (2) choosing new spheres that would steer the growth of the structure in a certain di-

rection. In this implementation, since the random sphere generating domain was not changing (see discussion of this in Section 4.2), the human user was responsible for guiding the structure to achieve the loose goal of spanning from one end of the work-space to the other. Without input from the human, the direction of growth could not be controlled. Aesthetic considerations (i.e. favouring long branches) were also involved in this decision. Therefore, all paths from the human perspective were not self-similar.

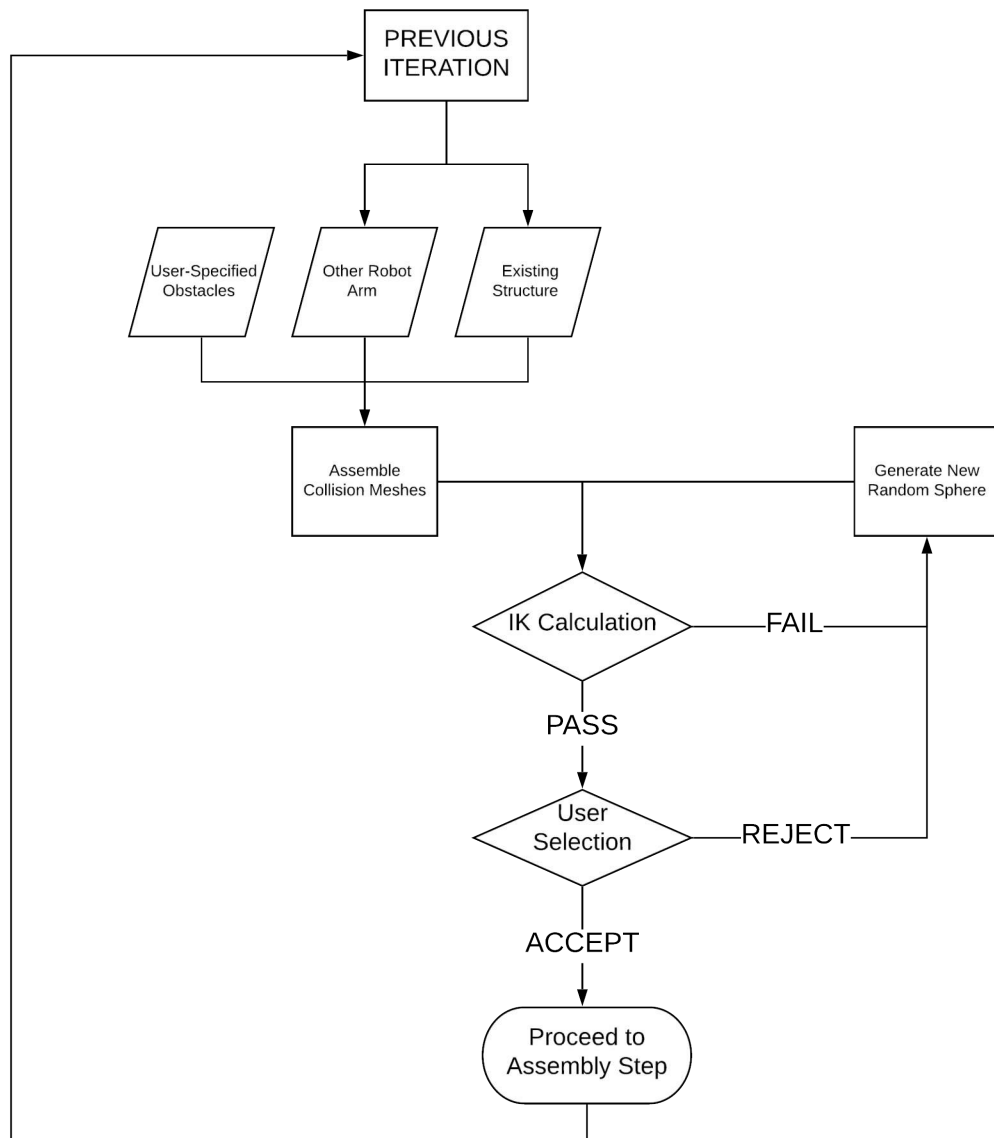


**Figure 3.7:** Flowchart for robotic path planning calculation loop.

### 3.3.4 Robotic Control

Once a new sphere that passes all criteria is found, it is added to the existing structure by sending the following set of assembly commands to the active robot arm:

1. Release grip on existing structure.
2. Reset the robot arm to rest position.
3. Pickup up new sphere and connector.
4. Reset the robot arm to rest position.
5. Position new sphere along approach trajectory.
6. Attach sphere to existing structure.

This aggregation loop is repeated, alternating between each robot. A full cycle for both is shown in [Figure 3.8](#).

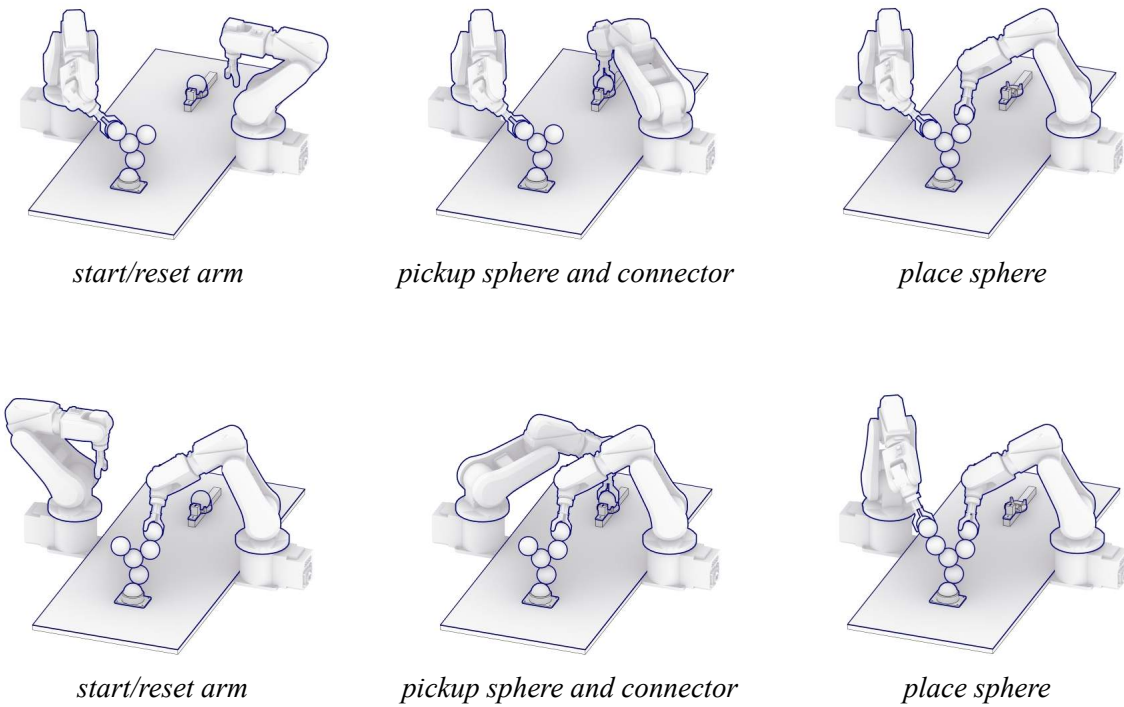


**Figure 3.8:** Example of one full aggregation cycle (top = robot 1, bottom = robot 2).

### 3.4 Final Structure

The progressive assembly of 16 spheres that comprise the final structure is shown in [Figure 3.9](#), where each image represents the end of a single aggregation cycle. [Figure 3.10](#) shows the final structure. To illustrate the contribution of each robot, the spheres have been coloured (white = robot 1, grey = robot 2) to reflect which arm was used to place them.

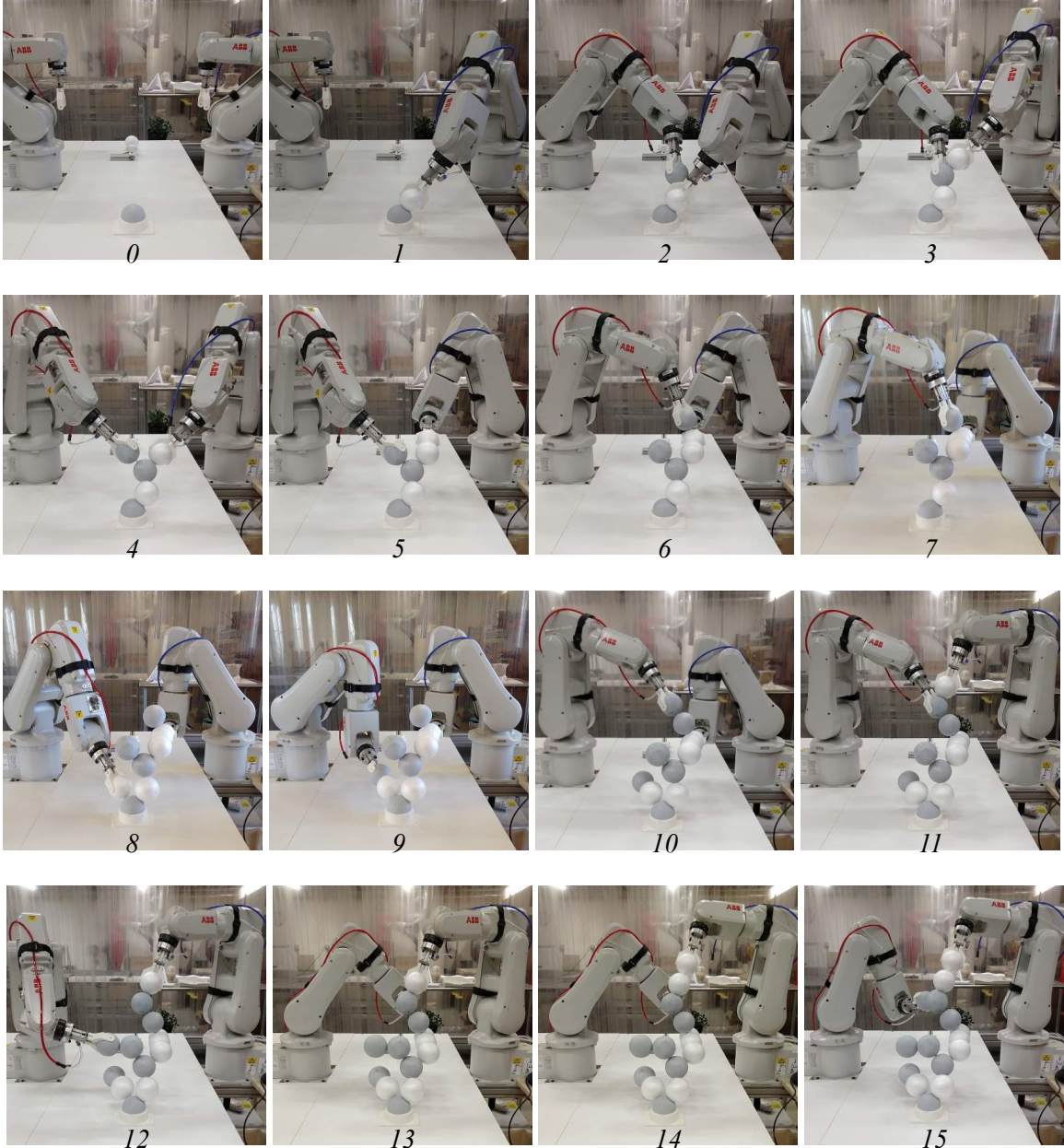


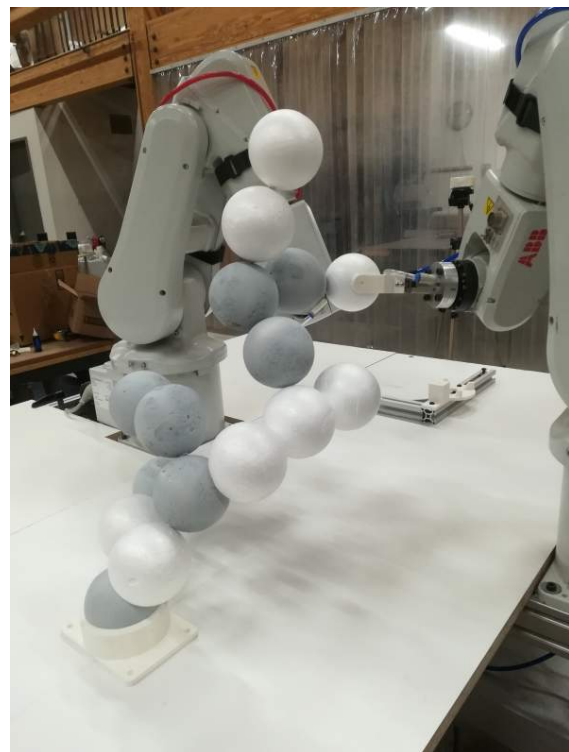
**Figure 3.9:** Structure at the end of each aggregation cycle.



*front perspective*



*left perspective*



*right perspective*

**Figure 3.10:** Final structure.

## 3.5 Discussion

### 3.5.1 Inverse Kinematics Computations

This project was successful in implementing pseudo-realtime kinematic evaluation, which is used as input to design the structure during the actual process of building. The result of the kinematic evaluation required a manual action by the user in response to the binary PASS/FAIL returned by the calculation (see [fig. 3.7](#) for the logic flowchart). As such, it became a collaborative design between the robot and human. This is one of the first aggregation projects in the architectural robotics field to actually focus on evaluating the feasibility of each new component during a sequential design process.

The inverse kinematic calculation, which was the driving force behind the final design, was successful in identifying the following constraints: when a sphere was out of reach, and when a collision in the scene was expected to happen. At the beginning of the build it was mainly the out of reach constraint that governed the placement of the spheres ([fig. 3.11a](#)), as the robots were required to stretch to almost their maximum capacity to reach the starting point. Therefore, most of the initial spheres were placed at an angle close to horizontal pointing towards the robots. Then as the structure grew towards the middle of the domain, the governing constraint became the collision between one robot arm and the other ([figs. 3.11b](#) and [3.11c](#)) — more dynamic sphere placements were therefore necessary to avoid these collisions.

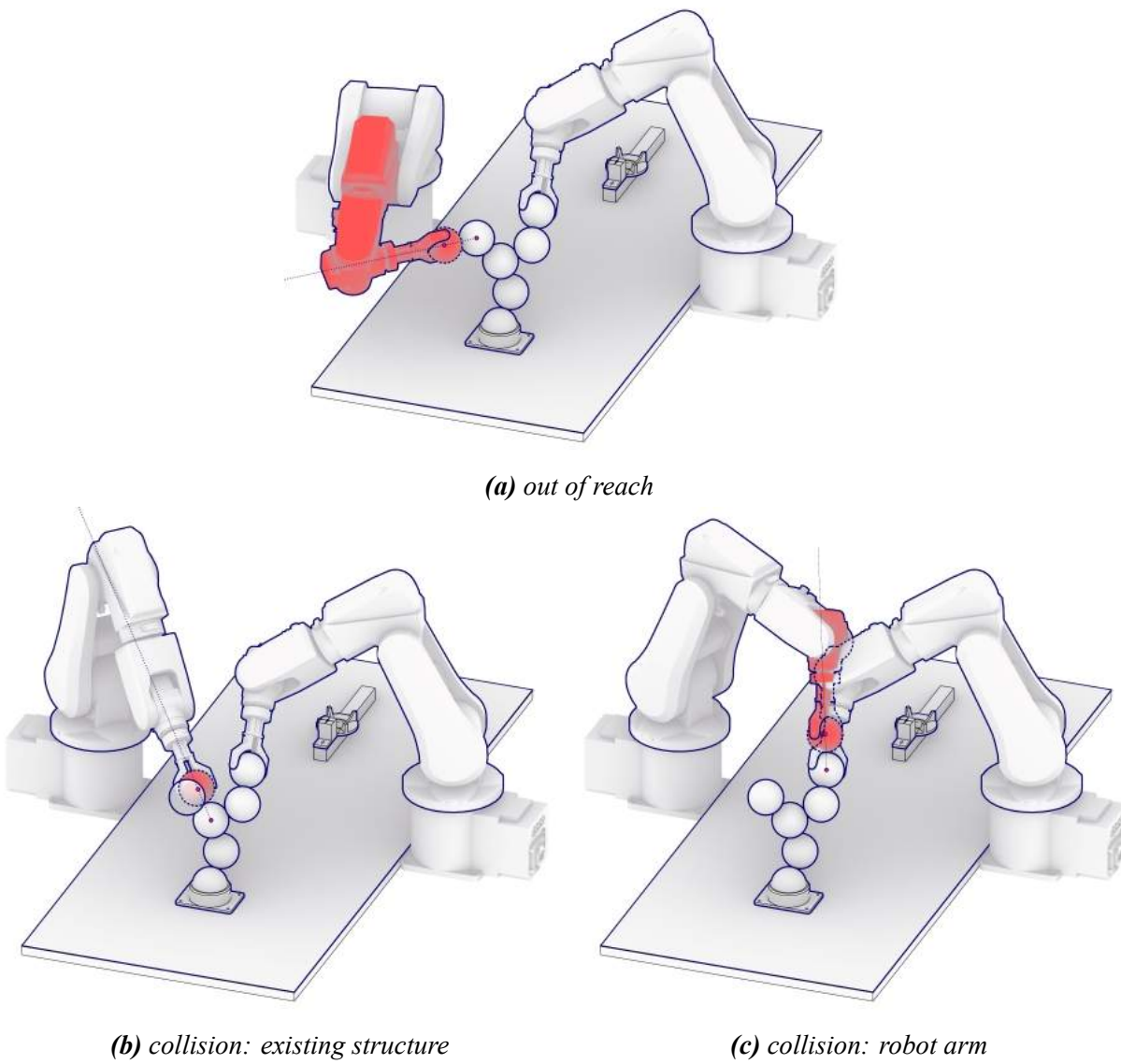


**Figure 3.11:** Example of inverse kinematics constraints during construction.

### 3.5.2 Factors Influencing the Final Result

Defining the volumetric domain within which new points were generated in the geometry creation process (Step 1 in [section 3.3.2](#)) played an important role in determining the general direction of growth for the structure. For example, a tall domain would tend to grow the resulting structure upwards, while a short domain would lead to a shallower form ([figs. 3.13a](#) and [3.13b](#)). In this fabrication case study, a simple bounding box is used, which encompassed the work sur-

face area and the vertical reach of the robots, to define the point generation domain. However, various user-specified alternative options exist for the definition of this bounding box.

In addition to modifying the shape and size of the point generation domain, separate domains could be defined per robot ([figs. 3.13c](#) and [3.13d](#)). Because new points are generated per assembly cycle, this would present the opportunity for the different position and work area of each robot to be accounted for during its turn. Additionally, this manner of differentiated domain has the potential to generate points resolving in spheres with an approach angle (for the placement action; Step 4, [section 3.3.2](#)) more likely to be within the kinematic range of the robot.

Finally, employing a dynamically changing domain would further increase the capacities of the generating system. Right now the human chooses the direction of growth to roughly satisfy a goal (e.g. going from one end of the domain to the other). But in the future a programmable objective can be built into the generation scheme. For instance, a domain which shrinks towards a point would bias the structure in a certain direction, allowing the for specification of a ‘goal’ ([fig. 3.12](#)). Linking the domain space to the state of the assembled structure might allow for a more construction aware structure generating process, or simply introduce another element of unpredictability. The design of the domain system represents a level of input which is responsive not only to formal objectives, but also to parameters of its own assembly and of the robotic agents.

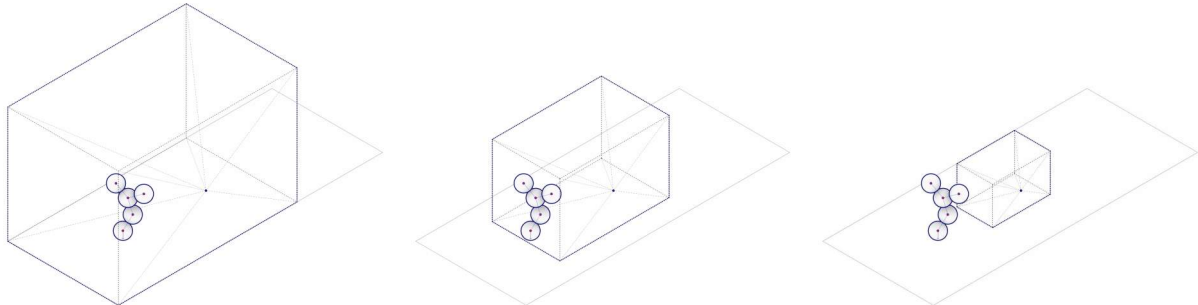
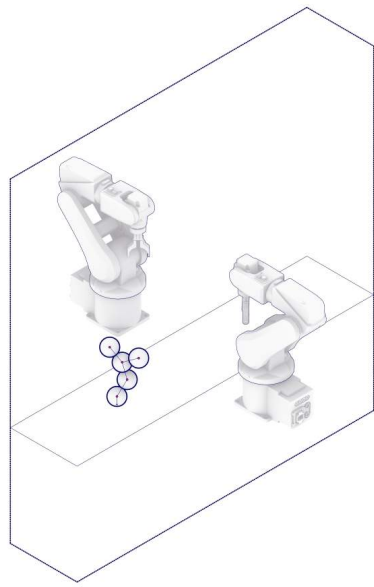
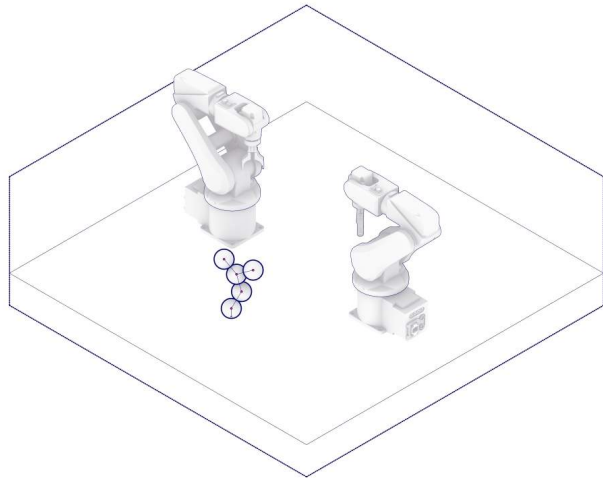


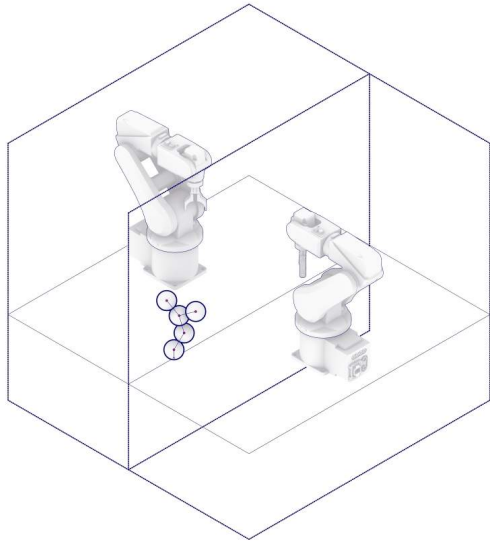
**Figure 3.12:** Hypothetical graduated constraint of domain space towards goal.



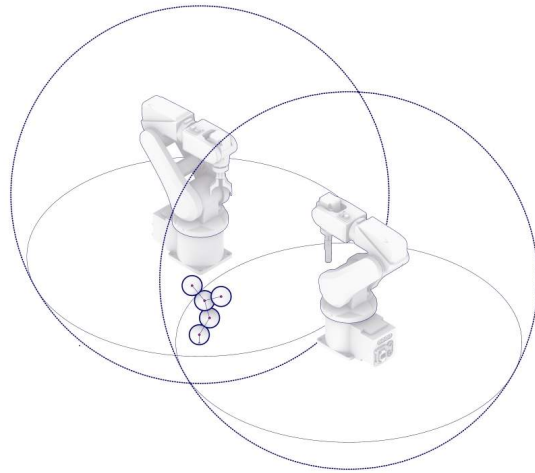
(a) 'tall' domain



(b) 'wide' domain



(c) simple split domain



(d) work-area based split domain

**Figure 3.13:** Examples of different domain space configurations for point generation.

## 3.6 Conclusion

This chapter presents the implementation of a CRF process using two 6-axis robotic arms, which was applied in a novel sequential design and construction framework to build a complex spatial structure. This research successfully extended the function of robots in architectural fab-

rication beyond their traditional role as passive facilitators of an end design. This was achieved by using kinematic constraints as actual inputs to steer the design; the structure was unplanned at the outset of the process and was instead designed sequentially as it was being built. Therefore, the robots became creative agents by virtue of suggesting the position of new spheres to add to the existing structure. Asking the user to offer input on this robotic input allowed an interesting dialogue to flourish between algorithmic and human creativity. The result of this collaboration was an unplanned structure – a complex 3D aggregation of solid spheres – sequentially designed and built on the basis of physical constraints associated with the fabrication domain.

In the current project, user and robotic input is limited to a binary yes/no response to a suggested sphere location. Strategies for giving users more input in directing the end form of the aggregation remain to be explored, such as: dynamic domain definitions, setting a goal point, and sub-domains with varying probabilistic weights for point generation. A more complex decision-making process for accepting or rejecting possible new spheres, based on the history of prior decisions, might also represent a direction for further work.

From the perspective of collaborative creation, there are several improvements to the process of generating structures based on external feedback that can be done in future work performed on a larger scale. The generative workflow implemented here relies entirely on simulated randomness as a surrogate for natural variability that would exist in a real-world open design context. A main finding from this preliminary work is that a local rule-based design process can use randomness as a catalyst to create global structure. The next step would be to apply this type of approach working with found materials (i.e. stones or recycled components) where such a flexible design method would be necessary to account for all the variability.

Further improvements to the process would involve integrating sensor feedback with robotic fabrication, which would allow for actual realtime adjustment, rather than a pseudo-realtime scheme used here. This would increase the possibilities for digital and human collaboration, and make better use of robotic manipulators as a design-fabrication tool. Although there exist many types of sensors for measuring a wide range of physical conditions, the prevalent modes for collecting data on physical assembly are visual and force sensing. One application would be to introduce a computer vision system, allowing the spatial positioning of the structure to guide the robotic placement of new components. This would allow unpredictable changes or deformations

to be taken into account directly during the aggregation process. Another option would be to use a force sensor mounted on the robot gripper to inform the placement of new components in locations that would minimize the total unbalanced force.

In summary, a robot is considered to have creative potential not because it can perform a calculation, or suggest an action that cannot be predicted or replicated by a human, but because the act of suggestion is itself the essence of a creative process. The interactive “just-in-time design” process developed in this case study is evidence that robots have the potential to be used both earlier in the design process, and in more creative roles. The aim is that the research presented in this chapter serves as an overall catalyst for future research on the topic of collaborative creation in architecture.

## References

- [1] S. T. Allen, Field Conditions Revisited, Stan Allen Architect, Long Island City, NY, 2010.
- [2] S. T. Allen, Field Conditions, in: M. Carpo (Ed.), *The Digital Turn in Architecture 1992–2012*, John Wiley & Sons, Inc., Hoboken, NJ, USA, 2013, pp. 62–79. doi:10.1002/9781118795811.ch5.
- [3] S. Wolfram, *A New Kind of Science*, 1st Edition, Wolfram Media, 2002.
- [4] C. G. Langton, Life at the Edge of Chaos, in: *Artificial Life II: Proceedings of the Workshop on Artificial Life*, Santa Fe Institute studies in the sciences of complexity, Addison-Wesley, Santa Fe, New Mexico, 1992, pp. 41–93.
- [5] T. Bonwetsch, D. Kobel, F. Gramazio, M. Kohler, The informed wall: Applying additive digital fabrication techniques on architecture, in: *Proceedings of the 25th Annual Conference of the Association for Computer-Aided Design in Architecture*, 2006, pp. 489–495, (ISBN: 978-0-9789463-0-2).
- [6] T. Bonwetsch, F. Gramazio, M. Kohler, Digitally fabricating non-standardised brick walls, in: *ManuBuild*, 2007, pp. 191–196, (ISBN: 978-0-86017-710-4).
- [7] S. Parascho, A. Gandia, A. Mirjan, F. Gramazio, M. Kohler, Cooperative fabrication of spatial metal structures, in: *Fabricate 2017: Rethinking Design and Construction*, UCL Press, London, 2017, pp. 24–29. doi:10.3929/ethz-b-000219566.
- [8] S. Parascho, T. Kohlhammer, S. Coros, F. Gramazio, M. Kohler, Computational design of robotically assembled spatial structures: A sequence based method for the generation and evaluation of structures fabricated with cooperating robots, in: *Advances in Architectural Geometry 2018*, Klein Publishing GmbH, Gothenburg, Sweden, 2018, pp. 112 – 139.  
URL <https://research.chalmers.se/en/publication/504188>
- [9] S. Parascho, Cooperative robotic assembly: Computational design and robotic fabrication of spatial metal structures, PhD Thesis, ETH, Zurich (2019).  
URL <https://doi.org/10.3929/ethz-b-000364322>

- [10] A. Thoma, A. Adel, M. Helmreich, T. Wehrle, F. Gramazio, M. Kohler, Robotic fabrication of bespoke timber frame modules, in: *Robotic Fabrication in Architecture, Art and Design 2018*, Springer International Publishing, Zurich, 2018, pp. 447–458. doi:10.1007/978-3-319-92294-2\_34.
- [11] A. Gandia, S. Parascho, R. Rust, G. Casas, F. Gramazio, M. Kohler, Towards Automatic Path Planning for Robotically Assembled Spatial Structures, in: *Robotic Fabrication in Architecture, Art and Design 2018*, Springer International Publishing, Zurich, 2018, pp. 59–73. doi:10.1007/978-3-319-92294-2\_5.
- [12] K. Dierichs, A. Menges, Towards an aggregate architecture: designed granular systems as programmable matter in architecture, *Granular Matter* 18 (2) (2016) 25, number: 2. doi:10.1007/s10035-016-0631-3.
- [13] K. Dierichs, O. Kyjánek, M. Loučka, A. Menges, Construction robotics for designed granular materials: in situ construction with designed granular materials at full architectural scale using a cable-driven parallel robot, *Construction Robotics* 3 (1-4) (2019) 41–52, number: 1-4. doi:10.1007/s41693-019-00024-6.
- [14] N. Davis, C.-P. Hsiao, K. Yashraj Singh, L. Li, B. Magerko, Empirically Studying Participatory Sense-Making in Abstract Drawing with a Co-Creative Cognitive Agent, in: *Proceedings of the 21st International Conference on Intelligent User Interfaces - IUI '16*, ACM Press, Sonoma, California, USA, 2016, pp. 196–207. doi:10.1145/2856767.2856795.
- [15] A. Bidgoli, P. Veloso, Deepcloud: The application of a data-driven, generative model in design, in: *Proceedings of the 38th Annual Conference of the Association for Computer Aided Design in Architecture*, Mexico City, 2018, p. 10.
- [16] A. Barqué-Duran, M. Klingemann, M. Marzenit, My Artificial Muse (2018).  
URL <https://albertbarque.com/myartificialmuse/>
- [17] M. Akten, Learning to See (2017).  
URL <http://www.memo.tv/portfolio/learning-to-see-hello-world/>

- [18] A. Bidgoli, E. Kang, D. C. Llach, Machinic Surrogates: Human-Machine Relationships in Computational Creativity, in: 25th International Symposium on Electronic Arts, Gwangju, South Korea, 2019, p. 7.
- [19] A. Liapis, G. N. Yannakakis, C. Alexopoulos, P. Lopes, Can Computers Foster Human Users' Creativity? Theory and Praxis of Mixed-Initiative Co-Creativity, *Digital Culture & Education* 8 (2) (2016) 17, number: 2.
- [20] A. Bidgoli, Towards an Integrated Design-Making Approach in Architectural Robotics, Master of Architecture, Pennsylvania State University, Centre County, Pennsylvania (2016).
- [21] S. M. LaValle, J. J. Kuffner, Randomized Kinodynamic Planning, *The International Journal of Robotics Research* 20 (5) (2001) 378–400, number: 5.
- [22] S. Karaman, E. Frazzoli, Sampling-Based Algorithms for Optimal Motion Planning, *The International Journal of Robotics Research* 30 (7) (2011) 846–894, number: 7. doi:10.1177/0278364911406761.
- [23] T. V. Mele, et al., COMPAS: A framework for computational research in architecture and structures. (2017).  
URL <https://doi.org/10.5281/zenodo.2594510>
- [24] R. Rust, G. Casas, S. Parascho, D. Jenny, K. Dörfler, M. Helmreich, A. Gandia, Z. Ma, I. Ariza, M. Pacher, B. Lytle, Y. Huang, C. Kasirer, E. Bruun, COMPAS FAB: Robotic fabrication package for the COMPAS Framework (2018).  
URL <https://doi.org/10.5281/zenodo.3469478>

# 4

## Three Cooperative Robotic Fabrication Methods for the Scaffold-Free Construction of a Masonry Arch

This chapter is based on the following publication(s):

**Bruun, E. P. G.**, Pastrana, R., Paris, V., Beghini, A., Pizzigoni, A., Parascho, S., & Adriaenssens, S. (2021). Three cooperative robotic fabrication methods for the scaffold-free construction of a masonry arch. *Automation in Construction*, 129, 103803.

<https://doi.org/10.1016/j.autcon.2021.103803>

Contributor roles in publication:

- Bruun: Conceptualization, Methodology, Software, Validation, Investigation, Writing (Original Draft), Writing (Review and Editing), Visualization
- Pastrana & Paris: Conceptualization, Validation, Writing (Original Draft), Visualization
- Beghini & Pizzigoni: Writing (Review and Editing)
- Parascho: Conceptualization, Resources, Writing (Review and Editing), Supervision, Project Administration
- Adriaenssens: Conceptualization, Writing (Review and Editing), Supervision, Funding



**Figure 4.1:** A glass-brick masonry vault assembled with two cooperating robots.

## Abstract

Geometrically complex masonry structures are traditionally built with scaffolding or falsework to provide stability during construction. The process of building such structures can be improved through the use of multiple robots working together in a cooperative assembly framework. Here a robot is envisioned as both a placement and external support agent during fabrication – the unfinished structure is supported in such a way that scaffolding is not required. The research in this chapter validates the efficacy of three cooperative fabrication approaches using two or three robots, for the scaffold-free construction of a stable masonry arch from which a medium-span vault is built (as shown in [fig. 4.1](#)). A simplified numerical method to represent a masonry structure is first presented and validated to analyse systems composed of discrete volumetric elements. This method is then used to evaluate the effect of the three cooperative robotic fabrication strategies on the stability performance of an arch. The *sequential method* and *cantilever method*, which utilize two robotic arms, are shown to be viable methods, but have challenges related to scalability and robustness. By adding a third robotic agent, it becomes possible to determine a structurally optimal fabrication sequence through a multi-objective optimization process. The *optimized three robot method* is shown to improve the structural behavior over all fabrication steps.

## 4.1 Introduction

A self-supporting construction process is one where no external support (e.g., temporary scaffolding or formwork) is required for the structure to remain stable as it is being built. The terms self-supporting [1] or self-balancing [2] are used interchangeably in the literature – self-supporting is used herein to describe this structural behavior. Such methods have been used throughout history to build large-scale complex masonry structures, relying on both the brick tessellation pattern and a careful design of the overall form to guarantee stability at all phases [3–9]. Although the contemporary building industry has generally moved away from many of these traditional methods, recently there has been a resurgence of interest on the investigation of self-supporting construction methods [1, 2, 10–14]. The emergence of automation, pre-fabrication, computational design, and robotic construction has created an opportunity to re-imagine how self-supporting construction techniques can find new relevance today [15].

In striving to develop self-supporting construction methods for masonry construction, a robot becomes more than just a fabrication tool, but is central to shaping what type of structure is feasible to build – informing the fabrication process through a Robot Oriented Design (ROD) framework [16]. Due to their task-versatility [17] and spatial precision [18], standardized industrial robotic arms have seen continuing widespread growth in industry adoption over the last decade [19]. Their application is improved by virtue of being able to perform a wide range of functions when paired with customized end-effectors designed for versatility [20]. In a cooperative robotic fabrication (CRF) context (i.e., multiple robots working together), robots with a gripping functionality can take turns performing either the function of picking up and aggregating structural components, or holding and providing temporary support over indefinite periods of time to a partially completed structure [21–23]. Therefore, when properly sequenced, a cooperative fabrication method has the potential to achieve complex structural goals – such as building a discrete element structure without temporary scaffolding while maintaining appropriate structural behaviour.

Developing such fabrication-informed construction sequences presents a departure from a traditional structural engineering workflow, which places emphasis on the design of the finished structure [24]. While this final state is conceivably optimized for a certain structural behaviour

or load combination, the construction sequencing and intermediate form required to reach this finished state is seldom optimized. But designing and optimizing a fabrication strategy around the goal of self-support is computationally intensive as all intermediate steps in the construction process need to be evaluated for structural performance – for the construction of a masonry system this can mean potentially evaluating the placement of 100's of bricks. Thus the goal of this chapter is twofold: (1) to develop, validate, and apply a computationally efficient framework for a high-level structural analysis of discrete element assemblies, (2) to apply the framework to validate the viability of three different cooperative robotic approaches used for to the scaffold-free construction of the central arch, which is part of a complex curved masonry vault.

#### 4.1.1 Summary of Contents

The chapter starts in [Section 4.2](#) with a brief review of literature on the topic of automation in masonry construction, cooperative robotic fabrication for discrete element structures, and modeling approaches for such structures. [Section 4.3](#) provides a description of the masonry vault prototype referred to in this chapter, and the development and calibration of a simplified modeling approach used to represent it. In [Sections 4.4](#) and [4.5](#), three cooperative robotic methods are analyzed in the context of the scaffold-free construction: *sequential method*, *cantilever method*, and the *optimized three robot method*. The chapter concludes in [Section 4.6](#) with a discussion of the results from applying these methods and a summary of the main contributions of this research.

## 4.2 Review of Robotic Fabrication and Masonry Structures

In the context of the Architecture, Engineering and Construction (AEC) field, robotic manufacturing was first applied at a significant scale to the prefabrication of modular homes in Japan in the 1970s [[25](#), [26](#)] and proliferated in numerous specialized applications in that country over the next decade [[27–30](#)]. The industry has experienced increasing adoption through technological improvements to automation and as a robot's ability to work in unstructured site environments has improved [[31](#), [32](#)]. Continuing future growth in adoption is motivated by numerous advantages to the construction industry: substantially improving productivity for complex structures [[33](#)], improving worker safety [[34](#)], and reducing material and labour costs [[35](#), [36](#)].

#### 4.2.1 On-site Automated Bricklaying in Industry

While construction robotics has seen a growth in application for off-site prefabrication [37], adoption has lagged for certain complex structural forms or material systems that are typically assembled on-site (e.g., stone/brick masonry [38–41] or cast-in-place concrete shells [42, 43]). Although Single Task Construction Robots (STCRs) [44] can be developed for specialized on-site applications, these are generally less common and harder to implement as they are motivated by project-specific economic factors [31].

Discrete element assemblies, such as masonry structures, are favourable candidates for robotic automation as they are physically taxing to construct manually [45, 46]. The construction of masonry structures is also highly repetitive and individual units are relatively lightweight, which makes such structures fit for development around an automated framework [47]. While robotic prefabrication of masonry in the factory setting is possible, the output is geometrically limited to highly standardized vertical block walls due to fixed space and equipment design constraints [37]. Thus, automation in masonry construction is generally better suited to in-situ fabrication approaches as a means to better address site variability or construct more complex geometry. The technical exploration of automated in-situ masonry construction dates back to the beginning of the 20th century, with a patent for an automated brick-laying machine submitted in 1904 [48]. A functioning automated linear bricklaying machine prototype was documented on-site in the 1960s [49]. But it was first in the late 1980s that developments in the automation of in-situ masonry construction started to flourish [50–52], from balancer and handling assistance machines [37], to Selective Compliance Articulated Robot Arm (SCARA) systems such as the Solid Material Assembly System (SMAS) [53, 54], the Robotic Construction System for Computer Aided Construction (ROCCO) [16, 55], and the Blockbot [56, 57]. Recent years have seen further commercial developments in the form of the Semi-Automated Mason (SAM100) [58] and Hadrian X robot [59], which can be thought of as technical successors to the previously developed articulated robotic arm systems [60, 61]. SAM100 consists of a robotic arm mounted on a track, while Hadrian X uses a custom gripper mounted on a mobile truck crane for improved reachability [47, 62].

## 4.2.2 Digital Fabrication and Geometric Complexity

The automated brick-laying systems summarized in [Section 4.2.1](#) were focused on industry applications for the construction of straight walls and generally improving construction productivity. But only in the last two decades has the field of digital fabrication (DFab) been seriously applied in an academic context to construction at the large-scale with the specific intention of expanding the geometric design space through the use of robots [63, 64]. The first such project saw stationary industrial robots used to stack bricks to build prefabricated load-bearing but non-standardised undulating walls [65–67]. Later the DFAB house [68] became the showcase for how different non-standardized components in a building can be shaped through digital design and robotic fabrication process [69–71]. In the context of masonry construction, the development of specialized digital design software [72, 73] and augmented reality frameworks [74–76] have allowed for more geometrically complex geometries to be materialized on site. Industrial robotic arms have also been applied in complex setups, for example on gantry cranes [77] and as mobile platforms [78, 79].

## 4.2.3 Cooperative Robotics and Discrete Element Structures

Despite the technical advances associated with the DFab movement, robotic fabrication is still rarely utilized beyond the construction of vertical layer-based structures [80, 81]. Structural stability and the detrimental effect of tensile forces in cantilevered or spanning forms are reasons why masonry robotic brick fabrication projects have been limited to vertical assemblies. Similar challenges are faced in additive concrete manufacturing, which draws inspiration from self-supporting masonry approaches as a means to develop more robust methods for 3D printing overhanging geometry [82–84].

Recent work has suggested that cooperative fabrication can be a means to address issues surrounding stability during construction and to therefore realize complex structural forms that would not be possible otherwise. An example of this is the assembly of metal rods into complex (i.e. non-uniform) space frame structures [23, 85] where complex joints between rods had to be carefully sequenced using two robots. Or in the fabrication of custom non-planar timber modules where cooperating robots were used to minimize the need for scaffolding [86]. Another

example is the construction of a small-scale branching structure, where two robots would take turns supporting the structure as it was being assembled [87]. While operating at different scales, these projects all explore the potential of creating a construction sequence where two robots work together cooperatively to assemble a geometrically complex discrete element structure.

#### 4.2.4 Analysis and Modeling of Masonry Structures

A number of modeling strategies exist to analyze the structural behavior of three-dimensional masonry structures. As recently surveyed in [88–90], finite element (FE), discrete element (DE), and geometric approaches are all feasible. In a FE setting, a continuum mesh of shell elements are calibrated to approximate the macro-behaviour of a masonry structure [88, 91]. The interaction between masonry elements and joint interfaces is homogenized. Meanwhile, DE strategies are able to accurately capture in- and out-of-plane behavior [92, 93], for varied types of geometry [94, 95], at both global- and local-scales [96–99] by representing a masonry structure as a system of three-dimensional rigid or deformable bodies. As shown in the literature [100–103], DE approaches are particularly suitable to highlight the detailed structural phenomena that occur between masonry elements and their joint interfaces, such as detachment, collision and sliding. While commercial software packages exist to facilitate the structural analysis of a masonry structure using a FE (e.g. Abaqus [104]) or a DE focus (e.g. 3DEC [105]), creating and running these models can be time-consuming and computationally expensive, which is unsuitable for explorative optimization processes. Inspired by Heyman’s safe theorem [6, 106], geometric strategies instead assess the static equilibrium of a masonry structure by modeling it as a network of compression forces. In the literature, geometrical approaches tailored to two-dimensional [107–109] and three-dimensional masonry structures [10, 110, 111] have been proposed. Unlike their FE or DE counterparts, geometric strategies do not solicit material information about a masonry structure and are agnostic to the arrangement of contact interfaces between masonry elements and joint types. While this can simplify and speed up the modeling process, geometric approaches overlook potentially relevant structural actions occurring at the joint interfaces which may be critical to assessing the inter-construction states in a masonry structure.

### **4.2.5 Next Steps in Robotic Fabrication**

Research on robotic construction in industry has focused on technical advances in the automation of traditional building practices, which are wasteful from the perspective of material usage. Meanwhile, recent academic research has focused on expanding design possibilities, using robots to achieve local geometric differentiation without a specific emphasis on material efficiency. There are opportunities in utilizing robotic construction to combine both of these approaches – keeping material efficiency and geometric complexity central to the process with the overall goal of making construction less labor intensive and more productive. Recent work [20–22] has demonstrated the feasibility of moving away from the vertical construction paradigm common to robotic masonry fabrication, by sequencing two robotic arms to build a complex vaulted structure without temporary scaffolding. The research presented in this chapter builds on this work by providing a numerical basis for how to develop and evaluate such robotic fabrication sequences. It also extends the fabrication framework developed in [20–22] by introducing the concept of multi-objective optimization to determine how robotic support positions can be determined while satisfying structural performance criteria.

## **4.3 Methodology**

### **4.3.1 Masonry Vault Prototype**

The research presented in this chapter explores cooperative robotic building sequences in the context of a recently constructed masonry vault prototype [22]. Figures 4.2 and 4.3 show the 338-brick building-scale vault, which is tiled using a herringbone tessellation pattern. This structure is assembled using two ABB 6400 industrial robotic arms (referred to as rob1 and rob2 throughout the chapter), with a maximum reach of 2.55 m and payload of 40 kg. These robots have a position repetition accuracy of 0.4 mm, with 98% of movements within 1 mm [112]. Previous work related to the development of the robotic fabrication method, the prototyping process, and the construction of the final vault are described in a series of recent publications [20–22].

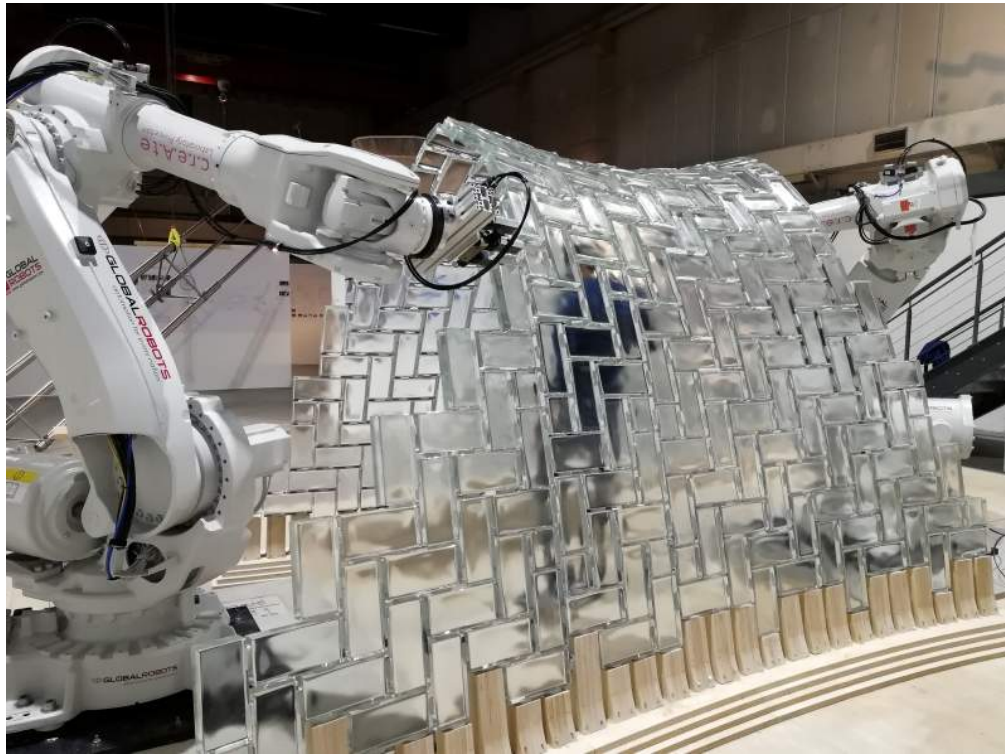


**Figure 4.2:** The vault prototype assembled with two industrial robotic arms.

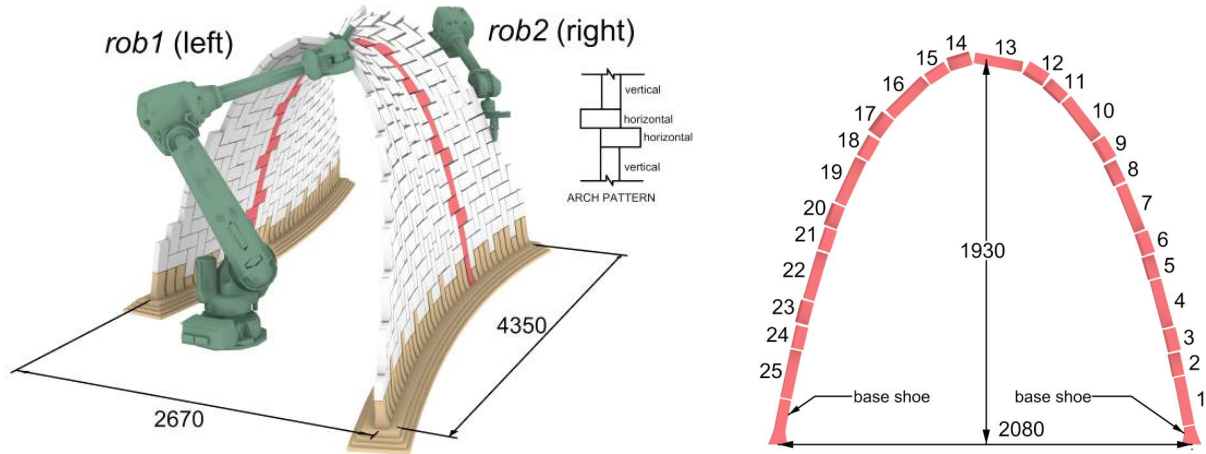


**Figure 4.3:** Geometry of the vault prototype and central arch (dimensions in mm).

The construction of this prototype can be split up into two main phases: (1) the central arch, and (2) the full vault. The central arch consists of 25 rectangular bricks, arranged with a span/height of 2.08/1.93 m respectively as shown in [Figure 4.3](#). Each brick has standardized dimensions of  $246 \times 116 \times 53 \text{ mm}$ , and is made from cast glass with a density of  $2420 \text{ kg/m}^3$  (i.e., self-weight of  $3.66 \text{ kg}$  per brick). This structure represents a significant step forward in the

field of robotic masonry construction, breaking with the vertical layer-based construction that is demonstrated in preceding robotic construction projects discussed in [Sections 4.2.1](#) and [4.2.2](#). The first construction phase is critical when developing a scaffold-free fabrication method since the arch is not self-stable in its unfinished state. Thus the robotic fabrication methods must break from the traditional two-sided construction approach where external scaffolding is required as shown in [Figure 4.4](#). Instead, the arch is built up from only one end, while utilizing the robots as mobile temporary supports to the unfinished arch during the full construction sequence as outlined in [21].

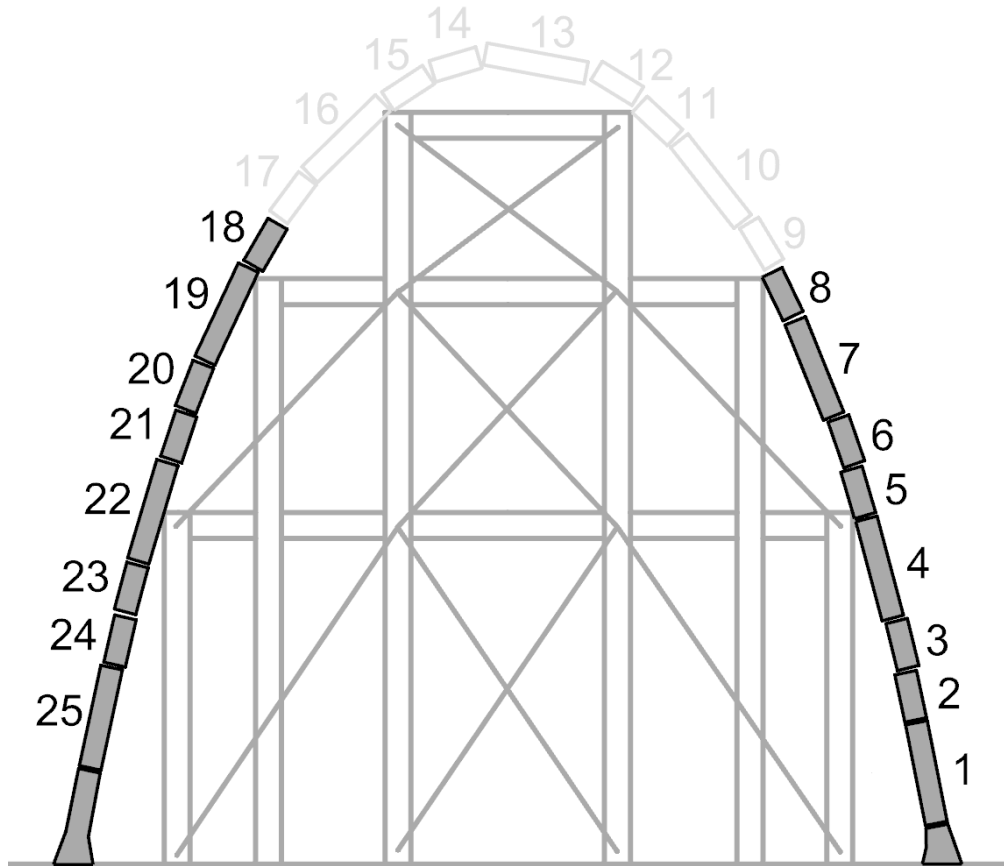


**Figure 4.4:** Scaffolding in traditional two-sided masonry arch construction.

Once the central arch is completed (see [Figure 4.3](#)), the second phase consists of building up the rest of the vault around it over a skewed plan area of 2670x4350mm. A step-wise sequence is used, where the central arch acts as a support from which to extend the structure out in overlapping diagonal layers. An interlocking herringbone tessellation pattern is used throughout the

full vault since this pattern provides local support to the surrounding bricks during construction [2, 8]. Thus, the central arch is built with a horizontal-horizontal-vertical 3-brick pattern, which allows it to interlock with the surrounding herringbone-patterned vault. Details on the tessellation and layered construction sequence are outlined in [21].

### 4.3.2 Computational Modeling Approach

The purpose of the computational modeling is to obtain values of displacements, forces and stability feedback throughout all the stages in the construction process for the masonry arch. The three robotic fabrication sequences proposed in Sections 4.4 and 4.5 are evaluated on the basis of their structural performance. The complexity or precision of a Finite Element (FE) mesh-based or Discrete Element (DE) model is deemed unnecessary since only the linear elastic behaviour of the masonry vault is required to assess performance in the context of the construction sequence. Therefore, only the static force distribution and instantaneous displacements are used as the basis for evaluating performance (i.e., nonlinear or long-term responses are not being evaluated). Furthermore, the large number of independent models that need to be evaluated to fully characterise the solution space of a building sequence optimization problem of this scale also preclude the use of FE mesh-based or DE analysis methods as they are computationally taxing. For example, the placement of each new brick constitutes a new structural model, which requires updating geometry, loading, and support conditions. Finally, a traditional modeling environment (i.e., non-parametric) is not suited to the optimization process used to calculate support points described in Section 4.5.

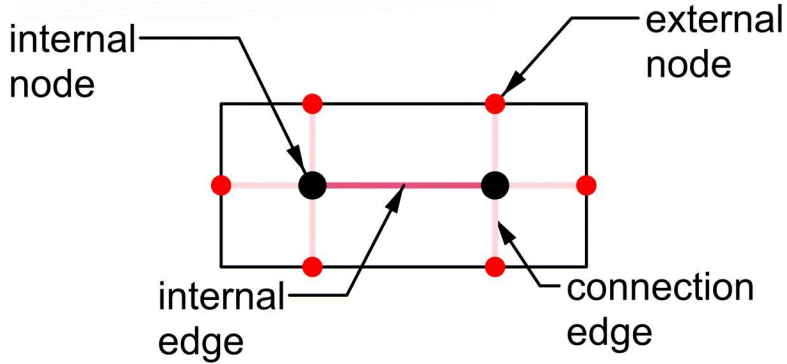
Based on these analysis requirements, a method based on a highly abstracted structural model using only linear elements is proposed here. First, the masonry structure is modelled as a geometric system, represented as a network graph (i.e., a collection of nodes connected by edges) as a way to simplify the discrete element assembly while still capturing its geometry and topology [113, 114]. Next, this geometric representation of the structure is turned into a simplified FE model, using linear elements and joints to represent the edges and nodes of the network. Specifically, edges become the structural elements (i.e., bricks) and nodes become either the centroids of the bricks or flexible connection joints between bricks (i.e., mortar bond) as shown in Figure 4.5.

Generating such a model from a given set of discrete elements can be scripted in a parametric environment [115], allowing for the rapid generation of numerous models representing the different construction steps, and simultaneous linear elastic analysis using existing FE software [116]. Linear and rotational stiffness values can be assigned to the elements and joints respectively. Rigid elements and flexible joints are used to represent the deformations that occur in the masonry assembly analysed in the linear range.

With such a model, based on a network representation, one compromises in accuracy but gains far more in “explorativity” by virtue of its simplicity and application in a parametric environment. [Section 4.3.2](#) describes this approach in more detail as it is specifically applied to the analysis of the masonry vault prototype, highlighting the calibration performed to determine reasonable joint spring stiffness values.

## The Double-Cross Model

To model masonry assemblies the geometry of each masonry unit is simplified to a “double-cross” network; the name is derived from the schematic appearance of this representation shown in [Figure 4.5](#). This configuration is chosen since it represents the physical geometry and connection topology in a typical masonry structure. Each brick is assigned a total of six external nodes (two per long side and one on either short side) and two inner nodes (at the quarter-points, or centroids of each half-brick). In a typical assembly, individual bricks can be joined together by connecting their neighboring centroids with a connection edge, and splitting this element to create an external node at the location where the gap between the bricks occurs (i.e., the external nodes of two connected bricks coincide). Both internal (between two internal nodes) and external (between an internal and external node) edges are modeled as rigid elements. They connect to at least one rigid internal joint, which by formulation does not allow for any relative rotation in the edges connected to it. The result is capturing the overall rigidity of a masonry unit using only simple joint and linear elements. Meanwhile, the external nodes represent the connection points between rigid bricks, and are modeled as joints with linear and rotational spring stiffness that represent the flexibility of the connection mortar. [Figure 4.5](#) shows such a representation for a small subset of bricks arranged in a herringbone pattern taken from the vault prototype.



(a) components of a double-cross network model for a single brick

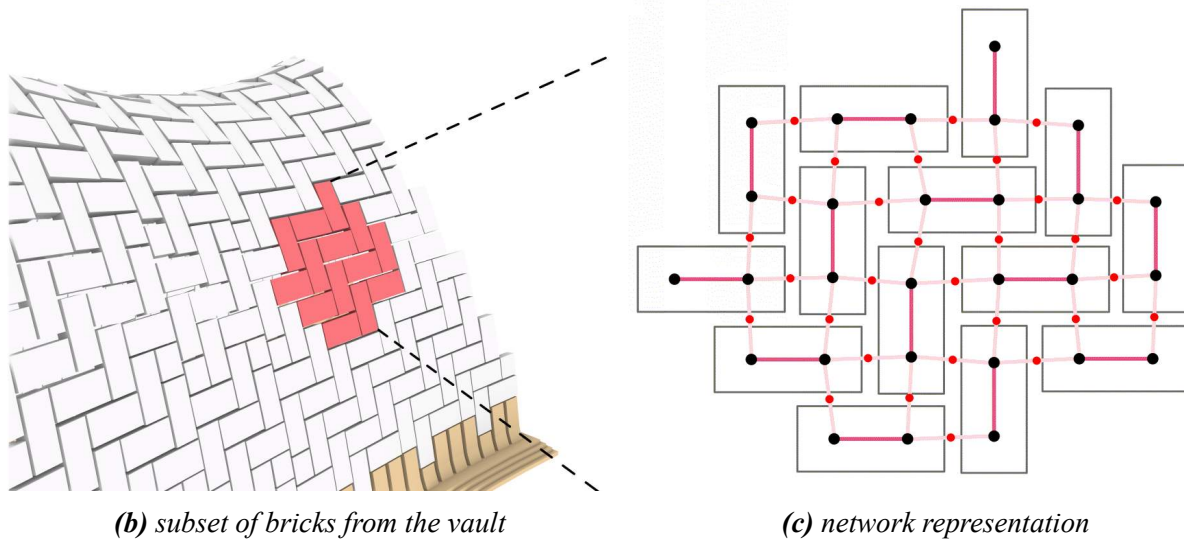


**Figure 4.5:** Representing a masonry structure with the double-cross model.

## Joint and Element Calibration

Despite being a simplification, the double-cross representation must still be able to capture displacements and force redistribution in a realistic manner. Structural stiffness is used as a proxy for this – if an analyzed structure exhibits accurate stiffness (i.e., load/deflection), then the assumption is that deflections and force redistribution are also accurate in the structure [117].

To improve the results from the double-cross model, the linear and rotational springs in the connection joints are calibrated on the basis of existing experimental results from full-scale masonry barrel vault load tests documented in the literature [118–124]. The reader is referred to [Table 4.1](#) for a list of references and values for all parameters defining the different structures:  $L$  = span length,  $r$  = vault radius,  $b$  = vault width (into the page),  $t$  = vault thickness,  $\#_{bricks}$  = number

**Table 4.1:** Summary of structural parameters for full-scale masonry arch tests with published load-deflection data

Reference	<i>L</i>	<i>r</i>	<i>b</i>	<i>t</i>	#bricks	<i>h</i>	$\gamma_f$	$\gamma_m$	<i>x</i>
	[m]	[m]	[m]	[mm]		[mm]	$\left[\frac{kg}{m^3}\right]$	$\left[\frac{kg}{m^3}\right]$	[m]
1 Royles and Hendry (1991) [118]	2.180	1.090	1.690	103	46 <sup>1</sup>	240	1430	2000 <sup>1</sup>	0.750
2 Melbourne and Walker (1988) [119]	1.600	0.800	1.000	100	31	150	1560	2100	0.550
3 Melbourne et al. (1997) [120]	3.220	0.860	2.880	215	48 <sup>1</sup>	170	2260	2400	0.860
4 Melbourne and Gilbert (1995) [121]	3.220	0.860	2.880	215	48 <sup>1</sup>	300	2260	2400	0.860
5 Melbourne and Gilbert (1995) [121]	5.450	1.470	3.010	445	81 <sup>1</sup>	350	2260	2400	1.470
6 Gilbert et al. (2007) [122]	3.220	0.860	1.010	215	48 <sup>1</sup>	305	1950	2360	0.860
7 Towler and Sawko (1982) [123]	4.220	1.110	1.100	215	70 <sup>2</sup>	250	2000 <sup>2</sup>	2000 <sup>2</sup>	2.110
8 Swift et al. (2013) [124]	3.220	0.860	1.010	215	48	300	2040	2000 <sup>2</sup>	0.860

<sup>1</sup> data not found in original paper, taken from summary by [91]

<sup>2</sup> data not found in original paper, estimated

of bricks in the vault,  $h$  = infill height above the crown,  $\gamma_f$  = infill density,  $\gamma_m$  = masonry density,  $x$  = loading distance. A generic experimental setup is schematically shown in Figure 4.6. These experiments take a monotonically increasing load ( $P$ ) and apply it across the width ( $b$ ) of the barrel vault, measuring the displacement under the load ( $\Delta$ ). For calibration purposes, only results in the literature where experimental load-deflection data is provided are used, and where spandrels are detached from the arch structure.

Linear elastic FE analysis models are created for each of the masonry vaults summarized in Table 4.1. These models are based on the same approach described in the Section 4.3.2: each brick in the arch is modeled as a rigid element connected to its neighbor at a flexible joint as shown in Figure 4.6. The full width (into the page) of the arch is represented by a single element since only in-plane behavior is examined in these tests. From this linear elastic analysis, the stiffness ( $k_m$ ) is obtained as a ratio of the applied load to the vertical displacement at the loaded location. This analytical stiffness is then compared to the experimental secant stiffness ( $k_e$ ) in the initial linear elastic region, which is based on the published load-displacement test data. Figure 4.7 shows an example of this process using the data from Test #1 [118]. The rotational and linear spring stiffness of the joints are then calibrated to ensure the best agreement between experimental and analytical stiffness for all the available tests.

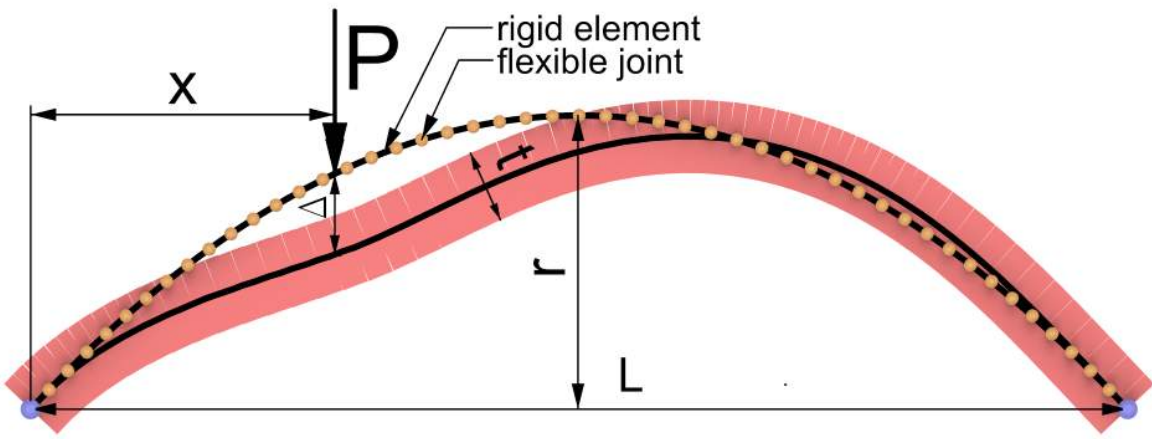


**Figure 4.6:** Deformed shape superimposed on the analytical representation of a generic masonry barrel vault load test.

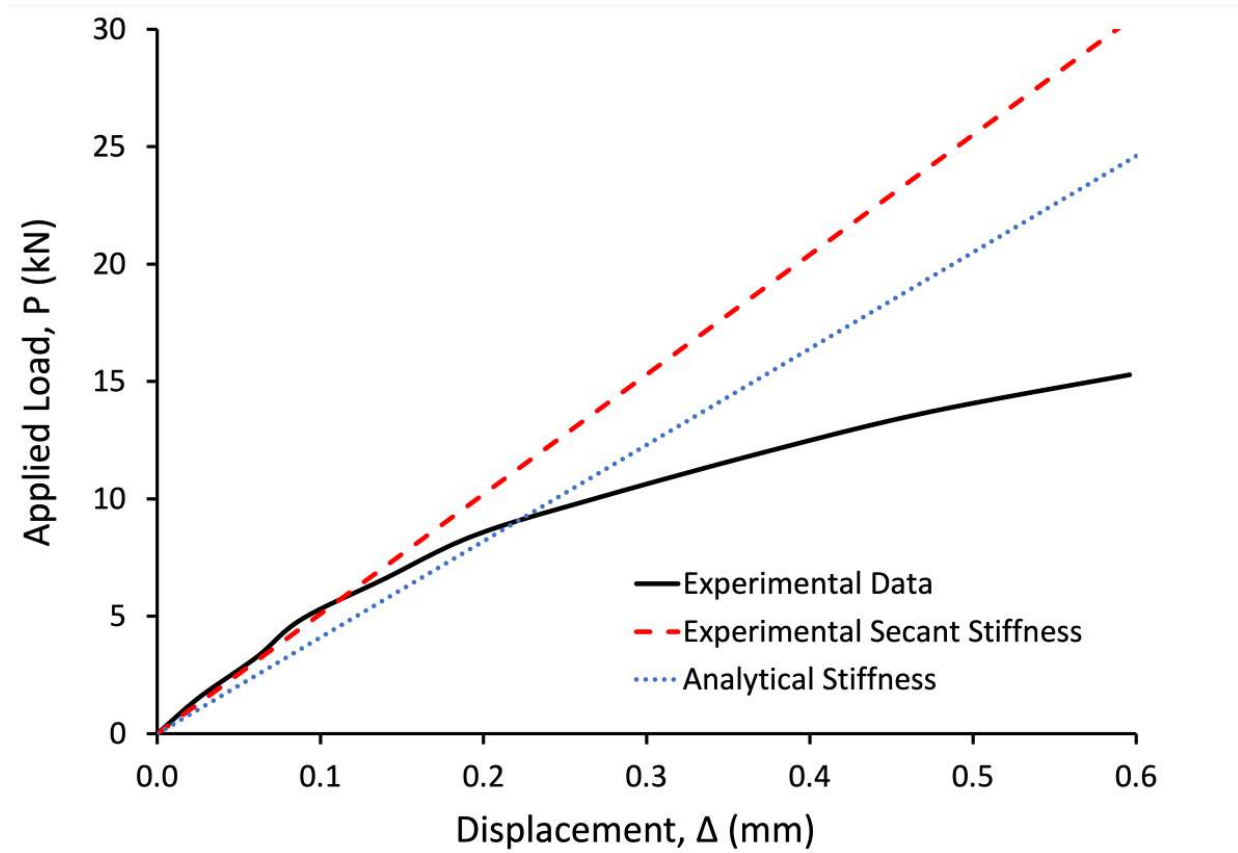


**Figure 4.7:** Tuning the analytical to the initial experimental secant stiffness.

The results of the calibration are summarized in [Table 4.2](#), which also shows the relative error ( $e_{rel}$ ) between the experimental ( $k_e$ ) and analytical ( $k_m$ ) stiffness when using calibrated linear

and rotational joint springs in the analytical model. When compared to the experimental data, a calibrated linear spring stiffness of  $100 \times 10^6 \text{ kN/m}^3$  and rotational spring stiffness of  $0.9 \times 10^6 \text{ kN/(rad} \cdot \text{m}^2)$  are determined to minimize the error across the full data set. The linear spring stiffness falls within the  $100 \times 10^6 - 100 \times 10^7 \text{ kN/m}^3$  range as per recommendations in the literature [97]. The rigid element and flexible joint approach used in the double-cross model is thus capable of capturing the in-plane load-deflection behaviour of a masonry structure in the elastic range.

**Table 4.2:** Initial experimental secant arch stiffness compared to calibrated element-spring model stiffness

Reference	$k_e$	$k_m$	$e_{rel}$
	$[\frac{\text{kN}}{\text{mm}}]$	$[\frac{\text{kN}}{\text{mm}}]$	[%]
1 Royles and Hendry (1991) [118]	51	41	-19.6
2 Melbourne and Walker (1988) [119]	138	143	3.6
3 Melbourne et al. (1997) [120]	378	434	14.8
4 Melbourne and Gilbert (1995) [121]	535	417	-22.1
5 Melbourne and Gilbert (1995) [121]	803	264	-67.1
6 Gilbert et al. (2007) [122]	132	140	6.1
7 Towler and Sawko (1982) [123]	70	71	1.4
8 Swift et al. (2013) [124]	120	141	17.5

### 3D Validation of Model

Further validation of the proposed model is performed to verify the ability of the double-cross model to capture out-of-plane displacements when using the joint stiffness results determined in Section 4.3.2. This validation is performed against static DE models implemented using the 3DEC software [105], representing snapshots of the prototype arch during various stages of construction. These models are numerical approximations of the real behavior, but by formulation are more realistic and accurate and computationally more expensive. Thus, the goal is to verify that the results of the DE models show good agreement with those of the simplified double-cross representation for situations that cause out-of-plane effects in the arch.

In the DE model, the partial arch is modelled as an assembly of rigid bodies, whose shape corresponds to the masonry bricks (i.e., rectangular prisms with 8 vertices). The joints between the bricks are modelled by interfaces ruled by a Mohr-Coulomb model [97], with the parameters

based on the characteristics of the epoxy mortar used (i.e., Oatey® Fix-It™ Stick [125]). The cohesion used is 2 MPa and the tensile stress cut-off is 3 MPa. Joint stiffness and shear stiffness are set to  $jK_n = 100 \times 10^6 \text{ kN/m}^3$  and  $jK_s = 10 \times 10^6 \text{ kN/m}^3$  with a friction angle of  $25^\circ$ , which is based on [97].

For the construction stages investigated, the robotic arm acting as a support to the structure is simulated with two fixed rigid bodies. These are labelled at (A) and (B) in Figure 4.8, which otherwise shows a visualization of the discrete element model with the brick interfaces highlighted. These two rigid bodies effectively support the active block in the arch at two small interfaces to simulate how a robot grips the brick. Unlike the typical brick-brick mortar joints, at the pinch location the normal and shear stiffness values are an order of magnitude greater to mimic the effect of a robotic gripper support, thus preventing any sliding deformation. Therefore, the arch is vertically supported while still able to rotate about the axis formed by the rigid support blocks. Global out-of-plane displacements of the arch are determined as a function of this support condition.

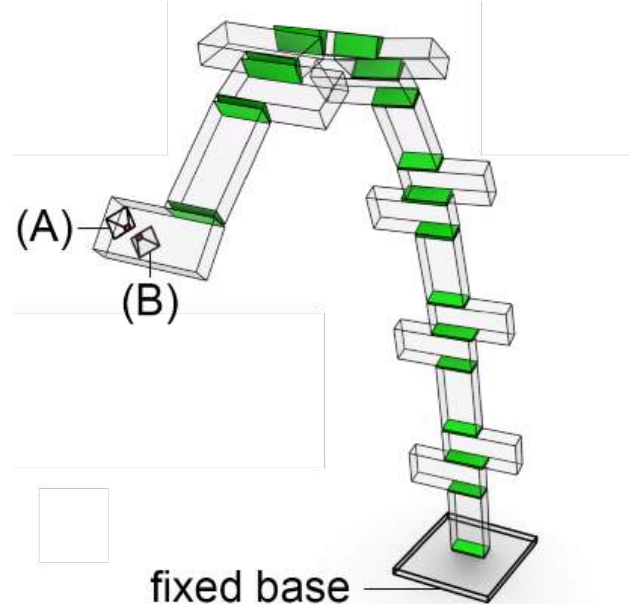


**Figure 4.8:** 3DEC model where robotic support is modelled as a two-block interface restraint (A and B).

The validation is performed across four separate models corresponding to steps in the arch construction sequence where the robot places and supports bricks 17, 18, 23 and 24. These construction steps are expected to produce out-of-plane twisting as seen in the *sequential method* dis-

cussed further in [Section 4.4](#). All DE analyses are performed with self-weight loading and supports at both the location where the robotic arm holds a brick and the fixed base. The DE computations are carried out over a sufficient time scale for the structure to reach equilibrium (i.e., until the unbalanced force is 0 kN), and in that state the displacements at the vertices of the discrete blocks are output. These rigid block vertex displacements are then converted to equivalent displacements at nodal locations coinciding with the inner nodes in the double-cross representation (see [Figure 4.9](#)). This conversion is performed based on weighted averages of the corner displacements as the blocks are rigid and therefore experience no relative deformation between vertices.

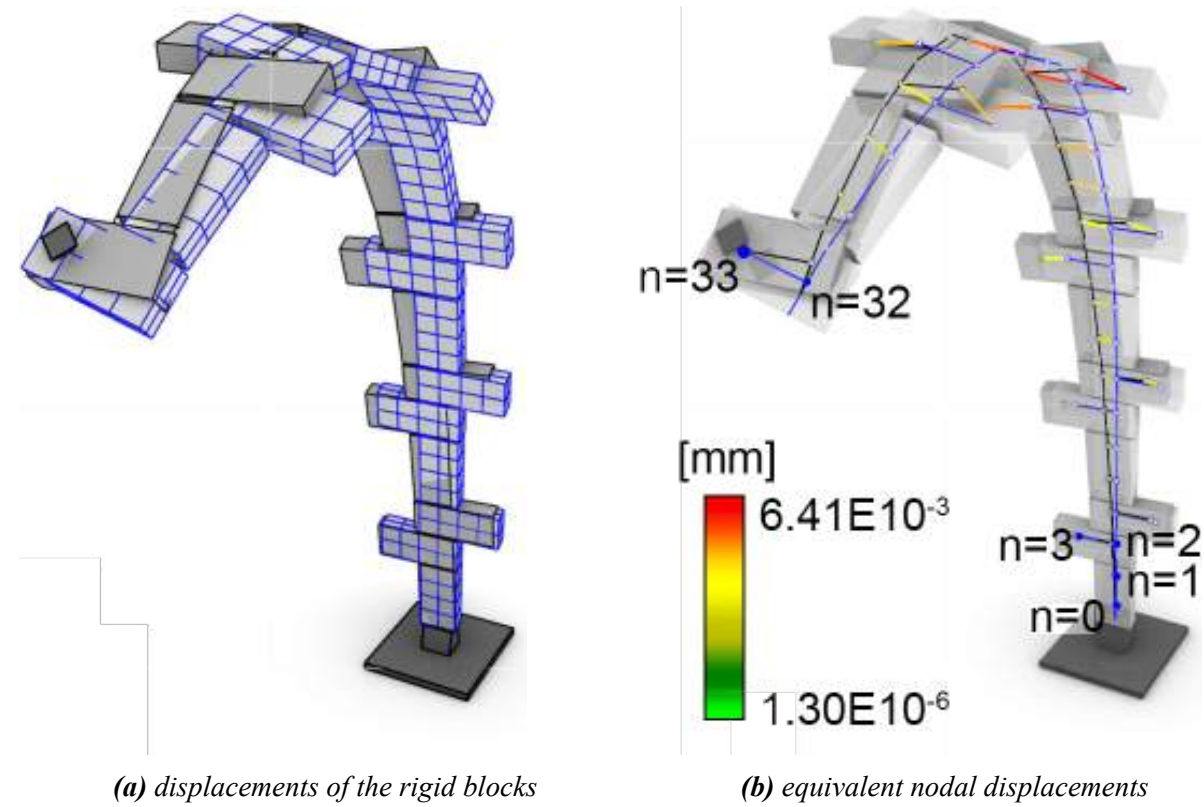


**Figure 4.9:** DE analysis of the partial arch.

The results of this comparison are shown in [Table 4.3](#), where the average relative error in the displacements between nodes across the discrete and finite element models is used as the comparison metric for each of the four partial arches modeled. This average error is based on results ranging from 33 to 47 data points for model 1 to 4 respectively. The magnitude of the errors is at a similar order of magnitude to those obtained in the in-plane calibration (see [Section 4.3.2](#)),

which means that the results for the out-of-plane behaviour are satisfactory using the simplified formulation. A comparison between the experimental calibration and DE validation tests show that when calibrated the tuned double-cross model is capable of representing both the in-plane and out-of-plane behaviour of a masonry structure within a 20% margin.

**Table 4.3:** Average relative error in displacements across models between the proposed simplified model and DE analysis results.

Model	Bricks	#nodes	%error
1	17	33	20.9
2	18	35	24.7
3	23	45	-14.9
4	24	47	-15.3

## 4.4 Central Arch Fabrication with Two Robots

The first phase of the vault's construction (i.e., the central arch) represents a challenge from the perspective of a scaffold-free construction method, since the structure is not self-stable before the central arch is complete. To unlock the construction potential of using two robots, this research builds on an existing cooperative robotic fabrication strategy first introduced in [21]. A

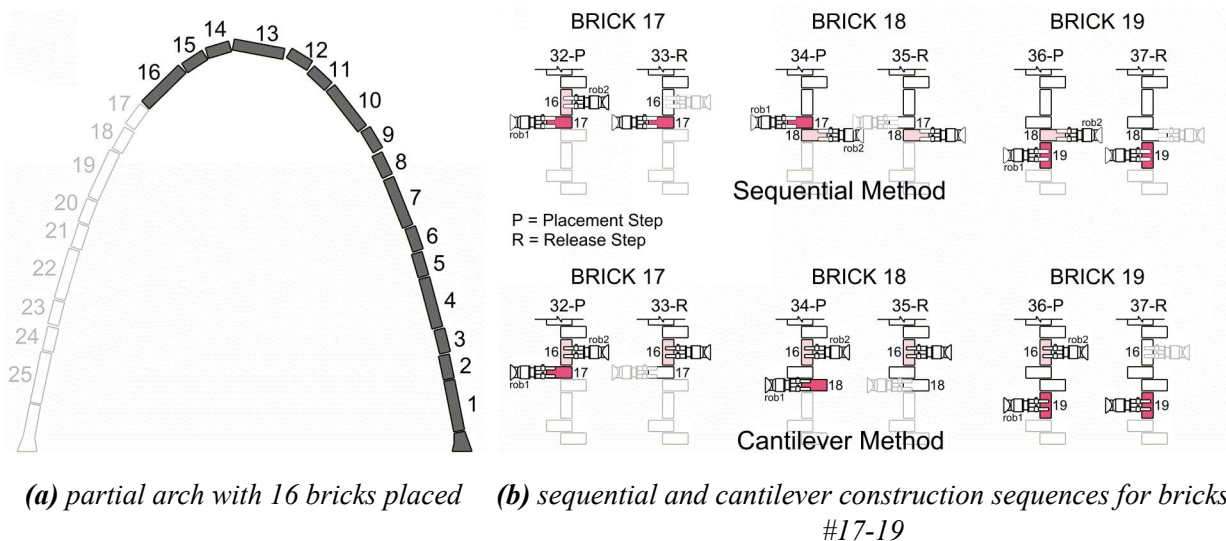


**Figure 4.10:** Unidirectional construction sequences where two robots alternate the support of the partial arch and the placement of new bricks.

unidirectional construction approach is implemented, where the arch is built up from one end to the other. Contrary to the traditional method, discussed in [Section 4.3.1](#), there is only one active build edge. This means that the robots can be sequenced in a cooperative manner by taking turns either placing or supporting the partial arch at this active edge. In this way, the full arch can be constructed without any external scaffolding by relying on robotic support.

Two different build strategies, referred to as the *sequential method* or *cantilever method* are defined in [21]. [Figure 4.10](#) schematically shows an example of these methods at work when adding three bricks to the partial arch starting from brick #17. In both sequences, each build step consists of one robot performing either of two actions: placement of a brick (P), or release of a brick (R) (i.e., adding a new brick takes two discrete steps). The strengths and weaknesses of each method are discussed in [Sections 4.4.1](#) and [4.4.2](#), with detailed structural results for each build step when constructing the full 25-brick central arch using each sequence in Appendix A.

#### 4.4.1 Sequential Method

The *sequential method* (shown in the top of [Figure 4.10b](#)), where the left and right robots alternate placing bricks, is the intuitive way to sequence two robots. This is a relatively simple sequence to implement robotically, but there are structural issues that arise from the support position location as function of the herringbone tessellation pattern. The bricks in the arch must be placed in a horizontal-horizontal-vertical pattern (as shown in [Figures 4.3](#) and [4.11a](#)) to allow the arch to later interlock with the rest of the vault. When using two robots (i.e., rob1 and rob2) on either side of the arch, there are stages in the construction when there is only one robot supporting the structure (i.e., a release (R) step) as the other robot releases the structure to retrieve the next brick. At these stages there is only one robot supporting the arch while gripping a horizontal brick. [Figure 4.11](#) illustrates this condition and the force couple,  $M = F \cdot e$ , that results from such a situation, causing critical out-of-plane twisting displacement that the arch is not capable of resisting. This moment scales with the magnitude of the force (F), which is equal to the thrust exerted by the partial arch on the robot as a function of the geometry and self-weight distribution in the structure. The lever arm (e) is equal to the deviation between the thrust line and support

point, which is  $135 \pm 15\text{mm}$ .

This off-center loading condition occurs at eight different steps in the full construction sequence (i.e., steps 9, 11, 21, 23, 33, 35, 45, and 47). [Table 4.4](#) summarizes the main structural results from these steps, showing the following: sequence step number; type of step (release or placement); total bricks in the arch; what brick (b) and node (n) each robot is gripping;  $F_{rob}$  = load supported by the robot;  $F_{sup}$  = load at the base support;  $M_{sup}$  = moment at the base support;  $\Delta_{max}$  = maximum nodal displacement.  $C_1 = M_{sup}/M_{sup,avg}$  is the moment multiple based on an average support moment of  $6.8 \text{ N} \cdot \text{m}$  over the full sequence, and  $C_2 = \Delta_{max}/\Delta_{max,avg}$  is the displacement multiple based on an average maximum nodal displacement of  $7.3 \times 10^{-3} \text{ mm}$  over the full sequence. The full data for all 49 steps required to build the 25-brick arch with the *sequential method* can be found in Appendix A, [Table A.1](#).

**Table 4.4:** Analysis results for the off-center support steps in the sequential method

Step	Type	Total Bricks	rob1		rob2		$F_{rob1}$	$F_{rob2}$	$F_{sup}$	$M_{sup}$	$C_1$	$\Delta_{max}$	$C_2$
			b	n	b	n							
9	release	5	5	8	—	—	75.0	—	106.1	6.8	1.0	1.3	0.2
11	release	6	—	—	6	11	—	85.2	132.2	8.3	1.2	2.2	0.3
21	release	11	11	20	—	—	86.6	—	311.7	21.5	3.2	12.8	1.8
23	release	12	—	—	12	23	—	89.7	347.9	22.0	3.2	16.9	2.3
33	release	17	17	33	—	—	170.8	—	470.0	21.3	3.1	70.8	9.7
35	release	18	—	—	18	35	—	203.8	468.9	29.6	4.4	97.5	13.4
45	release	23	23	44	—	—	369.3	—	477.1	56.4	8.3	264.4	36.2
47	release	24	—	—	24	47	—	405.5	474.7	66.0	9.7	306.5	42.0

Four of the off-center steps occur while building up to the crown (steps 9, 11, 21, and 23) and four while building down from the crown (steps 33, 35, 45, and 47). The four steps after the crown experience maximum nodal displacements at multiples of 9.7 to 42.1 times greater than the average maximum displacements for all other typical loading steps ( $7.3 \times 10^{-3} \text{ mm}$ ), and moment multiples of 4.1 to 9.7 times the average moment across all the steps ( $6.8 \text{ N} \cdot \text{m}$ ). An example of such a twisting step is 35-R where *rob2* is holding brick 18 at node 35, which is schematically shown in [Figure 4.11b](#). This step has a displacement and moment multiple of 13.4 and 4.4 respectively. In general, the large displacement multiples experienced during this fabrication process suggest that the sequential method, while easy to implement, is not robust and scalable. This

method is not suitable for structures with larger axial thrusts. Ideally maximum out-of-plane displacements and moments should be kept below the value for Step 35 (i.e.,  $\approx 100 \times 10^{-3} \text{ mm}$  and  $\approx 30 \text{ N} \cdot \text{m}$ ), which can be detrimental and lead to collapse of the arch. While this collapse mechanism is a function of the geometry, small and medium span arches can be fabricated without collapse using the *sequential method*, but at the larger scale this twisting behavior must be avoided.

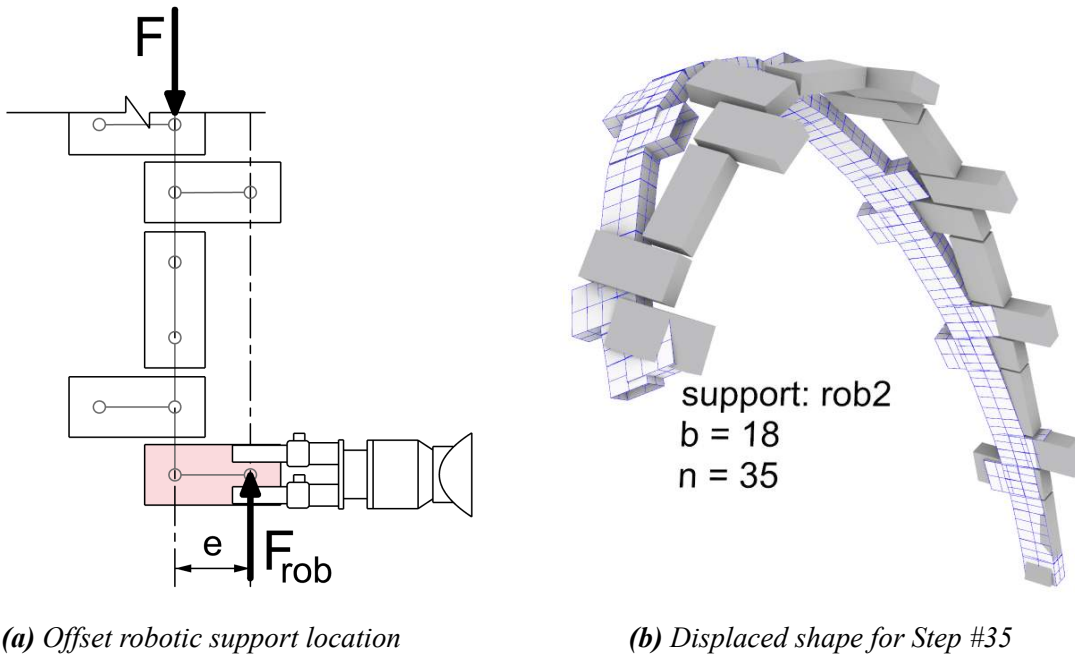


**Figure 4.11:** Twisting of the arch during construction with the sequential method.

#### 4.4.2 Cantilever Method

The *cantilever method* (shown in the bottom of Figure 4.10b) is a more complex 2-robot sequence that was developed to solve the twisting issue experienced in the *sequential method* [21]. The method is based around an alternating three brick placement sequence for each robot. Figure 4.10 illustrates one full construction loop: *rob2* supports the arch at brick 16, while *rob1* places 3 bricks in sequence (i.e., steps 32, 34 and 36), after which their roles swap. Despite this difference, the *cantilever method* shares 1/3 of its steps in common with the *sequential method*. For example, as shown in Figure 4.10, steps 32 and 37 out of the six steps in one loop are the same across both methods. These common steps are also highlighted in the full 49 step build-

ing sequence for the 25-brick arch in Appendix A, [Table A.2](#). The main benefit of the *cantilever method* is that the support point swap (brick 19 in step 37 in the example above) always occurs when a robot is supporting the arch on a vertical brick, which is centered on the thrust line of the arch.

**Table 4.5:** Comparison of cantilever to sequential method at critical steps

Step	$M_{sup}$			$\Delta_{max}$			$T_{max}$		
	$C$	$S$	$C/S$	$C$	$S$	$C/S$	$C$	$S$	$C/S$
	[ $N \cdot m$ ]	[ $N \cdot m$ ]		[ $10^{-3} mm$ ]	[ $10^{-3} mm$ ]		[ $N$ ]	[ $N$ ]	
9	2.9	6.8	0.43	0.4	1.3	0.31	68.6	36.9	1.9
11	1.6	8.3	0.19	0.6	2.2	0.27	69.1	45.5	1.5
21	20.7	21.5	0.96	8.5	12.8	0.66	78.4	23.7	3.3
23	18.6	22.0	0.85	7.3	16.9	0.43	90.8	11.4	8.0
33	4.6	21.3	0.22	11.2	70.8	0.16	29.6	0.8	37.0
35	5.3	29.6	0.18	10.4	97.5	0.11	59.3	0.8	74.1
45	3.7	56.4	0.07	15.9	264.4	0.06	34.8	0.8	43.5
47	0.9	66.0	0.01	11.1	306.5	0.04	69.6	0.8	87.0

C = Cantilever Method, S = Sequential Method

Avoiding a support point swap while gripping a horizontal brick off-center leads to more consistent structural behavior across all the fabrication steps (i.e., no large jump in moments and displacements between steps). This consistency is shown in [Table 4.5](#) when comparing the moment and maximum displacement between the two methods, for all the critical steps discussed in [Section 4.4.1](#). Based on the moment and maximum displacement metrics, the *cantilever method* consistently outperforms the *sequential method*. This performance is exemplified in the four critical steps after the crown (i.e., steps 33, 35, 45 and 47), where moments and maximum displacements are reduced by 78-99% and 84-96% respectively. Eliminating the twist allows the central arch to maintain stability and to be constructed without temporary scaffolding, as shown in [Figure 4.12](#).

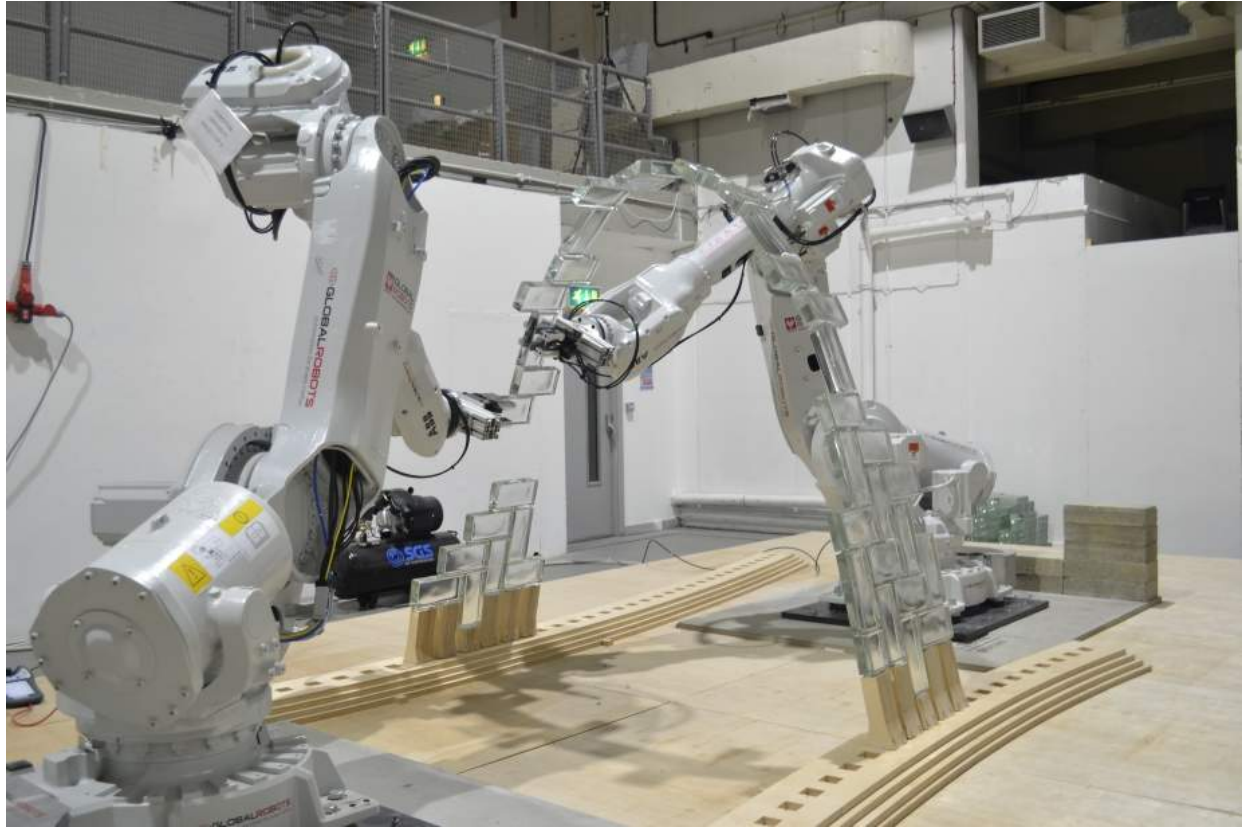


**Figure 4.12:** Two robots build the central arch using the cantilever method.

While the *cantilever method* successfully mitigates the critical twisting action, it does introduce a new challenge: during certain stages in the sequence there are up to three bricks being cantilevered from the closest robotic support point. This partial assembly is therefore relying on the tensile capacity of a single brick-brick connection at the fixed support. This is not a reliable strategy since it is highly sensitive to the connection and brick material used. For the prototype, this is solved by using fast-setting epoxy putty [125] that can support a cantilevered load equivalent to five bricks [21]. But in general, this direct reliance on the mortar strength raises questions about scalability and efficiency of the *cantilever method*. The connection material needs to be fully cured before proceeding to the next step, which slows down construction significantly. But this was not a significant factor as the epoxy only required  $\approx 15$  mins to cure. But if traditional mortar is used, coupled with heavier construction loads (i.e., heavier or larger bricks), resisting the tension caused by the cantilevered support condition within a reasonable time-frame would not be feasible.

In general, the *cantilever method* performs worse with respect to tensile forces in the members

than the *sequential method*, which is typically undesirable in masonry construction. This comparison is made in the  $T_{max}$  column in [Table 4.5](#), where the maximum tensile force in an element at a step is shown for both methods. [Table 4.6](#) shows the average maximum tension forces in the elements across all steps in the full construction sequence, steps before the crown, and steps after the crown. These values are consistently 40-80% higher for the *cantilever method*, although the absolute maxima are the same for both.

**Table 4.6:** Tensile forces in both 2-robot sequences (in N)

	Sequential	Cantilever
Average $T_{max}$ in full sequence	38.0	53.7
Average $T_{max}$ before crown	55.2	80.0
Average $T_{max}$ after crown	17.4	30.6
Maximum $T_{max}$	114.4	111.5

#### 4.4.3 General Challenges with 2-Robot Fabrication Methods

Neither of the 2-robot construction methods discussed in [Sections 4.4.1](#) and [4.4.2](#) are a perfect solution to the scaffold-free construction goal. The *sequential method* suffers from twisting displacements at certain steps, but minimizes overall tensile forces since the arch is always supported on the last brick placed. On the other hand, the *cantilever method* minimizes the out-of-plane deformations during construction but suffers from a reliance on the tensile capacity of the mortar. These two methods do not constitute all the possible sequences, but all 2-robot fabrication sequences face issues related to scaling the size of the structure and reaching the maximum load capacity of the robots themselves. Regardless of the specific fabrication sequence, when using two robots there is always a situation where only one robot is gripping the structure. The load path is determinate, so the support force grows proportional to the size and weight of the arch. The maximum forces in the robots for the full construction sequences are shown in [Table 4.7](#). Although the two methods have different overall behaviors, the maximum force in each robot required to support the arch is similar.

**Table 4.7: Maximum forces supported by the robots**

	rob1	rob2
	$N$	$N$
Sequential Method	369	406
Cantilever Method	362	409

## 4.5 Central Arch Fabrication with Three Robots

Adding a third robot to the construction sequence can mitigate many of the issues that arise from using either of the 2-robot methods discussed in [Sections 4.4.1](#) and [4.4.2](#), and thereby improving the overall scalability of a scaffold-free fabrication method by reducing the maximum support force in each robot, and minimizing tension forces, moments and displacements in the structure. A third robot (*rob3*) is envisioned as a mobile agent, that has additional flexibility to place and support bricks from either side of the arch, unlike *rob1* and *rob2* which are fixed on either side of the structure. In the research presented in this chapter, only the structural influence of this third robot is investigated, omitting the challenges associated with the developing the fabrication setup around reachability and collision concerns.

Based on the conclusions drawn from developing the 2-robot methods come the following design criteria for a 3-robot sequence as desired:

1. no twisting: two robots must always be gripping the structure
2. no cantilevering: a robot must always be supporting the very last brick in the partially constructed arch

The inclusion of a third agent capable of placing and supporting means that the fabrication sequence is no longer prescriptive – there is an additional robotic support available at each step beyond what is required for stability, which can be moved to support any free location on the structure. The selection of the location of the additional robotic support can be formulated as an optimization problem, where the new support position is calculated to improve a user-specified set of structural criteria. In [Sections 4.5.1](#), [4.5.2](#) and [4.5.3](#) the following is discussed: the optimization approach that is used to select support points, how a 3-robot optimization-based fabrication could be implemented, and the structural results of using an optimized fabrication sequence.

### 4.5.1 Optimization Algorithm

The goal of the optimization is to minimize the displacement and forces experienced by the partial arch during each construction step, and thus to determine the location on the structure that a robotic support should move to at the start of each optimization loop (outlined in [Sections 4.5.2](#) and [4.5.2](#)). The optimization process is formulated in [Equation \(4.1\)](#), where an optimal node ( $n^*$ ) is defined as the support node on the structure that minimizes the sum of the average R-terms (i.e., performance ranks) at each of the fabrication steps for which the support is present. These rank terms represent the relative performance in a particular structural criterion when placing a support at the node being examined. First, an exhaustive set of FE structural analyses based on the double-cross representation are performed at each fabrication step, where the support point is moved to every possible support location on the structure. The number of possible support locations increases with the size of the partial arch. The structural behavior from each of these models is recorded (i.e., maximum tension in the element interfaces, moment at the support, forces in the robotic supports, and maximum displacement), and once all locations have been evaluated they are ranked from best to worst.

For example, if there are a total of 17 bricks already placed in the partial arch structure, there are a potential  $17 \times 2 = 34$  possible support nodes in the structure for a robot to move to in the following step (less any that are not reachable based on kinematics and if a robot is already supporting that location). Thus, 34 models would be run for this step, varying the support location in each, and then ranking these models based on how they performed in each of the structural categories of interest. The sets of criteria can be chosen by the user, in the case of the arch, the two criteria to improve are shown in [Equations \(4.2\)](#) and [\(4.3\)](#). [Equation \(4.2\)](#) minimizes the following: maximum tension in the bricks ( $T_{max}$ ), support moment at the base ( $M_{sup}$ ), forces in all supporting robots ( $R_{rob1}, R_{rob2}, R_{rob3}$ ). [Equation \(4.3\)](#) minimizes: maximum tension in the bricks ( $T_{max}$ ), support moment at the base ( $M_{sup}$ ), forces in the active robot moving to an optimized location ( $R_{rob}$ ), and the maximum displacement in the arch ( $\Delta_{max}$ ).

$$n^* = \underset{(support\ node)}{\operatorname{argmin}} \sum_{i=1}^4 \bar{R}_i \quad (4.1)$$

where :

$$\bar{R} = \text{avg} (R^{T_{max}} + R^{M_{sup}} + R^{F_{rob1}} + R^{F_{rob2}} + R^{F_{rob3}}) \quad (4.2)$$

$$\bar{R} = \text{avg} (R^{T_{max}} + R^{M_{sup}} + R^{F_{rob}} + R^{\Delta_{max}}) \quad (4.3)$$

This optimization, based on multiple structural criteria, ensures that the selected support location leads to general improvements to all the important structural behavior criteria while minimizing negative side-effects. For example, to avoid reducing the deflection at the cost of higher forces in the supporting robots. [Equation \(4.2\)](#) is used for optimizations that occur before the crown of the arch has been reached, since deflections are not significant up to this point. [Equation \(4.3\)](#) is used for the optimizations after the crown, where the deflection and support force criteria are critical. Only the active robot – the robot that is being moved in the optimization loop – has its support force optimized.

### 4.5.2 Optimization-Based Fabrication Sequences

#### Modified Sequential Method

Given an existing 2-robot sequence, one can determine where the third support should be placed to mitigate any structural issues. For example, starting with the *sequential method* and the challenges with twisting, the 3rd support could be placed on the structure to counteract this action. [Table 4.8](#) illustrates such a hypothetical scenario, starting with the partial arch during the *sequential method* at step 8. Normally the following step would cause off-center twisting to occur as *rob2* releases its grip (see Appendix A, [Table A.1](#) for the full sequential sequence). But the third support is free to be placed at an optimal location on the structure before this twisting occurs, which is highlighted by the cells labelled “O1” in [Table 4.8](#). This location is identified on the basis of an optimization; the selected brick and node to grip must lead to improved structural behavior in all three of the steps it will be present in. The objective function is thus formulated as choosing a support location that leads to the best cumulative performance in displacements,

forces, and moments in the structure over all three steps. The issue with twisting on step 9 has thereby been resolved through the inclusion of the *rob3* support, and this process is continued for the full fabrication sequence as the third support is continuously moved to optimize the behavior over the following range of three steps:  $O_2, O_3, O_4, \dots, O_n$ . But not all fabrication steps are optimized when adding a third support to an existing 2-robot method in this way. For example, the steps when *rob3* releases the structure and moves (10 and 12 in [Table 4.8](#)) are the same as in the standard 2-robot *sequential method*.

**Table 4.8:** Modifying the sequential method with an optimized third support

Step <sup>1</sup>	Total Bricks	<i>rob1</i>		<i>rob2</i>		<i>rob3</i>	
		b	n	b	n	b	n
:	:	:	:	:	:	:	:
8	4	5	8	4	7	—	—
	4	5	8	4	7	O1	O1
9 <sup>2</sup>	4	5	8	—	—	O1	O1
	5	5	8	6	11	O1	O1
10	5	5	8	6	11	—	—
	5	5	8	6	11	O2	O2
11 <sup>2</sup>	5	—	—	6	11	O2	O2
	6	7	13	6	11	O2	O2
12	6	7	13	6	11	—	—
:	:	:	:	:	:	:	:

= optimized support location

<sup>1</sup> step numbering corresponds to the sequential method sequence

<sup>2</sup> steps experiencing off-center twisting in sequential method

## Optimized Three Robot Method

In contrast to a partially optimized sequence, as described in [Section 4.5.2](#), a fully optimized fabrication sequence is one where each step is covered by an optimization calculation for any one of the robots. Such a sequence is superior to a modified 2-robot sequence, as the position of all three robots is actively included in the optimization process. Therefore, the whole fabrication sequence can be redefined with respect to a set of user-specified structural optimization criteria in addition to the no twisting and cantilevering design criteria, rather than just building on an existing and potentially limited 2-robot sequence. [Table 4.9](#) describes a fully *optimized three*

*robot method*, where every step is covered by an optimization calculation performed for the active robot (represented by the cell highlighted in blue).

**Table 4.9:** 3-robot cascading optimization

Step	Total Bricks	rob1		rob2		rob3	
		b	n	b	n	b	n
1	1	1	1	—	—	—	—
2	2	1	1	2	2	—	—
3	3	1	1	2	2	O1	O1
4	3	—	—	2	2	O1	O1
5	4	4	7	2	2	O1	O1
6	4	4	7	—	—	O1	O1
7	4	4	7	O2	O2	O1	O1
8	4	4	7	O2	O2	—	—
9	5	4	7	O2	O2	5	8
10	5	—	—	O2	O2	5	8
11	5	O3	O3	O2	O2	5	8
12	5	O3	O3	—	—	5	8
13	6	O3	O3	6	11	5	8
14	6	O3	O3	6	11	—	—
15	6	O3	O3	6	11	O4	O4
16	6	—	—	6	11	O4	O4
17	7	7	13	6	11	O4	O4
18	7	7	13	—	—	O4	O4
19	7	7	13	O5	O5	O4	O4
20	7	7	13	O5	O5	—	—
21	8	7	13	O5	O5	8	15
⋮	⋮	⋮	⋮	⋮	⋮	⋮	⋮
58	17	—	—	O14	O14	17	33
59	17	O15	O15	O14	O14	17	33
60	17	O15	O15	—	—	17	33
61	18	O15	O15	18	35	17	33
62	18	O15	O15	18	35	—	—
⋮	⋮	⋮	⋮	⋮	⋮	⋮	⋮

■ = optimized support location

An optimization is performed for each brick placed into the arch (excluding the first two), where  $\sum_{n=3}^{n_{max}} 4 \cdot 2n$ , is the number of individual analysis models that are needed for the full fabrication (i.e., 2,576 models with  $n_{max} = 25$  bricks). It is important to point out that this constitutes a simplification to a cascading optimization, where each cycle is linked to the next as their first

and last steps overlap. For example, looking at [Table 4.9](#), Step 11 falls on the last step in O2 and the first step in O3. This means that an exhaustive evaluation would require  $(2n)(2(n - 1))$  models to run for each of these overlapping steps, resulting in a total  $\sum_{n=3}^{n_{max}} 3 \cdot 2n + (2n)(2(n - 1))$  individual analysis models that would need to be run for the full fabrication (i.e., 22,724 models with  $n_{max} = 25$  bricks). Even with the simplified modeling approach this is considered an excessive number of analyses to perform. Therefore this overlapping step is treated as pertaining only to one of the optimizations, thereby reducing the order of the problem from  $O(n^2)$  to  $O(n)$ .

The general fabrication process can be described by the four-step loop (a to d) in [Figure 4.13](#). This loop is repeated over the construction of the whole arch, with the roles of the three robots varying depending on what stage of the construction is being completed. The placement of bricks is sequential, but each robot takes a turn being the optimized support every three bricks, creating the cascading pattern of optimizations as seen in [Table 4.9](#).

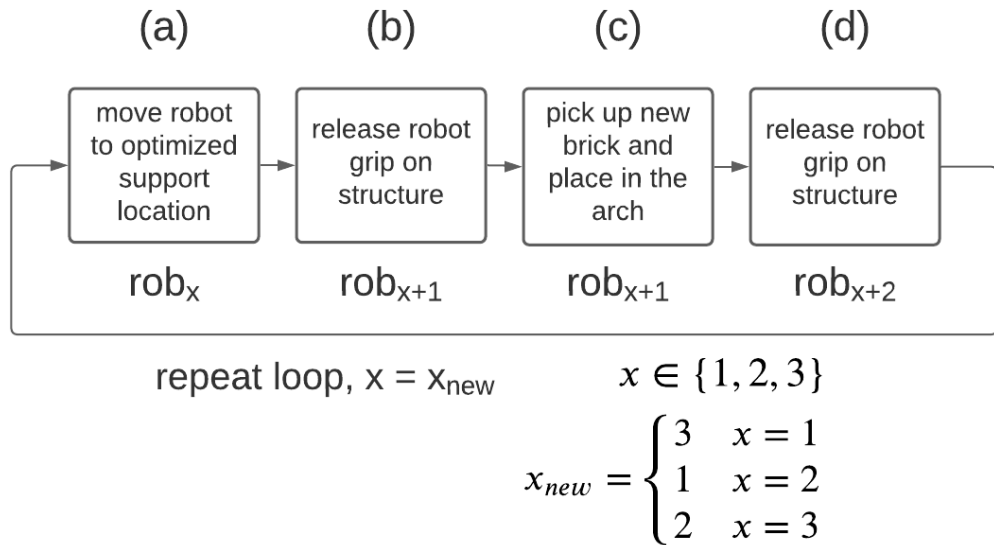


*Figure 4.13: Four-step fabrication loop.*

[Figure 4.14](#) shows a concrete implementation of this for just one loop starting at step #59 (the full arch fabrication sequence can be found in Appendix B, [Table A.3](#)), where the four-step loop (a to d) is described in detail at each step. In [Figure 4.14](#) the optimized location (O15) in step #59 is calculated for the structure based on the algorithm explained in [Section 4.5.1](#).

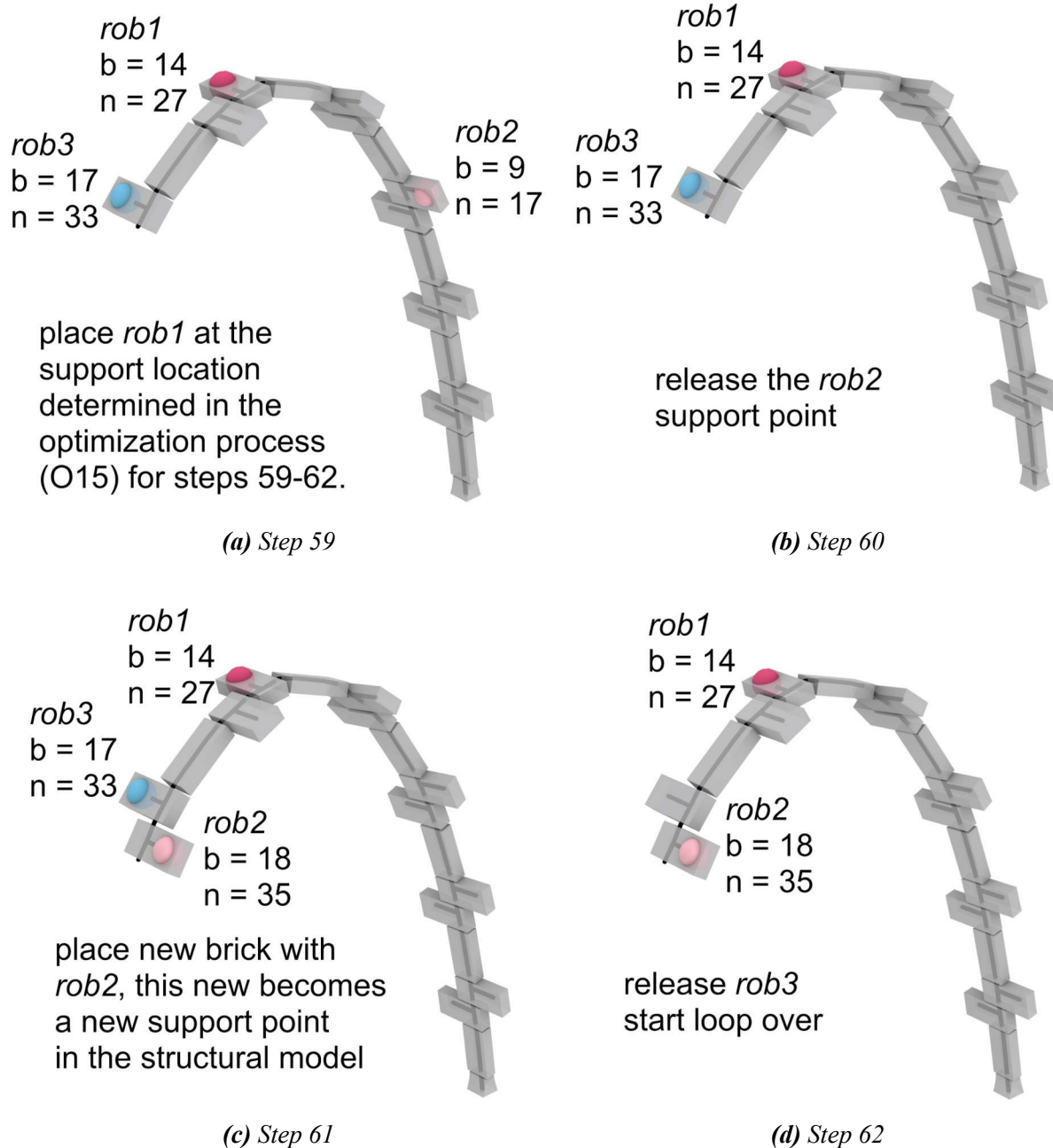


**Figure 4.14:** An example four step loop in the 3-robot construction sequence.

### 4.5.3 Optimization Results

A total of 23 independent optimizations (each corresponding to 4 steps in the sequence) were required in the fabrication simulation of the 25-brick arch based on the *optimized three robot method*. The full set of structural analysis results using these optimized locations are shown in

Appendix B, [Table A.3](#). With this method the construction takes a total of 90 steps, which is almost double what is required in a 2-robot method. However, this is due to the re-positioning of the optimized support every four steps. This longer fabrication sequence is partially offset by the fact that waiting for mortar curing is not required as there is always a robot supporting the latest brick in the sequence and there is no cantilevering action.

The *optimized three robot method* is able to significantly improve the structural behavior over the full construction sequence when compared to both 2-robot methods discussed in [Sections 4.4.1](#) and [4.4.2](#). [Table 4.10](#) compares the maximum structural forces, moments, and displacements measured during each of the three fabrication sequences. The 3-robot sequence is able to re-distribute the forces in the robotic supports reducing the maximum force in *rob1* and *rob2* by 27% and 37% respectively. Twisting behavior is also mitigated, thereby reducing the maximum moment and displacement by 67% and 93% respectively when compared to the *sequential method*. The maximum tension in an element is reduced by 23% when compared to the 2-robot sequences.

**Table 4.10:** Improvement to structural behavior with 3-robot optimized sequence

		Seq.	Cant.	3-rob
$F_{rob1}$	[N]	369	362	270
$F_{rob2}$	[N]	406	409	257
$F_{rob3}$	[N]	—	—	254
$M_{sup}$	[N · m]	66.0	21.7	21.5
$T_{max}$	[N]	114.4	111.5	87.7
$\Delta_{max}$	[ $10^{-3}$ mm]	306.5	15.9	21.9

## 4.6 Conclusion

The research presented in this chapter builds on previous research [[20–22](#)] that has demonstrated how industrial robots sequenced in a cooperative manner are a viable method for building a discrete brick arch without temporary scaffolding. In the context of fabricating a masonry arch, a minimum of two robots are needed to successfully execute a scaffold-free cooperative placement and support sequence. A simplified geometric structural analysis framework, based on rigid

elements and flexible joints, is presented, validated and used to evaluate three fabrication methods: sequential, cantilever, and optimized. While the *sequential method*, where two robots take turns placing bricks, is simple to implement, the out-of-plane twisting observed is detrimental in larger-scale structures. The *cantilever method*, where the robots take turns placing three bricks in a row, solves the issue of twisting. But this method raises questions about applicability to larger masonry structures due to a reliance on the strength of the mortar to support bricks throughout the fabrication.

The addition of a third robot was analyzed to further improve upon the 2-robot scaffold-free fabrication methods. It is shown that including a third robot improves the structural behavior during fabrication when formulating the fabrication sequence as the result of an optimization problem. This approach creates an opportunity to design a fabrication sequence on the basis of a set of user-specified structural optimization targets (e.g., displacements, forces, moments) in addition to the goal of removing the need for temporary scaffolding. Generally, the *optimized three robot method* is an improvement as it combines many positive aspects of the 2-robot methods, while simultaneously mitigating the negative: twisting deformations, tensile forces, and large support moments.

Geometrically complex discrete element systems have significant economic and environmental consequences due to their challenging construction process, which is still deeply rooted in a pre-robotic construction rationale. This work re-imagines the construction of discrete element structures in response to emerging innovations in robotic fabrication in the building industry and thus hopes to bring about transformative sustainable changes in construction practices while increasing onsite productivity. The research presented in this chapter has generated new knowledge on how to design and analyze robotic sequences for spatial structural systems, and illustrates further the potential of utilizing cooperative robotic fabrication for scaffold-free construction applications.

## References

- [1] M. Deuss, D. Panozzo, E. Whiting, Y. Liu, P. Block, O. Sorkine-Hornung, M. Pauly, Assembling self-supporting structures, *ACM Transactions on Graphics* 33 (6) (2014) 1–10. doi:10.1145/2661229.2661266.
- [2] V. Paris, A. Pizzigoni, S. Adriaenssens, Statics of self-balancing masonry domes constructed with a cross-herringbone spiraling pattern, *Engineering Structures* 215 (2020) 1–10. doi:10.1016/j.engstruct.2020.110440.
- [3] A. Choisy, *L'Art de bâtir chez les Byzantins*, Société anonyme de publications périodiques, Paris, 1883, (ISBN: 978-88-271-1911-2).
- [4] S. El-Naggar, *Les voûtes dans l'architecture de l'Egypte ancienne*, Institut français d'archéologie orientale, Le Caire, 1999, (ISBN: 978-2-7247-0252-1).
- [5] R. Besenval, *Technologie de la boûte dans l'orient ancien*, Éditions Recherche sur les Civilisations, Paris, 1984, (ISBN: 978-2-86538-082-4).
- [6] J. Heyman, *The stone skeleton: Structural engineering of masonry architecture*, reprint Edition, Cambridge University Press, 1997, (ISBN: 978-0-521-62963-8).
- [7] A. Pizzigoni, Brunelleschi's bricks, *Journal of the International Association for Shell and Spatial Structures* 56 (2) (2015) 137–148, (ISSN: 1028-365X).
- [8] A. Pizzigoni, V. Paris, M. Pasta, M. Morandi, A. Parsani, Herringbone naked structure, in: *Proceedings of IASS Annual Symposia 2018*, Boston, 2018, pp. 1–6, (ISSN: 2518-6582).
- [9] J. A. Ochsendorf, *Guastavino vaulting: The art of structural tile*, Princeton Architectural Press, New York, 2010, (ISBN: 978-1-56898-741-5).
- [10] E. Vouga, M. Höbinger, J. Wallner, H. Pottmann, Design of self-supporting surfaces, *ACM Transactions on Graphics* 31 (4) (2012) 1–11. doi:10.1145/2185520.2185583.
- [11] S. Goessens, C. Mueller, P. Latteur, Feasibility study for drone-based masonry construction of real-scale structures, *Automation in Construction* 94 (2018) 458–480. doi:10.1016/j.autcon.2018.06.015.

- [12] SOM, University of Alcalá, Bricks, mortar, and robots: Solutions for sustainable construction (Aug. 2019).  
URL <https://som.medium.com/bricks-mortar-and-robots-solutions-for-sustainable-construction-f404b90fe9ab>
- [13] V. Loing, O. Baverel, J.-F. Caron, R. Mesnil, Free-form structures from topologically interlocking masonries, *Automation in Construction* 113 (2020) 1–15. doi:10.1016/j.autcon.2020.103117.
- [14] J. Drew, Lock-Block Ltd. (2021).  
URL <http://www.lockblock.com/>
- [15] K. Wu, A. Kilian, Robotic equilibrium: Scaffold free arch assemblies, in: Proceedings of the 38th Annual Conference of the Association for Computer Aided Design in Architecture, Mexico City, 2018, pp. 342–349, (ISBN: 978-0-692-17729-7).
- [16] T. Bock, T. Linner, Robot-oriented design: Design and management tools for the deployment of automation and robotics in construction, Vol. 1, Cambridge University Press, 2015, (ISBN: 978-1-107-07638-9).
- [17] G. Bravo-Palacios, A. D. Prete, P. M. Wensing, One robot for many tasks: Versatile co-design through stochastic programming, *IEEE Robotics and Automation Letters* 5 (2) (2020) 1680–1687. doi:10.1109/LRA.2020.2969948.
- [18] P. Eversmann, F. Gramazio, M. Kohler, Robotic prefabrication of timber structures: towards automated large-scale spatial assembly, *Construction Robotics* 1 (2017) 49–60. doi:10.1007/s41693-017-0006-2.
- [19] IFR, World robotics report (2018).  
URL <https://ifr.org/ifr-press-releases/news/global-industrial-robot-sales-doubled-over-the-past-five-years>
- [20] I. X. Han, E. P. Bruun, S. Marsh, S. Adriaenssens, S. Parascho, From concept to construction: A transferable design and robotic fabrication method for a building-scale vault, in:

Proceedings of the 40th Annual Conference of the Association for Computer Aided Design in Architecture, 2020, p. 12.

- [21] S. Parascho, I. X. Han, S. Walker, A. Beghini, E. P. Bruun, S. Adriaenssens, Robotic vault: A cooperative robotic assembly method for brick vault construction, *Construction Robotics* 4 (3) (2020) 1–10. doi:10.1007/s41693-020-00041-w.
- [22] S. Parascho, I. X. Han, A. Beghini, M. Miki, S. Walker, E. P. Bruun, S. Adriaenssens, LightVault: A design and robotic fabrication method for complex masonry structures, in: *Advances in Architectural Geometry 2021*, Paris, France, 2021, p. 25.
- [23] S. Parascho, A. Gandia, A. Mirjan, F. Gramazio, M. Kohler, Cooperative fabrication of spatial metal structures, in: A. Menges, B. Sheil, R. Glynn, M. Skavara (Eds.), *Fabricate 2017*, UCL Press, London, 2017, pp. 24–29. doi:10.3929/ethz-b-000219566.
- [24] S. Sharif, R. Gentry, BIM for masonry: Development of BIM plugins for the masonry unit Database, in: *Proceedings of the 33rd Education and Research in Computer Aided Architectural Design in Europe Conference*, Vienna, Austria, 2015, pp. 567–576, (WOS: 000372317300061).
- [25] T. Bock, Construction robotics, *Autonomous Robots* 22 (3) (2007) 201–209. doi:10.1007/s10514-006-9008-5.
- [26] T. Bock, The future of construction automation: Technological disruption and the upcoming ubiquity of robotics, *Automation in Construction* 59 (2015) 113–121. doi:10.1016/j.autcon.2015.07.022.
- [27] J. S. Albus, Trip report: Japanese progress in robotics for construction, *Robotics* 2 (2) (1986) 103–112, publisher: North-Holland. doi:10.1016/0167-8493(86)90047-1.
- [28] L. Cousineau, N. Miura, *Construction robots: The search for new building technology in Japan*, American Society of Civil Engineers, Reston, VA, 1998, (ISBN: 978-0-7844-0317-4).

- [29] P. Y. Huang, M. Sakurai, Factor automation: the Japanese experience, *IEEE Transactions on Engineering Management* 37 (2) (1990) 102–108. doi:10.1109/17.53712.
- [30] T. Ueno, J. Maeda, T. Yoshida, S. Suzuki, Construction robots for site automation, in: Proceedings of the 3rd ISARC, Marseille, France, 1986, pp. 627–639. doi:10.22260/ISARC 1986/0049.
- [31] T. Bock, T. Linner, Site automation: Automated/robotic on-site factories, Vol. 3, Cambridge University Press, 2016, (ISBN: 978-1-107-07597-9).
- [32] M. J. Skibniewski, Robotics in civil engineering, Van Nostrand Reinhold, Southampton, 1989, (ISBN: 978-0-442-31925-0).
- [33] J. M. Davila Delgado, L. Oyedele, A. Ajayi, L. Akanbi, O. Akinade, M. Bilal, H. Owolabi, Robotics and automated systems in construction: Understanding industry-specific challenges for adoption, *Journal of Building Engineering* 26 (2019) 1–11. doi:10.1016/j.jobe.2019.100868.
- [34] D. Castro-Lacouture, Construction automation, in: S. Y. Nof (Ed.), *Springer Handbook of Automation*, Springer Handbooks, Springer, Berlin, Heidelberg, 2009, pp. 1063–1078, (ISBN: 978-3-540-78831-7).
- [35] B. García de Soto, I. Agustí-Juan, J. Hunhevicz, S. Joss, K. Graser, G. Habert, B. T. Adey, Productivity of digital fabrication in construction: Cost and time analysis of a robotically built wall, *Automation in Construction* 92 (2018) 297–311. doi:10.1016/j.autcon.2018.04.004.
- [36] V. R. P. Kumar, M. B. a. S. J. Raj, Robotics in construction industry, *Indian Journal of Science and Technology* 9 (23) (2016) 1–12. doi:10.17485/ijst/2016/v9i23/95974.
- [37] T. Bock, T. Linner, Robotic industrialization: Automation and robotic technologies for customized component, module, and building prefabrication, Vol. 2, Cambridge University Press, 2015, (ISBN: 978-1-107-07639-6).

- [38] P. Block, T. Van Mele, A. Liew, M. DeJong, D. Escobedo, J. Ochsendorf, Structural design, fabrication and construction of the Armadillo Vault, *The Structural Engineer* 96 (5) (2018) 10–20.
- [39] M. Rippmann, T. V. Mele, M. Popescu, E. Augustynowicz, T. M. Echenagucia, C. C. Barentin, U. Frick, P. Block, Computational design and digital fabrication of a freeform stone shell, in: *Advances in Architectural Geometry 2016*, Zurich, 2016, pp. 344–363. doi:10.3929/ethz-a-010709080.
- [40] L. Davis, M. Rippmann, T. Pawlofsky, P. Block, Innovative funicular tile vaulting: A prototype in Switzerland, *The Structural Engineer* 90 (11) (2012) 46–56.
- [41] E. Borne, E. e. a. Heathcote, The Droneport project, *AA: L'Architecture d'Aujourd'hui* (2016) 92.  
URL <https://www.lafargeholcim-foundation.org/media/publications/aa-perspectives-the-droneport-project>
- [42] J. Chilton, Heinz Isler's infinite spectrum: Form-finding in design, *Architectural Design* 80 (4) (2010) 64–71. doi:10.1002/ad.1108.
- [43] J. Chilton, C.-C. Chuang, Rooted in nature: Aesthetics, geometry and structure in the shells of Heinz Isler, *Nexus Network Journal* 19 (3) (2017) 763–785. doi:10.1007/s00004-017-0357-5.
- [44] T. Bock, T. Linner, Construction robots: Elementary technologies and single-task construction robots, Vol. 4, Cambridge University Press, 2016, (ISBN: 978-1-316-78517-1).
- [45] P. Vink, M. Miedema, E. Koningsveld, H. v. d. Molen, Physical effects of new devices for bricklayers, *International Journal of Occupational Safety and Ergonomics* 8 (1) (2002) 71–82. doi:10.1080/10803548.2002.11076515.
- [46] J. Hess, M. Weinstein, L. Welch, Ergonomic best practices in masonry: Regional differences, benefits, barriers, and recommendations for dissemination, *Journal of Occupational and Environmental Hygiene* 7 (8) (2010) 446–455. doi:10.1080/15459624.2010.484795.

- [47] Z. Dakhli, Z. Lafhaj, Robotic mechanical design for brick-laying automation, *Cogent Engineering* 4 (2017) 1–22. doi:10.1080/23311916.2017.1361600.
- [48] J. Thomson, Brick-laying machine, patent Number: US772191A (Oct. 1904).  
URL <https://patents.google.com/patent/US772191A/en>
- [49] British Pathé, Mechanical bricklayer (1967).  
URL <https://www.youtube.com/watch?v=4MWald1Goqk>
- [50] E. Y. Malinovsky, A. A. Borshchevsky, E. A. Elder, V. M. Pogodin, A robotic complex for brick-laying applications, in: 7th International Symposium on Automation and Robotics in Construction, Bristol, England, 1990, pp. 32–38. doi:10.22260/ISARC1990/0005.
- [51] D. Chamberlain, P. Speare, S. Ala, Progress in a masonry tasking robot, in: 8th Int. Symposium on Automation and Robotics in Construction, Stuttgart, Germany, 1991, pp. 909–918. doi:10.22260/ISARC1991/0087.
- [52] F. Altobelli, H. F. Taylor, L. E. Bernold, Prototype robotic masonry system, *Journal of Aerospace Engineering* 6 (1) (1993) 19–33. doi:10.1061/(ASCE)0893-1321(1993)6:1(19).
- [53] T. Bock, T. Linner, From early trials to advanced computer integrated prefabrication of brickwork, in: G. Grimscheid, F. Scheublin (Eds.), *New Perspective in Industrialization in Construction – A State-of-the-Art Report*, CIB International Council for Research and Innovation in Building and Research, Zurich, 2009, pp. 161–181, (ISBN: 978-3-906800-17-2).
- [54] Y. Kodama, Y. Yamazaki, H. Kato, Y. Iguchi, H. Naoi, A robotized wall erection system with solid components, in: Proceedings of the 5th International Symposium on Automation and Robotics in Construction (ISARC), Tokyo, Japan, 1988, pp. 441–448. doi:10.22260/ISARC1988/0052.
- [55] J. Andres, T. Bock, F. Gebhart, W. Steck, First results of the development of the masonry robot system ROCCO: A fault tolerant assembly tool, *Automation and Robotics in Construction XI* (1994) 87–93doi:10.1016/B978-0-444-82044-0.50016-3.

- [56] A. H. Slocum, B. Schena, Blockbot: A robot to automate construction of cement block walls, *Robotics and Autonomous Systems* 4 (2) (1988) 111–129. doi:10.1016/0921-8890(88)90020-6.
- [57] H. Lehtinen, E. Salo, H. Aalto, Outlines of two masonry robot systems, in: Proceedings of the 6th International Symposium on Automation and Robotics in Construction., San Francisco, California, 1989, pp. 143–150. doi:10.22260/ISARC1989/0018.
- [58] N. Podkaminer, L. Peters, SAM100 – Construction robotics (2021).  
URL <https://www.construction-robotics.com/sam100/>
- [59] M. Pivac, M. Pivac, M. Sheridan, Hadrian X - Fastbrick robotics (2021).  
URL <https://www.fbr.com.au/>
- [60] G. Pritschow, M. Dalacker, J. Kurz, J. Zeiher, A mobile robot for on-site construction of masonry, *Proceedings of IEEE/RSJ International Conference on Intelligent Robots and Systems (IROS'94)* 3 (1994) 1701–1707. doi:10.1109/IROS.1994.407628.
- [61] G. Pritschow, M. Dalacker, J. Kurz, M. Gaensle, Technological aspects in the development of a mobile bricklaying robot, *Automation in Construction* 5 (1) (1996) 3–13. doi:10.1016/0926-5805(95)00015-1.
- [62] J. Sklar, Robots lay three times as many bricks as construction workers (2015).  
URL <https://www.technologyreview.com/2015/09/02/10587/robots-lay-three-times-as-many-bricks-as-construction-workers/>
- [63] F. Gramazio, M. Kohler, Digital materiality in architecture, 1st Edition, Lars Muller, Baden, 2008, (ISBN: 978-3-03778-122-7).
- [64] F. Gramazio, M. Kohler (Eds.), Made by robots: Challenging architecture at a larger scale, 1st Edition, Academy Press, London, 2014, (ISBN: 978-1-118-53548-6).
- [65] T. Bonwetsch, D. Kobel, F. Gramazio, M. Kohler, The informed wall: Applying additive digital fabrication techniques on architecture, in: Proceedings of the 25th Annual Conference of the Association for Computer-Aided Design in Architecture, 2006, pp. 489–495, (ISBN: 978-0-9789463-0-2).

- [66] T. Bonwetsch, F. Gramazio, M. Kohler, Digitally fabricating non-standardised brick walls, in: ManuBuild, 2007, pp. 191–196, (ISBN: 978-0-86017-710-4).
- [67] M. Kohler, F. Gramazio, J. Willmann, Gantenbein vineyard façade, in: The Robotic Touch: How Robots Change Architecture, The University of Chicago Press, 2014, pp. 66–75, (ISBN: 978-3-906027-37-1).
- [68] EMPA, DFAB HOUSE – Digital fabrication and living. (2021).  
URL <https://www.empa.ch/web/nest/digital-fabrication>
- [69] J. Willmann, M. Knauss, T. Bonwetsch, A. A. Apolinarska, F. Gramazio, M. Kohler, Robotic timber construction — Expanding additive fabrication to new dimensions, Automation in Construction 61 (2016) 16–23. doi:10.1016/j.autcon.2015.09.011.
- [70] N. Hack, T. Wangler, J. Mata-Falcón, K. Dörfler, N. Kumar, N. Walzer, K. Graser, L. Reiter, H. Richner, J. Buchli, W. Kaufmann, R. J. Flatt, F. Gramazio, M. Kohler, Mesh mould: An on site, robotically fabricated, functional formwork, in: Second Concrete Innovation Conference, Vol. 19, Tromsø, Norway, 2017, p. 11, (ISBN: 978-82-8208-054-5).
- [71] N. Hack, K. Dörfler, A. N. Walzer, T. Wangler, J. Mata-Falcón, N. Kumar, J. Buchli, W. Kaufmann, R. J. Flatt, F. Gramazio, M. Kohler, Structural stay-in-place formwork for robotic in situ fabrication of non-standard concrete structures: A real scale architectural demonstrator, Automation in Construction 115 (2020) 1–13. doi:10.1016/j.autcon.2020.103197.
- [72] T. Bonwetsch, R. Bärtschi, M. Helmreich, BrickDesign, in: Robotic Fabrication in Architecture, Art and Design 2012, Springer International Publishing, Vienna, 2012, pp. 102–109. doi:10.1007/978-3-7091-1465-0\_9.
- [73] T. V. Mele, A. Liew, T. M. Echenagucia, M. Rippmann, COMPAS: A framework for computational research in architecture and structures. (2017).  
URL <https://compas-dev.github.io/>
- [74] G. Jahn, C. Newnham, N. v. d. Berg, M. Beanland, Holographic design, fabrication, assembly and analysis of woven steel structures, in: Proceedings of the 38th Annual Confer-

ence of the Association for Computer Aided Design in Architecture, Mexico City, 2018, p. 11, (ISBN: 978-0-692-17729-7).

- [75] G. Jahn, C. Newnham, N. Berg, M. Iraheta, J. Wells, Holographic construction, in: Design Modelling Symposium, Berlin, 2019, p. 13. doi:10.1007/978-3-030-29829-6.
- [76] D. Mitterberger, K. Dörfler, T. Sandy, F. Salveridou, M. Hutter, F. Gramazio, M. Kohler, Augmented bricklaying, *Construction Robotics* 4 (3) (2020) 151–161. doi:10.1007/s41693-020-00035-8.
- [77] L. Piškorec, D. Jenny, S. Parascho, H. Mayer, F. Gramazio, M. Kohler, The brick labyrinth, in: Robotic Fabrication in Architecture, Art and Design 2018, Springer International Publishing, Zurich, 2018, pp. 489–500. doi:10.1007/978-3-319-92294-2\_37.
- [78] K. Dörfler, T. Sandy, M. Gifthalter, F. Gramazio, M. Kohler, J. Buchli, Mobile robotic brickwork: Automation of a discrete robotic fabrication process using an autonomous mobile robot, in: Robotic Fabrication in Architecture, Art and Design 2016, Springer International Publishing, Sydney, Australia, 2016, pp. 204–217. doi:10.1007/978-3-319-26378-6-15.
- [79] M. Gifthalter, T. Sandy, K. Dörfler, I. Brooks, M. Buckingham, G. Rey, M. Kohler, F. Gramazio, J. Buchli, Mobile robotic fabrication at 1:1 scale: The in situ fabricator, *Construction Robotics* 1 (1) (2017) 3–14. doi:10.1007/s41693-017-0003-5.
- [80] R. Bärtschi, M. Knauss, T. Bonwetsch, F. Gramazio, M. Kohler, Wiggled brick bond, in: Advances in Architectural Geometry 2010, Springer, Wien/New York, 2010, pp. 137–147. doi:10.1007/978-3-7091-0309-8.
- [81] M. Kohler, F. Gramazio, J. Willmann, The programmed column, in: The Robotic Touch: How Robots Change Architecture, The University of Chicago Press, 2014, pp. 208–215, (ISBN: 978-3-906027-37-1).
- [82] P. Carneau, R. Mesnil, N. Roussel, O. Baverel, An exploration of 3d printing design space inspired by masonry, in: Proceedings of IASS Annual Symposium 2019, Zenodo, Barcelona, 2019, p. 9. doi:10.5281/ZENODO.3563672.

- [83] P. Carneau, R. Mesnil, N. Roussel, O. Baverel, Additive manufacturing of cantilever - From masonry to concrete 3D printing, *Automation in Construction* 116 (2020) 1–16. doi:10.1016/j.autcon.2020.103184.
- [84] M. Motamedi, R. Oval, P. Carneau, O. Baverel, Supportless 3D printing of shells: Adaptation of ancient vaulting techniques to digital fabrication, in: *Proceedings of the Design Modelling Symposium Berlin*, Berlin, 2019, pp. 714–726. doi:10.1007/978-3-030-29829-6-55.
- [85] S. Parascho, Cooperative robotic assembly: Computational design and robotic fabrication of spatial metal structures, PhD Thesis, ETH, Zurich (2019).  
URL <https://doi.org/10.3929/ethz-b-000364322>
- [86] A. Thoma, A. Adel, M. Helmreich, T. Wehrle, F. Gramazio, M. Kohler, Robotic fabrication of bespoke timber frame modules, in: *Robotic Fabrication in Architecture, Art and Design 2018*, Springer International Publishing, Zurich, 2018, pp. 447–458. doi:10.1007/978-3-319-92294-2\_34.
- [87] E. P. G. Bruun, I. Ting, S. Adriaenssens, S. Parascho, Human–robot collaboration: A fabrication framework for the sequential design and construction of unplanned spatial structures, *Digital Creativity* 31 (4) (2020) 320–336. doi:10.1080/14626268.2020.1845214.
- [88] V. Sarhosis, S. D. Santis, G. d. Felice, A review of experimental investigations and assessment methods for masonry arch bridges, *Structure and Infrastructure Engineering* 12 (11) (2016) 1439–1464. doi:10.1080/15732479.2015.1136655.
- [89] A. M. D’Altri, V. Sarhosis, G. Milani, J. Rots, S. Cattari, S. Lagomarsino, E. Sacco, A. Tralli, G. Castellazzi, S. de Miranda, Modeling strategies for the computational analysis of unreinforced masonry structures: Review and classification, *Archives of Computational Methods in Engineering* 27 (4) (2020) 1153–1185. doi:10.1007/s11831-019-09351-x.
- [90] D. L. Fang, R. K. Napolitano, T. L. Michiels, S. M. Adriaenssens, Assessing the stability of unreinforced masonry arches and vaults: a comparison of analytical and numer-

ical strategies, International Journal of Architectural Heritage 13 (5) (2019) 648–662.

doi:10.1080/15583058.2018.1463413.

- [91] T. Kamiński, Tests to collapse of masonry arch bridges simulated by means of FEM, in: Proceedings of the Fifth International Conference on Bridge Maintenance, Safety and Management, CRC Press, Philadelphia, USA, 2010, pp. 1431–1438. doi:10.13140/2.1.4381.2649.
- [92] B. Pulatsu, E. Erdoganmus, E. M. Bretas, P. B. Lourenço, In-plane static response of dry-joint masonry arch-pier structures, in: Architectural Engineering Institute (AEI) Conference, 2019, pp. 240–248. doi:10.1061/9780784482261.028.
- [93] B. Pulatsu, E. Erdoganmus, P. B. Lourenço, Comparison of in-plane and out-of-plane failure modes of masonry arch bridges using discontinuum analysis, Engineering Structures 178 (2019) 24–36. doi:10.1016/j.engstruct.2018.10.016.
- [94] J. McInerney, M. J. DeJong, Discrete element modeling of groin vault displacement capacity, International Journal of Architectural Heritage 9 (8) (2015) 1037–1049. doi:10.1080/15583058.2014.923953.
- [95] D. Foti, V. Vacca, I. Facchini, DEM modeling and experimental analysis of the static behavior of a dry-joints masonry cross vaults, Construction and Building Materials 170 (2018) 111–120. doi:10.1016/j.conbuildmat.2018.02.202.
- [96] A. Thavalingam, N. Bicanic, J. I. Robinson, D. A. Ponniah, Computational framework for discontinuous modelling of masonry arch bridges, Computers & Structures 79 (19) (2001) 1821–1830. doi:10.1016/S0045-7949(01)00102-X.
- [97] J. Simon, K. Bagi, Discrete element analysis of the minimum thickness of oval masonry domes, International Journal of Architectural Heritage 10 (4) (2016) 457–475. doi:10.1080/15583058.2014.996921.
- [98] P. A. Cundall, Formulation of a three-dimensional distinct element model—Part I. A scheme to detect and represent contacts in a system composed of many polyhedral blocks,

- in: International Journal of Rock Mechanics and Mining Sciences & Geomechanics Abstracts, Vol. 25, 1988, pp. 107–116. doi:10.1016/0148-9062(88)92293-0.
- [99] R. Hart, P. A. Cundall, J. Lemos, Formulation of a three-dimensional distinct element model—Part II. Mechanical calculations for motion and interaction of a system composed of many polyhedral blocks, in: International journal of rock mechanics and mining sciences & Geomechanics abstracts, Vol. 25, Elsevier, 1988, pp. 117–125. doi:10.1016/0148-9062(88)92294-2.
- [100] G. M. Roberti, F. Calvetti, Distinct element analysis of stone arches, Arch Bridges: History, Analysis, Assessment, Maintenance and Repair (1998) 181–186doi:doi.org/10.1201/9781003078494.
- [101] N. Kassotakis, V. Sarhosis, T. Forgàcs, K. Bagi, Discrete element modelling of multi-ring brickwork masonry arches, in: 13th Canadian Masonry Symposium, Newcastle University, 2017, p. 11.
- [102] P. Meriggi, G. de Felice, S. De Santis, F. Gobbin, A. Mordanova, B. Pantò, Distinct element modelling of masonry walls under out-of-plane seismic loading, International Journal of Architectural Heritage 13 (7) (2019) 1110–1123.
- [103] T. Michiels, R. Napolitano, S. Adriaenssens, B. Glisic, Comparison of thrust line analysis, limit state analysis and distinct element modeling to predict the collapse load and collapse mechanism of a rammed earth arch, Engineering Structures 148 (2017) 145–156. doi:10.1016/j.engstruct.2017.06.053.
- [104] ABAQUS Inc., Abaqus FEA (2020).  
URL <https://www.3ds.com/products-services/simulia/products/abaqus/>
- [105] Itasca Consulting Group Inc., 3DEC (2016).  
URL <https://www.itascacg.com/software/3dec>
- [106] J. Heyman, The stone skeleton, International Journal of Solids and Structures 2 (2) (1966) 249–279. doi:10.1016/0020-7683(66)90018-7.

- [107] P. Block, M. DeJong, J. Ochsendorf, As hangs the flexible line: Equilibrium of masonry arches, *Nexus Network Journal* 8 (2) (2006) 13–24. doi:10.1007/s00004-006-0015-9.
- [108] W. W. Lau, Equilibrium analysis of masonry domes, PhD Thesis, Massachusetts Institute of Technology (2006).  
URL <https://dspace.mit.edu/handle/1721.1/34984>
- [109] T. Michiels, S. Adriaenssens, Form-finding algorithm for masonry arches subjected to in-plane earthquake loading, *Computers & Structures* 195 (2018) 85–98. doi:10.1016/j.compstruc.2017.10.001.
- [110] D. O'Dwyer, Funicular analysis of masonry vaults, *Computers & Structures* 73 (1) (Oct. 1999). doi:10.1016/S0045-7949(98)00279-X.
- [111] P. Block, J. Ochsendorf, Thrust network analysis: A new methodology for three-dimensional equilibrium, *Journal of the International Association for Shell and Spatial Structures* 48 (3) (2007) 167–173, (ISSN: 1028-365X).
- [112] ABB, Product specification - IRB 4600, Tech. Rep. 3HAC032885-001, ABB Group, workspace 20D, version a7 (Dec. 2020).
- [113] A. Kaveh, The role of algebraic graph theory in structural mechanics, in: B. Topping, C. Mota Soares (Eds.), *Progress in Computational Structures Technology*, 1st Edition, Saxe-Coburg Publications, 2005, pp. 77–110, (ISBN: 978-1-874672-21-0).
- [114] A. Kaveh, H. Rahami, An efficient analysis of repetitive structures generated by graph products, *International Journal for Numerical Methods in Engineering* 84 (1) (2010) 108–126. doi:10.1002/nme.2893.
- [115] D. Rutten, Grasshopper (2007).  
URL <https://www.grasshopper3d.com/>
- [116] C. Preisinger, M. Heimrath, Karamba — A toolkit for parametric structural design, *Structural Engineering International* 24 (2) (2014) 217–221. doi:10.2749/101686614X13830790993483.

- [117] M. J. Turner, R. W. Clough, H. C. Martin, L. J. Topp, Stiffness and deflection analysis of complex structures, *Journal of the Aeronautical Sciences* 23 (9) (1956) 805–823. doi: 10.2514/8.3664.
- [118] R. Royles, A. W. Hendry, Model tests on masonry arches, *Proceedings of the Institution of Civil Engineers* 91 (2) (1991) 299–321. doi:10.1680/iicep.1991.14997.
- [119] C. Melbourne, P. Walker, Load tests to collapse of model brickwork masonry arches, in: *Proceedings of the 8th International Brick/Block Masonry Conference*, Dublin, Ireland, 1988, pp. 991–1002, (ISBN: 1-85166-265-0).
- [120] C. Melbourne, M. Gilbert, M. Wagstaff, The collapse behaviour of multispan brickwork arch bridges, *The Structural Engineer* 75 (17) (1997) 297–305, (ISSN: 1466-5123).
- [121] C. Melbourne, M. Gilbert, The behaviour of multi-ring brickwork bridges, *The Structural Engineer* 73 (1995) 39–47, (ISSN: 1466-5123).
- [122] M. Gilbert, C. C. Smith, J. Wang, Small and large-scale experimental studies of soil-arch interaction in masonry bridges, in: *5th International Conference on Arch Bridges*, Funchal, Madeira, 2007, pp. 381–388, (ISBN: 978-972-8692-31-5).
- [123] K. Towler, F. Sawko, Limit state behaviour of brickwork arches, in: *6th International Conference on Brick Masonry*, Rome, Italy, 1982, pp. 422–429.
- [124] G. Swift, L. Augustus-Nelson, C. Melbourne, M. Gilbert, Physical modelling of masonry arch bridges, in: *7th International Conference on Arch Bridges*, Split, Croatia, 2013, pp. 621–628, (ISBN: 978-953-7621-16-2).
- [125] Oatey, Oatey® Fix-It™ Stick Epoxy Putty (2020).  
URL <https://www.oatey.com/products/oatey-fixit-stick-epoxy-putty-1829259701>

# 5

## Cooperative Robotic Scaffold-Free (Dis)Assembly of Triangulated Space Frames Designed with Rigidity Theory

This chapter is primarily based on the following publication:

**Bruun, E. P. G.**, Adriaenssens, S., & Parascho, S. (2022). Structural rigidity theory applied to the scaffold-free (dis)assembly of space frames using cooperative robotics. *Automation in Construction*, 141, 104405. <https://doi.org/10.1016/j.autcon.2022.104405>

Contributor roles in publication:

- Bruun: Conceptualization, Methodology, Software, Validation, Investigation, Writing (Original Draft), Writing (Review and Editing), Visualization
- Parascho: Resources, Writing (Review and Editing), Supervision, Funding Acquisition
- Adriaenssens: Writing (Review and Editing), Supervision, Funding Acquisition

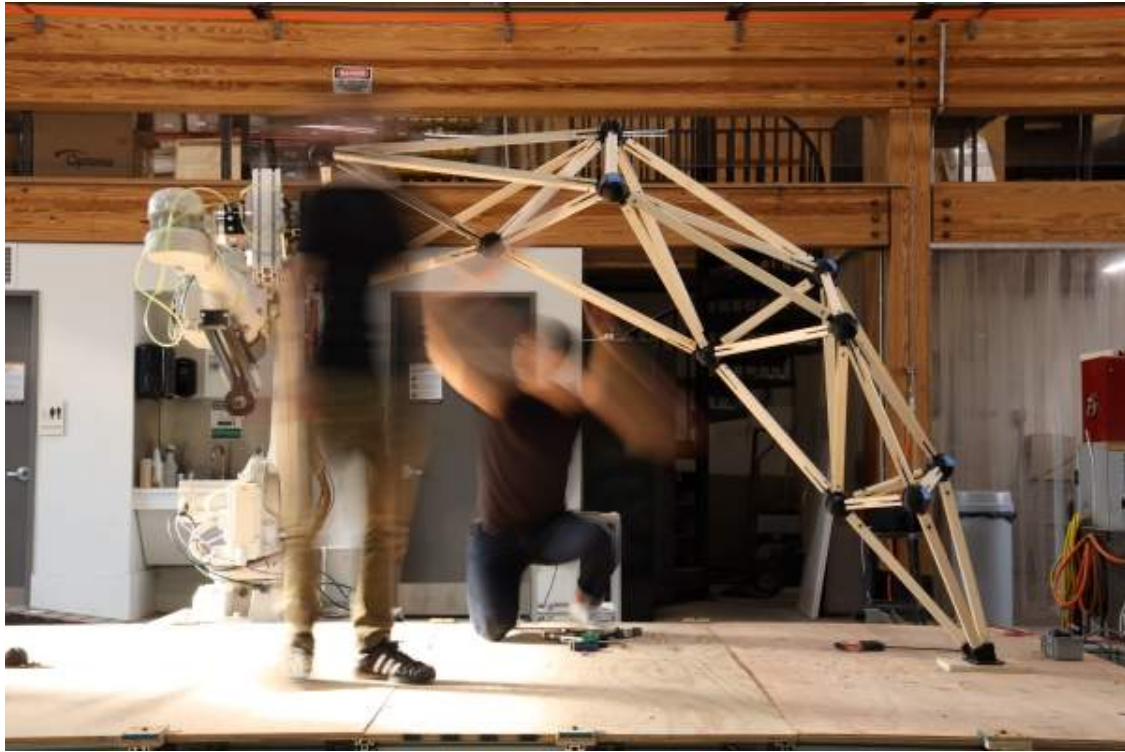


**Figure 5.1:** A snapshot from the cooperative robotic assembly of a space frame arch structure.

## Abstract

This chapter presents a fabrication-informed design method for triangulated space frame structures that remain stable during all phases of their robotic assembly and disassembly without requiring external scaffolding. A graph theoretic framework, based on rigidity theory, is developed to allow the structure, its support conditions, and the impact of robotic support constraints to be simultaneously represented in a single topological framework. The structural system is sequentially designed with an assembly logic based on Henneberg graph-construction steps, which are executed with two robots through a cooperative rigidity-preserving sequence. Ensuring planarity of the resulting graph during these construction steps is shown to lead to intrinsic disassembly potentials within the system. A graph-based algorithm is presented to locate, isolate and remove locally rigid tetrahedral cells formed in the structural system. This algorithm is then utilized to compute a rigidity-preserving robotic disassembly sequence. The method is demonstrated in the design of a space frame arch structure (shown in fig. 5.1) that is robotically (dis)assembled.

## 5.1 Introduction

Traditionally, architects and structural engineers place emphasis on the preliminary design of a structure in its finished state [1], but rarely account for the relationship between structural form and the resulting construction sequence that is necessary to reach this finished state. This can result in an expensive, time-consuming, or materially wasteful construction process. Construction costs can be substantial – for example, formwork amounts to about 40% of the total cost for reinforced concrete thin shells [2]. Looking at the other end of the building life-cycle, a structure is rarely designed with considerations for its efficient disassembly and potential reuse as a means to mitigate the large amount of waste construction activities currently contribute to landfill volumes [3]. Such a wasteful single-use design philosophy serves as a negative multiple on the high embodied energy associated with resource extraction and material processing requirements for building components [4]. Technological developments to improve construction efficiency and material usage can help address some of these environmental impacts. The challenge is that the Architecture, Engineering and Construction (AEC) industry lags other industries when it comes to leveraging contemporary automation techniques and the associated productivity and environmental benefits [5].

The motivation behind this research is thus to aid in addressing the waste generation and productivity gap in the construction industry [6], specifically when considering geometrically complex truss and space frame structures. This is accomplished through the development of a structural design framework for efficient construction using a cooperative robotic fabrication setup. Efficiency, in the context of fabrication, is herein defined as maintaining stability without requiring external formwork or scaffolding during all stages of assembly or disassembly. This framework thus addresses the AEC industry challenges by both improving construction productivity through automation, reducing construction waste by eliminating the need for temporary support material, and planning for disassembly of the structure. Planning for disassembly as a core consideration in the design process provides opportunities for future structural reconfiguration and reuse [7–9].

Industrial robots are applicable to architectural fabrication setups for discrete element structures due to their application versatility [10] and spatial precision in picking and placing material

[11]. They are also experiencing growing adoption in both industry and academic contexts [12] and are promising tools to tackle the AEC industry's lagging productivity and labor efficiency [13, 14]. This chapter presents a *fabrication-informed* design framework, which is defined as a framework where the structural design directly accounts for how the structure will be built and taken apart, in this case utilizing the capabilities of a robotic setup (specifically with respect to sequencing). This constitutes a departure from a more traditional linear approach to construction, where a robot would act as a generic tool at the end of the workflow to materialize a structure designed in a separate design phase. On the otherhand, a *fabrication-informed* framework specifically developed for a cooperative robotic setup, in this chapter incorporates the multiple complimentary functions possible when several robots are working together: either placing members (during assembly) or removing parts of the structure (during disassembly), while also supporting the structure in its temporary state [15].

The proposed design method utilizes a graph-theoretic approach, based on rigidity theory, to link cooperative robotic construction with structural topology. This approach allows for the design of structures that have intrinsic scaffold-free assembly and disassembly potentials built directly into their preliminary design formulation.

### 5.1.1 Chapter Organization

Section 5.2 begins with a literature review on cooperative robotic fabrication and graph theory for the analysis of structural rigidity, followed by a more detailed explanation in Section 5.3 of the specific concepts from rigidity theory that are necessary when representing bar and joint frameworks (i.e., trusses and space frames). Section 5.4 presents a topology-driven design method for structures that can be assembled with cooperating robots in a rigidity-preserving manner. Section 5.5 then presents a graph-based algorithm that is used to plan a rigidity-preserving cooperative robotic disassembly sequence for the same structure. The method is demonstrated in the design of a spanning wooden space frame arch structure, with a discussion of the results from its physical assembly and disassembly presented in Section 5.6. The chapter concludes in Section 5.7.

## 5.2 Literature Review

### 5.2.1 Cooperative Robotic Fabrication in Construction

In the AEC industry, industrial robotic arms were first applied to the construction of modular homes [16, 17] and then in single-purpose automation systems [18–21]. Since their first adoption, robotic systems have continued to improve their functionality in unstructured environments [22, 23], which has substantially improved their viability in the construction of structures with complex geometries [24].

Growth in the field of digital fabrication (dfab) saw the first large-scale explorations in an architectural context of robots applied to the construction of geometrically complex structures [25–27]. At the outset, robots were used to build prefabricated load-bearing but non-standardized undulating walls made of discrete volumetric elements [28–30], followed by the DFAB house [31] as an example of how digital design and robotic fabrication processes can be used to build different non-standardized components and assembled in a structure [32–34]. Yet despite these advancements, when specifically applied to the construction of discrete element structures, robotic fabrication is still predominantly utilized for the construction of vertical layer-based structures [28–30, 35–38]. A review of recent trends in multi-agent fabrication, applied in a collaborative (human-robot) or cooperative (robot-robot, cobot) framework, shows how multi-agent approaches can help to expand the feasible design space of robotic fabrication [39–41].

Maintaining stability and mitigating unwanted forces and deflections during construction can prove a significant challenge when using additive fabrication processes [42–44]. This can be a limitation to the design freedom of discrete element structures realized with robotic fabrication methods. One solution to the challenge of maintaining stability is to work with specially designed discrete elements that allow some level of interlocking to provide local stability during construction [45, 46]. Another approach is to utilize a cooperative robotic fabrication strategy (i.e., multiple robots working together to perform a task that cannot be performed with one robot alone), which can lead to new self-supporting construction processes, a concept proposed for space frame construction by Parascho [15, 47, 48]. In Parascho’s work, structural stability during construction was achieved without scaffolding by designing the structure specifically for fabrication using two robots sequenced in a cooperative manner. The robots take turns performing either

the function of: (1) picking up and accurately placing structural components, or (2) holding and providing temporary support over indefinite periods of time to a partially completed structure. These are tasks that a human would struggle with but are well-suited to a robotic agent. Thus, these structures were only realizable in a self-stable way (i.e., without external scaffolding) when explicitly leveraging the use of multiple robots.

The support/place approach has been used in a number of subsequent cooperative robotic fabrication projects to construct complex discrete element structural forms in a range of materials and scales. For example, the fabrication of non-planar timber modules, where cooperating robots were used as a way to minimize the need for scaffolding in the intermediate stages of fabrication [49]. Several geometrically complex spanning structures have also been constructed without scaffolding using a cooperative robotic strategy: a bifurcating arch structure built out of foam blocks [50], and a doubly-curved brick shell [51–53], and a branching tree structure [54]. In general, the trend of moving from single to multiple agents for collaborative processes increases the complexity of the relationship between fabrication sequence and structural design. It is thus necessary to develop a design framework that can handle the increasing complexity of setups with multiple robots working together.

### 5.2.2 Graph Theory and Structural Isomorphism

Designing a discrete element structure for stability during assembly and disassembly requires a numerical formulation that characterizes this objective. The goal is to integrate the fabrication sequence with the structural design, while considering the interaction of the multiple robotic agents without an overly prescriptive method that stifles geometric exploration and creativity in the preliminary design. These objectives are formulated here as a topological problem: relating the connection between the structural elements and the structural stability during construction, while taking into account the potential of utilizing robotic support.

A topological problem can be expressed as a graph,  $G = (V, E)$ , which is a discrete mathematical structure in  $\mathbb{R}^2$  made up of vertices,  $V$ , connected by edges,  $E$ , that represent pairwise relations between objects. The foundations of graph theory (i.e., the study of such structures) were laid by Euler in his solution to the *Seven Bridges of Königsberg* problem [55]. Graph theory

has since seen broader application in the study of topology and in applied science applications to model how objects are distributed and connected in complex systems including circuits [56, 57], elastic networks [58], and structures [59–61]. More recently, topological representations have also been used in geometric form-finding methods [62–64].

A graph is isomorphic to a physical system if it has a one-to-one mapping with the elements in the system it represents. Given such a representation, one can determine properties of the underlying system with graph theoretic approaches based only on topological information [65]. The general principle is that certain properties of the graph represent the intrinsic physical behavior of the system it represents. Isomorphic graphs have thus been used to show parallels in the analysis and formulation of a broad class of physical systems such as: trusses, dynamic mass-spring-damper oscillator systems, and planetary gear systems [65–67]. In the context of bar and joint frameworks (i.e., trusses and space frames), this relationship between a graph and its isomorphic structure can be used to compute force and displacement quantities [66, 68, 69] or generic properties such as rigidity and stability [65].

### 5.2.3 Infinitesimal Rigidity and the Laman Count Condition

For a bar and joint framework, a necessary condition for infinitesimal rigidity was first formulated by Maxwell as a counting rule relating the number of nodes,  $v$ , to the number of members,  $e$ , in the framework. A structure needs a minimum of  $e = 2v - 3$  members in  $\mathbb{R}^2$ , and a minimum of  $e = 3v - 6$  members in  $\mathbb{R}^3$  to be infinitesimally rigid [70]. An infinitesimally rigid structure is one where every infinitesimal motion is a Euclidean one (i.e., a rigid body motion); a structure is infinitesimally rigid iff it is statically rigid, meaning that every equilibrium load has a resolution [71]. The relationship between the number of nodes and members was later refined by Calladine to characterize the number of mechanisms present in a framework [72, 73]. However, the overall Maxwell count condition is a necessary, but not sufficient, condition for infinitesimal rigidity. This is demonstrated with the two trusses in Figure 5.2, where both satisfy the count condition but only the right one is infinitesimally rigid. Thus, a more generalized approach, based on rigidity theory (a branch of graph theory), is necessary to determine if a bar and joint framework is rigid based on the topology of its isomorphic graph.

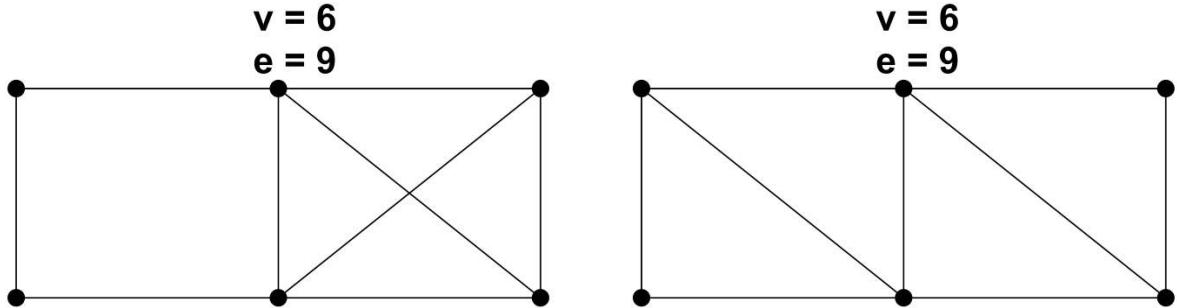


**Figure 5.2:** Two trusses that both satisfy the planar Maxwell count condition but only the right is infinitesimally rigid.

If for a graph,  $G = (V, E)$ , where the number of edges is  $|E| = 2|V| - 3$ , every subgraph,  $G' = (V', E')$ , satisfies the count condition,  $|E'| \leq 2|V'| - 3$ , then the graph is minimally rigid (i.e., infinitesimally rigid with the least amount of edges possible). Theorem 5.6 of Laman's paper [74] proved that this condition is not only necessary, but also sufficient, for a graph to be generically minimally rigid in the plane. The term *generic*, in reference to rigidity, refers to a graph that has at least one isomorphic realization (i.e., a specific mapping of vertices to physical nodes corresponding to a truss structure) that is statically rigid [71]. This theorem, when applied to the cases shown in Figure 5.2, correctly identifies the 6-noded truss on the right as statically rigid with the minimum required 9 members. A sub-graph counting condition, with  $|E'| \leq 3|V'| - 6$  instead, can also be used to determine if a graph is generically minimally rigid with respect to realizations in  $\mathbb{R}^3$ . These principles can be used to build generically rigid graphs, which thus have at least one isomorphic realization as a space frame in  $\mathbb{R}^3$  that is isostatic (i.e., statically rigid and infinitesimally rigid). This procedure, and certain caveats, are further explained in Section 5.3.

### 5.2.4 Research Contributions

This research extends past work on the scaffold-free cooperative robotic fabrication of space frames [15] by redefining the design process and assembly logic through a novel graph theoretic framework based on rigidity theory. A spatial structure is represented as its isomorphic graph [65], where the structural topology and influence of robotic support is simultaneously evaluated from the perspective of preserving rigidity in the graph. The topology-driven design method

developed using this framework is able to unify the generation of a space frame geometry with the criteria that the resulting structure has a feasible scaffold-free assembly and disassembly sequence. The design method is also considered *fabrication-informed* since the resulting structure is directly designed based on what is possible when sequencing two robots in a cooperative manner. The following is a summary of the main contributions of the research presented in this chapter:

- Presentation of the isomorphic *stability graph* as a unified framework to represent a structure and its supports, and the impact of robotic support on the rigidity of a graph.
- Recontextualization of an existing cooperative robotic assembly sequence for space frames [15] through the lens of rigidity-preserving Henneberg assembly steps used for the mathematical construction of rigid graphs.
- Development of a sequential topology-driven design method that links physical assembly and disassembly with the properties of graph planarity and minimal rigidity. These properties, resulting in a structure comprised of locally rigid tetrahedral cells, are used to guarantee that a scaffold-free assembly (member-by-member) and disassembly (cell-by-cell) sequence exist for the structure.
- Demonstration of the proposed method in the design of a space frame arch structure, and implementation of a cooperative robotic sequence for both its scaffold-free assembly and disassembly.

### 5.3 Graph Representation for Space Frame Structures

This section expands the general principles of rigidity theory and structural isomorphism introduced in Sections 5.2.2 and 5.2.3 with specific concepts that are required to represent a space frame structure as a graph. This representation forms the basis for the design method that guarantees a rigidity-preserving assembly and disassembly sequence. The following topics are covered: Henneberg assembly steps to build generic minimally rigid graphs isomorphic to 3D bar and joint frameworks (section 5.3.1), representing a minimally rigid tetrahedral building block (or cell)

as a graph ([section 5.3.2](#)), and accounting for structural supports and evaluating their impact on rigidity through a stability graph representation ([section 5.3.3](#)).

The terms *vertex* and *edge* are used when referring to a graph, which is a representation that lives in  $\mathbb{R}^2$ , and *node* and *element* are used when referring to an *realization* or *physical embedding* (used interchangeably) of the graph in  $\mathbb{R}^2$  (i.e., a truss) or  $\mathbb{R}^3$  (i.e., a space frame). The term *rigidity* will also henceforth be used to refer to *generic infinitesimal rigidity* unless noted otherwise.

### 5.3.1 Constructing Rigid Graphs: Henneberg Assembly Steps

While the Laman condition provides a definitive way to check rigidity in the plane ( $\mathbb{R}^2$ ), its naïve algorithmic implementation results in an exponential time algorithm [[65](#)]. Modern algorithms exist that reduce the complexity of verifying minimal rigidity to polynomial [[75](#), [76](#)], quadratic [[77](#), [78](#)], or even sub-quadratic [[79](#)] time. However, these algorithms can be complex to implement. But rigidity can for large and complex graphs be more easily checked through a particular graph's sequential assembly sequence (if this information is available), since every minimally rigid graph can be built up starting from a single edge using only a simple set of rules. This process is named after Henneberg, who first introduced the idea of preserving rigidity in the plane by sequentially aggregating a low-valent vertex to the existing graph [[80](#)]. Thus, if a larger graph is found to be the result of a series of rigidity-preserving Henneberg steps then by inductive reasoning it is guaranteed to be rigid itself.

Extending this concept to graphs embedded in space ( $\mathbb{R}^3$ ), starting from a  $C_3$  graph (i.e., 3-vertex cycle) with non-collinear embedding, every minimally rigid graph can be built up through a sequence of the following three Henneberg assembly steps [[71](#)], illustrated in [Figure 5.3](#):

Type 1: (i) add a new vertex, (ii) connect the new vertex to any 3 vertices in the graph.

Type 2: (i) delete any edge, (ii) add a new vertex, (iii) connect the new vertex to the 2 vertices incident to the deleted edge, (iv) connect the new vertex to any 2 other vertices in the graph.

Type 3a: (i) delete any 2 edges, (ii) add a new vertex, (iii) connect the new vertex to the 4 vertices incident to the deleted edges, (iv) connect the vertex to any other vertex in the graph.

Type 3b: (i) delete any 2 edges, (ii) add a new vertex, (iii) connect the new vertex to the 3 vertices incident to the deleted edges, (iv) connect the vertex to any 2 other vertices in the graph.

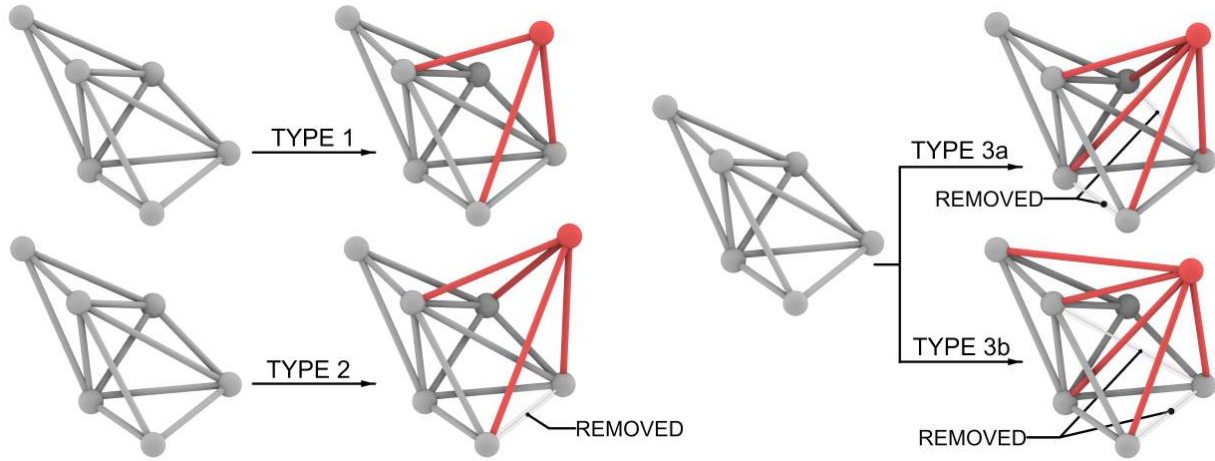


**Figure 5.3:** Henneberg assembly steps for the construction of a graph with a generic rigid embedding in space ( $\mathbb{R}^3$ )

Only after executing a Type 1 or Type 2 step is the resulting graph guaranteed to be a generically minimally rigid (i.e., it has at least one possible rigid realization in space). A Type 3 step has been shown to result in a graph without a rigid realization in some special cases [71, 81, 82]. The failure of Type 3 steps to definitively preserve rigidity is related to the fact that the Laman condition is a necessary, but not sufficient condition, for a minimally rigid graph embedded in space, as shown by the *double banana* counter-example in the literature [83, 84]. Providing a combinatorial characterization of rigidity in space, as exists in the plane, is a major open problem in graph theory [85]. This issue can be mitigated through imposing additional topological and geometric constraints on the resulting physical structure that the graph is isomorphic to. For example, explicitly avoiding the formation of an axis of rotation in the *double banana* structure. Another way to preserve the property of rigidity in the overall graph is to construct the graph through the aggregation of smaller sub-graphs (referred to here as cells) with proven rigid realizations.

Thus, the design method presented in this chapter is based on a strictly Type 1 assembly logic, which is guaranteed to preserve rigidity. But using Type 2 or 3 Henneberg steps for assembling rigid structures is a possible foundation for the development of bi-directional (i.e., both adding and removing elements) fabrication sequences for more topologically varied structures.

### 5.3.2 The Tetrahedral Cell as a Rigid Building Block

The tetrahedron, which can be represented with a skeletal framework of 4 nodes and 6 elements, is the simplest platonic solid and corresponds to a minimally rigid cell from which larger rigid structures can be assembled. Due to their geometric simplicity, they are used as the fundamental building block for space frame structures designed to be assembled and disassembled with the cooperative robotic method described in this chapter. More complex rigid cells, composed of more vertices, could also be used in this method, but their stability-preserving assembly feasibility is contingent on the number of robotic agents available in the setup.

The graph representing the topology of a tetrahedron is minimally rigid, with generic rigid realizations in  $\mathbb{R}^3$  under the geometric constraint that no three nodes are collinear and that all four nodes are not coplanar [71]. Based on inductive reasoning, these constraints, when coupled with the Laman count condition, are sufficient to guarantee rigidity in a structure that is built up from a collection of rigid tetrahedral cells. [Figure 5.4](#) illustrates the isomorphic graph representation of such a cell as a planar realization (i.e., no edges crossing) of the  $K_4$  graph, which is built from,  $G_0 = C_3$ , with a Henneberg Type 1 step:  $G_1 = (V_0 \cup \{3\}, E_0 \cup \{e_2, e_3, e_4\})$ . The resulting graph satisfies the Laman count requirements, has a valid Henneberg construction sequence characterization, and known rigid realizations in  $\mathbb{R}^3$  under the geometric constraints mentioned above. The representation of a structure without support conditions, as in [Figure 5.4](#), is defined as a rigidity graph.

Planarity is another important property of the graph of the tetrahedral cell, which will be discussed in the context of the assembly logic ([section 5.4.4](#)) and the disassembly sequence algorithm ([section 5.5.2](#)).

### 5.3.3 Structural Supports Represented in a Graph

When representing a structure including its support conditions, its isomorphic graph is herein defined as a stability graph. For example, a structure might be rigid based on its topology but still undergo rigid-body motion based on its support conditions. One of the strengths of a topological approach is that the same methodology to assess rigidity, can be extended to evaluate stability based on the degrees of freedom (DOFs) being constrained at vertices in the graph. Thus, if the

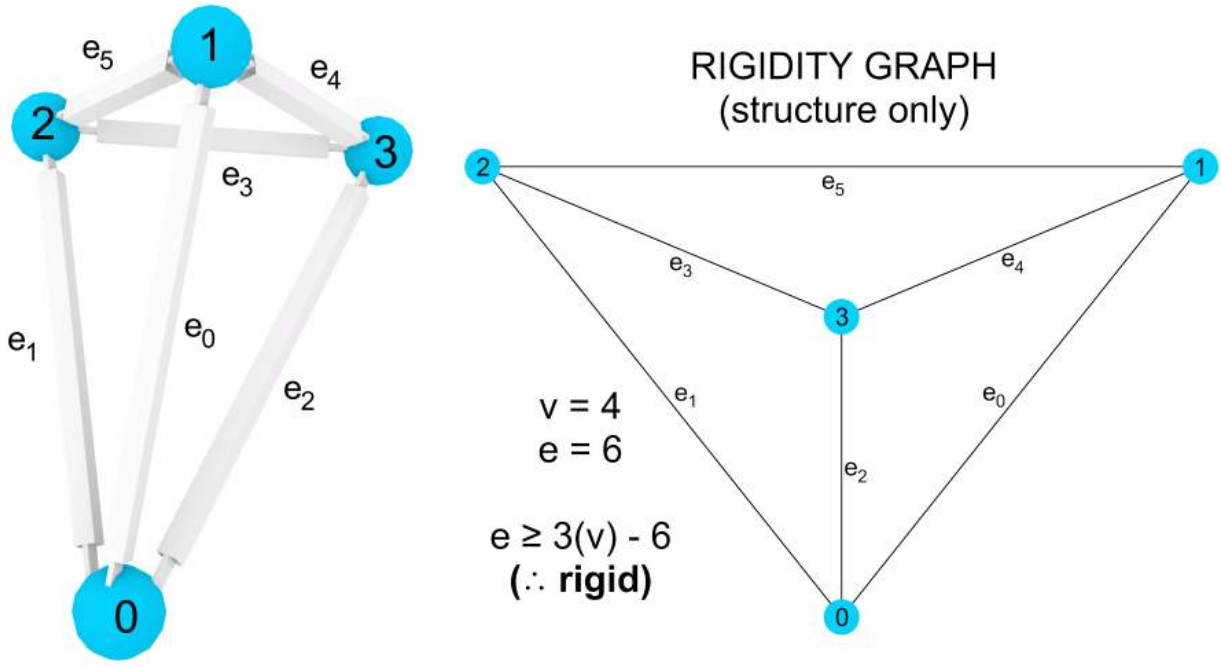


**Figure 5.4:** Rigidity graph (right) and rigid realization (left) of a minimally rigid tetrahedral cell ( $|V| = 4$ ,  $|E| = 6$ ).

stability graph is found to be rigid (i.e., through the Laman count and Henneberg sequence characterization), then the structure it is isomorphic to is stable. This process is described for trusses ( $\mathbb{R}^2$ ) in [65] and extended to space frames ( $\mathbb{R}^3$ ) in this chapter.

A stability graph is built by representing the DOFs in the system as additional graph vertices, which - for a graph realized in  $\mathbb{R}^3$ - are the three translations in Euclidean space. Edges are then added between these support vertices and the vertices that represent structural nodes restrained in translation by a support. Figure 5.5 shows two different support conditions: (1) a single pin at the base of the structure, and (2) a base pin, roller, and directional pin (X & Z). Condition (1) is unstable as the structure, one rigid tetrahedral cell, is free to rotate about its base. This rigid body motion can equivalently be proved by analysis on the graph representation: each supported DOF is shown as an edge in the graph,  $E_{support} = \{a, b, c\}$ , hence the global count for this graph is now 12, which does not satisfy the required global Laman count, 15. Condition (2) on the other hand is stable, with  $E_{support} = \{a, b, c, d, e, f\}$ , hence the total count is 15, which satisfies the global Laman count, 15. But for a stability graph to be generically rigid it must also satisfy certain constraints when considering realizations in  $\mathbb{R}^3$ , similar to how the rigidity graph of the tetra-

hedral cell must satisfy certain geometric constraints as discussed in [Section 5.3.2](#). If adjacent support edges are not independent this has the effect of removing a supported DOF from the system and destabilizing it. For example, in [Figure 5.5](#), if edges  $\{e, f\}$  (i.e.,  $(z, 2)$  and  $(z, 3)$ ) represent supports that are in the axis of member  $(2, 3)$  (i.e., the support forces are collinear), then the system would not be stable. Additionally, a minimum of three nodes in the structure must at any time have at least one DOF constrained, to prevent an axis of rotation forming. This result corresponds to the principles of statics, where every equilibrium load can only be resolved through the global equations of force and moment equilibrium when precisely 6 independent support reactions are acting in at least one plane.

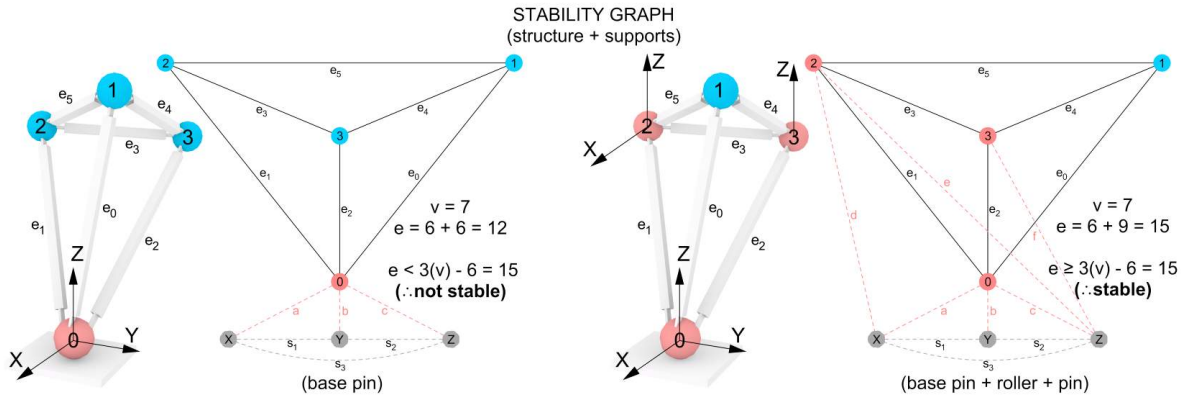


**Figure 5.5:** Stability graphs representing two different sets of support conditions on the same minimally rigid space frame structure. Condition 1 (left) is unstable since  $|E| = 12 < 3|V| - 6$ , while condition 2 (right) is stable since  $|E| = 15 \geq 3|V| - 6$ , a Henneberg assembly sequence exists, and the geometric constraints specified in Sections 5.3.2 and 5.3.3 are satisfied.

Using this topological representation, unifying structure and support, the structure can be said to be stable if its stability graph is rigid. Minimal rigidity of the stability graph is verified through the same process as the for the graph of the structure, by showing that there exists a sequence,  $S$ , of Henneberg Type 1 or 2 steps ( $h_1$  or  $h_2$ ) to build the final graph,  $G_n$ , starting from a rigid graph,  $G_0 = (V_0, E_0)$ :

$$\exists S\{H_1 \dots H_n\} \text{ s.t. } G_0 \rightarrow G_n \mid H \in \{h_1, h_2\} \quad (5.1)$$

There may exist numerous valid Henneberg sequences,  $S$ . The stability graph,  $G_3$ , referring to support condition (2) in Figure 5.5, can be built from the starting graph,  $G_0$ , referring to the graph

of the tetrahedral cell in [Figure 5.4](#), through one such sequence:

- $H_1 = h_1: G_1 = (V_0 \cup \{Z\}, E_0 \cup \{c, e, f\})$
- $H_2 = h_1: G_2 = (V_1 \cup \{Y\}, E_1 \cup \{b, s_2, (Y, 2)\})$
- $H_3 = h_2: G_3 = (V_2 \cup \{X\}, E_2 \setminus (Y, 2) \wedge E_2 \cup \{a, d, s_1, s_3\})$

## 5.4 Designing a Space Frame Structure for Cooperative Robotic Assembly

In this section, principles of graph rigidity, and their characterization through Henneberg assembly steps, are implemented to develop a topology-driven design method for the scaffold-free construction of space frame structures. The main objective is to design the structure explicitly considering a cooperative fabrication sequence with two robots [15]. Thus, the structure's stability graph must remain rigid throughout the full assembly process while planarity must be preserved in the graph isomorphic to the structure. The property of planarity is shown to result in the formation of locally rigid cells arranged in a linear manner in the overall structure, which will be crucial in ensuring that a scaffold-free disassembly sequence is also embedded in the structural design. Thus, the design method is introduced through the lens of efficient rigidity-preserving assembly, but has explicit considerations for disassembly in its formulation.

### 5.4.1 Cooperative Robotic Assembly Strategy

The structural design method is based on a cooperative fabrication sequence with two robots ( $R_1$  and  $R_2$ ) that alternate their role in placing members and providing temporary support to the structure, as described in [15, p.74-77]. After placing a member, a robot is left supporting the structure, while the other robot is free to release the structure and retrieve and add the following member.

The axial forces in individual members are resolved at concurrent points at the structural joints, illustrated for a system of three members in [Figure 5.6](#). There is only one possible physical arrangement of members at the joint level for each spatial mapping of the vertices. As a

result, there exists a true one-to-one relation between the graph and the load path in the realized structure. A translational restraint shown as an edge in the graph, also represents the resulting force equilibrium in this pin-joint when a support is acting on it. This relation only exists for an idealized bar and joint structure where axial forces are resolved at concurrent points, because a graph representation only carries information about the connection topology. Capturing more complex equilibrium conditions, such as moments in the connections, requires information about offsets and distances not present in a topological representation. For example, the joint-level load paths cannot be fully characterized in a reciprocal frame style connection system where numerous relative member placements are possible for the same joint (as in previous work [47, 48]).

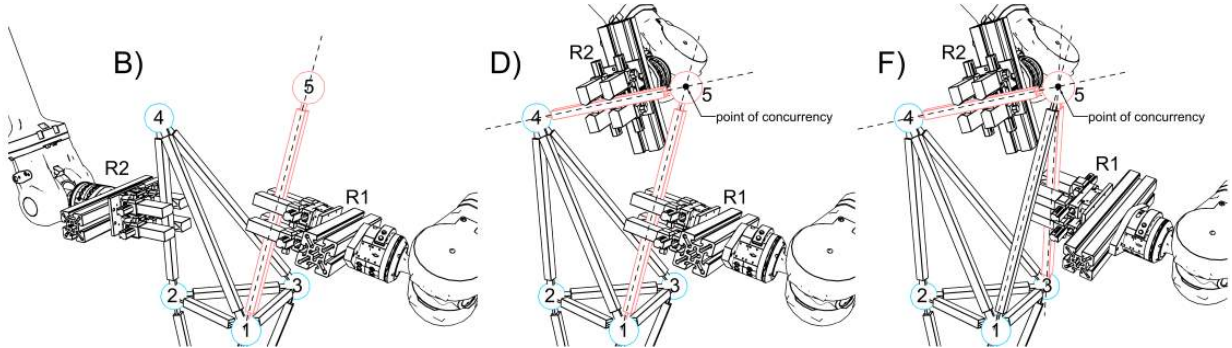


**Figure 5.6:** Cooperative robotic sequence to execute a 3-member rigidity-preserving Henneberg Type 1 step for members with concurrent lines of action at the added node. Stage B (left): R1 = Place, R2 = Support; Stage D (middle): R1 = Support, R2 = Place; Stage F (right): R1 = Place, R2 = Support (adapted [15, fig. 3.19])

### 5.4.2 Robotic Support and Henneberg Assembly

In a structure constructed from concurrent members, according to a cooperative assembly strategy, the action of a temporary robotic support on the structure can be represented in the stability graph. The two vertices incident to the member a robot is supporting, are connected to the three graph vertices representing the translational constraints using the methodology described in [Section 5.3.3](#) and shown during the execution of a Henneberg Type 1 step in [Figure 5.7](#). The robot thus affects the property of rigidity in the stability graph by altering the edge counts in the overall graph and its subgraphs.

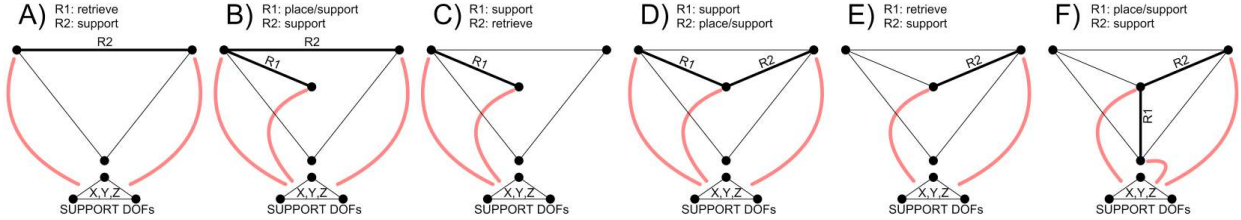


**Figure 5.7:** The stability graphs at each of the 6 stages (A-F) for a Henneberg Type 1 step executed with two robots ( $R_1$  and  $R_2$ ) either supporting a member or retrieving the next member to add to the structure. Each edge highlighted in red represents three independent edges connecting a supported vertex in the structure to each of the three vertices representing the  $X$ ,  $Y$ ,  $Z$  translation constraints.

However, from the perspective of rigidity, despite utilizing the support provided by two robots during fabrication, there are limitations to the feasible sequence of adding members. For example, in a situation where elements are built off an existing rigid structure, but are placed without being incident to the same end node: one member can initially be placed and supported by either robot, but would later become unstable since it is only connected at one pinned end once the robot releases it to retrieve the next element. In the graph representation, this can be verified with a failure to achieve the global Laman count. One way to overcome this failure, is to add new members to the structure in mutually reinforcing ways (i.e., incident to the same new node) so that they assemble towards states of rigidity in the graph isomorphic to the structure.

Building towards stages of rigidity can be evaluated through the lens of Henneberg assembly steps. A Type 1 step requires an additional vertex to be connected to the graph at three distinct vertices to maintain rigidity. In an applied context, during physical construction, such a step cannot happen instantaneously, but is instead executed through the sequential placement of three separate members. This process is shown in [Figure 5.7](#) through the stability graph representation at each of the 6 stages (placing and retrieving members) required to execute a full Henneberg sequence with two robots. The sequence starts with a generic rigid structure supported by a robot in stage A; for clarity the graph of the rest of the structure and its non-robotic foundation supports are not shown in [Figure 5.7](#). Each vertex that is supported by a robot at a stage is connected to the vertices representing the  $X$ ,  $Y$ ,  $Z$  translational support DOFs. During the first two member placements (stages B and D), there must be at least one robot supporting the partially completed Henneberg structure (i.e., the sub-structure of members connecting to the newly added node) for

it to be rigid. Once the third and final member in the sequence is placed (stage F), the Henneberg step is complete, and the graph of the structure (in this case representing a simple tetrahedral cell) becomes minimally rigid without requiring robotic support. The aggregation process can then be repeated with the addition of another vertex to the existing graph, which is realized through the execution of another 3-member cooperative sequence with two robots. To compliment the graph representation in [Figure 5.7](#), the physical representation of such a sequence is illustrated in [Figure 5.6](#) for the member placement stages (B, D, F) in the process of adding a node to an existing rigid structure. Depending upon the type of external non-robotic foundation support, a robotic support to the structure might still be required to guarantee stability of the overall structure, even at the completion of a Henneberg step. It is possible for the rigidity graph to be rigid while the stability graph is not, as is the case for a structure supported on a single external base pin (i.e., Condition 1 in [Figure 5.5](#)).

In [Section 5.3.3](#) it was explained that a total of 6 DOFs, represented as 6 edges in the graph, must be constrained on a minimum of 3 vertices (i.e., embedded as a plane) for the stability graph to remain rigid. This requirement is satisfied in a 3-member Henneberg sequence as there is always at least one robot supporting the structure. Since the robot constrains the movement of two vertices incident to the member it supports, this provides more support than is strictly necessary for the minimally rigid criteria. For example, the stability graph in [Figure 5.5](#) has 3 additional edges,  $E = \{(Y, 2), (Y, 3), (X, 3)\}$ , if member  $e_3$  was supported by a robot (i.e.,  $V_{support} = \{2, 3\}$ ). But although such a structure would result in an over-constrained system (i.e., statically indeterminate), this over-constraining does not negatively impact the stability in the structure. Adding edges representing supports to a minimally rigid stability graph does not undermine its underlying property of rigidity; if a structure is stable under certain set of support conditions, additional supports only add to the structural redundancy of the system.

### 5.4.3 Assembly Logic

A structure is designed sequentially to reflect its order of assembly, where each new node is connected back to three existing nodes in the structure, as per a Henneberg Type 1 step, forming a triangulated configuration as in [15, pg. 52-53]. This assembly logic has been recontextualized for the use of two robots, as shown in [Figure 5.6](#).

tualized and developed in this chapter through the graph-based analysis approach described in Sections 5.4.1 and 5.4.2, to show that the properties of rigidity can be preserved at both the local and global level when utilizing a cooperative robotic place/support strategy as illustrated in Figure 5.6. However, the assembly logic used here differs from previous work [15] as a new node in the structure is further specified to always connect to three nodes on the most recently formed tetrahedral cell. This approach guarantees that a rigid tetrahedral cell is formed after each 3-member aggregation phase. Thus, each added member is guaranteed to be part of at least one rigid cell. This is equivalent to specifying that a new vertex must be added to the current graph such that the resulting graph has a 1) planar realization (i.e., can be drawn with no edges crossings), and 2) linear partial order (i.e., a collection of rigid cells in series).

The process of adding new nodes to three nodes on the most recently completed cell in the existing structure is not strictly necessary when just considering rigidity during assembly. But this aggregation logic becomes important when planning for a disassembly sequence as it guarantees the topological uniformity of the graph. The property of planarity and the linear partial order in the nested graph that is produced when utilizing the this assembly logic guarantees that an efficient stability-preserving cooperative robotic sequence can later be found for disassembly. Each member is guaranteed to be part of at least one rigid cell, which allows for an algorithmic process to locate, isolate, and remove these self-contained rigid cells during disassembly. This algorithm is explained in detail in Section 5.5.2. Thus, a design process utilizing the assembly logic described in this section is considered fabrication-informed as it has considerations for not just efficient assembly, but also for ease of disassembly, built directly into its formulation.

In contrast, if an assembly logic based on connecting to any three nodes is used, the structure can still be assembled without requiring support but is now not guaranteed to be composed of rigid cells. This case is illustrated in Figure 5.8, where node 5 is connected to the existing structure with  $E = \{(0, 5), (3, 4), (4, 5)\}$ . The result is a supergraph of the utility graph (UG), and is therefore non-planar [86]. It is possible to find two  $K_4$  subgraphs, which correspond to the existence of two tetrahedral cells,  $C_1$  and  $C_2$ , in the original structure. But there is no such subgraph formed with the new edges in the graph, so no valid cell is formed when adding these members. A cell can be formed given the existing configuration by adding a single edge,  $e = (0, 4)$ , or by swapping  $e = (0, 5)$  for  $e = (1, 5)$  as can be observed in Figure 5.8. But in general, if such an

assembly logic, allowing connection to any three nodes, is applied for a large structure with numerous assembly steps, there is no guarantee that the resulting topology can be characterized as a collection of elements that form tetrahedral cells.

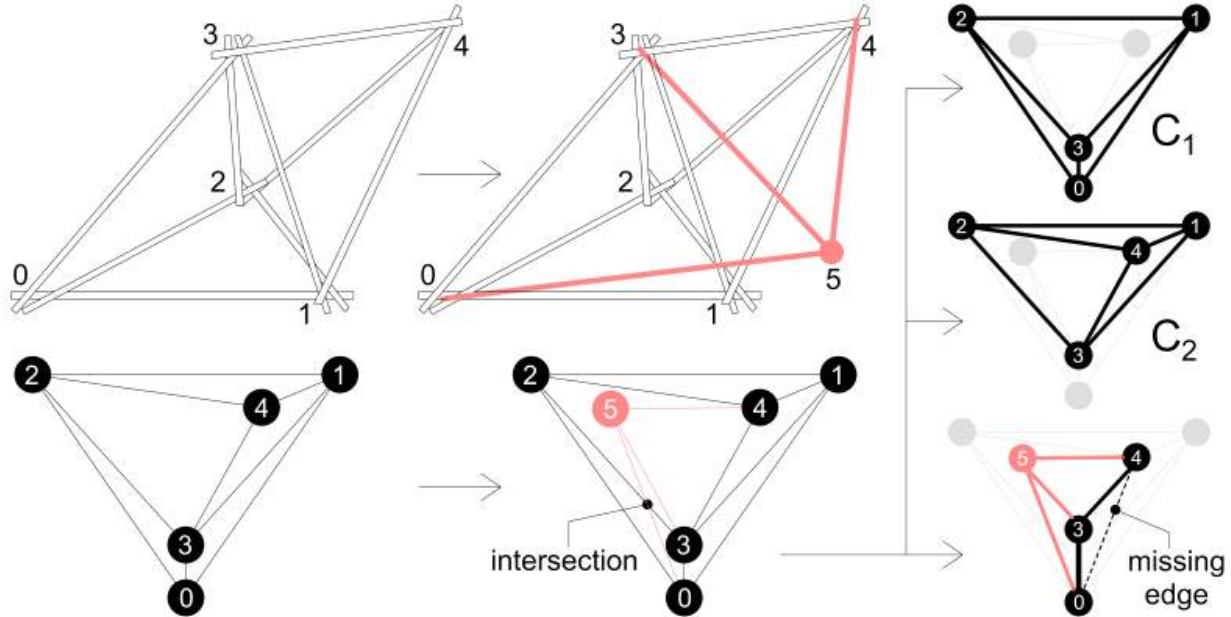


**Figure 5.8:** An assembly approach where a new node can connect to any three nodes results in a non-planar graph where a subgraph isomorphic to a tetrahedral rigid cell is not formed.

#### 5.4.4 Design Method

The cooperative robotic support strategy and structural assembly logic can be implemented to design space frame structures that can be efficiently assembled and disassembled. The following steps are a schematic implementation of the concepts discussed thus far in this chapter, which are meant to guide the preliminary design of such structures:

1. Specify a curve, or a collection of curves, that represent the overall target form or backbone of the target structure.
2. Choose the target number of nodes that the structure is to be built from.
3. Specify geometric constraints on the realization of graph vertices. For example, those necessary in the formation of rigid realizations of tetrahedral cells ([section 5.3.2](#)).

4. Connect a new vertex to a region of the existing graph ensuring a tetrahedral cell topology while maintaining the property of planarity.
5. Calculate the physical realization of the new graph vertex on the basis of the geometric constraints specified.

Steps 4 and 5 occur in a loop executed as many times as specified in Step 3: sequentially updating the current isomorphic graph as each new vertex is added based on the physical realization of the structure from the previous stage. Step 4 is equivalent to assigning a valid topological configuration in the graph representation, and Step 5 maps this new graph vertex to a feasible structural node (i.e., physical embedding in space) -  $N : V \rightarrow \mathbb{R}^3$  s.t.  $n_a \neq n_b \mid (a, b) \in G(E)$ .

As per the assembly logic introduced in [Section 5.4.3](#), each new vertex only has three potential regions it can connect to, with each corresponding to a face on the most recently completed tetrahedral cell in the structure. Once the region is selected, the new vertex is connected to each of the three adjacent vertices with an edge, as per a Henneberg Type 1 step, to preserve rigidity. This process can be thought of as building a sequential nesting graph of vertices that connect to form a series of tetrahedral subgraphs.

Choosing which of the three regions to connect to is determined by calculating which face in the most recently calculated cell has a normal vector closest to the tangent vector at a point on the target geometry curve closest to the cell. The process for selecting this face and choosing the region on the graph to add the next vertex to is shown schematically for three sequential iterations in [Figure 5.9](#). The three potential regions in each iteration, and their corresponding faces on the structure, are shown in red, green, or blue on both the planar graph and its resulting embedding. In [Figure 5.9](#), the selected region and corresponding face to build from are shown in red; the vertices in the graph are shifted to make this region larger for clarity. The mapping of this new vertex is then calculated in Step 5 so that no new resulting member is co-linear with an existing member in the structure, and satisfying any remaining geometric constraints specified in Step 3.

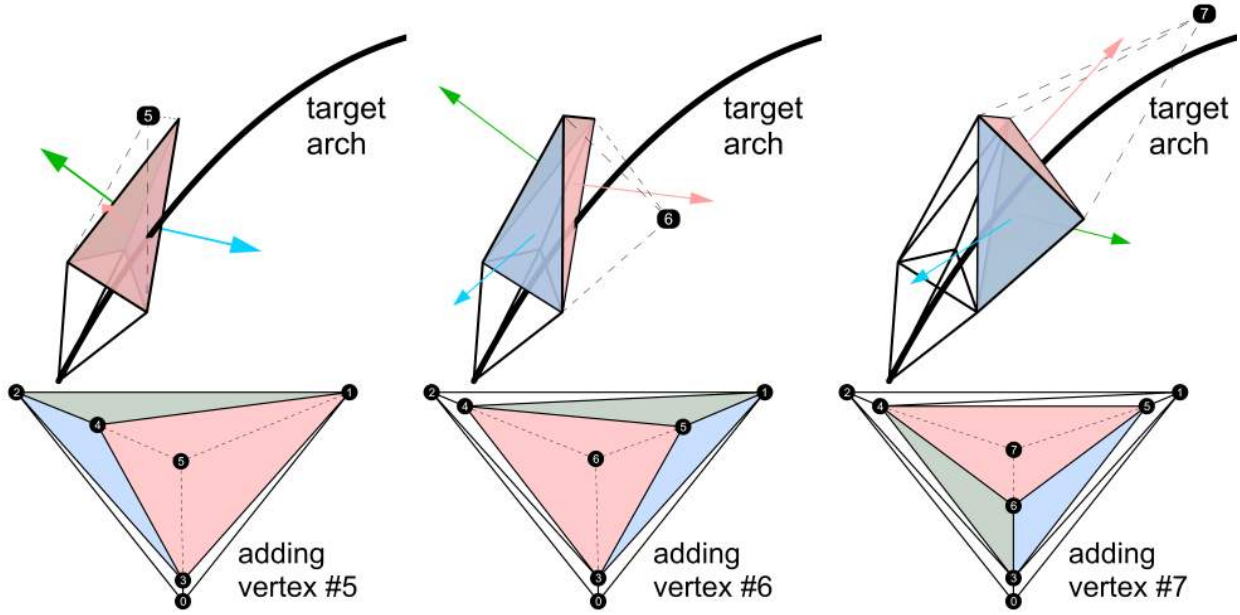


**Figure 5.9:** The sequential design of a structure and its realization in space (top) corresponds to the sequential addition of vertices to the existing graph (bottom), forming a topology that can be characterized as a series of nested tetrahedral cells preserving the property of planarity in the overall graph at each aggregation phase.

### 5.4.5 Design of a Space Frame Arch Structure

To test the implementation of the method, a design was performed with an input backbone curve of an arch, pin supported at its 2 extremities, with a final span of 3m and a central height of 1.6m. An arch is chosen as a structural system since its sequential fabrication requires working from one end to the other, which highlights the stability preserving nature of the fabrication method. If such a spanning structure was built using a more typical fabrication method (i.e., element-by-element construction starting from either end and meeting at the crown) it would be neither globally or locally stable during construction without external scaffolding. Using the assembly logic and design method described in Sections 5.4.3 and 5.4.4 respectively, an isomorphic planar graph is sequentially constructed. The graph ( $|V| = 17$ ,  $|E| = 45$ ) corresponding to the finished structure is shown in Figure 5.10, with the corresponding vertex connectivity and embeddings in  $\mathbb{R}^3$  that were computed at each stage summarized in Appendix A, Table B.1

The only geometric constraint, in addition to those necessary for rigid realizations of tetrahedral cells outlined in Section 5.3.2, is that the vertex mapping function results in nodes satisfying the following:  $0.3m \leq |n_a - n_b| \leq 1.2m \mid (a, b) \in G(E)$ . Individual members must be

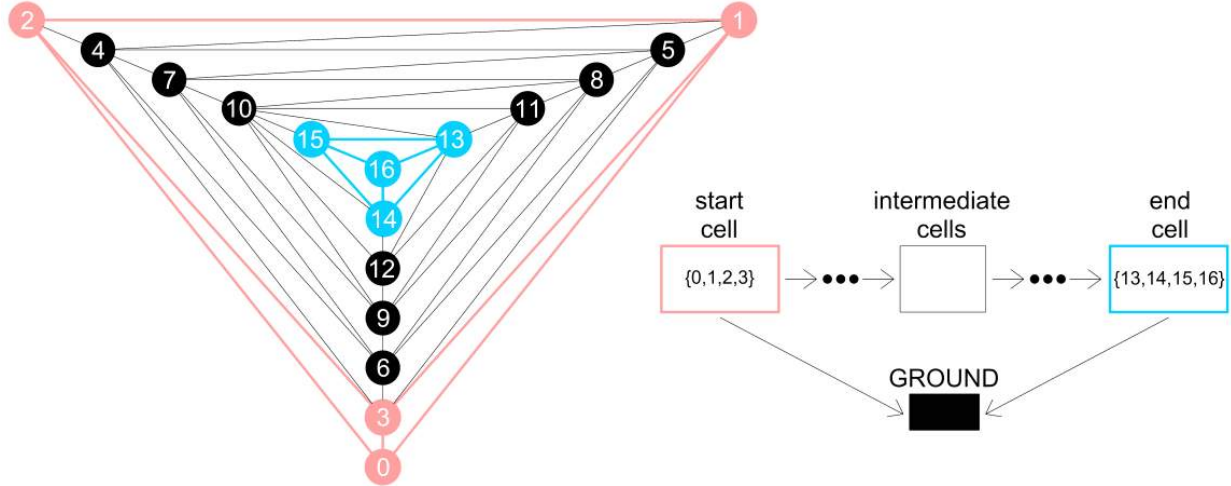


**Figure 5.10:** The planar graph (left) isomorphic to the designed space frame structure, represented as a linear partial order of rigid tetrahedral cells (right).

longer than the width of the fingers spacing on robotic gripper to allow for an adequate gripping surface, but not exceed the length of the available construction material stock. Additional constraints based on optimization criteria (i.e., minimizing forces and displacements in the structure) can be used to further modify the mapping function to control of the design of the final structure. These were not implemented since the focus at this stage of the research is only linking topology and stability with the execution of a cooperative fabrication sequence.

The resulting arch structure starts and ends with the cells defined by the vertex subsets,  $V_{start} = \{0, 1, 2, 3\}$  and  $V_{end} = \{13, 14, 15, 16\}$ , shown in the condensed partial order of rigid cells in Figure 5.10 and in the rendering of the final structure in Figure 5.11. This partial order specifies the directionality of the assembly, based on the nesting order of the planar  $K_4$  graphs representing the tetrahedral cells (i.e., from outside  $\rightarrow$  inside of the graph). This direction is a function of how the graph is originally drawn. In some cases, it might be easier to draw new cells surrounding, rather than nesting into, the existing graph, thus the direction of assembly would be flipped (i.e., from inside  $\rightarrow$  outside of the graph).

The final space frame arch (fig. 5.11) that results from the topology-driven approach to the construction of its isomorphic graph (fig. 5.10), is explicitly designed for fabrication efficiency. It is possible to assemble this structure without external scaffolding during any assembly step by utilizing robotic support.

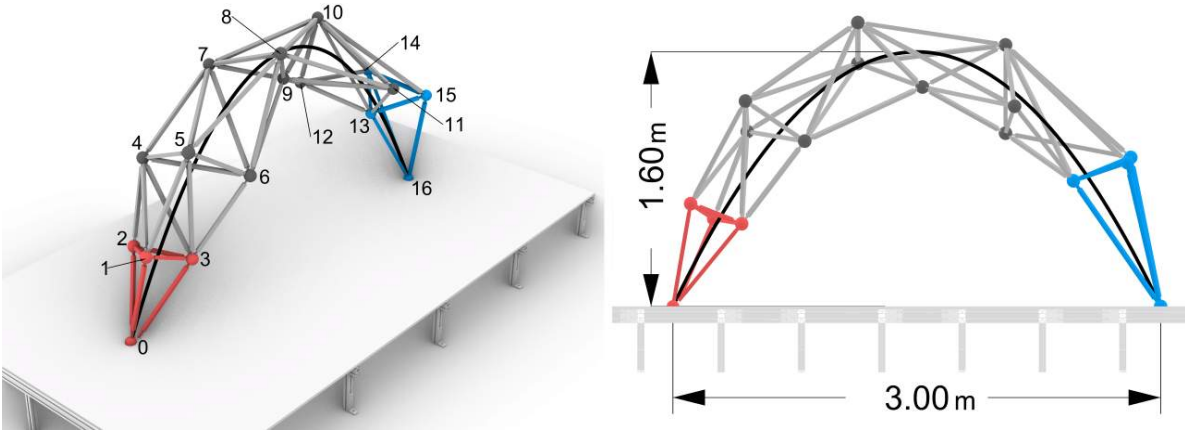


**Figure 5.11:** Renderings of the designed space frame arch structure showing the node numbers and start/end tetrahedral cells (red/blue).

## 5.5 Planning a Cooperative Robotic Disassembly Sequence

When designing a structure for robotic assembly, the emphasis is on allowing for geometric complexity in the design, which can be achieved by placing individual elements to build up a series of rigid cells. In contrast, a disassembly sequence is an operation on a completed structure, and thus a fixed final geometry. Therefore, the resulting process of taking the structure apart can occur through the hybrid removal of existing rigid cells and individual members, to minimize the total number of robotic operations necessary to complete the process. The fewer operations, the faster the full structure can be disassembled.

Planning the disassembly sequence is presented here based on subtractive operations on the graph representation of the structure. Instead of reducing the graph vertex by vertex, with inverse 3-member Henneberg steps, a more efficient approach is to locate, disconnect and then remove larger locally rigid regions of the graph. These regions correspond to the rigid cells formed in the structure during its design and assembly. The challenge is that their removal must be sequenced such that stability is maintained throughout the full disassembly process.

### 5.5.1 Cooperative Robotic Disassembly Strategy

The approach to disassembly is similar to assembly in that the two robots are sequenced to provide temporary support to the structure while they also actively participate in its sequential disassembly. But although the overall goal of maintaining rigidity at intermediate stages is the

same in both assembly and disassembly, the implementation here differs from assembly as performing the removal operation, does not need to occur element by element.

The disassembly sequence takes advantage of the fact that the structure is specifically designed as a series of nested rigid tetrahedral cells, represented in a planar graph. A sequence can thus be determined where a rigid cell is located, supported, isolated from the rest of the structure, and then independently removed, while preserving the property of rigidity in the stability graph. Having the two robots dedicated to supporting the structure at all times offers more flexibility in this type of disassembly approach as it is now possible to support two distinct regions, and potentially disconnected components, of the structure at all times.

The process starts by identifying a rigid cell in the structure that is targeted for removal, and assigning a robot to grab and support any member in this cell. Another distinct rigid cell, adjacent to the cell to be removed, is then located in the structure and the second robot is placed there as support. A distinct adjacent cell shares no members with another cell, and is separated by only one member from the cell it is adjacent to. These two cells,  $C_{remove}$  and  $C_{support}$ , are now supported by the two robots, and the edges in the graph between them become redundant from the point of view of minimal rigidity in the stability graph. These edges are effectively locked between two regions of the graph that are rigid when robotic support is provided to them. Thus, the physical members represented by these edges can be removed one by one without compromising either overall stability of the structure or the rigidity of the local region the members are adjacent to. Once the intermediate members are removed, the result is a graph partitioned into two independent rigid components: (1) a disconnected single rigid cell supported by a robot, (2) the remaining structure supported by the other robot and the external foundation support. The single cell can now be removed as a whole component from the work area by the robot supporting it, and the process of disconnection and removal begins again, now starting with the rigid cell that was supported by the other robot (i.e.,  $C_{support} \rightarrow C_{remove}$ ). This process is schematically shown in [Figure 5.12](#) for a simple 2D truss.

Using a cell-by-cell approach allows the full structure to be disassembled with fewer robotic repositioning steps than would be required in a member-by-member approach. Determining which rigid cells to remove and support in each disassembly phase is performed through operations on the isomorphic graph representation – utilizing the property of planarity and the tetra-

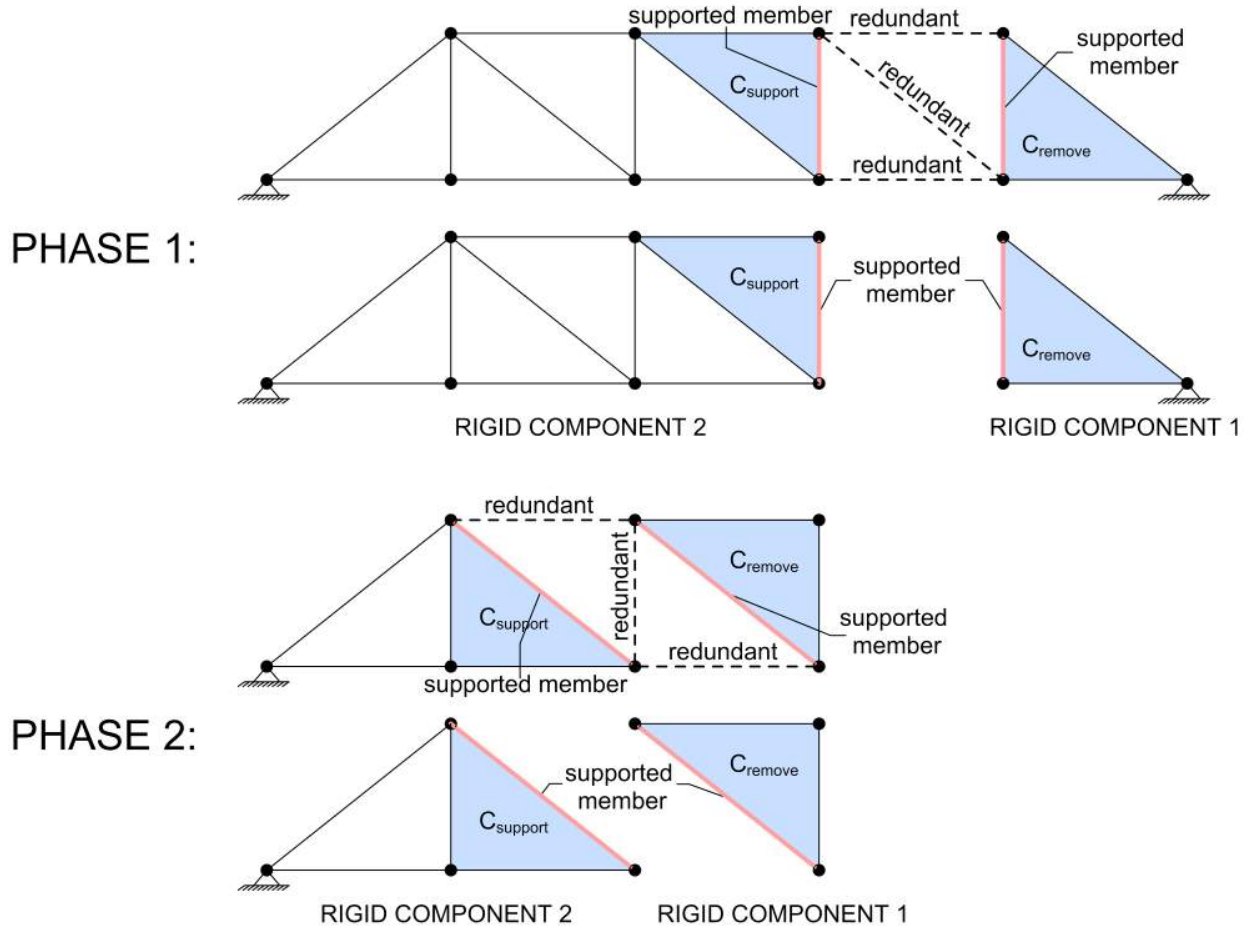


**Figure 5.12:** Demonstration of a disassembly sequence where rigid cells are sequentially located, supported, isolated and then removed from a structure.

hedral topology that was explicitly generated in the design process. A non-planar graph would imply a more complex connection hierarchy within the structure, representing sub-structures that are not independently rigid and can therefore not be isolated and removed in a stability-preserving way.

The removal of the intermediate members is done manually, as an example of Human-Robot Interaction (HRI) in a collaborative fabrication process [39, 54]. *Collaborative* refers to a process where the human works alongside the robot, while *cooperative* refers to a process where multiple robotic agents work together to accomplish a task one of them alone could not. The task of removing intermediate members is best performed manually, rather than robotically, because spatial accuracy and support capabilities are not required when members can be removed individually without compromising the stability of the structure.

### 5.5.2 Algorithm for Locating Rigid Cells

Establishing a feasible disassembly sequence requires locating 1) rigid cells in the structure for the robots to support (sections 5.5.2 and 5.5.3), and 2) intermediate elements to remove (section 5.5.4). This procedure is performed through topological computations on the isomorphic planar graph generated from the design process described in Section 5.4.4. A graph-based algorithm finds rigid cells in the structure, and uses this information when planning a stability-preserving disassembly sequence. The rigid cell locating algorithm is initialized by choosing an edge in the graph to support, and then identifying the corresponding rigid tetrahedral cells to which it belongs. This procedure is described through pseudo-code in Algorithm 1 and in greater detail in the remainder of this section.

---

#### Algorithm 1 Rigid Tetrahedral Cell Locating Algorithm

---

```

1: Choose supported edge,  $e_{support} = \{v_1, v_2\}$ 

2: for Every  $v \in e_{support}$  do
3:   calculate closed neighbourhood graph,  $N_G[v_i]$ 
4: end for
5: find common vertices,  $V' = N_G[v_1] \cap N_G[v_2]$ 

6: for Every  $N_G$  do
7:   eliminate edges that are not adjacent to  $V'$ 
8:   remaining edges,  $E'_i$ , to form graph,  $N'_i = G(V', E'_i)$ 
9: end for
10: form adjacent cell subgraph,  $N' = N'_1 \cup N'_2$ 

11: calculate complete edge set,  $E'_f$ 
12:  $E'_c = E'_f - N'$  = edges missing

13: for Every  $e \in E'_c$  do
14:   form a tetrahedral cell,  $C_i$  by adding,  $e_i$ , to  $N'$ 
15:   then remove vertices that are not 3-connected
16: end for

17: evaluate if support member and corresponding tetrahedral cell(s) are adequate to support
   based on procedure described in Section 5.5.3
18: repeat algorithm until valid cell is located

```

---

Next, the algorithm is further explained with a demonstration of its step-wise execution given an example starting edge,  $e_{support} = (11, 12)$ , operating on the graph generated in [Section 5.4](#). This edge is indicated in the graph of the finished space frame arch structure that was designed ([fig. 5.13](#)). The algorithm can be executed given a random edge, or an edge informed by the overall geometry and load-path. This decision is based on the type of structure being disassembled. For example, in a linear structure such as the arch, the disassembly should start from either end of the structure, rather than the middle, so that there are no more than two disconnected regions of the graph at any one time.

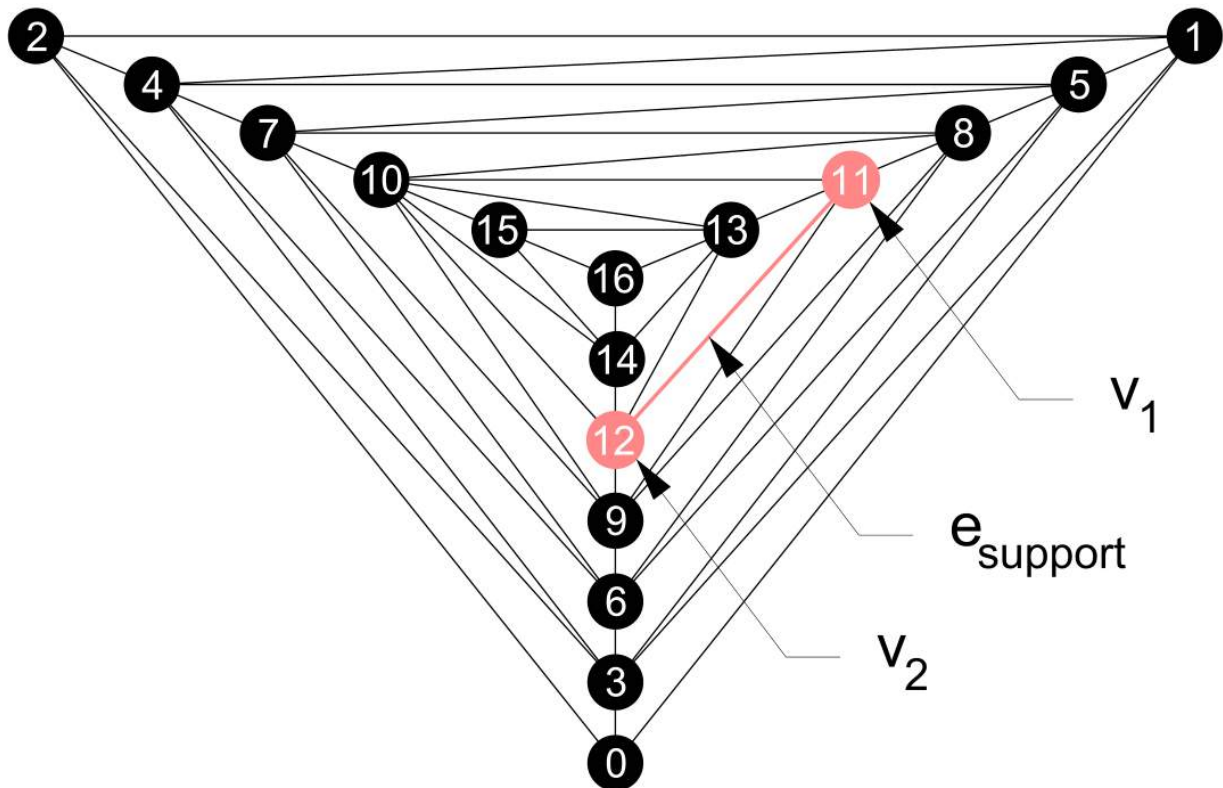


**Figure 5.13:** Isomorphic planar graph of a space frame arch structure indicating a potential support edge,  $e_{support} = (11, 12)$ , used to initialize the rigid cell finding algorithm.

The process starts with choosing a set of supported edges in  $G = (V, E)$ , the planar isomorphic graph of the space frame structure. The supported vertices,  $V_{support} = \{v_1 \dots v_n\}$ , are adjacent to these edges. For a single supported edge,  $n = 2$ . A set,  $S$ , of closed neighborhood graphs is then calculated from each supported vertex in  $G$ :

$$S = \{N_G[v] \mid v \in V_{support}\} \quad (5.2)$$

To simplify the notation,  $N_G[v_i] = N_i$ . Edges that are not components of the same rigid tetrahedral cells as the supported member must be removed from the neighborhood graphs. First, a subset of common vertices,  $V'$ , is created across the neighborhood graph vertices:

$$V' = N_1(V) \cap N_2(V) \quad (5.3)$$

Next, for each neighborhood graph,  $N_i \in S$ , a reduced neighborhood subgraph,  $N'_i = (V', E'_i)$ , is created by eliminating edges that are not adjacent to the common vertices in  $V'$ :

$$E'_i = \{(v_i, u) \in N_i \mid u \in V'\} \quad (5.4)$$

$N'$ , defined as the *adjacent cell subgraph*, is then formed as the union of these reduced neighborhoods:

$$N' = N'_1 \cup N'_2 \quad (5.5)$$

$N'$  only has vertices and edges that are part of a rigid cell that contains the supported element. Searching for a tetrahedral cell topology, it is evident that there are two potential cells that contain the supported member as seen in [Figure 5.14](#). But while all the vertices are present, there is one edge missing per cell.

The complete edge set,  $E'_f$ , for the rigid cells containing the supported member, is computed as all edges in the original graph,  $G = (V, E)$ , adjacent to the common vertices in  $V'$ :

$$E'_f = \{(u, v) \in G \mid u, v \in V'\} \quad (5.6)$$

The set of missing edges,  $E'_c$ , to complete the partial cells in  $N'$ , is computed as the difference between the full edge set,  $E'_f$ , and the edges of the *adjacent cell subgraph*:

$$E'_c = E'_f \setminus N'(E) = \{e_1 \dots e_n\} \quad (5.7)$$

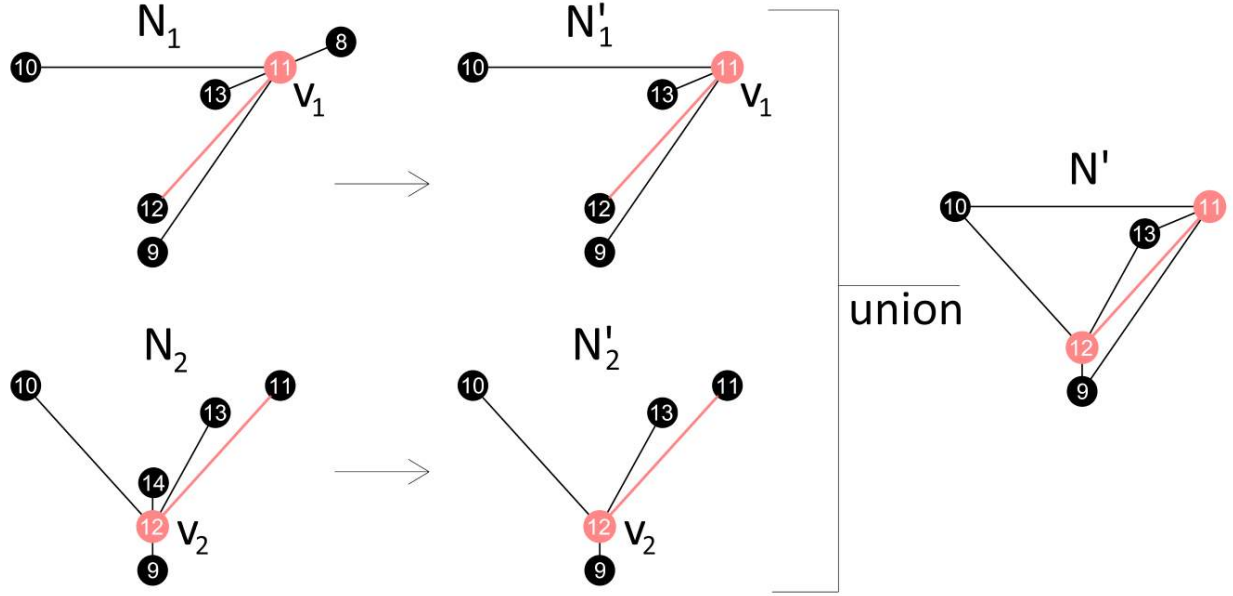


**Figure 5.14:** The adjacent cell subgraph,  $N'$ , is formed from the union of the reduced support neighborhood subgraphs,  $N'_1$  and  $N'_2$ .

The size of this edge set (i.e.,  $|E'_c|$ ) indicates the number of tetrahedral cells containing the supported element. This operation is based on the knowledge that the overall structure is specified to be made up of a series of tetrahedral rigid cells, thus the algorithm is locating as many copies of this specific topology that exist in the neighborhood of the supported member.

The individual subgraphs of each cell are created by first adding each edge,  $e_i \in E'_c$ , separately to the *adjacent cell subgraph*:

$$C_i = N'(V, E \cup e_i) \quad (5.8)$$

Then removing vertices,  $v$ , in the resulting graph,  $C_i$ , that are not 3-connected:

$$C_i = C_i - \{v \mid v \in C_i(V) \wedge \deg(v) \neq 3\} \quad (5.9)$$

In this example, with  $e_{support} = (11, 12)$ , the result is two cells,  $C_1$  and  $C_2$ , in the overall graph,  $G$ , that contain the supported edge, shown in Figure 5.15. They have vertex sets  $V_{C1} = \{9, 10, 11, 12\}$  and  $V_{C2} = \{10, 11, 12, 13\}$ , which share three common vertices (i.e.,  $|V_{C1} \cap V_{C2}| = 3$ ) because the cells share a common face.

It is possible that an edge is only part of one rigid cell (i.e.,  $|E'_c| = 1$ ). The reader can verify

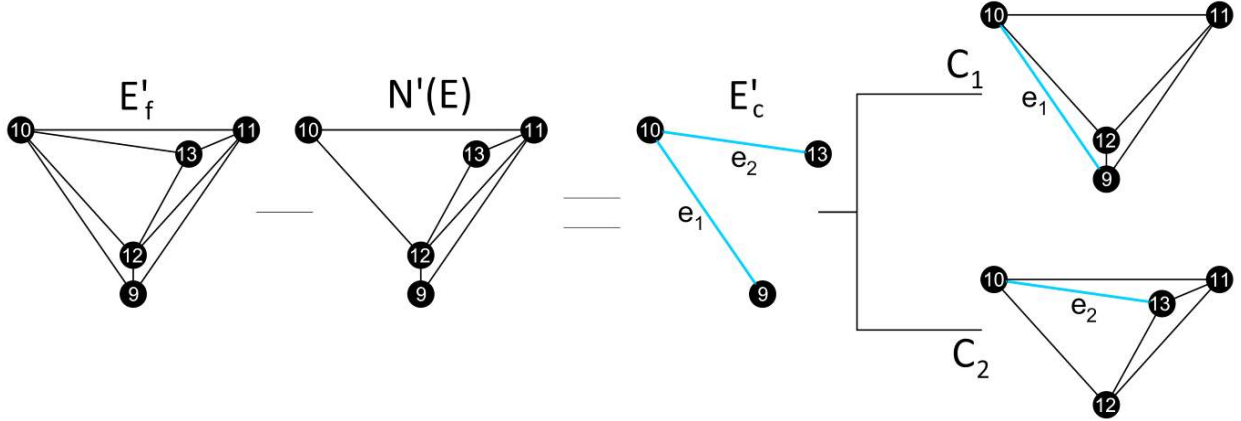


**Figure 5.15:** Rigid tetrahedral cell subgraphs containing the supported member,  $e_{\text{support}} = (11, 12)$ . These cells are computed from the addition of a single edge,  $e_i \in E'_c$ , to the cell adjacency subgraph, and then removing vertices that are not 3-connected.

this result by following the steps outlined in this section given a different starting support edge (e.g.,  $e_{\text{support}} = (8, 11)$ ).

### 5.5.3 Selecting a Rigid Cell to Support

In each disassembly phase, the current cell being isolated and removed is referred to as  $C_{\text{remove}}$ , and the other supported cell in the structure is referred to as  $C_{\text{support}}$  (fig. 5.16). Once a phase is complete,  $C_{\text{support}} \rightarrow C_{\text{remove}}$  in the next phase, and the process repeats. The algorithm described in Section 5.5.2 is executed multiple times per phase, varying the supported member initialization to generate an aggregated set of potential rigid cells,  $\{C_1 \dots C_n\}$ . Naively this requires  $|G'(E)|$  runs for a complete characterization of the structure, where  $G'$  is a subgraph representing the structure in a partially disassembled state. In practice, this procedure can be reduced significantly as  $C_{\text{support}}$  must be located adjacent to  $C_{\text{remove}}$  in the structure. Once the set of rigid cells has been assembled, one cell from here must be chosen as the cell to support in the current phase.

$C_{\text{support}}$  is chosen based on the criteria that all intermediate edges connecting it to  $C_{\text{remove}}$  can be individually removed without breaking apart a non-supported cell in the structure or  $C_{\text{remove}}$  itself (i.e., compromising rigidity). Thus, the requirement for  $C_{\text{support}}$  is that it must be immediately adjacent to  $C_{\text{remove}}$ , expressed as the following two conditions:

1. No vertex overlap between  $C_{support}$  and  $C_{remove}$  (i.e., not too close):

$$C_{support}(V) \cap C_{remove}(V) = \emptyset \quad (5.10)$$

2. No unsupported vertices between  $C_{support}$  and  $C_{remove}$  (i.e., not too far):

$$v \in \{C_{support}(V) \cup C_{remove}(V)\} \wedge v \in P \quad (5.11)$$

where,  $P$ , is a set of vertices representing all the possible walks of length two between both cells in the graph.

For example, [Figure 5.16](#) illustrates the two rigid cells,  $\{C_1, C_2\}$ , that are located when initializing the algorithm with  $e_{support} = (11, 12)$ , and the single cell,  $C_3$ , that is located when initializing the algorithm with  $e_{support} = (8, 11)$ .  $C_2$  fails criterion #1 ([eq. \(5.10\)](#)) as one of the vertices overlaps with  $C_{remove}$ , thus it cannot be removed as a complete cell without destabilizing the rigid cell  $C_2$  by removing one of its vertices.  $C_3$  fails criterion #2 ([eq. \(5.11\)](#)) as supporting this cell leaves a region of the remaining structure directly connected to  $C_{remove}$  unsupported. When removing individual members during the disassembly process this unsupported region of the graph is destabilized. Meanwhile,  $C_1$  is feasible cell as a robot placed here supports the remaining structure while not leaving any unsupported intermediate vertices connected to  $C_{remove}$ . Thus, the intermediate members can be manually removed without compromising stability, as each member is immediately adjacent to a rigid supported cell.

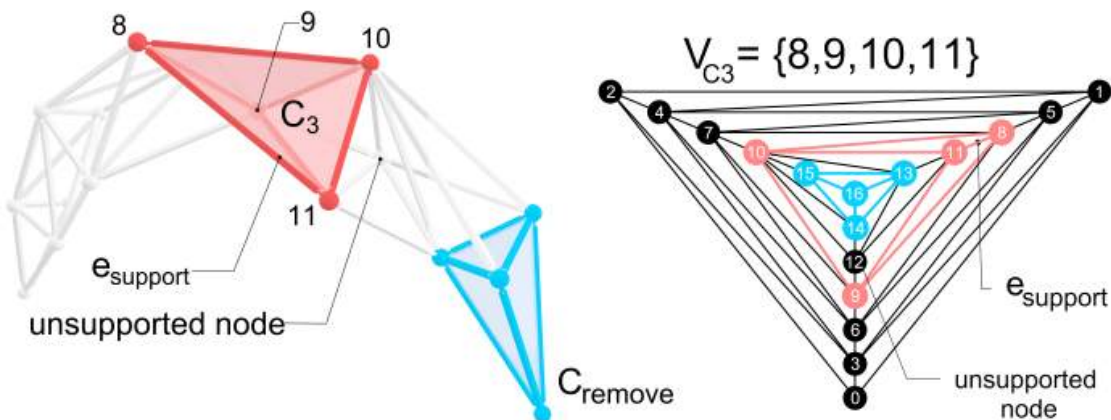
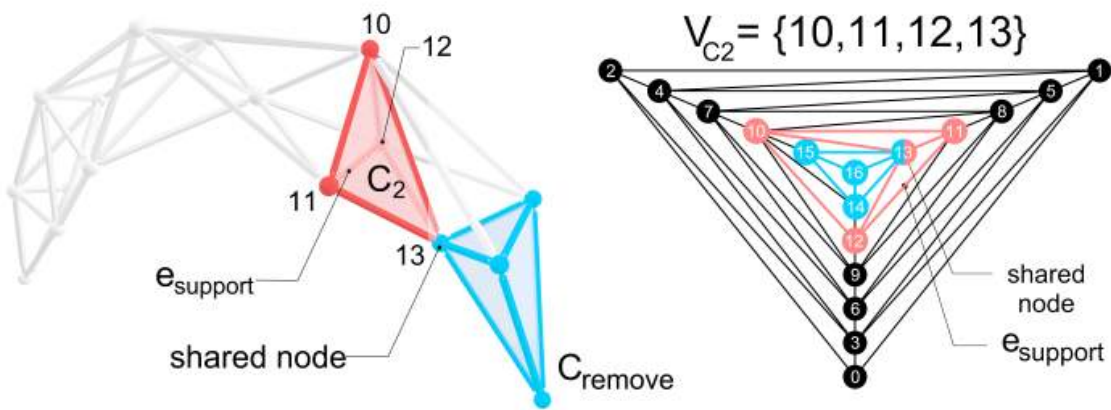
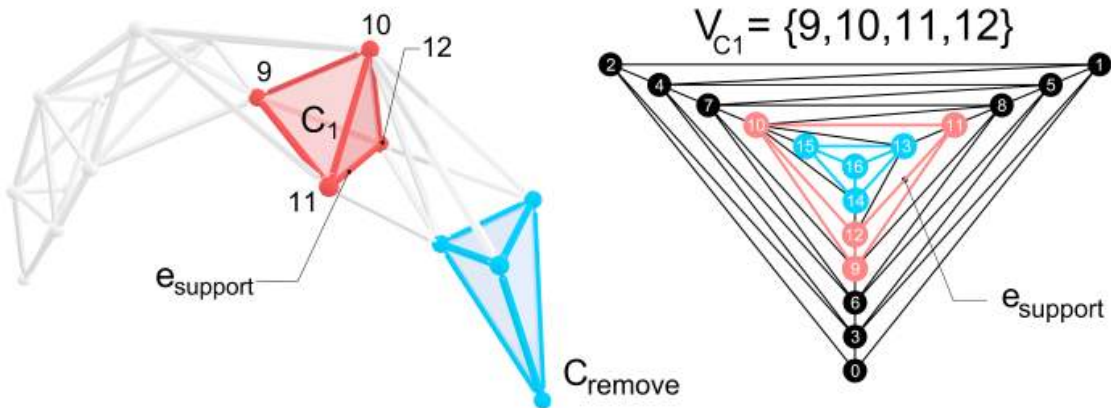


**Figure 5.16:** Checking the viability of a rigid cell to support in relation to the location of the current cell being removed.  $C_1$  is a valid cell to support, while  $C_2$  and  $C_3$  violate the adjacency criteria.

### 5.5.4 Selecting Individual Members to Remove

Once a viable rigid cell to support is chosen based on the criteria outlined in [Section 5.5.3](#), the set of edges,  $E_{remove}$ , that connect  $C_{remove}$  and  $C_{support}$ , is computed as per [Equation \(5.12\)](#).  $G'$  is the graph of the full structure in the current disassembly phase. Following the removal of the intermediate members in any order, the cell  $C_{remove}$  is disconnected from the remaining structure and is removed as an independent component.

$$E_{remove} = \{(u, v) \in G' \mid u \in C_{remove}, v \in C_{support}\} \quad (5.12)$$

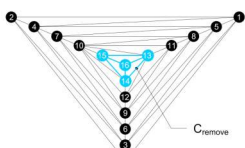
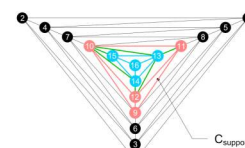
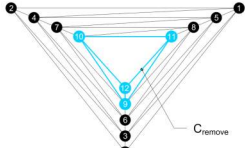
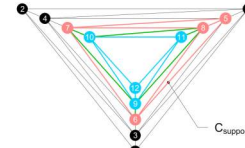
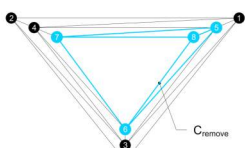
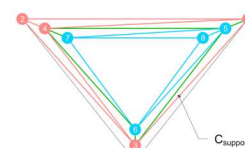
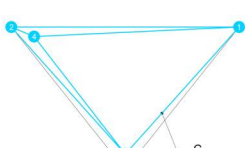
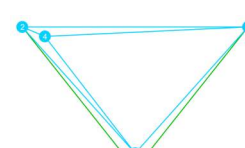
### 5.5.5 Planning the Disassembly Sequence for a Spanning Space Frame

#### Arch

Computing a stability-preserving disassembly sequence using two robots is implemented on the space frame structure designed in [Section 5.4.5](#). The complete disassembly of the structure is found to only require four phases. Each phase starts with the repositioning of a robot to support a viable rigid cell,  $C_{support}$ , located as per [Sections 5.5.2](#) and [5.5.3](#), and ends with the removal of a set of intermediate members,  $E_{remove}$  as per [Section 5.5.4](#), followed by the removal of  $C_{remove}$ . [Table 5.1](#) summarizes the key information computed for each phase, where  $G'$  is the graph of the remaining structure at the start of each disassembly phase.  $G'_{end}$  shows the results of the algorithm operating on  $G'$ , with the location of  $C_{remove}$  in blue,  $C_{support}$  in red, and  $E_{remove}$  in green. The vertex and edge sets for each of these components are listed in the table for each phase.

The process starts by choosing  $C_{remove}$  as the rigid cell at one end of the arch, and progresses over the whole structure, with  $C_{support} \rightarrow C_{remove}$  in the following phase.

**Table 5.1:** The four disassembly phases planned for the arch structure designed in Section 5.4.5.

	$G'$	$C_{remove}$	$C_{support}$	$E_{remove}$	$G'_{end}$
Phase 1	 $V = \{13, 14, 15, 16\}$	$C_{remove} = \{$ (13,14) (13,15) (13,16) (14,15) (14,16) (15,16) } 	$V = \{9, 10, 11, 12\}$	$E = \{$ (9,10) (9,11) (9,12) (10,11) (10,12) (11,12) } 	 $C_{support} = \{$ (10,13) (10,14) (10,15) (11,13) (12,13) (12,14) }
Phase 2	 $V = \{9, 10, 11, 12\}$	$E = \{$ (9,10) (9,11) (9,12) (10,11) (10,12) (11,12) }	$V = \{5, 6, 7, 8\}$	$E = \{$ (5,6) (5,7) (5,8) (6,7) (6,8) (7,8) }	 $C_{support} = \{$ (6,9) (7,10) (7,9) (8,9) (8,10) (8,11) }
Phase 3	 $V = \{5, 6, 7, 8\}$	$E = \{$ (5,6) (5,7) (5,8) (6,7) (6,8) (7,8) }	$V = \{1, 2, 3, 4\}$	$E = \{$ (1,2) (1,3) (1,4) (2,3) (2,4) (3,4) }	 $C_{support} = \{$ (1,5) (3,6) (4,5) (4,6) (4,7) (5,6) }
Phase 4	 $V = \{1, 2, 3, 4\}$	$E = \{$ (1,2) (1,3) (1,4) (2,3) (2,4) (3,4) }	—	$E = \{$ (0,1) (0,2) (0,3)	 $C_{support} = \{$ —

## 5.6 Assembly and Disassembly Results and Discussion

### 5.6.1 Space Frame Assembly

The 17-noded space frame structure, designed for the target  $3.0m \times 1.6m$  arch geometry in [Section 5.4.5](#), is physically assembled in the Embodied Computation Lab lab at Princeton University. This is done using a robotic cell comprised of two ABB IRB4600-40/2.55 robotic arms on 3.9 m linear tracks. The purpose of this exercise is to validate the design method presented in this chapter and to test the rigidity-preserving cooperative robotic fabrication sequence that the structure is designed for. The material system used for the structure is 85 mm diameter 3D-printed PETG hollow nodes (with embedded slots for the member connection tabs) and 30 mm square wood members, which are fastened manually with 6mm machine screws drilled through a 3D-printed tapered PETG tab inserted through a slot at each member's end. This tabs acts as the connector between the member and the node, and is itself manually placed after the member is maneuvered to the correct location with the robotic arm, which is instrumented with a pneumatic gripper ([fig. 5.17](#)).

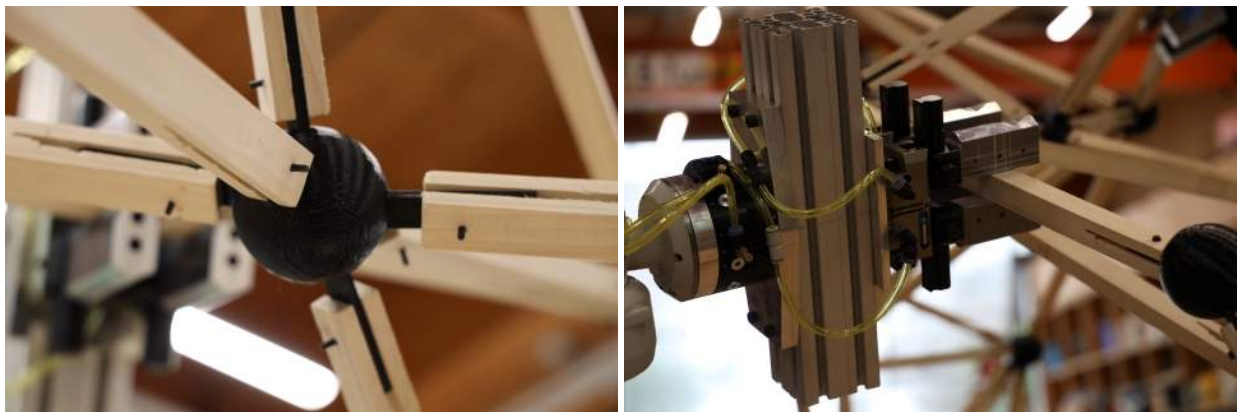
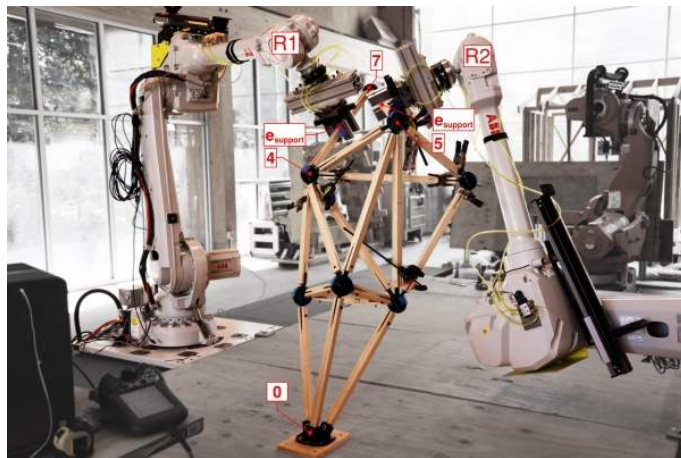


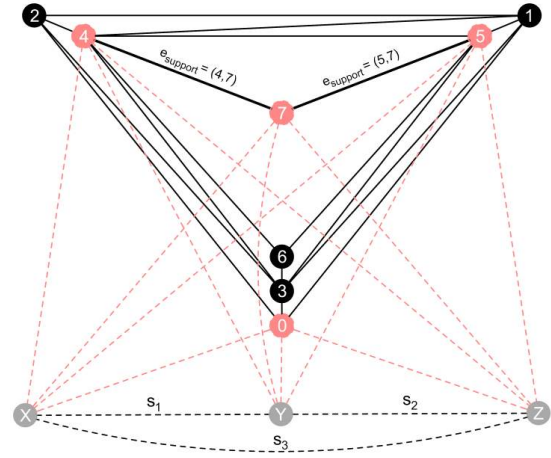
**Figure 5.17:** A typical structural node with connecting tabs (left). A robotic arm with pneumatic gripper placing and supporting a member in the structure (right).

Snapshots of the structure, and its corresponding stability graph, as examples of the assembly process are shown in [Figure 5.18](#) during the execution of a 3-member aggregation sequence for nodes 7 and 11. [Figures 5.18a](#) and [5.18b](#) show the structure during a partially completed Henneberg sequence for node 7, where only two of the three members have been placed and the structure is supported by both robots:  $e_{support} = \{(4, 7), (5, 7)\}$ . [Figures 5.18c](#) and [5.18d](#) show

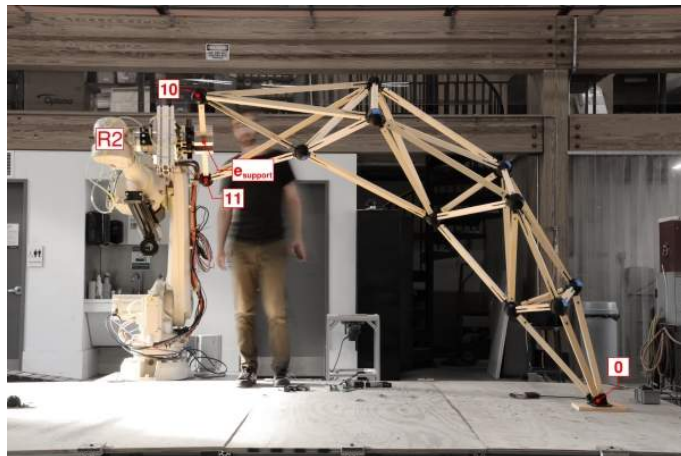
the stage where node 11 is fully connected and the structure itself becomes minimally rigid (i.e., at the end of a Henneberg 3-member sequence), with support from one robot only required for overall stability:  $e_{support} = \{(10, 11)\}$ . The full fabrication sequence is shown in Appendix A, **Table B.2**, which summarizes the order of assembly, the edge in the graph each member corresponds to, and the robot ( $R1$  or  $R2$ ) that was used to place a member as part of a 3-member sequence. The finished structure is shown in [Figure 5.19](#).



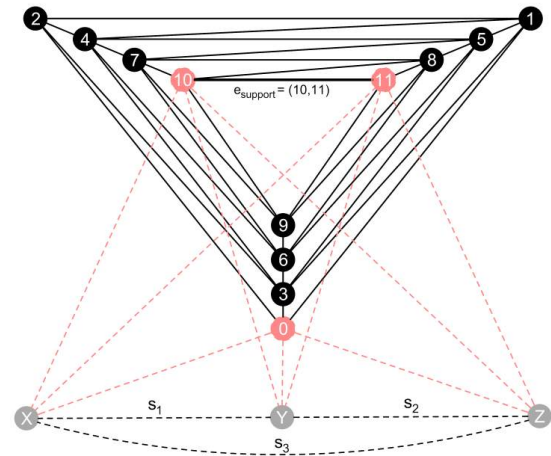
**(a)** both robots supporting the structure in a partially completed Henneberg Type 1 step for node 7.



**(b)** rigid stability graph of the structure showing the 4 supported vertices in red.



**(c)** a single robot supporting the structure after a completed Henneberg Type 1 step for node 11.



**(d)** rigid stability graph of the structure showing the 3 supported vertices in red.

**Figure 5.18:** Snapshots of the cooperative robotic assembly process for the space frame arch structure. Robotic support is shown on the structure and its isomorphic graph for a partially completed (top) and completed (bottom) 3-member Henneberg sequence.

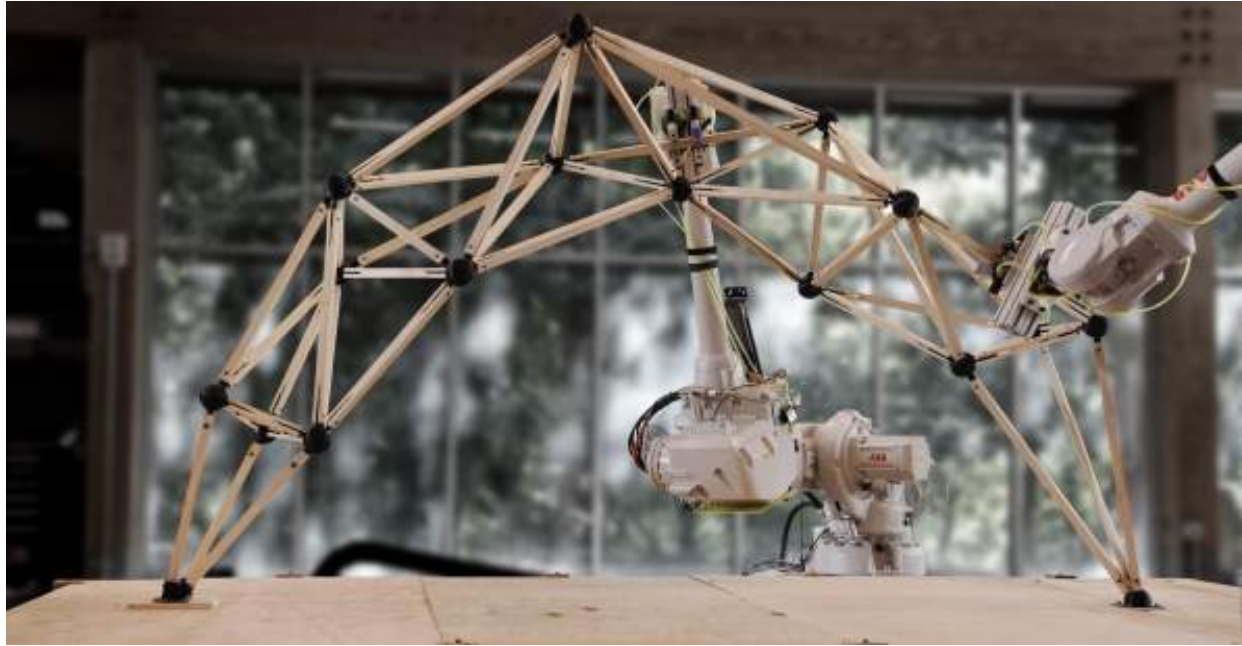


**Figure 5.19:** The 17-noded space frame arch structure as the realization of a planar graph designed to have a rigidity-preserving (dis)assembly sequence.

The robotic fabrication sequence for the full structure is planned using the COMPAS FAB framework [87] to calculate feasible collision-free paths for the robots to take while placing members. For a geometrically complex structure, individual members can be more easily maneuvered in space by the robots, which improves the likelihood of a feasible collision-free path to be found. But even so, as assembly progresses and the structure grows in size, it becomes more difficult to find feasible collision-free paths. To help with the path planning process in later stages of assembly, the calculation of trajectories is split into two discrete planning operations: (1) from the fixed pick-up location to an unobstructed intermediate plane in space; (2) from the intermediate plane to the final location of the member, also expressed as a plane located at the member's geometric center. The intermediate plane is located approximately 500 mm away from the structure and is parallel to the member's final location plane, which is based on the cartesian position and orientation taken from an accurate 3D model of the structure. The likelihood of a feasible path being calculated is improved as the first operation would maneuver the robot in unobstructed space to a position in line with the member's final location, and the second operation would perform a relatively simple linear cartesian move to the final location. The control of the robots, and execution of the calculated trajectories for the placement of each member, is

then done using the COMPAS RRC framework [88]. Placement errors (i.e., positional differences between the digital model and as-built structure) ranged from 1-10 mm between the end of members and connection slots in the nodes. This was within the tolerance of the material system, therefore no correction using sensors or 3D imaging (as in [89]) was required during construction.

The rigidity-preserving assembly logic, and the resultant structure designed using the method developed in this chapter, is specifically based around the use of two robotic arms. Adding an additional robotic support agent to the setup would greatly expand the design space for rigidity-preserving space frame structures, by allowing more complex cooperative robotic sequences to be performed. For example, it would be possible to construct rigid cells composed of five or six vertices, rather than the four as in the tetrahedral cell. These rigid cells can be realized through more complex rigidity-preserving fabrication sequences based on combinations of both Henneberg Type 1 and 2 steps. The ability to build cells with six vertices is particularly promising as there are four different rigid topological configurations that are possible, which would thus allow for additional flexibility during the design stage. Finally, a third robotic agent would allow for a more complex load-path, allowing for stable branching structures to be built beyond the linear partial order that is currently possible with two robots.

### 5.6.2 Space Frame Disassembly

The disassembly sequence computed in [Section 5.5.5](#) is implemented on the completed structure at the end of the assembly sequence ([fig. 5.19](#)). The results of the physical implementation of this rigidity-preserving sequence are documented for each of the four phases in [Table 5.2](#). The left column shows the disconnected structure, with one robot supporting the rigid tetrahedral cell to remove ( $C_{remove}$ ) and the other robot supporting the remaining rigid portion of the arch structure. The right column shows close-up images of the rigid cell and the six intermediate members removed ( $E_{remove}$ ) in the process of disconnecting the cell from the rest of the structure.

**Table 5.2:** Documentation of the four phases of the rigidity-preserving disassembly sequence calculated and executed for the space frame arch structure.

	Disconnected Supported Structure	$C_{remove}$ and $E_{remove}$
Phase 1		
Phase 2		
Phase 3		
Phase 4		

The computation of the disassembly sequence does not provide information about which of the six elements comprising each selected cell a robot should support. While this choice does not impact rigidity (i.e., any of the six elements are valid), an additional finite element analysis was performed to inform which robot should support which cell in each phase, and the optimal combination of supported elements in each of the two cells ( $C_{remove}$  and  $C_{support}$ ). The combination of supported elements that result in the minimum average strain energy during the full disassembly process in each phase are summarized in [Table 5.3](#). The methodology for this analysis and the full data for all possible support combinations in each phase are shown in Appendix B. Robotic reachability also impacts which members can be supported, but is not an issue in this specific case as most members are within reach of at least one robot, which is verified using the path-planning functionality in COMPAS FAB [87]. In general, supporting members that are located close to the central axis of the arch results in lower average axial strain energy in the structure, for all steps in a particular disassembly phase. This result is due to the structure experiencing less out-of-plane twisting when supported at these central locations.

**Table 5.3:** The two members supported by either robot resulting in the minimum average axial strain energy ( $10^{-9} \text{ kN} \cdot \text{m}$ ) in each disassembly phase.

	$R_1$	$R_2$	$E_{\epsilon,avg}$
Phase 1	$C_{support}$ member = 31 $e = (11,12)$	$C_{remove}$ member = 41 $e = (14,15)$	9.51
Phase 2	$C_{support}$ member = 15 $e = (5,7)$	$C_{remove}$ member = 31 $e = (11,12)$	4.42
Phase 3	$C_{support}$ member = 6 $e = (1,4)$	$C_{remove}$ member = 16 $e = (6,7)$	1.55
Phase 4	$C_{remove}$ member = 6 $e = (1,4)$	-	0.87

Using a closed-form algorithm to locate and isolate rigid cells in a structure during disassembly, such as the one presented in [Section 5.5.2](#), is a valid approach when given a structure with a

uniform topology. For example, as with the example presented in this chapter, where the structure is known to be composed of tetrahedral cells. But a more generic method is necessary when expanding the feasible design space to include structures composed of both more complex and varied rigid cells, and branching load paths (i.e., not a linear partial order of rigid cells). With the future inclusion of a third robotic agent in the fabrication setup, assembling such structures will be possible. The calculation of a feasible rigidity-preserving disassembly sequence must thus be generalized for use in such structures with unknown and varied topologies by developing a more generic approach to the cell locating and isolating algorithm. This will be accomplished in future work through the implementation of a graph-search approach based on the rigidity-finding *pebble game* algorithm [77].

## 5.7 Conclusion

In this chapter, a novel graph theoretic approach, based on rigidity theory, is presented as a way to assess the stability of spatially complex bar and joint structures (i.e., trusses and space frames) during any phase of their construction. A topological framework, referred to as a *stability graph*, is developed as an isomorphic representation of the physical structure (i.e., there exists a one-to-one mapping between the graph and structure). The structural elements, support conditions, and temporary robotic supports can all be represented in the *stability graph*, and their collective effect on the stability of the structure can thus be evaluated using only graph rigidity principles (e.g., Laman count and Henneberg construction steps).

A schematic design method, based on a topology-driven approach to rigidity and structural stability, is then developed. The method is used to design space frame structures that remain stable during all stages of their assembly and disassembly without requiring external scaffolding. The design method is *fabrication-informed*, because it is specifically developed to take advantage of the fabrication capabilities (with respect to sequencing) when two industrial robotic arms work together in a cooperative manner: placing elements (during assembly), removing cells (during disassembly), while also supporting the structure in its temporary state.

The proposed method is demonstrated in this chapter through the design, and robotic assembly and disassembly, of a rigidity-preserving space frame arch, composed of 17 nodes and 45

elements. The structure is sequentially designed to be assembled element-by-element with two robots, mirroring a Henneberg rigid-graph assembly step in the topological design space of the *stability graph*. The design process and assembly logic guarantee that the property of planarity is maintained in the graph, which physically corresponds to a structure that is composed of a series of rigid tetrahedral cells. The property of planarity, coupled with a tetrahedral cell topology, results in a structure that can then also be efficiently disassembled through the application of a graph-based algorithm to sequentially locate and isolate rigid cells in the graph. After the cells are located, they are robotically supported and removed from the physical structure as independent components, all while the stability of the remaining structure is preserved.

As robotic technology improves, its applications in the AEC industry will continue to grow, with multi-robot setups becoming more prevalent. Engineers and architects should consider how the structures they design can better take advantage of the potential afforded them through such robotic fabrication setups. The generic support/place sequencing approach, that is demonstrated with two robots in this chapter, can help to further expand the feasible design space for geometrically complex discrete element structures. Future work will integrate feedback in the form of 3D imaging of the structure during assembly or disassembly to allow the fabrication process to better adapt to changing conditions such as deformation of the structure due to self-weight. Overall, the goal is to further promote the application of robotic fabrication and automation in construction, while simultaneously improving the material use and construction efficiency of geometrically complex trusses and space frames.

## References

- [1] S. Sharif, R. Gentry, BIM for masonry: Development of BIM plugins for the masonry unit database, in: Proceedings of the 33rd Education and Research in Computer Aided Architectural Design in Europe Conference, Vienna, Austria, 2015, pp. 567–576.  
URL [http://papers.cumincad.org/cgi-bin/works/paper/ecaade2015\\_261](http://papers.cumincad.org/cgi-bin/works/paper/ecaade2015_261)
- [2] C. Meyer, M. H. Sheer, Do Concrete Shells Deserve Another Look?, *Concrete International* 27 (10) (2005) 43–50.  
URL <https://www.concrete.org/publications/internationalconcreteabstractsportal.aspx?m=details&ID=14717>
- [3] R. Zimmann, H. O'Brien, J. Hargrave, M. Morrell, The circular economy in the built environment, Tech. rep., Arup (2016).  
URL <https://www.arup.com/perspectives/publications/research/section/circular-economy-in-the-built-environment>
- [4] S. Kaethner, J. Burridge, Embodied CO<sub>2</sub> of structural frames, *Structural Engineer* 90 (5) (2012) 33–40.  
URL <https://www.istructe.org/sitefiles/handlers/DownloadFile.ashx?productId=1583>
- [5] F. Barbosa, J. Woetzel, J. Mischke, M. Ribeirinho, M. Sridhar, M. Parsons, N. Bertram, S. Brown, Reinventing Construction: A Route to Higher Productivity, Tech. rep., McKinsey Global Institute (2017).  
URL <https://www.mckinsey.com/business-functions/operations/our-insights/reinventing-construction-through-a-productivity-revolution>
- [6] W. Lu, H. Yuan, A framework for understanding waste management studies in construction, *Waste Management* 31 (6) (2011) 1252–1260. doi:10.1016/j.wasman.2011.01.018.
- [7] J. Brütting, J. Desruelle, G. Senatore, C. Fivet, Design of truss structures through reuse, *Structures* 18 (2019) 128–137. doi:10.1016/j.istruc.2018.11.006.

- [8] J. Brütting, G. Senatore, M. Schevenels, C. Fivet, Optimum design of frame structures from a stock of reclaimed elements, *Frontiers in Built Environment* 6 (2020) 57. doi:10.3389/fbuil.2020.00057.
- [9] J. Brütting, G. Senatore, C. Fivet, Design and fabrication of a reusable kit of parts for diverse structures, *Automation in Construction* 125 (2021) 103614. doi:10.1016/j.autcon.2021.103614.
- [10] G. Bravo-Palacios, A. D. Prete, P. M. Wensing, One robot for many tasks: Versatile co-design through stochastic programming, *IEEE Robotics and Automation Letters* 5 (2) (2020) 1680–1687. doi:10.1109/LRA.2020.2969948.
- [11] P. Eversmann, F. Gramazio, M. Kohler, Robotic prefabrication of timber structures: towards automated large-scale spatial assembly, *Construction Robotics* 1 (2017) 49–60. doi:10.1007/s41693-017-0006-2.
- [12] IFR, World robotics report (2018).  
 URL <https://ifr.org/ifr-press-releases/news/global-industrial-robot-sales-doubled-over-the-past-five-years>
- [13] B. García de Soto, I. Agustí-Juan, J. Hunhevicz, S. Joss, K. Graser, G. Habert, B. T. Adey, Productivity of digital fabrication in construction: Cost and time analysis of a robotically built wall, *Automation in Construction* 92 (2018) 297–311. doi:10.1016/j.autcon.2018.04.004.
- [14] V. R. P. Kumar, M. B. a. S. J. Raj, Robotics in construction industry, *Indian Journal of Science and Technology* 9 (23) (2016) 1–12. doi:10.17485/ijst/2016/v9i23/95974.
- [15] S. Parascho, Cooperative robotic assembly: Computational design and robotic fabrication of spatial metal structures, PhD Thesis, ETH, Zurich (2019).  
 URL <https://doi.org/10.3929/ethz-b-000364322>
- [16] T. Bock, Construction robotics, *Autonomous Robots* 22 (3) (2007) 201–209. doi:10.1007/s10514-006-9008-5.

- [17] T. Bock, The future of construction automation: Technological disruption and the upcoming ubiquity of robotics, *Automation in Construction* 59 (2015) 113–121. doi:10.1016/j.autcon.2015.07.022.
- [18] J. S. Albus, Trip report: Japanese progress in robotics for construction, *Robotics* 2 (2) (1986) 103–112, publisher: North-Holland. doi:10.1016/0167-8493(86)90047-1.
- [19] L. Cousineau, N. Miura, Construction robots: The search for new building technology in Japan, American Society of Civil Engineers, Reston, VA, 1998, (ISBN: 978-0-7844-0317-4).
- [20] P. Y. Huang, M. Sakurai, Factor automation: the Japanese experience, *IEEE Transactions on Engineering Management* 37 (2) (1990) 102–108. doi:10.1109/17.53712.
- [21] T. Ueno, J. Maeda, T. Yoshida, S. Suzuki, Construction robots for site automation, in: Proceedings of the 3rd ISARC, Marseille, France, 1986, pp. 627–639. doi:10.22260/ISARC 1986/0049.
- [22] T. Bock, T. Linner, Site automation: Automated/robotic on-site factories, Vol. 3, Cambridge University Press, Cambridge, 2016, (ISBN: 978-1-107-07597-9).
- [23] M. J. Skibniewski, Robotics in civil engineering, Van Nostrand Reinhold, Southampton, 1989, (ISBN: 978-0-442-31925-0).
- [24] J. M. Davila Delgado, L. Oyedele, A. Ajayi, L. Akanbi, O. Akinade, M. Bilal, H. Owolabi, Robotics and automated systems in construction: Understanding industry-specific challenges for adoption, *Journal of Building Engineering* 26 (2019) 1–11. doi:10.1016/j.jobe.2019.100868.
- [25] F. Gramazio, M. Kohler, Digital materiality in architecture, 1st Edition, Lars Muller, Baden, 2008, ISBN: 978-3-03778-122-7.
- [26] F. Gramazio, M. Kohler (Eds.), Made by robots: Challenging architecture at a larger scale, 1st Edition, Academy Press, London, 2014, (ISBN: 978-1-118-53548-6).

- [27] M. Kohler, F. Gramazio, J. Willmann, The programmed column, in: The Robotic Touch: How Robots Change Architecture, The University of Chicago Press, Chicago, 2014, pp. 208–215, (ISBN: 978-3-906027-37-1).
- [28] T. Bonwetsch, D. Kobel, F. Gramazio, M. Kohler, The informed wall: Applying additive digital fabrication techniques on architecture, in: Proceedings of the 25th Annual Conference of the Association for Computer-Aided Design in Architecture, 2006, pp. 489–495, (ISBN: 978-0-9789463-0-2).
- [29] T. Bonwetsch, F. Gramazio, M. Kohler, Digitally fabricating non-standardised brick walls, in: ManuBuild, 2007, pp. 191–196, (ISBN: 978-0-86017-710-4).
- [30] M. Kohler, F. Gramazio, J. Willmann, Gantenbein vineyard façade, in: The Robotic Touch: How Robots Change Architecture, The University of Chicago Press, Chicago, 2014, pp. 66–75, (ISBN: 978-3-906027-37-1).
- [31] EMPA, DFAB HOUSE – Digital fabrication and living. (2021).  
URL <https://www.empa.ch/web/nest/digital-fabrication>
- [32] J. Willmann, M. Knauss, T. Bonwetsch, A. A. Apolinarska, F. Gramazio, M. Kohler, Robotic timber construction — Expanding additive fabrication to new dimensions, Automation in Construction 61 (2016) 16–23. doi:10.1016/j.autcon.2015.09.011.
- [33] N. Hack, T. Wangler, J. Mata-Falcón, K. Dörfler, N. Kumar, N. Walzer, K. Graser, L. Reiter, H. Richner, J. Buchli, W. Kaufmann, R. J. Flatt, F. Gramazio, M. Kohler, Mesh mould: An on site, robotically fabricated, functional formwork, in: Second Concrete Innovation Conference, Vol. 19, Tromsø, Norway, 2017, p. 11, (ISBN: 978-82-8208-054-5).
- [34] N. Hack, K. Dörfler, A. N. Walzer, T. Wangler, J. Mata-Falcón, N. Kumar, J. Buchli, W. Kaufmann, R. J. Flatt, F. Gramazio, M. Kohler, Structural stay-in-place formwork for robotic in situ fabrication of non-standard concrete structures: A real scale architectural demonstrator, Automation in Construction 115 (2020) 1–13. doi:10.1016/j.autcon.2020.103197.

- [35] R. Bärtschi, M. Knauss, T. Bonwetsch, F. Gramazio, M. Kohler, Wiggled brick bond, in: Advances in Architectural Geometry 2010, Springer, Wien/New York, 2010, pp. 137–147. doi:10.1007/978-3-7091-0309-8.
- [36] L. Piškorec, D. Jenny, S. Parascho, H. Mayer, F. Gramazio, M. Kohler, The brick labyrinth, in: Robotic Fabrication in Architecture, Art and Design 2018, Springer International Publishing, Zurich, 2018, pp. 489–500. doi:10.1007/978-3-319-92294-2\_37.
- [37] K. Dörfler, T. Sandy, M. Gifthalter, F. Gramazio, M. Kohler, J. Buchli, Mobile robotic brickwork: Automation of a discrete robotic fabrication process using an autonomous mobile robot, in: Robotic Fabrication in Architecture, Art and Design 2016, Springer International Publishing, Sydney, Australia, 2016, pp. 204–217. doi:10.1007/978-3-319-26378-6-15.
- [38] M. Gifthalter, T. Sandy, K. Dörfler, I. Brooks, M. Buckingham, G. Rey, M. Kohler, F. Gramazio, J. Buchli, Mobile robotic fabrication at 1:1 scale: The in situ fabricator, Construction Robotics 1 (1) (2017) 3–14. doi:10.1007/s41693-017-0003-5.
- [39] I. X. Han, F. Meggers, S. Parascho, Bridging the collectives: A review of collective human–robot construction, International Journal of Architectural Computing 19 (4) (2021) 20. doi:10.1177/14780771211025153.
- [40] K. H. Petersen, N. Napp, R. Stuart-Smith, D. Rus, M. Kovac, A review of collective robotic construction, Science Robotics 4 (28) (2019) 1–10. doi:10.1126/scirobotics.aau8479.
- [41] S. Bragança, E. Costa, I. Castellucci, P. M. Arezes, A Brief Overview of the Use of Collaborative Robots in Industry 4.0: Human Role and Safety, in: Occupational and Environmental Safety and Health, Studies in Systems, Decision and Control, Springer International Publishing, Cham, 2019, pp. 641–650. doi:10.1007/978-3-030-14730-3\_68.
- [42] E. P. G. Bruun, R. Pastrana, V. Paris, A. Beghini, A. Pizzigoni, S. Parascho, S. Adriænsens, Three cooperative robotic fabrication methods for the scaffold-free construction of a masonry arch, Automation in Construction 129 (2021) 103803. doi:10.1016/j.autcon.2021.103803.

- [43] P. Carneau, R. Mesnil, N. Roussel, O. Baverel, Additive manufacturing of cantilever - From masonry to concrete 3D printing, *Automation in Construction* 116 (2020) 1–16. doi:10.1016/j.autcon.2020.103184.
- [44] M. Motamedi, R. Oval, P. Carneau, O. Baverel, Supportless 3D printing of shells: Adaptation of ancient vaulting techniques to digital fabrication, in: *Proceedings of the Design Modelling Symposium Berlin*, Berlin, 2019, pp. 714–726. doi:10.1007/978-3-030-29829-6-55.
- [45] P. Latteur, A. Fascetti, S. Goessens, The droxel: A universal parametric construction component, *Engineering Structures* 250 (2022) 113363. doi:10.1016/j.engstruct.2021.113363.
- [46] S. Goessens, C. Mueller, P. Latteur, Feasibility study for drone-based masonry construction of real-scale structures, *Automation in Construction* 94 (2018) 458–480. doi:10.1016/j.autcon.2018.06.015.
- [47] S. Parascho, A. Gandia, A. Mirjan, F. Gramazio, M. Kohler, Cooperative fabrication of spatial metal structures, in: *Fabricate 2017: Rethinking Design and Construction*, UCL Press, London, 2017, pp. 24–29. doi:10.3929/ethz-b-000219566.
- [48] S. Parascho, T. Kohlhammer, S. Coros, F. Gramazio, M. Kohler, Computational design of robotically assembled spatial structures: A sequence based method for the generation and evaluation of structures fabricated with cooperating robots, in: *Advances in Architectural Geometry 2018*, Klein Publishing GmbH, Gothenburg, Sweden, 2018, pp. 112 – 139.  
URL <https://research.chalmers.se/en/publication/504188>
- [49] A. Thoma, A. Adel, M. Helmreich, T. Wehrle, F. Gramazio, M. Kohler, Robotic fabrication of bespoke timber frame modules, in: *Robotic Fabrication in Architecture, Art and Design 2018*, Springer International Publishing, Zurich, 2018, pp. 447–458. doi:10.1007/978-3-319-92294-2\_34.
- [50] K. Wu, A. Kilian, Robotic equilibrium: Scaffold free arch assemblies, in: *Proceedings of*

the 38th Annual Conference of the Association for Computer Aided Design in Architecture, Mexico City, 2018, pp. 342–349. doi:10.52842/conf.acadia.2018.342.

- [51] S. Parascho, I. X. Han, S. Walker, A. Beghini, E. P. G. Bruun, S. Adriaenssens, Robotic vault: A cooperative robotic assembly method for brick vault construction, *Construction Robotics* 4 (3) (2020) 117–126. doi:10.1007/s41693-020-00041-w.
- [52] S. Parascho, I. X. Han, A. Beghini, M. Miki, S. Walker, E. P. G. Bruun, S. Adriaenssens, LightVault: A design and robotic fabrication method for complex masonry structures, in: *Advances in Architectural Geometry 2020*, Presses des Ponts, Paris, France, 2021, pp. 350–375.  
URL <https://oar.princeton.edu/handle/88435/pr1s17ss4d>
- [53] I. X. Han, E. P. G. Bruun, S. Marsh, S. Adriaenssens, S. Parascho, From concept to construction: A transferable design and robotic fabrication method for a building-scale vault, in: *Proceedings of the 40th Annual Conference of the Association for Computer Aided Design in Architecture*, Online, 2020, pp. 614–623. doi:10.52842/conf.acadia.2020.1.614.
- [54] E. P. G. Bruun, I. Ting, S. Adriaenssens, S. Parascho, Human–robot collaboration: A fabrication framework for the sequential design and construction of unplanned spatial structures, *Digital Creativity* 31 (4) (2020) 320–336. doi:10.1080/14626268.2020.1845214.
- [55] L. Euler, *Solutio problematis ad geometriam situs pertinentis*, *Scientarium Imperialis Petropolitanque* 7 (1758) 9–28.  
URL <https://scholarlycommons.pacific.edu/euler-works/53/>
- [56] E. C. Kirby, R. B. Mallion, P. Pollak, P. J. Skrzyński, What Kirchhoff actually did concerning spanning trees in electrical networks and its relationship to modern graph-theoretical work, *Croatica Chemica Acta* 89 (4) (2016). doi:10.5562/cca2995.
- [57] G. Kirchhoff, Ueber die auflösung der gleichungen, auf welche man bei der untersuchung der linearen vertheilung galvanischer ströme geführt wird, *Annalen der Physik und Chemie* 148 (12) (1847) 497–508. doi:10.1002/andp.18471481202.

- [58] G. Kron, Elastic structures from the point of view of topological network theory, in: RAAG Memoirs of the Unifying Study of Basic Problems in Engineering and Physical Sciences by Means of Geometry, 1st Edition, Vol. 3, Gakujutsu Bunken Fukyu-Kai, 1962, pp. 329–337.  
URL <https://lccn.loc.gov/60004906>
- [59] S. J. Fenves, F. H. Branin, Network-topological formulation of structural analysis, *Journal of the Structural Division* 89 (4) (1963) 483–514. doi:10.1061/JSDEAG.0000954.
- [60] S. J. Fenves, Structural analysis by networks, matrices, and computers, *Journal of the Structural Division* 92 (1) (1966) 199–222. doi:10.1061/JSDEAG.0001379.
- [61] N. Lind, Analysis of Structures by System Theory, *Transactions of the American Society of Civil Engineers* 128 (2) (1963) 786–806. doi:10.1061/TACEAT.00088.
- [62] P. Block, J. Ochsendorf, Thrust network analysis: A new methodology for three-dimensional equilibrium, *Journal of the International Association for Shell and Spatial Structures* 48 (3) (2007) 167–173, (ISSN: 1996-9015).
- [63] P. O. Ohlbrock, P. D'Acunto, A computer-aided approach to equilibrium design based on graphic statics and combinatorial variations, *Computer-Aided Design* 121 (2020) 102802. doi:10.1016/j.cad.2019.102802.
- [64] R. Pastrana, P. O. Ohlbrock, T. Oberbichler, P. D'Acunto, S. Parascho, Constrained form-finding of tension-compression structures using automatic differentiation, *arXiv* (Nov. 2021). doi:arXiv:2111.02607.
- [65] O. Shai, K. Preiss, Isomorphic representations and well-formedness of engineering systems, *Engineering with Computers* 15 (1999) 303–314. doi:10.1007/s003660050025.
- [66] O. Shai, K. Preiss, Representation of embedded engineering knowledge for design, in: 5th International Conference on Artificial Intelligence in Design, Springer Netherlands, Dordrecht, 1998, pp. 149–167. doi:10.1007/978-94-011-5121-4\_8.
- [67] O. Shai, K. Preiss, Graph theory representations of engineering systems and their embedded knowledge, *Artificial Intelligence in Engineering* 13 (3) (1999) 273–285. doi:10.1016/S0954-1810(99)00002-3.

- [68] A. Kaveh, Structural mechanics: Graph and matrix methods, Macmillan International Higher Education, London, 1992, (ISBN: 978-1-349-87760-7).
- [69] A. Kaveh, The role of algebraic graph theory in structural mechanics, in: B. Topping, C. Mota Soares (Eds.), Progress in Computational Structures Technology, 1st Edition, Saxe-Coburg Publications, Scotland, 2005, pp. 77–110, (ISBN: 978-1-874672-21-0).
- [70] J. C. Maxwell, On the calculation of the equilibrium and stiffness of frames, *The London, Edinburgh, and Dublin Philosophical Magazine and Journal of Science* 27 (182) (1864) 294–299. doi:10.1080/14786446408643668.
- [71] T.-S. Tay, W. Whiteley, Generating isostatic frameworks, *Structural Topology* 11 (Jan. 1985).  
 URL <https://upcommons.upc.edu/handle/2099/1047>
- [72] C. Calladine, Buckminster Fuller’s “Tensegrity” structures and Clerk Maxwell’s rules for the construction of stiff frames, *International Journal of Solids and Structures* 14 (2) (1978) 161–172. doi:10.1016/0020-7683(78)90052-5.
- [73] R. Connelly, P. W. Fowler, S. D. Guest, B. Schulze, W. J. Whiteley, When is a symmetric pin-jointed framework isostatic?, *International Journal of Solids and Structures* 46 (3) (2009) 762–773. doi:10.1016/j.ijsolstr.2008.09.023.
- [74] G. Laman, On graphs and rigidity of plane skeletal structures, *Journal of Engineering Mathematics* 4 (4) (1970) 331–340. doi:10.1007/BF01534980.
- [75] M. Grötschel, L. Lovász, A. Schrijver, The ellipsoid method and its consequences in combinatorial optimization, *Combinatorica* 1 (2) (1981) 169–197. doi:10.1007/BF02579273.
- [76] S. J. Gortler, A. D. Healy, D. P. Thurston, Characterizing generic global rigidity, *American Journal of Mathematics* 132 (4) (2010) 897–939. doi:10.1353/ajm.0.0132.
- [77] D. J. Jacobs, B. Hendrickson, An algorithm for two-dimensional rigidity percolation: the pebble game, *Journal of Computational Physics* 137 (2) (1997) 346–365. doi:10.1006/jcph.1997.5809.

- [78] S. Bereg, Certifying and constructing minimally rigid graphs in the plane, in: Proceedings of the twenty-first annual symposium on Computational geometry, Association for Computing Machinery, New York, NY, USA, 2005, pp. 73–80. doi:10.1145/1064092.1064106.
- [79] O. Daescu, A. Kurdia, Towards an optimal algorithm for recognizing Laman graphs, *Journal of Graph Algorithms and Applications* 13 (2009) 219–232. doi:10.7155/jgaa.00185
- .
- [80] L. Henneberg, Die graphische Statik def starren Körper, in: Encyklopädie der mathematischen Wissenschaften mit Einschluss ihrer Anwendungen, Vol. IV, Vieweg+Teubner Verlag, Wiesbaden, 1908, pp. 345–434, (ISBN: 978-3-663-16021-2).
- [81] G. Grasegger, Realizations and Constructions of Minimally Rigid Graphs, in: Bridges 2018 Conference Proceedings, Stockholm, Sweden, 2018, pp. 539–542.  
URL <https://archive.bridgesmathart.org/2018/>
- [82] G. Grasegger, C. Koutschan, E. Tsigaridas, Lower Bounds on the Number of Realizations of Rigid Graphs, *Experimental Mathematics* 29 (2) (2020) 125–136. doi:10.1080/10586458.2018.1437851.
- [83] J. Cheng, M. Sitharam, I. Streinu, Nucleation-free 3D rigidity, in: Proceedings of the 21st Annual Canadian Conference on Computational Geometry, Vancouver, Canada, 2009, pp. 71–74.  
URL [http://cccg.ca/proceedings/2009/cccg09\\_19.pdf](http://cccg.ca/proceedings/2009/cccg09_19.pdf)
- [84] H. Pollaczek-Geiringer, Über die gliederung ebener fachwerke, *Zeitschrift für Angewandte Mathematik und Mechanik* 7 (1) (1927) 58–72. doi:<https://doi.org/10.1002/zamm.19270070107>.
- [85] J. Cruickshank, On Spaces of Infinitesimal Motions and Three Dimensional Henneberg Extensions, *Discrete & Computational Geometry* 51 (3) (2014) 702–721. doi:10.1007/s00454-014-9580-y.
- [86] R. J. Trudeau, Introduction to Graph Theory, 2nd Edition, Dover Publications, New York, 1994, (ISBN: 978-0-486-67870-2).

- [87] T. V. Mele, et al., COMPAS: A framework for computational research in architecture and structures. (2017).  
URL <https://doi.org/10.5281/zenodo.2594510>
- [88] P. Fleischmann, G. Casas, M. Lyrenmann, COMPAS RRC: Online control for ABB robots over a simple-to-use Python interface. (Jul. 2020).  
URL <https://doi.org/10.5281/zenodo.4639418>
- [89] L. Ding, W. Jiang, Y. Zhou, C. Zhou, S. Liu, BIM-based task-level planning for robotic brick assembly through image-based 3D modeling, *Advanced Engineering Informatics* 43 (2020) 100993. doi:10.1016/j.aei.2019.100993.

# 6

## Coopearative Robotic Disassembly and Reuse of a Timber Frame Structure

This chapter is based on the following publication:

**Bruun, E. P. G.**, Adriaenssens, S., Besler, E., & Parascho, S. (2024). ZeroWaste: Disassembly and Reuse of a Timber Frame Structure using Cooperating Robots. *Construction Robotics*. (Accepted)

Contributor roles in publication:

- Bruun: Conceptualization, Methodology, Software, Validation, Investigation, Writing (Original Draft), Writing (Review and Editing), Visualization
- Adriaenssens: Writing (Review and Editing), Supervision, Funding Acquisition
- Besler: Conceptualization, Resources, Writing (Review and Editing), Funding Acquisition
- Parascho: Conceptualization, Resources, Writing (Review and Editing), Supervision, Funding Acquisition



*Figure 6.1: An existing timber structure is disassembled and reassembled into a new configuration with a team of cooperating robots.*

## Abstract

This chapter presents the results of the ZeroWaste project, showcasing how circular economy principles are realized through cooperative robotic fabrication methods. A pavilion-scale conventional stick frame prototype structure is initially constructed (as shown on the left in [fig. 6.1](#)). Precise geometric data is then obtained using a robotic cell equipped with three large-scale robotic arms and 3D cameras, facilitating planning of robotic processes. A novel topological representation, the support hierarchy graph, is developed to generate fabrication sequences, assessed for robotic execution and structural feasibility. Leveraging the cooperative robotic setup, disassembly sequences are planned without external scaffolding, as the robots are used to provide temporary support. Three physical fabrication phases validate the computational and robotic workflow: Phase 1 involves small-scale disassembly, Phase 2 expands to full wall disassembly with minor reassembly, and Phase 3 disassembles remaining members while concurrently reassembling them to create a stiffer lattice structure. These fabrication phases result in a modified structural configuration (as shown on the right in [fig. 6.1](#)) that demonstrates the potential of existing buildings to be used as reservoirs of reusable materials through the implementation of scaffold-free cooperative robotic disassembly and reassembly methods.

## 6.1 Introduction

The Architecture, Engineering, Construction (AEC) industry has a significant negative impact on the environment due to its material and energy-intensive manufacturing and construction processes [1] and the high embodied carbon content of structural systems [2, 3]. For example, buildings and construction activities accounted for 36% of global energy-usage and of 37% of global CO<sub>2</sub> emissions in 2020 [4]. This impact is further exacerbated by the increasing waste generated by construction and demolition (C&D) processes [5, 6], which were estimated to account for up to 30% of total waste produced globally in the 1990s [7, 8].

To illustrate this worsening trend, in the mid-1990s in the United States, construction and demolition (C&D) activities were responsible for generating an estimated 100-135 million tons of waste, of which approximately 35-45% found its way to landfills [9, 10]. This C&D waste accounted for 29% of the total landfill volumes at that time [11]. However, by 2018, the volume of waste from C&D activities had surged to 600 million tons, with 144 million tons or 24% of this waste ending up in landfills [12]. Thus, approximately half of landfill volumes in 2018 were associated with C&D activities, with the remaining municipal solid waste contributing 146 million tons [12]. This trend is especially concerning when considering the substantial construction needs of the coming century. Aging infrastructure must be replaced while accommodating the requirements of a growing and rapidly urbanizing global population [13].

Reducing the construction industry's material usage and waste generation involves harnessing technological advancements such as robotics and automation to boost productivity and efficiency of construction processes. However, this is only one part of the solution, as addressing waste begins at the design phase, where strategic planning can significantly reduce material usage and waste generation throughout the project life cycle. Research indicates that a notable portion of construction waste stems from inadequate waste reduction measures early in the design stages, particularly in planning for building decommissioning [14]. With demolition accounting for over 90% of construction and demolition (C&D) debris generation [12], the industry faces a pressing need for transformation. Therefore, adopting a design paradigm centered on deconstruction and material reuse aligns with the principles of a circular economy [15], and presents a possible solution to the industry's waste challenges.

### **6.1.1 Chapter Organization**

The chapter is structured into several key sections to comprehensively present the research. First, in [Section 6.2](#), a literature review is presented, covering topics such as circular economy design frameworks and robotic fabrication within the context of material circularity. An overview of the ZeroWaste project, which forms the basis of this chapter, is also provided specifically describing how the project addresses circular economy and robotic fabrication through its research objectives. Following this, in [Section 6.3](#), the experimental setup is outlined, describing the physical robotic fabrication cell and the experimental prototype that is built and then experimented on in the three subsequent project phases. In [Section 6.4](#), the workflow and methods are detailed, focusing on the computational methods developed for various aspects of the project. This includes the use of robot-mounted 3D cameras to gather geometric information about the as-built conditions of the structure, the development of the topological support hierarchy representation, and the methods used to generate robotic fabrication sequences and assess their feasibility. In [Section 6.5](#), the results of implementing the computational methods described in the previous section to plan and then execute three different disassembly and reassembly robotic fabrication tasks on the prototype structure are presented and discussed. Finally, in [Section 6.6](#), the chapter concludes with a summary of the main results and discussions from the fabrication tasks performed on the prototype structure, and suggesting ideas for future work stemming from limitations of the current work.

## **6.2 Literature Review**

### **6.2.1 Circular Economy Design Frameworks**

The construction industry is actively moving away from the traditional linear single-use material flow model. To support this transition, there has been a focus on developing models for quantifying the environmental benefits of material circularity and the potential for reusing existing building stock, as evidenced in works such as [\[16, 17\]](#). In parallel, novel frameworks have emerged that break down the concept of circularity into distinct principles relating to material and energy flows. An illustrative framework is the “narrow, slow, close, and regenerate” framework

outlined in [18, 19], which serves as the basis for a recent book on shifting to the circular built environment while leveraging modern digital technologies [20].

Specifically, the “slow” principle, which focuses on extending the lifespan of products and components, encompasses a range of circular product design and business strategies that are applicable to the building industry [21]. One such strategy, known as “design for dis- and reassembly,” is demonstrated by a growing body of research that highlights practical implementation of design and optimization strategies for the disassembly, reuse, and reconfiguration of discrete element structures. This includes examples applied to a variety of structural systems like planar trusses [22, 23], space frames [24, 25], moment frames [26], reciprocal frames [27, 28].

### 6.2.2 Robotic Fabrication and Material Circularity

The construction industry, despite its potential to benefit from technological advancements that enhance efficiency, has been slow in embracing automation technology and realizing productivity gains in comparison to other sectors, as observed over the last five decades [29]. Nonetheless, an opportunity still exists to leverage modern technological innovations, with a particular focus on the use of robots to improve the productivity of construction [30], particularly when applied to the construction of geometrically complex and materially efficient bespoke structures [31].

In the initial phase of introducing robots to the construction industry during the 1980s, the primary focus was on utilizing single robots to automate individual human tasks [32, 33]. In recent years, however, researchers have shifted their focus from task-specific automation towards an approach that integrates robots into a broader construction context, using more complex robotic setups for collaborative and adaptive construction processes to expand the possibilities of what can be designed and built [34, 35]. This shift involves leveraging the unique capabilities of robots, such as their precision in repetitive movement, accurate spatial positioning of components, and ability to perform long-duration tasks. For instance, the adoption of a cooperative robotic fabrication framework, first demonstrated in [36], has emerged as a promising avenue, demonstrating the potential to enhance both fabrication complexity and the degree of automation [37, 38]. Cooperative robotic fabrication, a specialized form of robotic manufacturing, entails synchronized robotic agents working together to achieve greater system utility and unique out-

comes that would be unattainable with independent robot operation [39]. This stands in contrast to collaborative robotic processes, where human operators work alongside robotic setups, occurring in either a cooperative robotic [40] or non-cooperative robotic setting [41].

The benefits of utilizing multiple robots collaborating go beyond just improving production efficiency. Cooperative robotic fabrication projects have explicitly demonstrated principles of circular economy and material circularity. A recent review titled “Cooperative Robotic Fabrication for a Circular Economy” by [42] provides a comprehensive overview of the general applications of cooperative robotic fabrication in the construction industry. The review further delves into these applications within the specific context of material reuse and reduction as integral components of a circular economy strategy. Examples of material reduction include minimizing the need for scaffolding during masonry [43–45] and steel [36, 46] structure construction through robot-assisted temporary support. Additionally, designing a timber space frame structures from the outset to be (dis)assembled in a scaffold-free manner with a cooperating team of robots as first demonstrated in [25].

### 6.2.3 The ZeroWaste Project

This chapter presents a comprehensive exploration of the ZeroWaste project, extending the research documented in recent publications [42, 47]. It serves as a practical demonstrator and a pivotal link between the existing body of research in the field of circular economy (as outlined in [Section 6.2.1](#)) and the implementation of robotic automation technology in the construction industry (as outlined in [Section 6.2.2](#)).

The research is conducted on a prefabricated timber prototype, which is meant to represent a generic unknown existing structure built according to the common North American stick frame construction practices. This choice is based on the prevalence of this building type coupled with the frequency that timber buildings are disposed of at the end their lives, as noted in previous studies [48, 49]. Notably, of the 40.8 million tons of wood construction debris generated in 2018 in the US, 72% of this total is sent to landfills, where 92% of this amount is attributed to demolition processes [12]. To address this linear material flow, reimagining timber buildings as material depots is proposed, recognizing their potential as reservoirs of valuable resources in the context

of a circular economy [50]. This shift prioritizes the upstream flow of materials on construction sites, reducing reliance on upstream virgin materials and downstream recycling and waste industries [51]. In addition, the aim is to perform all processes in a scaffold-free manner to reduce the materials typically required to provide support during assembly and disassembly.

## Research Objectives

The ZeroWaste project is situated at the intersection of two key research areas: (1) circular economy and (2) robotic fabrication. The project aims to achieve various objectives that highlight the possibilities and benefits of combining these two research domains.

The objectives related to circular economy principles are the following:

1. **Physical Implementation Study:** Demonstrate how existing timber buildings can serve as reservoirs of reusable materials.
2. **Material Reuse:** Disassemble and reassemble portions of an existing prototype structure, demonstrating the potential for creating new configurations from previously used materials.

The objectives related to robotic fabrication are the following:

1. **Cooperative Fabrication:** Harness the capabilities of a cooperative robotic setup, consisting of three large-scale robotic arms, working in a coordinated manner to improve the fabrication utility of the setup.
2. **Fabrication Sequences:** Calculate feasible cooperative robotic assembly and disassembly sequences when considering constraints related to robotic reachability and structural stability.
3. **Scaffold-free Construction:** Execute the fabrication sequences without the need for external temporary scaffolding, utilizing the robots themselves as passive structural supports.
4. **Member Localization:** Utilize robot-mounted 3D cameras to generate geometrically pre-

cise as-built digital models of the existing timber prototype structure.

The significance of these objectives extends beyond the specific structural prototype under study. They offer a versatile framework applicable to a wide range of timber structures and discrete element topologies. The ZeroWaste project serves as a compelling illustration of how circular economy principles can be integrated into construction practices, and it highlights the potential for modern robotic fabrication setups to streamline the complex processes involved in efficient disassembly and reuse of building components.

## 6.3 Experimental Setup

### 6.3.1 Robotic Fabrication Cell

The cooperative robotic cell employed in this study is illustrated schematically in [Figure 6.2](#). It features two IRB4600-40/2.55 robotic arms mounted on parallel linear tracks, providing a maximum travel distance of 3.9 m in the North-South direction. Positioned at the South end of the cell is an IRB7600-400/2.55 robotic arm securely fixed to the ground. All three robots are equipped with standard linear grippers featuring custom fingers tailored for pick-and-place operations involving dimensional lumber. Additionally, each of the IRB4600s is equipped with a high-definition 3D machine vision camera, the details of which are further discussed in [Section 6.4.1](#).

The computational workflow relies on the COMPAS framework [52]. Robotic fabrication processes are planned and executed using the COMPAS FAB package in conjunction with a ROS backend [53]. The execution of robotic motion commands is facilitated through COMPAS RRC [54], and the corresponding RRC driver operates on the IRC5 controller.

### 6.3.2 Experimental Prototype

At the heart of this research project is a prefabricated physical prototype - a timber shed structure constructed in accordance with conventional American stick frame construction practices. This prototype serves as a representative example of an existing structure that will undergo robotic disassembly and reassembly, demonstrating the real-world application of

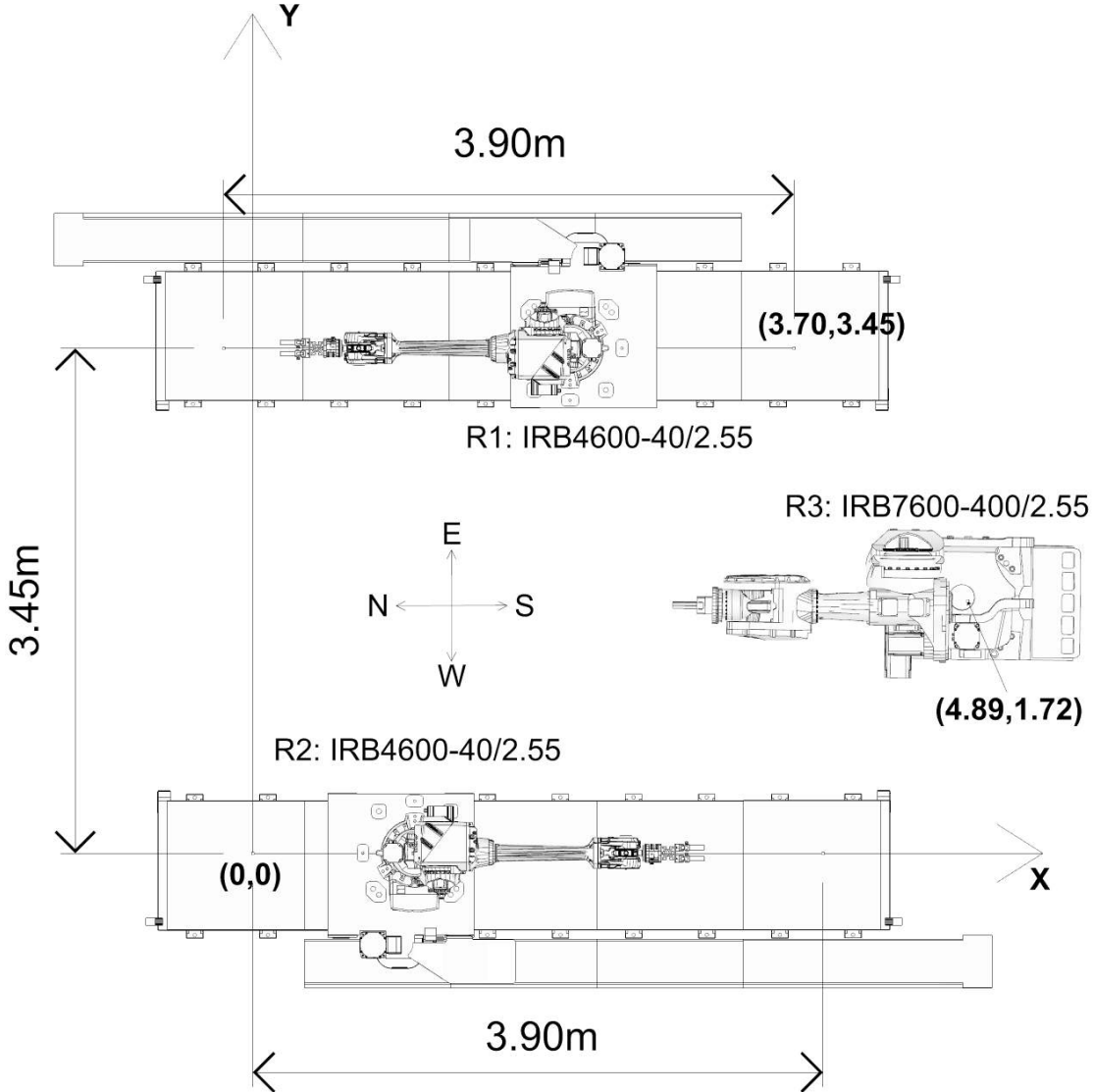
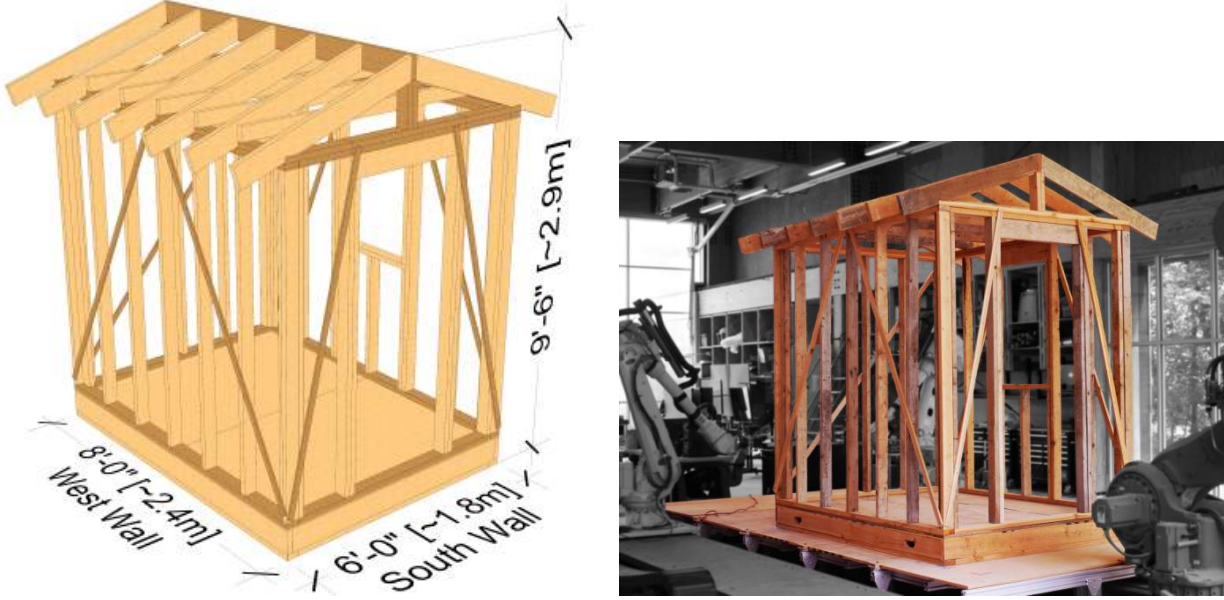


**Figure 6.2:** Layout of the three-robot cooperative fabrication cell with North defined towards the left.

the computational methods developed in this research. Illustrated in [Figure 6.3](#), the structure has dimensions of 8 x 6 ft (~2.4 x 1.8 m) in plan, a stud wall height of 8.0 ft (~2.6 m), and a crown height of 9.6 ft (~2.9 m). Constructed using 2x4" and 2x6" SPF dimensional lumber, the traditional planar wall sheathing is replaced with linear members positioned diagonally across the stud wall to impart the necessary shear stiffness.

To streamline the forthcoming presentation of results and discussion regarding robotic fabrication sequences, the overall prototype structure is represented as a composite of distinct sub-structures - namely, the four walls (East, West, North, South) and the roof. Each of these sub-



*(a)* Rendering of the structure showing the dimensions and naming convention for the walls.

*(b)* Image of structure showing its placement in the robotic work cell (from [47]).

**Figure 6.3:** The prototype timber structure.

structures is then comprised of individual linear members, systematically labeled, and color-coded according to their respective types as shown in [Table 6.1](#). The color-coded members and the five sub-structures are depicted in [Figure 6.4](#), where the individual members are labelled using the following convention  $AB\#\_\$$ , where:

A: The first letter indicates if it is part of the roof (R) or one of the four walls (N, S, E, W).

B: The second letter represents the type of member, as shown in the 2nd column of [Table 6.1](#).

#: The third digit is used to number a unique member of a particular type.

\$: The fourth digit (if required) is used to number a section of a single member.

The color-coding and member notation described in [Table 6.1](#) and [Figure 6.4](#) matches the topological support hierarchy representation, which is introduced in [Section 6.4.2](#). This convention is consistently used in all the subsequent results and discussions in the chapter.

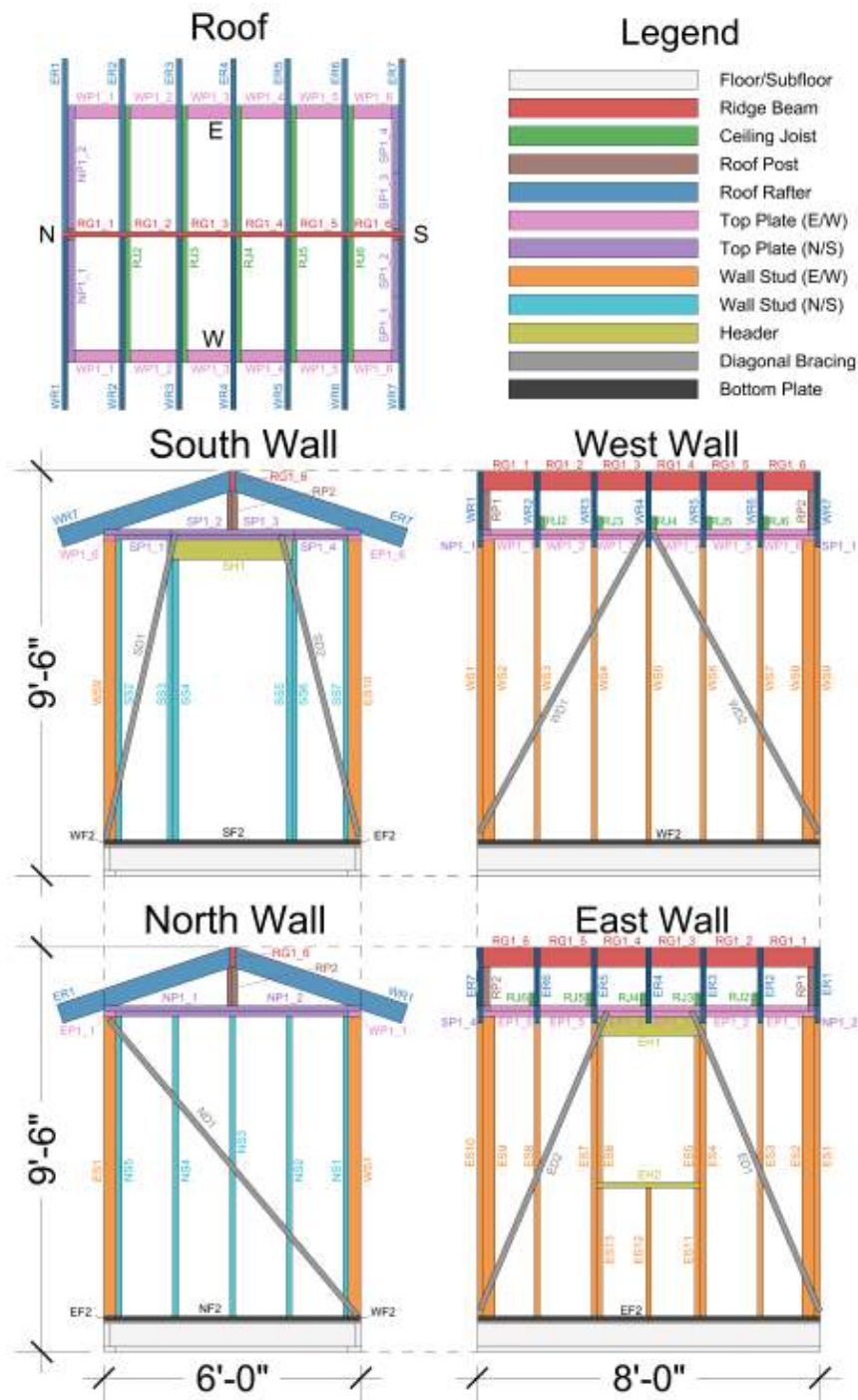


**Figure 6.4:** Prototype structure shown as an assembly of five sub-structures with the members in each color-coded according to their type.

**Table 6.1:** Members in the prototype structure

Member	Letter	Count	Color
Floor	N/A	N/A	white
Roof Girder	G	1	red
Ceiling Joist	J	5	green
Roof Post	P	2	brown
Roof Rafter	R	14	blue
Top Plate (E/W)	P	2	pink
Top Plate (N/S)	P	2	purple
Wall Stud (E/W)	S	22	orange
Wall Stud (N/S)	S	12	cyan
Header	H	3	yellow
Diagonal Bracing	D	7	grey
Bottom Plate	F	4	black

### 6.3.3 Project Phases

The ZeroWaste project aims to develop an integrated computational workflow for orchestrating a cooperative, scaffold-free robotic disassembly and reassembly process on an unknown existing structure. The practical manifestation of this goal involves a series of physical demonstrations on the prototype timber structure described in [Section 6.3.2](#). The overall project is strategically divided into three distinct fabrication phases, each serving as a milestone to incrementally evaluate the developed methods described in [Section 6.4](#). Each phase demonstrates increasing complexity in both the structural disassembly and reassembly tasks and the degree of cooperative robotic sequencing necessary to execute these tasks. These phases are as follows: Phase 1, single target member removal; Phase 2, full wall disassembly and partial reassembly; Phase 3, full wall removal and reassembly. Further details and the results of these fabrication phases are presented in [Section 6.5](#).

## 6.4 Workflow and Methods

The overarching computational workflow utilized across all phases of the ZeroWaste project is illustrated in [Figure 6.5](#), depicting three primary components. Firstly, the use of 3D cameras mounted on robots to capture geometric and positional data pertaining to the unknown existing timber structure, which is here represented by the prototype shed ([section 6.4.1](#)). Secondly, calculation of potential cooperative robotic disassembly and reassembly sequences when given user-specified member targets. This is achieved by leveraging the topological member support hierarchy representation of the structure ([section 6.4.2](#)). Lastly, the workflow incorporates an evaluative process, assessing the feasibility of generated fabrication sequences, given the generated geometric data on the structure, regarding both structural performance and constraints associated with robotic reach and path planning ([section 6.4.3](#)).

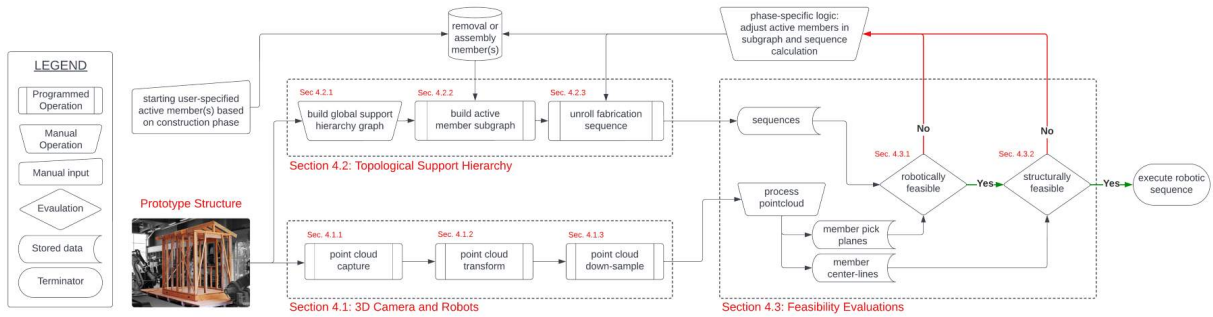


**Figure 6.5:** Computational workflow showing the interaction between the methods described in [Section 6.4](#).

### 6.4.1 3D Camera and Robots

Each of the two IRB4600 robots, positioned on tracks, is equipped with a Zivid 3D structured light camera with a spatial resolution of 0.39 mm at a distance of 700 mm [[55](#)]. The initial phase of the project involved creating a point cloud of the entire existing structure, which is a composite stitched together from several independent camera captures taken at various locations around the structure. Performing this procedure is essential before initiating any fabrication processes since an accurate digital representation of the as-built geometry of the unknown structure is required. Even if a pre-existing digital model of the structure is available, as is the case with the

prototype structure, this point cloud step must still be performed as the as-built conditions of the structure invariably differ from the perfect digital model.

Moreover, beyond generating an accurate geometric representation of the structure, accurately positioning this geometry within the workcell is equally vital. This requires that the structure is correctly situated with respect to robots. Precise relative positioning is essential for the execution of robot move commands, which are sent relative to robots' base coordinate frame - that is, where the robot perceives its spatial location to be. Therefore, maintaining alignment between the as-built digital representation of the real structure and the perceived location of the robots in the fabrication cell is crucial for the execution of all robotic movements.

## Point Cloud Capture

To construct an accurate as-built model of the structure, the robots capture 3D images from different spatial positions as they move around the structure ( $R1 = 105$ ,  $R2 = 62$  separate positions). Each capture generates a unique point cloud. The individual point clouds are then transformed to the correct global coordinate frame and combined into a single point cloud representing the whole structure, shown in [Figure 6.6](#).

## Point Cloud Transform

The cameras are mounted on the robots used for the fabrication tasks, which is known as an eye-in-hand setup. Since the Tool Center Point (TCP) location with respect to the robot base is always known by the robot controller, this can be used to perform coordinate transforms on point clouds captured by the fixed camera. A point in the camera's coordinate system (i.e., how the camera sees the object),  $P_{object\_camera}$ , can be transformed to a point in the global coordinate frame of the CAD model,  $P_{object\_world0}$ , aligned with where the robots are situated in the global coordinate frame in the following manner:

$$P_{object\_world0} = H_3 * H_2 * H_1 * P_{object\_camera}$$

Where the 4x4 transformation matrices are the following:

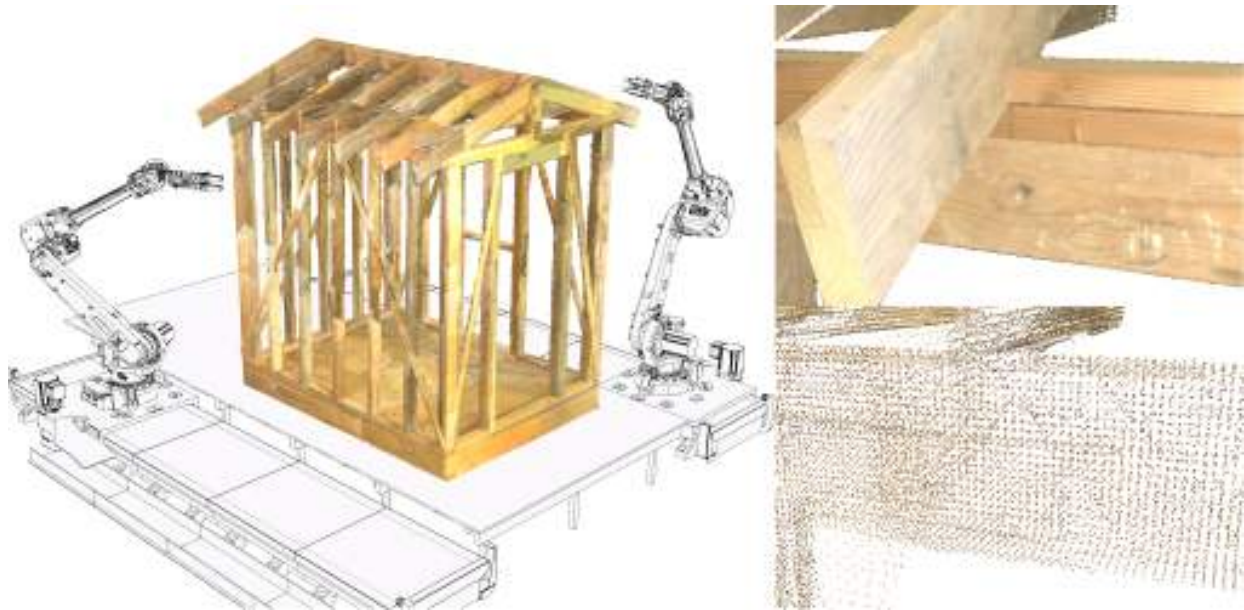


**Figure 6.6:** As-built point cloud of the prototype structure from combined individual captures transformed to the correct location in space with respect to the robotic cell (left). Point cloud density for a small region of the structure before (top-right) and after (bottom-right) down-sampling with low-definition settings.

- H1: from TCP to camera. This transformation is calculated from a single eye-in-hand calibration routine that must be performed only once each time the camera is re-mounted.
- H2: from robot base to TCP. This transformation is calculated from the positional frame representing the TCP, which is queried from the robot controller using the COMPAS RRC API [54] at each camera capture.
- H3: from World0 to Work Object (WOBJ) frame. This transformation is calculated from an user-defined coordinate frame set for each robot. This frame serves to establish a unified coordinate system for all the robots in multi-robot process, aligning them with the global coordinate frame of the CAD model. Consequently, all positional data is defined relative to this unified coordinate system.

### Point Cloud Down-Sample

The 3D cameras have a resolution that results in captured point clouds with greater fidelity than is strictly necessary for the subsequent robotic processes. Individual captures range from

50-200k points, resulting in raw combined point cloud model with 23.6M points ( $R1 = 14.5M$  and  $R2 = 9.1M$  points). A model of this size is computationally expensive to work with. In addition, the process of combining separate captures also leads to overlapping regions with duplicated points. Thus, further processing to reduce the overall point cloud density and remove the unnecessary duplicate points is required.

The raw point cloud undergoes down-sampling using statistical outlier, radius outlier, and voxel filters from the open3D package library [56]. The hyper-parameters for this process are shown in [Table 6.2](#), where the more aggressive low-definition (LD) settings result in a coarse overall model with only 0.55 million points, while the high-definition (HD) settings result in a model with 11.8M points. A final manual clean to remove unnecessary points, such as the ground, or any visible missed outliers, further reduces the model size slightly. The smaller LD model is used in computational processes where working with a minimal dataset is crucial, while the higher quality HD model is suitable for visual applications.

**Table 6.2:** Hyper-parameters and results for low-definition (LD) and high-definition (HD) down-sampling procedures

	LD	HD
pcd (start)	23.6M	23.6M
voxel_size (m)	0.010	0.001
nb_neighbor	30	20
std_ratio	1.0	2.0
nb_points	20	20
radius (m)	0.08	0.08
pcd (down-sample)	0.6M	11.8M
pcd (manual clean)	0.5M	11.3M

[Figure 6.6](#) displays the final stitched model of the as-built prototype structure accurately located with respect to the robotic cell after the process of transformation and down-sampling. This image also illustrates the difference in the density between the raw and down-sampled point clouds for a small region of the structure.

### 6.4.2 Topological Support Hierarchy

Creating a computational framework to plan disassembly and reassembly sequences that are both stable and feasible requires a robust representation of the interconnections and support relationships within a structure. One effective method for visualizing this connectivity is using a multidirected graph (multidigraph) data structure [57]. In the context of this research, a representation referred to as the topological support hierarchy graph was developed. In this graph, individual members are depicted as vertices, while physical connections between members are represented as edges. The direction of support is indicated by outgoing edges, effectively portraying the load-path.

However, representing geometric information, such as where along a member (e.g., a top plate) multiple members are being supported, poses a challenge in a topological data structure like a graph. To address this challenge, a more detailed and precise graph representation by decomposing certain elements into their constituent submembers is proposed. Each submember is then treated as an independent vertex in the graph. To signify their mutually supportive relationship, vertices corresponding to submembers of the same member are connected by two parallel, opposing edges — a situation referred to as a fixed connection.

[Figure 6.7](#) illustrates the methodology for how a structure can be represented as a topological support hierarchy graph, for two members (B) supported by members (A and C). This graph representation can be further refined by dividing members A and C into submembers, providing a more nuanced depiction of how individual members are supported within the structure.

#### Build Global Support Hierarchy Graph

The global support hierarchy graph representing the entire prototype structure, which is an input to the computational processes for planning robotic fabrication sequences, is shown in [Figure 6.8](#). Constructed manually, this graph adheres to the principles illustrated in [Figure 6.7](#). Vertex names and colors are aligned with the member naming and color scheme described in [Section 6.3.2](#), while edges are color-coded based on their originating vertices. To more accurately capture the support hierarchy of the numerous individual members supported on them, the top plate and roof ridge beam members are represented as a series of submembers with fixed sup-

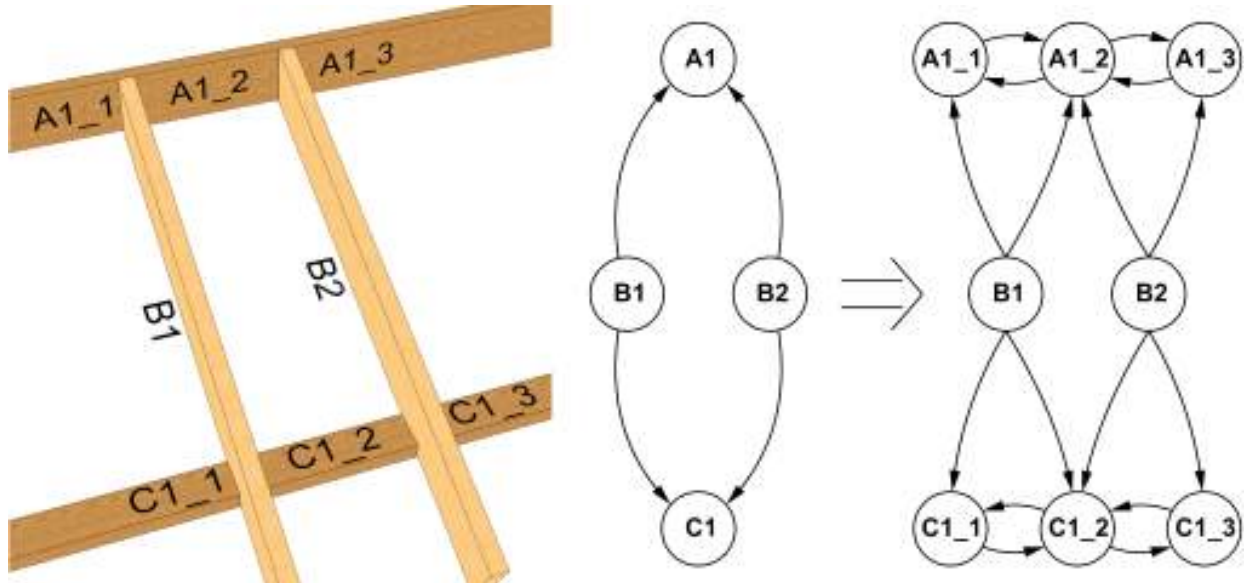


**Figure 6.7:** Directed edges show that members  $B1$ ,  $B2$  are supported by members  $A1$  and  $C1$ . These support members can also be shown subdivided into their constituent submembers that are connected with parallel and opposite edges to represent a fixed connection.

ports between them.

The graph in Figure 6.8 visually partitions the structure into five distinct regions, either the roof or one of the four walls. However, this segmentation is primarily for clarity since the relative positioning of vertices lacks significance, as a graph data structure exclusively conveys topological information. The structure terminates at the foundation supports, visually shown in the graph by hexagonal vertices that represent the connection between the bottom plate of each wall and the ground beneath.

### Build Active Member Subgraphs

Given an active member, such as a target specified for removal, an algorithmic operation can be executed on the global support member hierarchy graph of the entire structure. This procedure yields a subgraph encompassing the members that are directly affected during the removal of the active member.

This procedure is based on a customized breadth-first search algorithm [57], which is used to traverse the regions in the global support hierarchy graph adjacent to the vertex representing the target member. The rationale for this search approach is that achieving a feasible disassembly

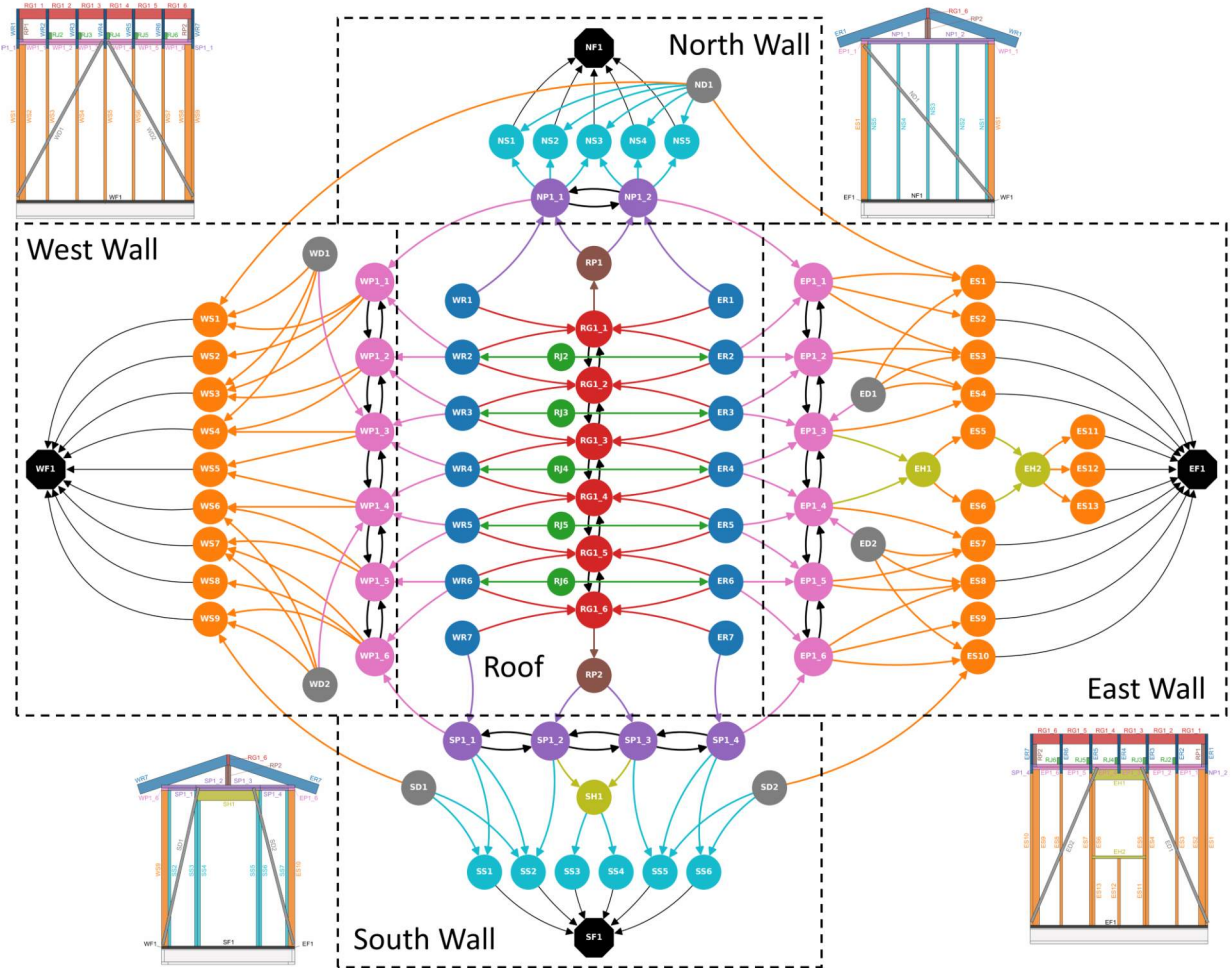


**Figure 6.8:** The global connection hierarchy in the timber prototype structure is represented as a multidirected graph with outgoing edges indicating the direction of support. The graph is organized into five regions, where the names and colors of the vertices are based on the convention introduced in Section 6.3.2.

sequence without leaving unstable or disconnected components in the structure is higher when all members in the region connected to the target member are also removed or identified as requiring some form of temporary support to during the overall removal process. For instance, if an active member is supporting several other members, it is logical to remove these supported members first as it is unlikely that they will remain structurally stable upon the removal of the active member. Thus, a breadth-first search is used to identify whether a member actively supports or is supported by other members, a condition represented by incoming and outgoing edges from neighboring vertices. Thus, any members connected to the active member will become part of the overall disassembly sequence. This procedure is then iterated to identify the members in turn

supported by these intermediate members, resulting in a subgraph of the global support hierarchy graph that represents all the affected members in for a user-specified active member.

The process of calculating subgraphs for individual user-specified active members is shown in [Algorithm 2](#), with the breadth-first search performed in the *calc\_subg* function ([section C.1.1](#)). When multiple user-specified active members are indicated for a single disassembly procedure, there is no need to repeat the breadth-first search. Instead, as shown in [Algorithm 3](#), the subgraphs representing the individual members can be joined to produce the subgraph for the multiple active member case. All graph-based computational processes are performed using the NetworkX package for Python [58].

---

**Algorithm 2** Single Member Subgraph(s) Calc

---

```

1: procedure bld_subg_single(G, rms)
2:   Ks  $\leftarrow$  []
3:
4:   for rm in rms do
5:     K  $\leftarrow$  calc_subg(G.copy(), rm)
6:     n_cut  $\leftarrow$  fxd_nodes_cut(G, K)
7:     fxd_nodes_support(G, K, rm, n_cut)
8:     Ks.append(K)
9:   end for
10:
11:  return Ks
12: end procedure
```

---



---

**Algorithm 3** Multi-Member Subgraph Calc

---

```

1: procedure bld_subg_multi(G, Ks, rms)
2:   K_joined  $\leftarrow$  nx.compose_all(Ks)
3:   add_in_extra_edge(G, K_joined)
4:   n_cut  $\leftarrow$  fxd_nodes_cut(G, K_joined)
5:   fxd_nodes_support(G, K_joined, rms, n_cut)
6:   return K_joined
7: end procedure
```

---

The breadth-first search concludes when the vertex-checking queue is empty. This occurs before traversing the entire graph due to certain conditions that lead to a vertex being labelled as an end, meaning its neighbors are not examined. For instance, a vertex with only outgoing edges implies that the member it represents can be removed without impacting any other parts of the

structure. Conversely, a vertex with only incoming edges designates a foundation support vertex that will not be removed.

The end condition is also triggered for any vertex possessing at least one fixed edge (i.e., equal and opposite parallel edges), indicating that it represents a submember. However, additional logic is necessary to determine whether these submembers qualify as valid end supports. A submember with only one fixed connection, designating it as the terminal segment of a larger member, may pose a potential stability hazard and requires further scrutiny. If such a submember shares a sole unidirectional edge with an active member, it necessitates removal, thus being treated as a standard vertex to be added to the breadth-first search queue. Alternatively, the submember may also require removal if all its edges are found in the subgraph, a condition verified in the *fxd\_nodes\_cut* function ([section C.1.2](#)). Otherwise, the submember is considered adequately supported and remains in the structure acting as an end support in the subgraph.

In the *fxd\_nodes\_support* function, all the ends that remain in the structure (i.e., submembers with fixed connections) are checked for adequate support at the culmination of the removal process ([section C.1.2](#)). Adequate support is defined by the requirement that at least two supports (i.e., outgoing edges) persist in the global support hierarchy graph once the subgraph has been deleted. For example, a submember with two fixed connections, signifying its placement within the interior of a larger member, is considered adequately supported. This condition serves as a safeguard against the formation of structurally undesirable cantilevered segments within the remaining structure after the disassembly process is completed. This is checked in both the single and multi-member subgraph procedures outlined in [Algorithms 2](#) and [3](#).

[Figure 6.9](#) shows example subgraphs calculated using the computational procedures outlined in this section given different user-specified targets: east side rafter #2 (ER2), east side stud #10 (ES10), north side top plate submember #1 (NP1\_1), east side top plate submember #2 (EP1\_2), and the composite of west side stud #3 (WS3) + west top plate submember #2 (WP1\_2). The colors for the edges and vertices in these subgraphs no longer indicate the physical member type, but instead represent output related to how the edges and vertices have been labelled in the computational process when generating the subgraph. For example, black is used for end members and green is used for start members. The shape of the vertices is also used to distinguish between different conditions. If an edge is black it represents typical support between members, but dashed

red edges indicate that a submember will require physical cutting from the overall member it is a part since it must be removed in the disassembly process. The complete legend for the nodes and edges are labelled in the active member subgraphs is shown in Figure 6.9.

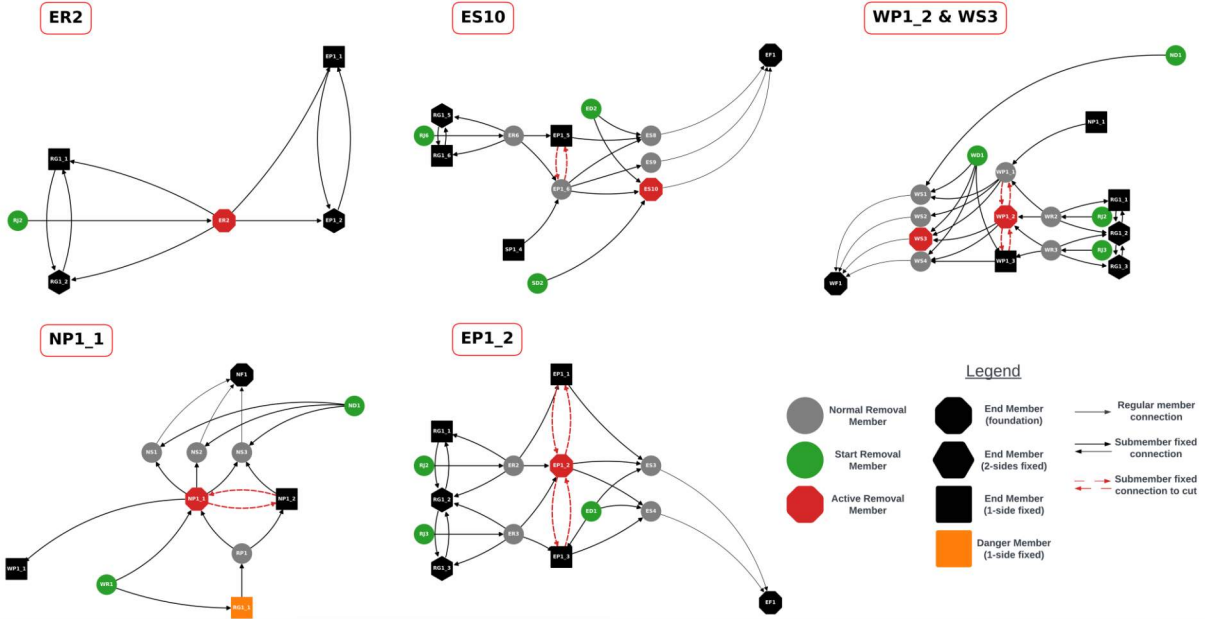


**Figure 6.9:** Examples of active member subgraphs constructed using the algorithmic procedures described in Section 6.4.2. Vertices and edges are drawn to represent the different conditions as per the legend.

## Calculate Fabrication Sequences

A computational procedure is employed to calculate a set of potential fabrication sequences, utilizing an active member subgraph generated through the methodology outlined in Section 6.4.2. Conceptually, this involves unfolding the subgraph data structure into a linear sequence of discrete fabrication steps. The overarching method for generating these sequences is summarized in Algorithm 4, with supplementary functions further explained in Section C.1.3.

The algorithm locates start vertices in the subgraph describing the full fabrication sequence. These vertices are first saved as a discrete disassembly step and then removed from the subgraph to represent the physical process occurring. The remaining subgraph is then relabeled with new start nodes to account for the resulting changes in the support hierarchy after this step is executed. This process of locating, removing, relabeling is iterated on the subgraph until all nodes are removed. The objective is to optimize the removal of the maximum number of members in

---

**Algorithm 4** Unroll subgraph into sequence

---

```
1: procedure bld_sequence(K, rms, num_agents)
2:   saved_K, saved_seq  $\leftarrow \[], []$ 
3:   n_active_type  $\leftarrow ["start", "rob_sprt"]$ 
4:
5:   while True do
6:     n1  $\leftarrow find\_n\_active(K, n\_active\_type)$ 
7:     n2  $\leftarrow set\_new\_to\_rob\_support(K)$ 
8:
9:     if n1  $\cup$  n2 is  $\emptyset$  then
10:      terminate loop
11:    end if
12:
13:    n_rmv, n_rob_sprt  $\leftarrow select\_n\_active(n1, n2)$ 
14:
15:    saved_K.append(K)
16:    saved_seq.append(n_rmv)
17:
18:    K.remove_nodes_from(n_rmv)
19:    K  $\leftarrow new\_subg\_relabel(K, rms)$ 
20:  end while
21:  return saved_K, saved_seq
22: end procedure
```

---

a single step, corresponding to the available robotic agents. In cases where the number of start nodes exceeds the count of robotic agents at a given step, a sequence is generated for each permutation. Subsequently, this exhaustive set of sequences is evaluated as outlined in [Section 6.4.3](#), to ascertain feasibility in terms of structural behavior and robotic reachability.

[Figure 6.10](#) illustrates a representative outcome of the fabrication sequence calculation process applied to the WP1\_2 & WS3 active member subgraph, as shown depicted in [Figure 6.9](#). These calculations consider the presence of two robotic agents, thus allowing the removal of a maximum of two members per step. In step #1, more than two start vertices are identified, implying the existence of multiple permutations at this stage, where the displayed sequence represents just one of these possibilities. All end nodes (depicted in black) are retained in the sequence graphs for better visualization; these nodes are not isolated components but are interconnected and adequately supported by the remaining structure beyond the boundaries of the specific subgraph.

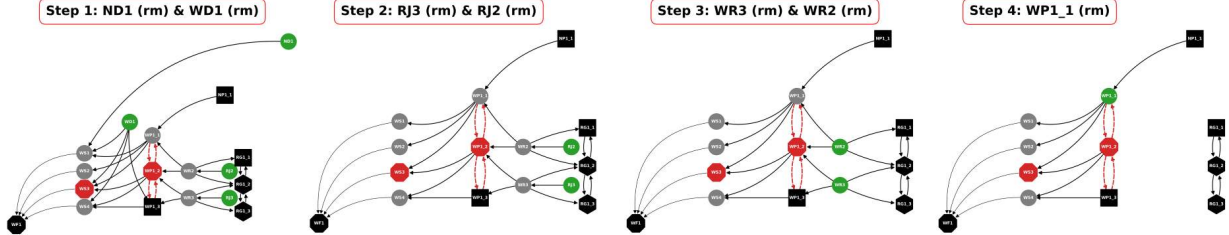


**Figure 6.10:** Example of a partial disassembly sequence (four steps) calculated from the subgraph for active members  $WP1\_2$  &  $WS3$ . After each step the subgraph is relabeled with new start nodes in green.

### 6.4.3 Feasibility Evaluations

The computational methods discussed in the preceding [Section 6.4.2](#), rooted in the topological support hierarchy representation of the structure, generate a sequence of fabrication plans when provided with a set of active members. The primary goal at this stage is just to discern fabrication sequences that could potentially be executed without external scaffolding while ensuring structural stability. Subsequently, these candidate sequences must undergo further examination, considering the physical structure itself, to verify feasibility and identify the optimal sequence.

An analysis of the generated sequences, evaluating both structural and robotic feasibility, precedes the selection of a sequence for execution. The verification process involves two concurrent procedures applied to the accurate as-built point cloud gathered as per the methods described in [Section 6.4.1](#). Firstly, the validation of robotic path planning and reachability is conducted using the COMPAS and COMPAS FAB package with a ROS backend [52, 53]. Secondly, a detailed parametric finite element (FE) analysis of the structure is carried out in Rhino/Grasshopper with Karamba3D [59, 60] to assess the structural behavior at each step in the fabrication sequence.

#### Robotic Feasibility

The first procedure involves assessing the physical executability of a proposed sequence from the robotic perspective. This evaluation focuses on ascertaining whether a robot can safely access and grip each building member specified in the sequence. This assessment is performed computationally through an inverse kinematic (IK) path planning operation, trying to move the robot to a target location on a specified member in the structure. This is done using the *Plan Motion* script implementing the RRT-connect path planning algorithm available as part of the COMPAS

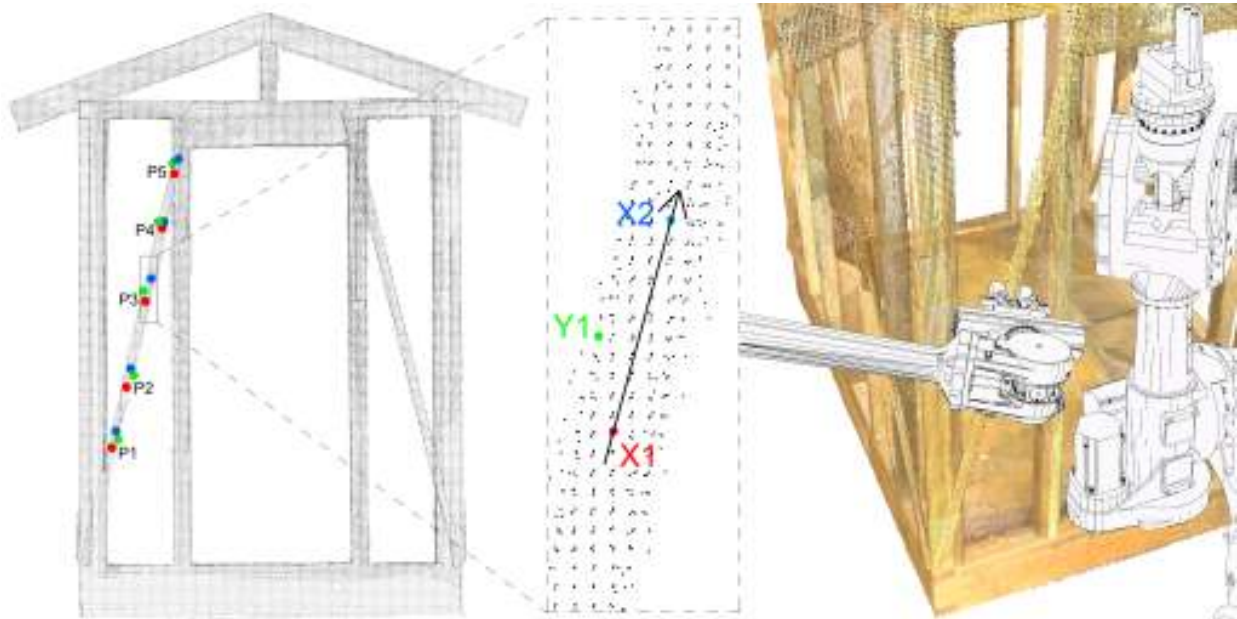


**Figure 6.11:** Left: Five pick locations ( $P_1 - P_5$ ) on a member are manually initialized from the as-built point cloud of the structure. Middle: At each location three points are used to define a spatial plane for the robot to reach. Right: Inverse kinematic path planning checks reveal that only  $P_3$  is reachable by a robot without encountering collisions with the structure or other robots in the work cell.

FAB computational package [53]. Generating a successful result from this operation ensures that the member is within the robot's reach. Furthermore, it confirms the existence of a feasible motion path from the initial position to the final target plane for the robot's tool center point (TCP), avoiding collisions with itself, other robots in the work cell, the ground, or any part of the existing structure.

To ensure realistic outcomes, accurate information about the as-built conditions of the structure is essential. Consequently, the as-built point cloud of the structure serves a dual purpose: it is utilized to establish authentic pick locations on the members and to define precise locations for collision meshes in the IK checks. The point cloud undergoes an initial manual processing phase, where the user selects multiple sets of three points from various locations along members, used to build planes in space. These planes represent potential locations and orientations for a robot to move and grasp a member during the execution of a planned sequence.

An illustrative example of the entire process is depicted in [Figure 6.11](#). The  $X_1$  point designates the plane's center, serving as the target for the robot's tool center point (TCP) to move to.

The orientation of the X-axis of the gripper is defined by the vector between X1 and X2. Y1, representing the third point on the member's surface, is necessary for establishing the spatial orientation of the plane. These designated pick locations are saved in a list and then undergo sequential testing during the evaluation of the disassembly sequence to assess which can be reached in a collision-free manner. If the IK checks return failure for all pick location on a member, indicating the impossibility of the robot reaching this member from a path planning perspective, adjustments are necessary to the original disassembly sequence. These adjustments may entail removing additional members before attempting to remove a target member or repositioning the robots strategically during the sequence to minimize obstructions.

## Structural Feasibility

The second step involves an assessment of the structural performance throughout a potential disassembly and assembly sequence. This evaluation is conducted through a linear elastic FE model representing snapshots of the structure at various stages during the execution of a sequence. Like the robotic feasibility check, the as-built point cloud is employed to create an accurate FE model, ensuring its fidelity to the real geometry of the structure. The beam elements in the model are located based on the center-line data of the members identified within the point cloud.

Utilizing the parametric Rhino/Grasshopper environment alongside the Karamba3D finite element package [59, 60] allows for the rapid investigation of candidate fabrication sequences. In this parametric environment, members can be selectively activated or deactivated to reflect a fabrication sequence being executed. Furthermore, additional supports, reflecting the positions of the robotic arms gripping the structure during the execution of a sequence, can be toggled on and off. This temporary support provided by the robots is represented as a standard pin support in the model. The structural members are themselves modeled as beam elements with semi-rigid joint connections. The overall FE model terminates at the bottom of the stud members, where their connection to the bottom plate is represented with a pin support.

While the actual structure only experiences self-weight loading, based on a dimensional lumber density of  $6 \text{ kN/m}^3$ , a more realistic loading condition is simulated by applying an additional uniform roof loading of  $2.0 \text{ kPa}$  distributed across the roof area. To further emulate real-world

conditions, a vertical load of  $1.0 \text{ kPa}$  is applied to the wall studs, representing the typical presence of hanging cladding and plywood sheathing in such structures.

The structural assessment fails if, at any step a given fabrication sequence, either the strength or serviceability conditions are exceeded. These conditions are calculated with the conservative assumption that SPF stud grade lumber is used, which has a bending strength of  $4.3 \text{ MPa}$  and a modulus of elasticity of  $3 \text{ GPa}$  [61]. The user-specified strength condition dictates that no member should experience a combined bending and axial stress exceeding  $3 \text{ MPa}$ . Additionally, the serviceability condition stipulates that beam deflections should not surpass  $2L/360$ ,  $L/360$ , or  $L/180$  for fixed, simply supported, and cantilever situations, respectively.

## 6.5 Results and Discussion

In the following section the planning and execution of three distinct fabrication phases are documented. The overall project is strategically divided into three phases to incrementally test the developed methods outlined in [Section 6.4](#). Each phase increases the complexity of the structural disassembly and reassembly tasks, as well as the degree of cooperative robotic sequencing required for execution. All phases are to be planned and then executed in such a way that the structure not only remains stable throughout the fabrication process that the resulting final structure also terminates in a state that is stable.

### 6.5.1 Phase 1 (P1): Single Target Member Removal

The initial phase focuses on validating the overall computational workflow developed for the project. Tasked with a straightforward fabrication objective, P1 demonstrates robotic sequence planning and execution where the starting goal is simply to remove a single simulated “damaged” member from the prototype structure. The cooperative robotic process involves two of the three available robots (R2 & R3), which is the minimum required for the robotic workflow to be considered cooperative. The planning of this phase was also the focus of a previous paper on the project [47], with further details presented herein.

## Preliminary Planning

Member SS1 (South Wall, Stud #1) is chosen as the member that is the target to be removed in P1. The active member disassembly subgraph for SS1 with all corresponding elements highlighted on the structure is shown in [Figure 6.12a](#).

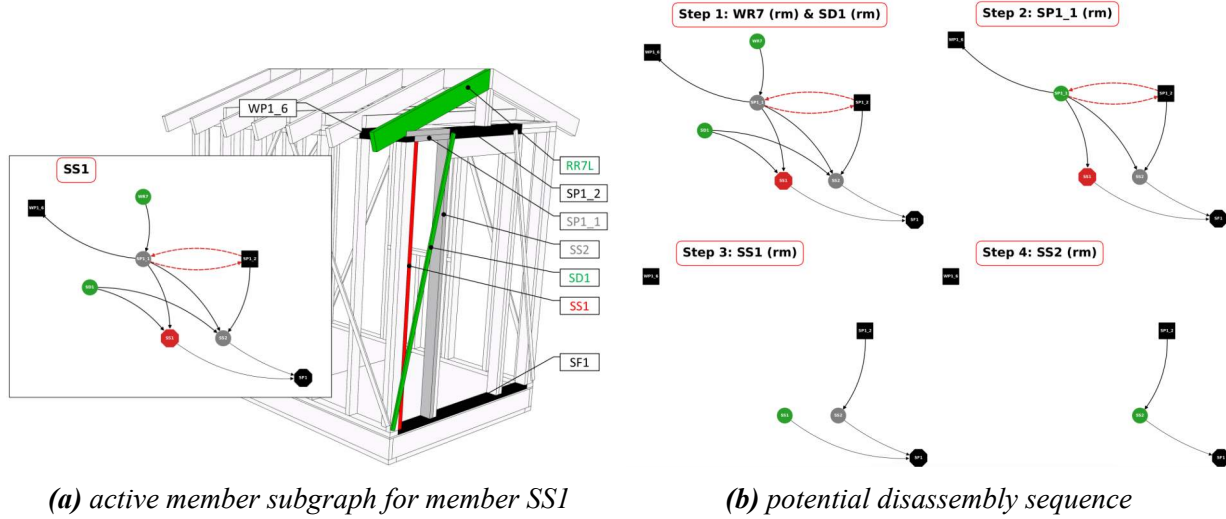


**Figure 6.12:** Planning the removal of member SS1

A potential four-step disassembly sequence generated from this subgraph is shown in [Figure 6.12b](#). The structural and robotic kinematic feasibility evaluation reveals that the sequence is structurally feasible but fails since no robot can reach member SS1 without colliding with either member WS9 or SS3 in its path. Thus, this first iteration indicates that the removal of either WS9 or SS3 must first occur as part of the overall fabrication task. This results in the generation of two new subgraphs representing the affected region of the structure when either of these members is added as an active member.

In [Figure 6.13a](#), the subgraph for option 1 is presented, involving the removal of SS3 before SS1. This option requires the removal of a total of 9 members but leads to inadequate support for member SP1\_2 upon the termination of the sequence. On the other hand, [Figure 6.13b](#) depicts the subgraph for option 2, removing WS9 before SS1. Despite a more extensive removal process involving 12 members, this option ensures a stable structure at the end of the sequence. Consequently, option 2 is chosen for P1.

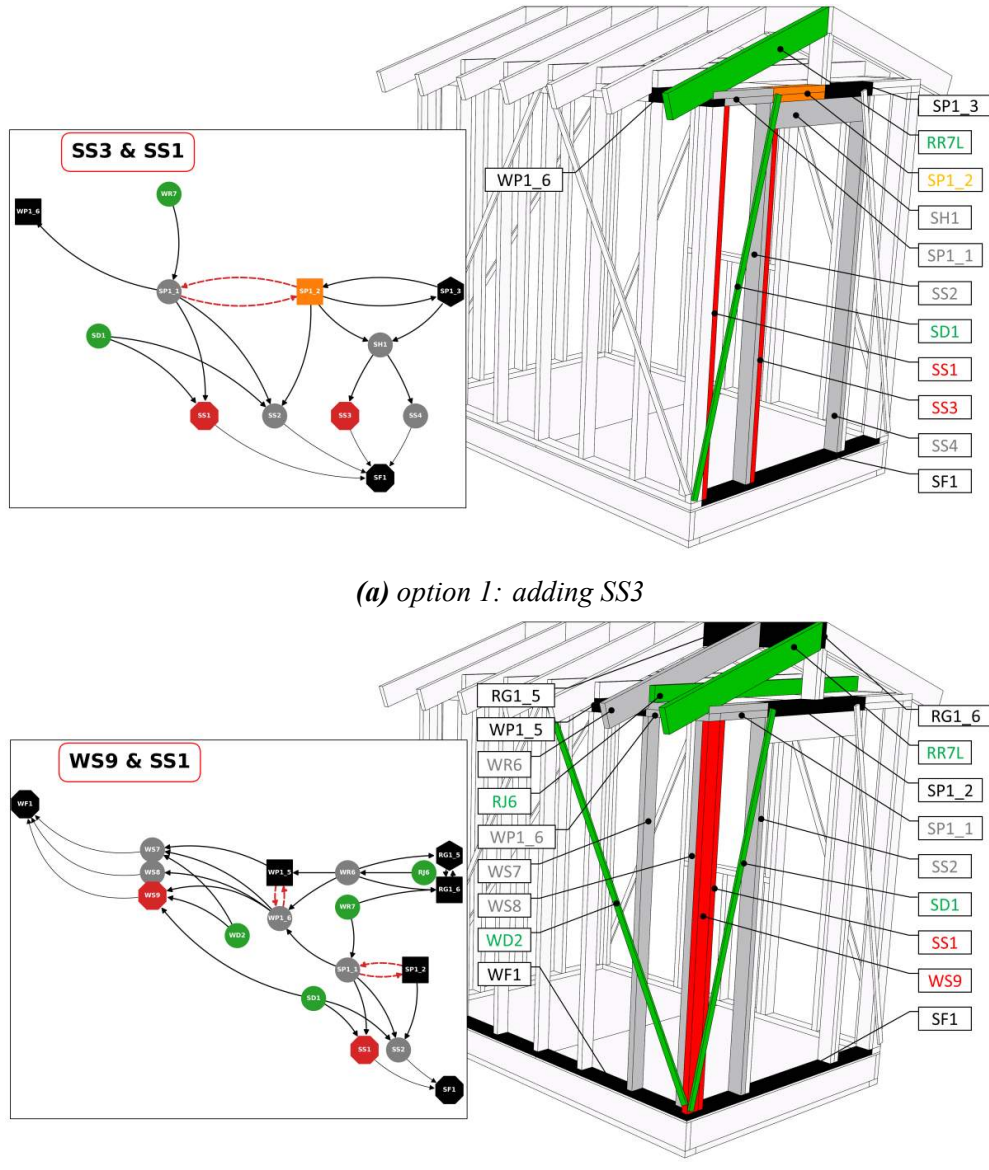
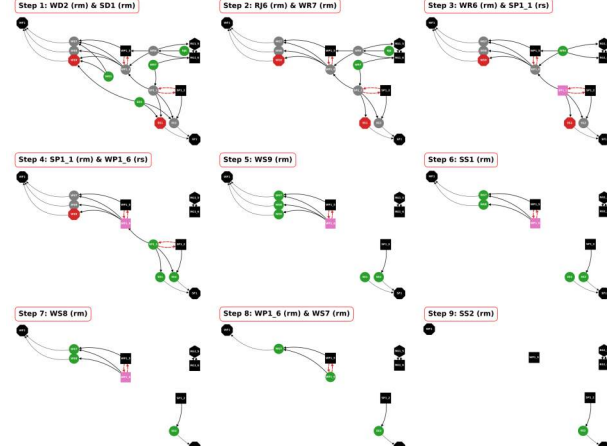


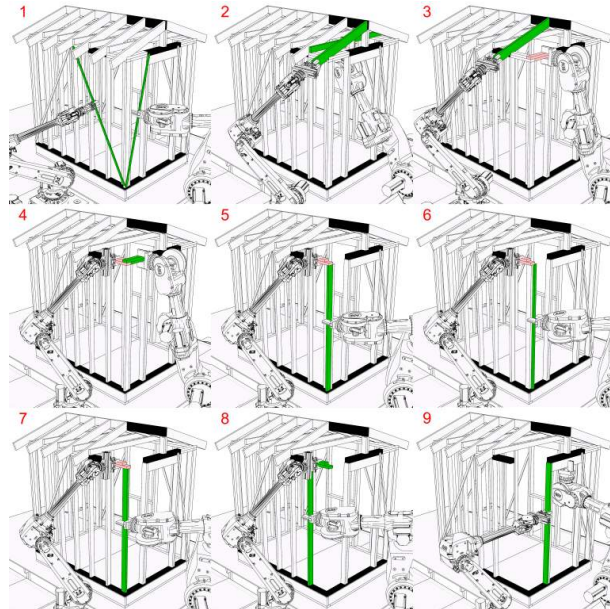
**Figure 6.13:** Two new active member subgraphs generated from the inclusion of additional removal targets determined by the feasibility evaluation for the planned removal of SS1.

## Fabrication Sequence

Assuming the availability of two robotic agents for executing the planned fabrication task, a viable disassembly sequence is derived from the active member subgraph generated for option 2 (members WS9 and SS1). This computed disassembly sequence encompasses 9 discrete steps, wherein one or two members in the subgraph are safely removed from the structure using robotic agents. The actions in each step are determined based on the current state of the structure, visu-



(a) sequence subgraphs



(b) sequence renderings

**Figure 6.14:** Phase 1 disassembly sequence.

ally represented by an updating subgraph at each step. The progression of the sequence and the planned action at each specific step is illustrated in Figure 6.14a. Simultaneously, renderings of the structure, highlighting the targeted members for removal/support at that step and depicting the robots in the correct position for execution, are presented in Figure 6.14b. In these figures, the pink denotes members that are temporarily physically supported by a robot, ensuring adequate stability during that step.

## Execution and Resulting Structure

The resulting structure after the completion of this 9-step disassembly sequence is displayed in [Figure 6.15](#). Further snapshots of the structure and robots at various stages of the phase are provided in [Section C.2.1](#).

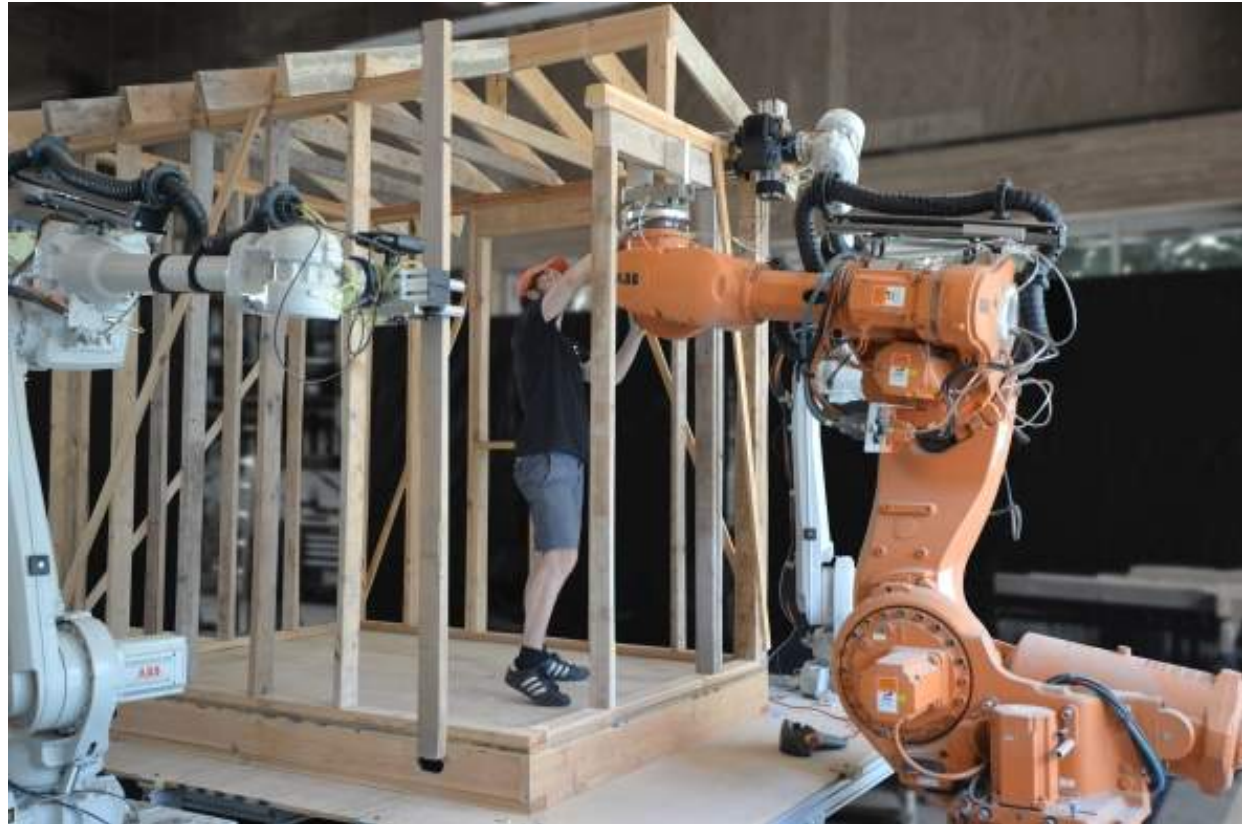


*Figure 6.15: Prototype structure at the end of the disassembly in Phase 1 (from [47]).*

### **6.5.2 Phase 2 (P2): Full Wall Disassembly and Partial Reassembly**

Building upon the methodologies explored in the initial phase, the second phase of the study extends the disassembly goal beyond a single-member target, as seen in P1. In P2, the objective is to safely remove a larger and more geometrically complex portion of the remaining South wall of the structure. This phase also introduces increased complexity in robotic planning by engaging all three available robots throughout the planned sequence.

In P2 the scope of the overall fabrication process is broadened by incorporating structural reassembly after completing the disassembly phase. This serves as a practical test for the reuse of members removed from the structure for alternative purposes. The disassembly goal in P2 is meant to explore what can be done when achieving a structurally sound final structure after disassembly is not possible without external support. Unlike P1, where a small disassembly intervention meant that finding a feasible sequence resulting in a stable final structure was possible, P2 involves a much larger and more complex disassembly operation where no safe resulting structure is identified within reasonable constraints (i.e., without calculating a sequence to dismantle the entire structure).

Thus, following the completion of disassembly in P2, the only viable means to safely conclude the process is either to provide external temporary support structures at the targeted location or to reuse several removed members to reassemble a new but simple supporting structure. Notably, this reassembly is considered partial, meaning that not all initially removed members are incorporated into the new structure. Additionally, in P2, the specific configuration of the new structure is not optimized; it solely acts as a prop, providing basic structural support to a region of the structure deemed unsafe after the disassembly is completed.

#### **Preliminary Planning**

To facilitate the removal of the entire South wall, the members chosen include the remaining top plate members SP1\_2, SP1\_3, and SP1\_4. This selection forms the disassembly subgraph depicted in [Figure 6.16a](#). Like the preceding phase (P1), the resultant disassembly sequence proves infeasible due to unavoidable collisions, particularly with member ES10. To address this challenge, as illustrated in [Figure 6.16b](#), ES10 is incorporated as a removal target prior to dismantling

the top plate. However, this adjustment also yields an unsatisfactory sequence, revealing inadequate support for the ridge beam member RG1\_6 upon completion of the disassembly process.

To rectify this structural instability, RG1\_6 is included in the disassembly sequence, leading to the configuration shown in [Figure 6.16c](#). Yet, the removal of RG1\_6 fails to resolve the issue, as the instability concern is transferred to the subsequent member, RG1\_5. Upon further examination, it becomes evident that achieving stability necessitates the removal of the entire ridge beam, along with all roof girders and joists. However, such an extensive intervention exceeds the intended scope of disassembly. Consequently, the disassembly process is limited to the members highlighted in the structure as shown in [Figure 6.16c](#), requiring a subsequent reassembly phase with additional support provided to stabilize member RG1\_5 at the conclusion of the sequence.

## Fabrication Sequence

Assuming the availability of all three robotic agents for executing the planned fabrication task, a viable disassembly sequence is calculated for the disassembly subgraph shown in [Figure 6.16c](#). The progression of the sequence and the planned action at each specific step is illustrated in [Figure 6.17a](#). Simultaneously, renderings of the structure, highlighting the targeted members for removal/support at that step and depicting the robots in the correct position for execution, are presented in [Figure 6.17b](#). In these figures, the pink denotes members that are temporarily physically supported by a robot, ensuring adequate stability during that step.

The disassembly sequence unfolds through steps 1 to 8, reminiscent of P1, employing only two robots. However, from step 9 onwards, the involvement of all three robots becomes necessary, orchestrating a leapfrogging strategy to dismantle the members supporting the roof girder. In step 12 the structure is shown in its temporary state, stabilized by R3. At this point, further disassembly is hindered, given that only R3 can access the final members but R3 must concurrently support the structure at this step. In addition, RG1\_5 will eventually require additional support at the conclusion of the disassembly as noted when planning this sequence. To address both challenges, a reassembly stage is initiated after step 12.

Several recently removed members — namely ER6, ER7, SS6, SS4, and SS4 — are strategically reassembled into a new supporting structure as shown in steps 13 to 17 in [Figure 6.18](#). This new structure not only provides crucial support to member RG1\_5 but also frees R3 since

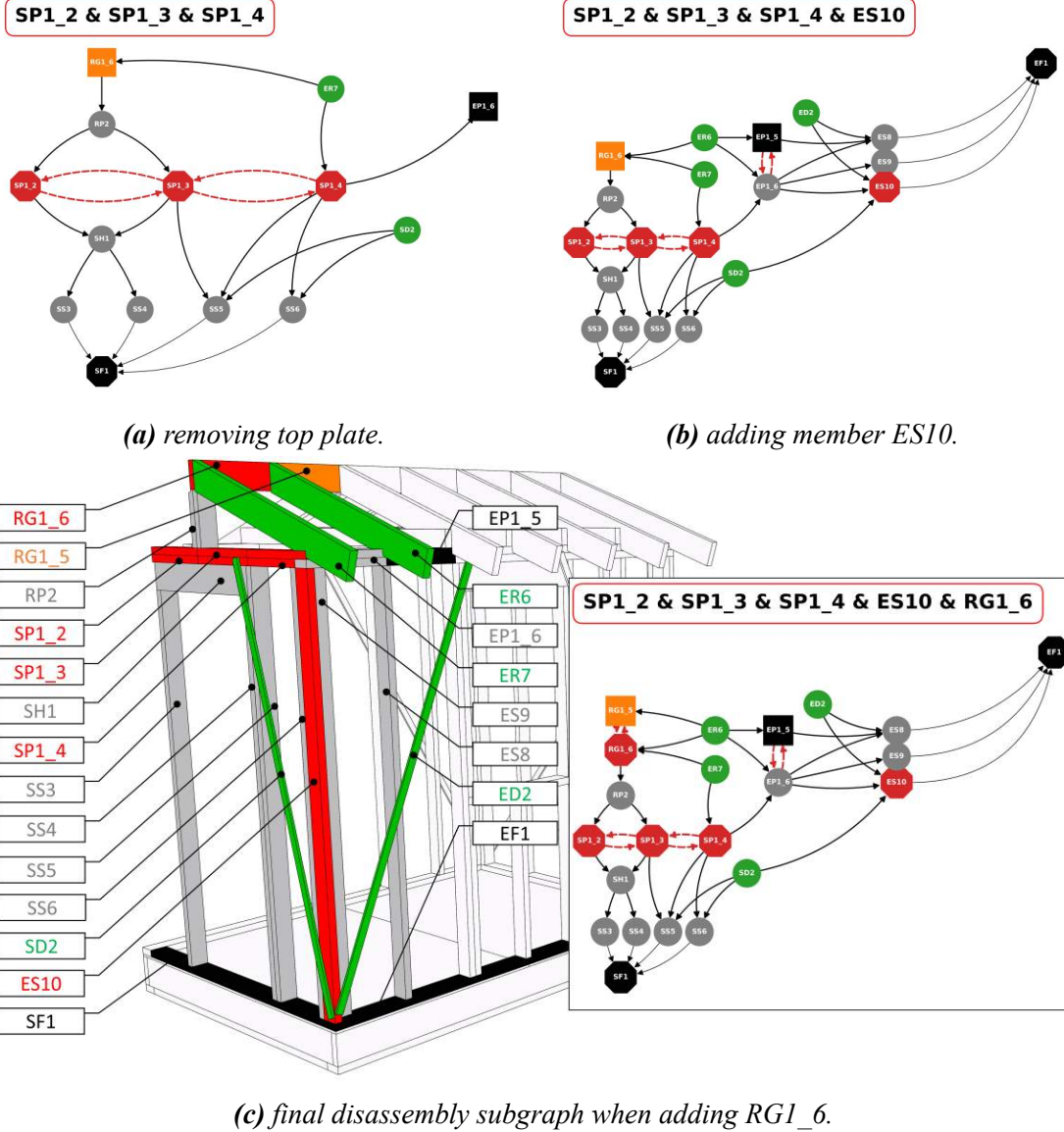


**Figure 6.16:** Planning the removal of the south wall as part of Phase 2 and resulting in a final structure that requires additional support.

it is no longer required for support and can thus continue with the remaining disassembly steps. The final members are removed by R3 in steps 17 and 18, completing the planned disassembly sequence while resulting in a structurally sound final configuration.

### Execution and Resulting Structure

Figure 6.19 shows snapshots of the disassembly sequence at two critical steps. In step 10, all three robots are required. In step 12, R3 is used to support the roof girder before the reassembly

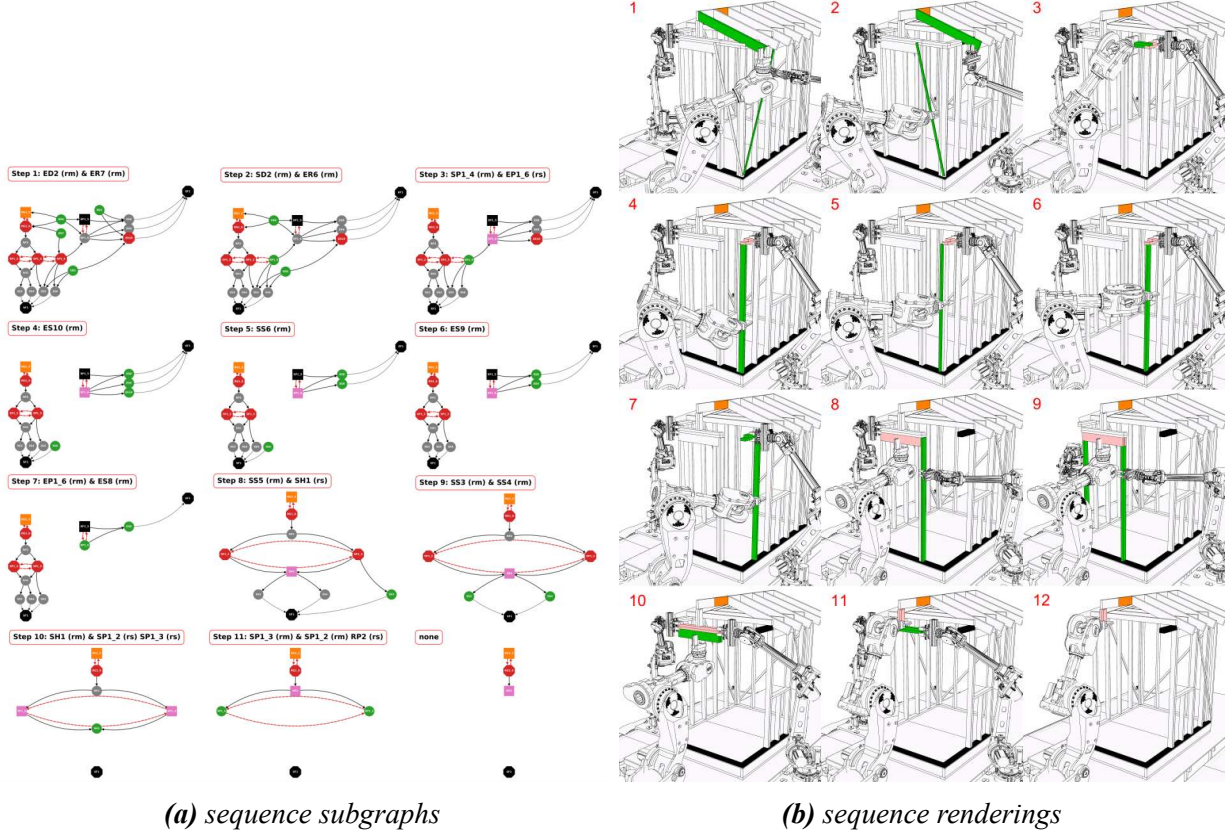
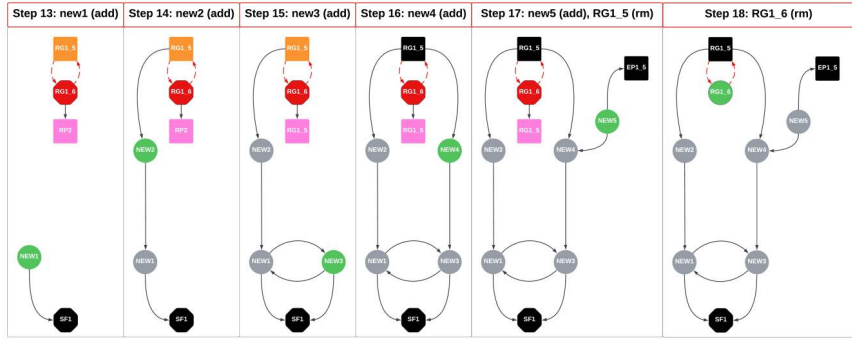


**Figure 6.17:** Phase 2 disassembly sequence.

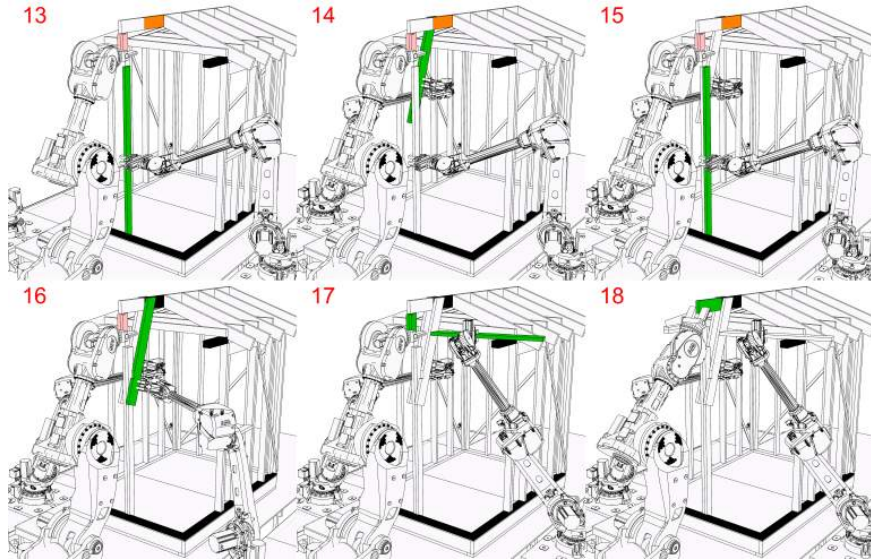
begins and additional support is added to the structure.

The completed structure resulting from the reassembly sequence is shown in [Figure 6.20a](#).

Additional snapshots illustrating various steps during disassembly and reassembly are presented in [Section C.2.2](#). Upon concluding Phase 2, in preparation for subsequent phases, the point cloud gathering procedure outlined in [Section 6.4.1](#) is repeated to capture deformations in the structure and the as-built position of the newly added members. This updated point cloud and the assembly hierarchy graph are shown in [Figure 6.20b](#).

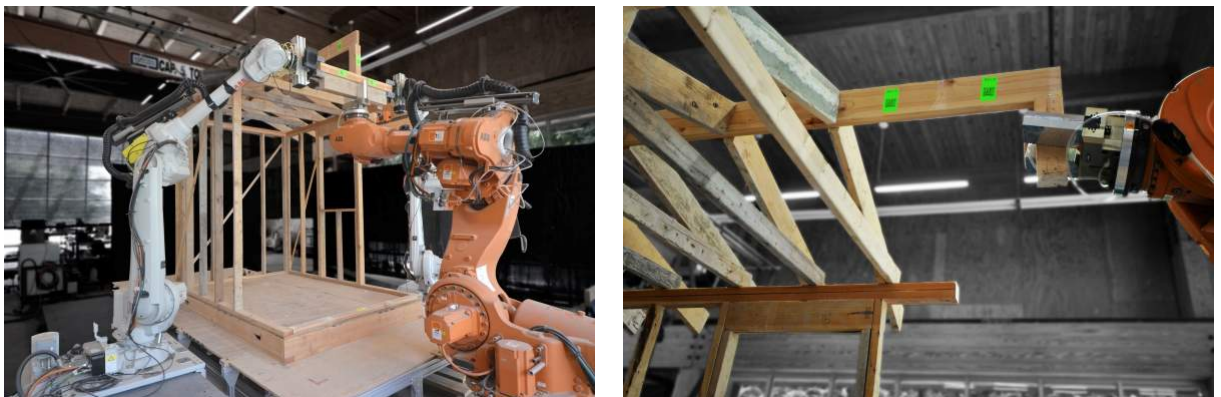


(a) sequence subgraphs



(b) sequence renderings

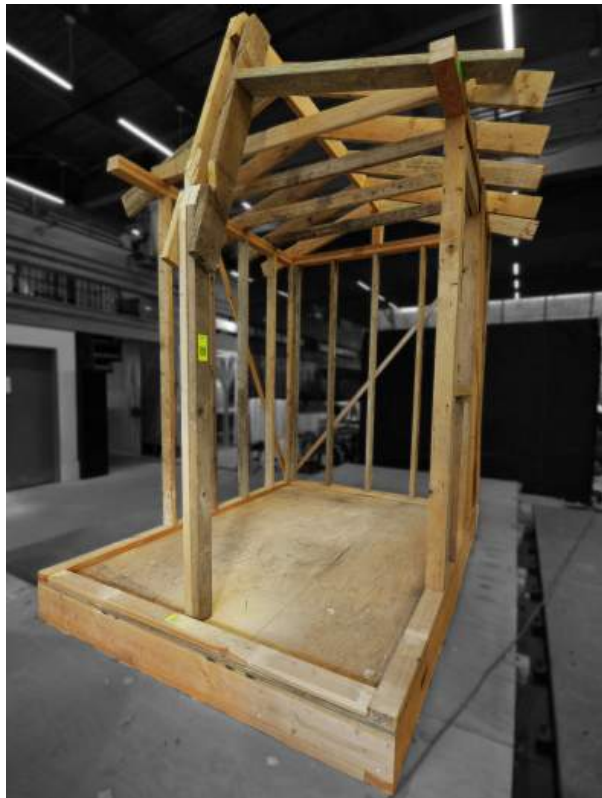
**Figure 6.18:** Phase 2 reassembly sequence.



(a) Step 10 in the disassembly sequence. R3 is ready to remove SH1, while R1 and R2 support SP1\_2 and SP1\_3 respectively (from [42]).

(b) Step 12 in the disassembly sequence. R3 is supporting the remaining roof structure before the start of the reassembly sequence.

**Figure 6.19:** Snapshots of Phase 2 disassembly.



(a) Prototype structure.



(b) As-built pointcloud & assembly hierarchy.

**Figure 6.20:** The prototype structure at the end of the disassembly and reassembly in Phase 2.

### **6.5.3 Phase 3 (P3): Full Wall and Roof Disassembly and Reassembly**

Phase 3 marks the project's culmination, surpassing the disassembly scopes of P1 and P2. In P3 the objective is to remove all remaining members in the West wall and roof sub-structures. Additionally, it introduces tighter constraints in reassembly, adopting a one-to-one approach: each extracted member is reincorporated to reshape the West wall into a lattice structure, improving its overall lateral stiffness.

#### **Preliminary Planning**

As illustrated in [Figure 6.21](#), Phase 3 designates twelve remaining members within the West wall and roof sub-structures for removal. The diagonal brace (WD1), is also planned for removal, but is not considered a valid member for reuse since the diagonal members take the place of typical planar sheathing used to provide lateral stiffness.

Only the two stud members in the North corner (WS1 and WS2) and the top plate (WP1) are not specified as removal targets. Retaining the corner stud members prevents the need to extend the disassembly sequence into the North wall, while the top plate acts as a support constraint for the newly reassembled wall. The planned goal for the reassembly process in P3 is to fit the new lattice wall structure within the current volume of the existing wall. This means that all the new members must fit within the original 4" thickness specified by the stud members in the wall (i.e., for a 2x4" stud wall).

#### **Fabrication Sequence**

The disassembly and reassembly of the twelve specified target members results in a fabrication sequence consisting of 25 steps. This sequence can be represented as two distinct sub-tasks: (1) Steps 1-12 involve the removal and reassembly of the initial set of 6 members, while (2) Steps 14-25 pertain to the removal and reassembly of the subsequent set of 6 members. The first set consists of disassembling and reassembling members WS6, RJ5, WR5, RJ4, WR4, and WS5 (in order) and the second set consists of disassembling and reassembling members RJ3, WR3, WS4, RJ2, WR2, WS3 (in order).

In [Figure 6.22](#), the planned fabrication sequence is shown as a series of renderings of the

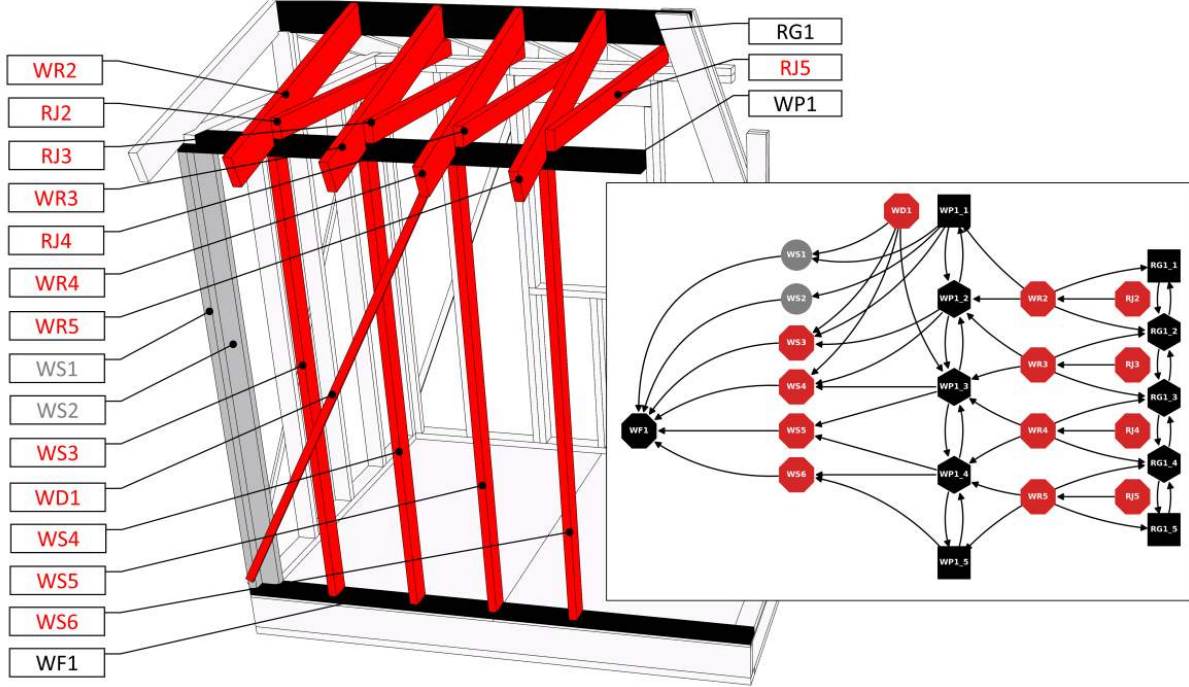
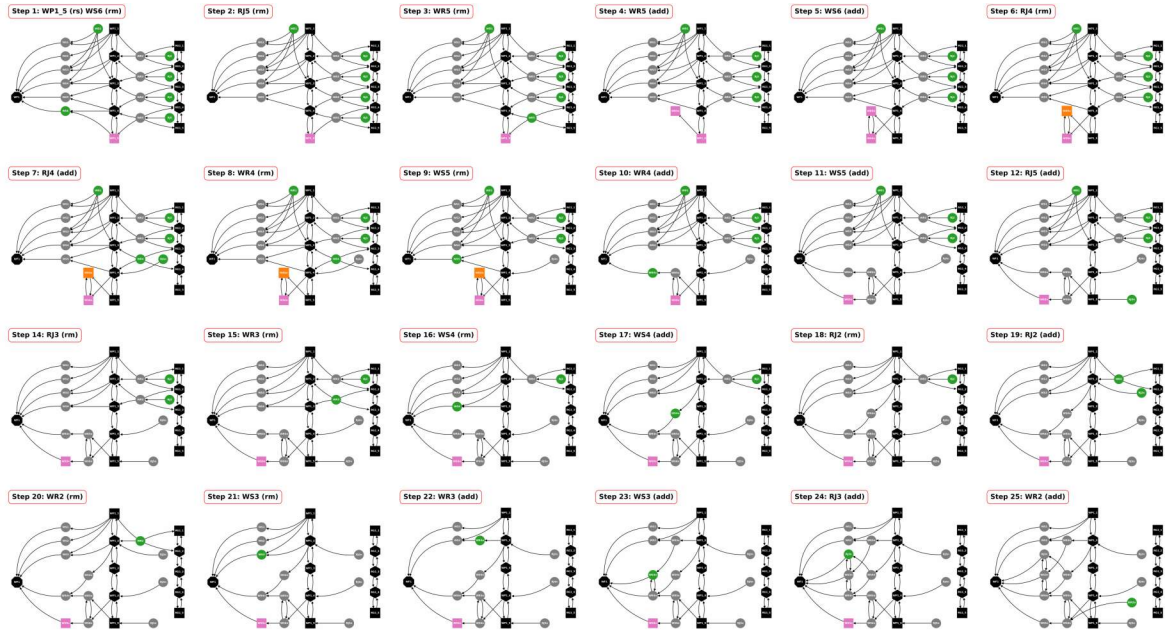
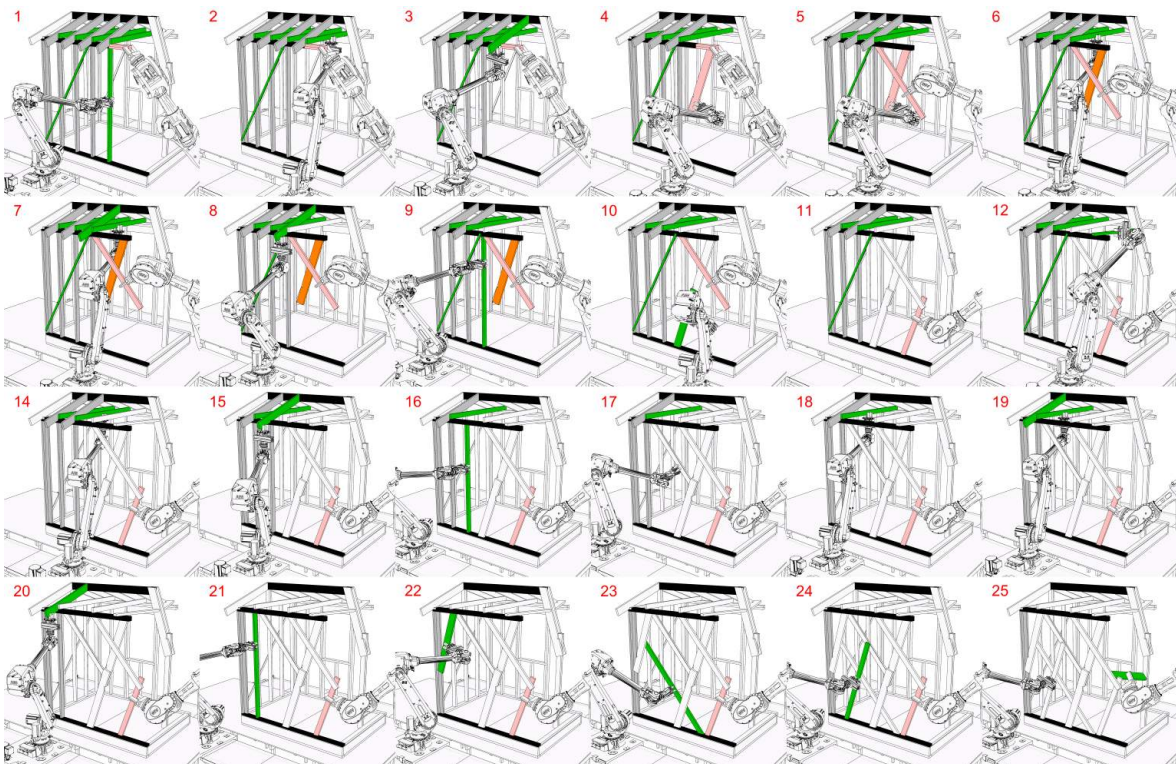


**Figure 6.21:** The disassembly subgraph for the removal of the West wall and roof members.

structure at each step, highlighting the remaining members in the structure still requiring removal/support, the newly placed members, and the position of the robots involved in each step. Upon reassembly into the structure, the members are depicted in white, signifying that they are no longer part of the active sequence plan. To streamline the presentation within the main body of the chapter, the corresponding support hierarchy subgraphs for each step are provided in [Section C.2.3](#). Step 13, which is omitted from [Figure 6.22](#), represents the removal of the diagonal member (WD1), which as previously established is just a placeholder element used in lieu of planar sheathing. In both the renderings and subgraphs, the pink denotes members temporarily supported by a robot, providing the necessary stability during the execution of the sequence.



(a) sequence subgraphs



(b) sequence renderings

**Figure 6.22:** Phase 3 disassembly and full reassembly (each member removed is reused).

## Execution and Resulting Structure

Figure 6.23a shows a snapshot of the newly assembled structure at the end of step 24, as R2 is positioning the final planar element into the wall. Four of the reassembled members (e.g., RJ4, RJ5, RJ2, WR2) are placed in the out-of-plane direction to provide bracing to the wall, thus the planar wall itself consists of only eight new members. As shown in Figure 6.23b the result is a planar wall where the standard vertical stud wall typology is replaced with a lattice typology. The lattice arrangement features members crossing at several points. At each of these points the members are connected to each other to stiffen the entire wall system. The members are arranged along their strong axis, meaning that the thickness into the plane of the wall is only 2", thus two members can cross and still fit within the original 4" wall cavity as specified by the original wall studs.



(a) Step 24 in the disassembly/reassembly sequence showing R2 placing the final member into the planar wall.

(b) Elevation of the finished West wall reassembled into a lattice structure.

**Figure 6.23:** The prototype structure at the end of the disassembly and reassembly in Phase 3.

Two linear elastic finite element analyses were conducted to compare the relative lateral stiffness of the original and reassembled West wall. Despite the mass increasing from 34.4 to 44.1 kg between the original and reassembled wall, a significant improvement in stiffness was noted. For instance, the unbraced original wall with vertical studs exhibited a maximum deflection at its top of 67.6 cm, whereas the reassembled wall with a lattice configuration experienced a lateral deflection of only 0.3 cm. This comparison was solely intended for relative assessment, thus the applied lateral loading of 5 kN at the top of the walls was arbitrarily chosen. Additionally,

to ensure comparability, identical support conditions were maintained across the models, with supports modeled as pins and connections between members fixed. Representing joints in a traditional stud wall as fixed is a conservative assumption since these connections are typically more flexible, suggesting that the actual performance of the traditional wall might be even worse if flexibility were introduced in the joints. The successful reassembly of the West wall in Phase 3 demonstrated the potential for rebuilding a structure with enhanced structural performance.

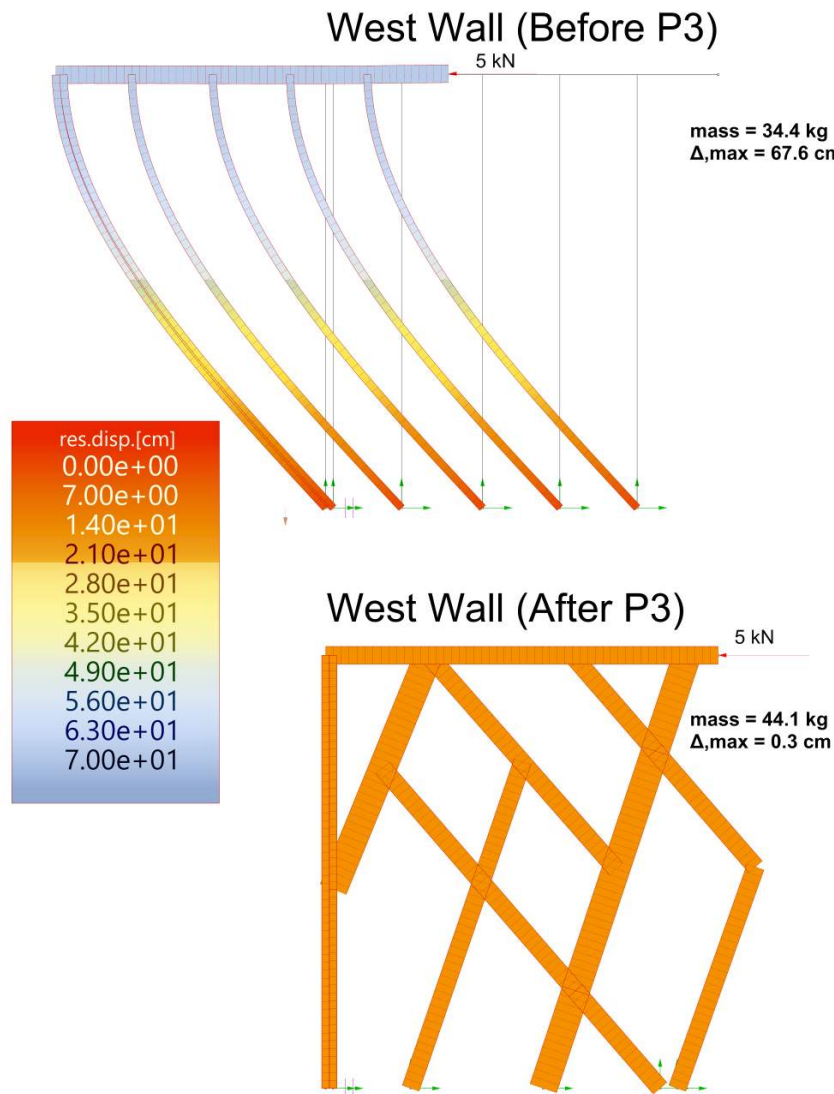


**Figure 6.24:** Finite element analysis comparing the lateral stiffness of the original (top) to the reassembled (bottom) West wall.

Figure 6.24 shows the results of the finite element analyses, visually depicting the relative difference in deflection between the two configurations. While conventional stud walls typically

rely on planar sheathing elements for lateral stiffness, advancements in digital fabrication raise questions about the necessity of this approach. Precise placement of elements in space allows for exploration of alternative geometries beyond conventional rectilinear forms. As demonstrated by the reassembled West wall, approximately the same amount of material arranged in a planar lattice structure can effectively resist both gravity and lateral loads, thus sheathing would not be required for structural performance, potentially leading to flexibility in how such a wall unit would be designed in the future. With the growing availability of flexible robotic fabrication setups these results challenge the traditional notion that timber framing must adhere to rectilinear forms, which have been developed for ease of manual construction.

## 6.6 Conclusion

This chapter presented the detailed computational workflow for performing scaffold-free cooperative robotic disassembly and reassembly processes for existing timber structures as a continuation of a preliminary publication on the topic [47]. It demonstrated how cooperative robotic cells could be used to collect data on unknown structures while enabling the planning and execution of feasible disassembly and reassembly without requiring external scaffolding. The ZeroWaste project exemplified how material reuse, as a consideration for a circular economy, can be paired with the capabilities of contemporary cooperative robotic fabrication systems. This research has advanced sustainability and technological sophistication in the construction sector, emphasizing efficiency, resource management, and environmental stewardship.

### 6.6.1 Summary of Results

The chapter first introduces the computational methods developed as part of the ZeroWaste project. These methods were subsequently applied to achieve various goals pertaining to circular economy principles and the integration of computational and cooperative robotic fabrication methods.

In terms of circular economy principles, the fabrication tasks undertaken on the prototype structure demonstrated the potential for existing timber buildings to function as reservoirs for reusable materials. By employing varying levels of disassembly and reassembly on an uniden-

tified timber prototype structure, the capacity to generate fresh structural configurations using previously utilized materials was highlighted.

In terms of computational and cooperative robotic fabrication methods, the project utilized a robotic cell equipped with three large-scale robotic arms. Initially, 3D cameras mounted on the robots captured precise geometric data of the prototype structure, aiding in efficient robotic sequence planning. Subsequently, a novel graph-based representation known as the support hierarchy graph was developed to depict the order of member support in the structure, facilitating the calculation of structurally stable fabrication sequences through algorithmic operations. These sequences were further assessed for feasibility considering factors such as robotic reach and structural stability. Leveraging the cooperative potential of the robotic setup, the planned fabrication sequences were executed, with the robots simultaneously removing/placing members while providing temporary structural support as needed for stability. This approach enabled the execution of fabrication sequences without external temporary scaffolding, as the robots served as passive structural support.

Across three distinct phases performed on the prototype structure, the ZeroWaste project highlighted the potential of treating existing timber buildings as reservoirs of reusable materials, thereby reducing reliance on scaffolding and virgin resources during construction. Phase 1 centered on the removal of a single targeted member, validating the computational and cooperative robotic workflow, and demonstrating scaffold-free cooperative robotic disassembly through a sequence executed by two robots. Phase 2 expanded the disassembly objective to encompass a larger portion of the structure—the full South wall—utilizing all three available robots and incorporating structural reassembly to highlight the potential for reusing extracted members. Phase 3 went further by disassembling all remaining members in the West wall and roof sub-structures, introducing stricter constraints in reassembly. Each extracted member was reincorporated to reshape the West wall into a new lattice configuration, thereby enhancing its lateral stiffness by two orders of magnitude. Through the successful execution of these phases, the ZeroWaste project illustrated the feasibility of orchestrating scaffold-free cooperative robotic disassembly and reassembly processes for existing timber structures, setting the stage for more sustainable construction practices.

## **6.6.2 Limitations and Future Work**

While the current study has made significant contributions in developing and demonstrating methods for advancing scaffold-free cooperative robotic disassembly and reassembly processes for existing timber structures, several limitations and avenues for future research remain to be addressed.

**Real-time Feedback on As-built Geometry:** An inherent limitation of the current approach lies in the reliance on pre-scanning the structure to generate a point cloud before beginning the planning of a particular fabrication phase. The method developed lacks the ability update the point cloud model promptly and accurately with changes during fabrication, necessitating a complete re-scan of the structure for any major changes to be updated in the model. Future research should prioritize the development of processes enabling the robots to dynamically collect information and update the as-built point cloud model of the structure while concurrently performing fabrication tasks. Such a real-time feedback mechanism would improve adaptability and accuracy in planning and executing fabrication processes, particularly for geometrically complex and dynamically changing structures.

**Automating Point Cloud Processing for Feasibility Assessments:** Another area requiring attention is the reduction of manual steps involved in setting up and processing the results of the path-planning and reachability feasibility assessments. Currently, users must manually select several locations on the point cloud representation of a member selected in a sequence only to conduct a series of brute force path-planning and reachability checks at these locations, a process that is both time-consuming and labor-intensive. Future research avenues would be to explore automated methods to streamline this process, potentially leveraging machine learning algorithms and computer vision techniques to automate point cloud processing with respect to performing these path-planning checks. Similarly, the implementation of a more automated approach to creating the Finite Element (FE) model based on the as-built point cloud holds promise for significant reductions in time required for the structural feasibility assessments. Currently, users are tasked with processing the point cloud manually to construct the structural analysis model for each sequence, based on the centerline locations of members.

**Integrating Results of Finite Element Analysis (FEA) with Graph Representation:** Enhanced integration between FEA results and the support hierarchy graph representation could optimize the generation and selection of fabrication sequences. Currently, all graph edges have uniform weights, but updating them dynamically based on previous analysis findings would facilitate a more informed sequence generation process. For example, this could take the form of updating edge weights based on the structural loading the members experienced in a previous step. But other user-specified criteria could also be set. Overall, better linking integration of the FEA and the graph representation would help reduce the extensive set of potential sequences currently generated and then verified.

**Use of Mobile Robots:** The inclusion of mobile robots for specific tasks, such as data gathering and material handling, holds promise for enhancing the overall scalability and broader applicability of the methods developed in this project. Utilizing mobile robots alongside stationary robotic arms would enable a better distribution of labor between the robots and broaden the overall reach of the cooperative setup allowing it to manage more diverse construction scenarios. It would also allow for larger structures to be disassembled, as currently the physical limit is set by the fixed volume of the robotic setup. In addition, fasteners are currently removed manually, and a mobile robot could instead be used to perform this function.

**Life-Cycle Analysis:** Analyzing the environmental impact of using robots to replace traditional methods on a job site would provide a clearer understanding of the pros and cons of different approaches. While our research primarily focused on showcasing cooperative robotic scaffold-free disassembly and reassembly processes, performing an energy balance or life-cycle analysis of these processes in the future is essential to determine the true impact of robot utilization.

In conclusion, addressing these limitations and pursuing future research directions will further advance the capabilities of cooperative robotic fabrication systems in the construction industry, contributing to more sustainable and efficient construction practices.

## References

- [1] International Energy Agency, United Nations Environment Programme, 2018 Global Status Report: Towards a zero-emission, efficient and resilient buildings and construction sector, Tech. rep., Global Alliance for Buildings and Construction (2018).  
URL <https://wedocs.unep.org/20.500.11822/27140>
- [2] S. Kaethner, J. Burridge, Embodied CO<sub>2</sub> of structural frames, Structural Engineer 90 (5) (2012) 33–40.  
URL <https://www.istructe.org/sitefiles/handlers/DownloadFile.ashx?productId=1583>
- [3] D. Fang, N. Brown, C. De Wolf, C. Mueller, Reducing embodied carbon in structural systems: A review of early-stage design strategies, Journal of Building Engineering 76 (2023) 107054. doi:10.1016/j.jobe.2023.107054.
- [4] United Nations, Global Status Report for Buildings and Construction, Tech. rep., UN (2021).  
URL [https://globalabc.org/sites/default/files/2021-10/GABC\\_Buildings-GSR-2021\\_BOOK.pdf](https://globalabc.org/sites/default/files/2021-10/GABC_Buildings-GSR-2021_BOOK.pdf)
- [5] US EPA, Construction and Demolition Debris Generation in the United States, 2015, Tech. rep., Office of Resource Conservation and Recovery (Sep. 2018).  
URL <https://www.epa.gov/facts-and-figures-about-materials-waste-and-recycling/studies-summary-tables-and-data-related>
- [6] US EPA, Construction and Demolition Debris Management in the United States, 2015, Tech. rep., Office of Resource Conservation and Recovery (Mar. 2020).  
URL [https://www.epa.gov/sites/production/files/2020-03/documents/final\\_cd-eol-management\\_2015\\_508.pdf](https://www.epa.gov/sites/production/files/2020-03/documents/final_cd-eol-management_2015_508.pdf)
- [7] C. K. Purchase, D. M. A. Zulayq, B. T. O'Brien, M. J. Kowalewski, A. Berenjian, A. H. Tarighaleslami, M. Seifan, Circular Economy of Construction and Demolition Waste: A Literature Review on Lessons, Challenges, and Benefits, Materials 15 (1) (Jan. 2022). doi: 10.3390/ma15010076.

- [8] B. K. Fishbein, Building for the future: strategies to reduce construction and demolition waste in municipal projects, Vol. 5 of INFORM Special Report, INFORM, Inc., New York, 1998.
- [9] T. H. Mills, E. Showalter, D. Jarman, A cost-effective waste management plan, Cost Engineering 41 (3) (1999) 35–43.  
URL <https://www.proquest.com/docview/220405711?pq-origsite=gscholar&fromopenvie w=true#>
- [10] US EPA, Characterization of building-related construction and demolition debris in the United States, Tech. Rep. EPA530-R-98-010, Municipal and Industrial Solid Waste Division (Jun. 1998).  
URL <https://archive.epa.gov/epawaste/hazard/generation/web/pdf/cd-rpt.pdf>
- [11] W. Lu, H. Yuan, A framework for understanding waste management studies in construction, Waste Management 31 (6) (2011) 1252–1260. doi:10.1016/j.wasman.2011.01.018.
- [12] US EPA, Advancing Sustainable Materials Management: 2018 Fact Sheet, Tech. rep., Office of Resource Conservation and Recovery (Dec. 2020).  
URL [https://www.epa.gov/sites/default/files/2021-01/documents/2018\\_ff\\_fact\\_sheet\\_dec\\_2020\\_fnl\\_508.pdf](https://www.epa.gov/sites/default/files/2021-01/documents/2018_ff_fact_sheet_dec_2020_fnl_508.pdf)
- [13] H. Ritchie, M. Roser, Urbanization (2018).  
URL <https://ourworldindata.org/urbanization>
- [14] M. Osmani, J. Glass, A. Price, Architects' perspectives on construction waste reduction by design, Waste Management 28 (7) (2008) 1147–1158. doi:10.1016/j.wasman.2007.05.011.
- [15] M. Geissdoerfer, P. Savaget, N. M. P. Bocken, E. J. Hultink, The Circular Economy – A new sustainability paradigm?, Journal of Cleaner Production 143 (2017) 757–768. doi:10.1016/j.jclepro.2016.12.048.  
URL <https://www.sciencedirect.com/science/article/pii/S0959652616321023>

- [16] D. Cottafava, M. Ritzen, Circularity indicator for residential buildings: Addressing the gap between embodied impacts and design aspects, *Resources, Conservation and Recycling* 164 (Jan. 2021). doi:10.1016/j.resconrec.2020.105120.
- [17] L. Eberhardt, J. Rønholt, M. Birkved, H. Birgisdottir, Circular Economy potential within the building stock - Mapping the embodied greenhouse gas emissions of four Danish examples, *Journal of Building Engineering* 33 (2021) 101845. doi:10.1016/j.jobe.2020.101845.
- [18] J. Konietzko, N. Bocken, E. Hultink, Circular Ecosystem Innovation: An Initial Set Of Principles, *Journal of Cleaner Production* 253 (2020) 119942. doi:10.1016/j.jclepro.2019.119942.
- [19] S. Çetin, C. De Wolf, N. Bocken, Circular Digital Built Environment: An Emerging Framework, *Sustainability* 13 (11) (2021) 6348. doi:10.3390/su13116348.
- [20] C. De Wolf, S. Çetin, N. Bocken, A Circular Built Environment in the Digital Age, *Circular Economy and Sustainability*, Springer Cham, 2023. doi:10.1007/978-3-031-39675-5.
- [21] N. M. P. Bocken, I. de Pauw, C. Bakker, B. van der Grinten, Product design and business model strategies for a circular economy, *Journal of Industrial and Production Engineering* 33 (5) (2016) 308–320. doi:10.1080/21681015.2016.1172124.
- [22] J. Brütting, J. Desruelle, G. Senatore, C. Fivet, Design of truss structures through reuse, *Structures* 18 (2019) 128–137. doi:10.1016/j.istruc.2018.11.006.
- [23] R. Naboni, A. Kunic, A. Kramberger, C. Schlette, Design, simulation and robotic assembly of reversible timber structures, *Construction Robotics* 5 (1) (2021) 13–22. doi:10.1007/s41693-020-00052-7.
- [24] J. Brütting, G. Senatore, C. Fivet, Design and fabrication of a reusable kit of parts for diverse structures, *Automation in Construction* 125 (2021) 103614. doi:10.1016/j.autcon.2021.103614.
- [25] E. P. G. Bruun, S. Adriaenssens, S. Parascho, Structural rigidity theory applied to the scaffold-free (dis)assembly of space frames using cooperative robotics, *Automation in Construction* 141 (2022) 104405. doi:10.1016/j.autcon.2022.104405.

- [26] J. Brütting, G. Senatore, M. Schevenels, C. Fivet, Optimum design of frame structures from a stock of reclaimed elements, *Frontiers in Built Environment* 6 (2020) 57. doi:10.3389/fbuil.2020.00057.
- [27] J. Glath, T. Gobin, R. Mesnil, M. Mimram, O. Baverel, Thinking and Designing reversible structures with non-sequential assemblies, in: *Design Modeling Symposium 2022: Towards Radical Regeneration*, Springer International Publishing, Cham, 2022, pp. 249–259. doi: 10.1007/978-3-031-13249-0\_21.  
 URL [https://doi.org/10.1007/978-3-031-13249-0\\_21](https://doi.org/10.1007/978-3-031-13249-0_21)
- [28] N. Zahiri, Sequential augmented assembly of interlocking timber elements for circular wood construction, in: *Proceedings of the IASS Annual Symposium 2023*, International Association for Shell and Spatial Structures, Melbourne, 2023, p. 12.  
 URL <https://www.ingentaconnect.com/contentone/iass/piass/2023/00002023/00000018/art00010>
- [29] F. Barbosa, J. Woetzel, J. Mischke, M. Ribeirinho, M. Sridhar, M. Parsons, N. Bertram, S. Brown, Reinventing Construction: A Route to Higher Productivity, Tech. rep., McKinsey Global Institute (2017).  
 URL <https://www.mckinsey.com/business-functions/operations/our-insights/reinventing-construction-through-a-productivity-revolution>
- [30] The Business Research Company, Global Construction Market Report And Strategies 2022, Tech. rep., The Business Research Company (2023).  
 URL <https://www.thebusinessresearchcompany.com/report/construction-market>
- [31] B. García de Soto, I. Agustí-Juan, J. Hunhevicz, S. Joss, K. Graser, G. Habert, B. T. Adey, Productivity of digital fabrication in construction: Cost and time analysis of a robotically built wall, *Automation in Construction* 92 (2018) 297–311. doi:10.1016/j.autcon.2018.04.004.
- [32] T. Bock, Construction robotics, *Autonomous Robots* 22 (3) (2007) 201–209. doi:10.1007/s10514-006-9008-5.

- [33] T. Bock, T. Linner, Construction robots: Elementary technologies and single-task construction robots, Vol. 4, Cambridge University Press, 2016, ISBN: 978-1-316-78517-1.
- [34] F. Gramazio, M. Kohler, Digital materiality in architecture, 1st Edition, Lars Muller, Baden, 2008, ISBN: 978-3-03778-122-7.
- [35] S. Parascho, Construction Robotics: From Automation to Collaboration, *Annual Review of Control, Robotics, and Autonomous Systems* 6 (1) (2023). doi:10.1146/annurev-contr-01-080122-090049.
- [36] S. Parascho, A. Gandia, A. Mirjan, F. Gramazio, M. Kohler, Cooperative fabrication of spatial metal structures, in: *Fabricate 2017: Rethinking Design and Construction*, UCL Press, London, 2017, pp. 24–29. doi:10.3929/ethz-b-000219566.
- [37] E. P. G. Bruun, R. Pastrana, V. Paris, A. Beghini, A. Pizzigoni, S. Parascho, S. Adriaenssens, Three cooperative robotic fabrication methods for the scaffold-free construction of a masonry arch, *Automation in Construction* 129 (2021) 103803. doi:10.1016/j.autcon.2021.103803.
- [38] R. Mesnil, T. Gobin, L. Demont, P. Margerit, N. Ducoulombier, C. Douthe, J.-F. Caron, Flexible digital manufacturing of timber construction: the design and fabrication of a free-form nexorade, *Construction Robotics* 7 (2) (2023) 193–212. doi:10.1007/s41693-023-00105-7.
- [39] Y. U. Cao, A. S. Fukunaga, A. Kahng, Cooperative Mobile Robotics: Antecedents and Directions, *Autonomous Robots* 4 (1) (1997) 7–27. doi:10.1023/A:1008855018923.
- [40] E. P. G. Bruun, I. Ting, S. Adriaenssens, S. Parascho, Human–robot collaboration: A fabrication framework for the sequential design and construction of unplanned spatial structures, *Digital Creativity* 31 (4) (2020) 320–336. doi:10.1080/14626268.2020.1845214.
- [41] C. Weckenborg, K. Kieckhäuser, C. Müller, M. Grunewald, T. S. Spengler, Balancing of assembly lines with collaborative robots, *Business Research* 13 (1) (2020) 93–132. doi:10.1007/s40685-019-0101-y.

- [42] E. P. G. Bruun, S. Parascho, S. Adriaenssens, Cooperative Robotic Fabrication for a Circular Economy, in: A Circular Built Environment in the Digital Age, Circular Economy and Sustainability, Springer Cham, 2024, pp. 129–149. doi:10.1007/978-3-031-39675-5\_8.
- [43] S. Parascho, I. X. Han, S. Walker, A. Beghini, E. P. G. Bruun, S. Adriaenssens, Robotic vault: A cooperative robotic assembly method for brick vault construction, *Construction Robotics* 4 (3) (2020) 117–126. doi:10.1007/s41693-020-00041-w.
- [44] S. Parascho, I. X. Han, A. Beghini, M. Miki, S. Walker, E. P. G. Bruun, S. Adriaenssens, LightVault: A design and robotic fabrication method for complex masonry structures, in: Advances in Architectural Geometry 2020, Presses des Ponts, Paris, France, 2021, pp. 350–375.  
 URL <https://oar.princeton.edu/handle/88435/pr1s17ss4d>
- [45] I. X. Han, E. P. G. Bruun, S. Marsh, S. Adriaenssens, S. Parascho, From concept to construction: A transferable design and robotic fabrication method for a building-scale vault, in: Proceedings of the 40th Annual Conference of the Association for Computer Aided Design in Architecture, Online, 2020, pp. 614–623. doi:10.52842/conf.acadia.2020.1.614.
- [46] S. Parascho, T. Kohlhammer, S. Coros, F. Gramazio, M. Kohler, Computational design of robotically assembled spatial structures: A sequence based method for the generation and evaluation of structures fabricated with cooperating robots, in: Advances in Architectural Geometry 2018, Klein Publishing GmbH, Gothenburg, Sweden, 2018, pp. 112 – 139.  
 URL <https://research.chalmers.se/en/publication/504188>
- [47] E. P. G. Bruun, S. Adriaenssens, E. Besler, S. Parascho, ZeroWaste: Towards Computing Cooperative Robotic Sequences for the Disassembly and Reuse of Timber Frame Structures, in: Proceedings of the 42nd Annual Conference of the Association for Computer Aided Design in Architecture, Philadelphia, USA, 2022, pp. 586–597.  
 URL <http://arks.princeton.edu/ark:/88435/pr1wp9t657>

- [48] E. O'Brien, B. Guy, A. S. Lindner, Life Cycle Analysis of the Deconstruction of Military Barracks: Ft. McClellan, Anniston, AL, *Journal of Green Building* 1 (4) (2006) 166–183.  
doi:10.3992/jgb.1.4.166.
- [49] V. Diyamandoglu, L. M. Fortuna, Deconstruction of wood-framed houses: Material recovery and environmental impact, *Resources, Conservation and Recycling* 100 (2015) 21–30.  
doi:10.1016/j.resconrec.2015.04.006.
- [50] R. Zimmann, H. O'Brien, J. Hargrave, M. Morrell, The circular economy in the built environment, Tech. rep., Arup (2016).  
URL [https://www.arup.com/perspectives/publications/research/section/circular-economy-i  
n-the-built-environment](https://www.arup.com/perspectives/publications/research/section/circular-economy-in-the-built-environment)
- [51] A. B. Garcia, I. Y. Cebeci, R. V. Calvo, M. Gordon, Material (data) Intelligence - Towards a Circular Building Environment, in: Proceedings of the 26th International Conference of the Association for Computer-Aided Architectural Design Research in Asia, Vol. 1, 2021, pp. 361–370. doi:10.52842/conf.caadria.2021.1.361.
- [52] T. V. Mele, et al., COMPAS: A framework for computational research in architecture and structures. (2017).  
URL <https://doi.org/10.5281/zenodo.2594510>
- [53] R. Rust, G. Casas, S. Parascho, D. Jenny, K. Dörfler, M. Helmreich, A. Gandia, Z. Ma, I. Ariza, M. Pacher, B. Lytle, Y. Huang, C. Kasirer, E. Bruun, COMPAS FAB: Robotic fabrication package for the COMPAS Framework (2018).  
URL <https://doi.org/10.5281/zenodo.3469478>
- [54] P. Fleischmann, G. Casas, M. Lyrenmann, COMPAS RRC: Online control for ABB robots over a simple-to-use Python interface. (Jul. 2020).  
URL <https://doi.org/10.5281/zenodo.4639418>
- [55] Zivid AS, Zivid Two, Technical Specifications, Zivid AS, Oslo, Norway (2021).  
URL <https://www.zivid.com/zivid-two?hsLang=en>

- [56] Q.-Y. Zhou, J. Park, V. Koltun, Open3D: A Modern Library for 3D Data Processing, arXiv:1801.09847 (2018).
- [57] G. Valiente, Algorithms on Trees and Graphs: With Python Code, 2nd Edition, Springer, Cham, 2021.
- [58] A. A. Hagberg, D. A. Schult, P. J. Swart, Exploring Network Structure, Dynamics, and Function using NetworkX, in: G. Varoquaux, T. Vaught, J. Millman (Eds.), Proceedings of the 7th Python in Science Conference, Pasadena, CA USA, 2008, pp. 11 – 15.
- [59] D. Rutten, Grasshopper (2007).  
URL <https://www.grasshopper3d.com/>
- [60] C. Preisinger, M. Heimrath, Karamba—A Toolkit for Parametric Structural Design, Structural Engineering International 24 (2) (2014) 217–221. doi:10.2749/101686614X13830790993483.
- [61] American Wood Council, National Design Specification for wood construction with commentary, 2015th Edition, American Wood Council, Leesburg, VA, 2015.

# 7

## Conclusions and Future Research

This chapter is based on the following publication(s):

**Bruun, E. P. G.**, Parascho, S., & Adriaenssens, S. (2024). Cooperative Robotic Fabrication for a Circular Economy. In A Circular Built Environment in the Digital Age (pp. 129–149). Springer Cham. [https://doi.org/10.1007/978-3-031-39675-5\\_8](https://doi.org/10.1007/978-3-031-39675-5_8)

Contributor roles in publication:

- Bruun: Conceptualization, Methodology, Investigation, Writing (Original Draft), Writing (Review and Editing), Visualization
- Parascho & Adriaenssens: Writing (Review and Editing), Supervision, Funding Acquisition

In this concluding chapter, the dissertation reviews the four main research projects that form the body of this dissertation, highlighting the key findings and conclusions drawn from each. These findings collectively demonstrate the fulfillment of the research objectives with respect to demonstrating the use of cooperative robotics for scaffold-free processes. Only [Section 7.1](#) is based on previously published work as acknowledged in the title page of this chapter. The subsequent [Section 7.2](#), which provides suggestions for future research endeavors within the realm of cooperative robotic fabrications, is a synthesis from all the future work sections throughout the main body chapters of this dissertation.

## 7.1 Cooperative Robotic Fabrication for a Circular Economy

The following section summarizes the four main chapters in the dissertation and how the research presented in each engages with the topic of cooperative robotic fabrication to achieve various goals of a circular economy. Specifically, this section summarizes examples of cooperative robotic discrete element assembly ([section 7.1.1](#), [section 7.1.2](#), [section 7.1.3](#)), disassembly ([section 7.1.3](#), [section 7.1.4](#)), and reassembly ([section 7.1.4](#)) processes, addressing the “narrow, slow, close” objectives integral to circular economy ideals.

### 7.1.1 Human-Robot Design Collaboration based on Kinematic Constraints for Scaffold-Free Structural Assembly

[Chapter 3](#) described the results of the initial research task focused on scaffold-free cooperative robotic fabrication, showcasing the early-stage implementation of a cooperative robotic support-place sequencing [1]. This first research project inspired and laid the foundation for subsequent research presented within this dissertation. It employed two small 6-axis industrial robotic arms to collaboratively aggregate solid spherical units, forming a branching spatial structure that was built up element-by-element ([fig. 7.1](#)). Notably, the construction of this structure was not pre-planned but rather designed in pseudo-real time during fabrication, utilizing a “design-as-you-build” approach. This method relied on a collaborative effort between humans and robots, where robotic input, in the form of kinematic and path-planning constraints, was combined with human

evaluation and decision-making.

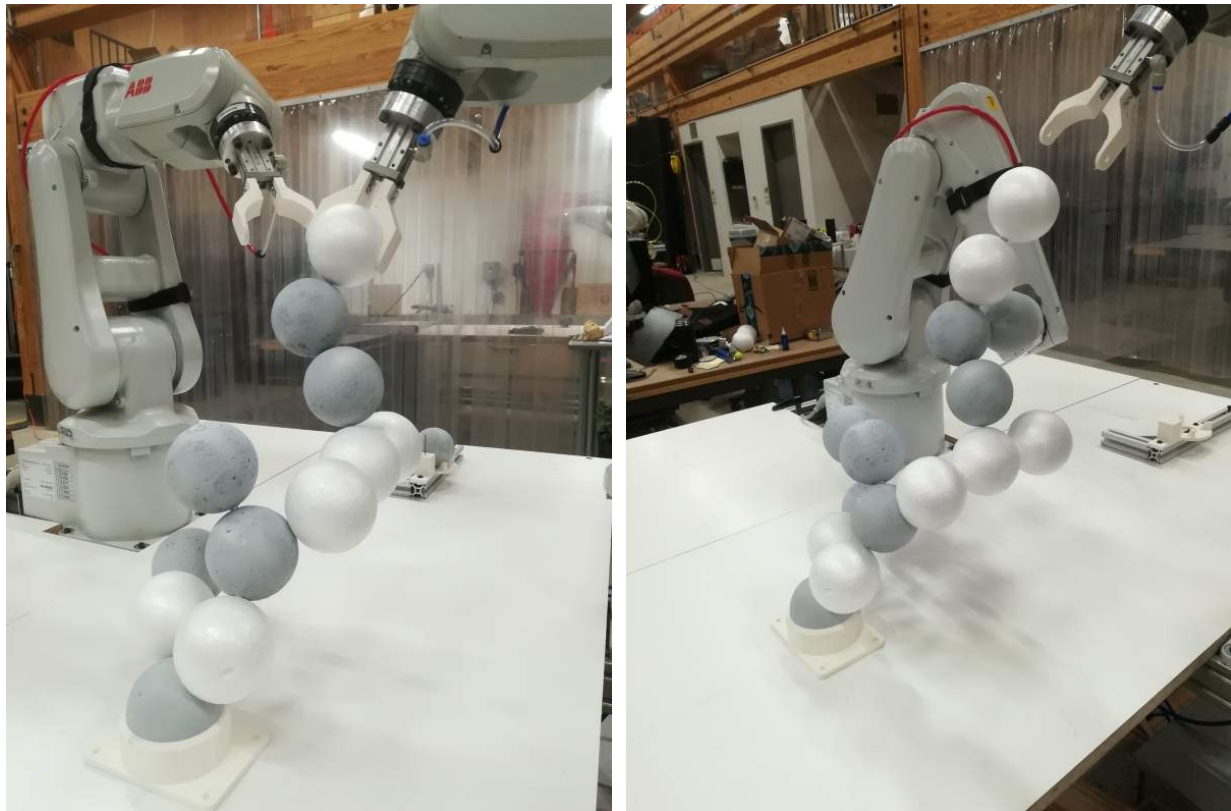


**Figure 7.1:** Snapshots from the cooperative robotic fabrication of an unplanned structure

This project revealed the versatility of robotic arms beyond active fabrication tasks, showcasing their ability to serve as passive supports during the fabrication process. Consequently, the need for external supporting structures during fabrication was eliminated addressing the goal of material reduction as per the “slow” circular economy principle. Although the scale and complexity of the structure assembled in this research project was modest, its significance lies in laying the groundwork for subsequent, more complex robotic fabrication tasks and developing an interactive design strategy that involves both humans and robots.

### 7.1.2 Cooperative Robotic Support-Place Sequencing for Scaffold-free Construction of Spanning Masonry Structures

Chapter 4 described the cooperative robotic sequencing and simulation studies as part of the LightVault project. In this project, a  $3.6 \times 6.5 \times 2.2m$  doubly-curved masonry vault was built

with two stationary robotic arms as a demonstration of CRF applied to an assembly process [2]. In the first phase of the project, a central arch was constructed utilizing the alternating cooperative robotic placement and support approach inspired by previous research on the assembly of metal space frame structures [3, 4]. One robot continuously acted as a support to the partially completed arch, while the other was used to place additional bricks into the structure (fig. 7.2). Thus, the arch was built from one end to the other without requiring any additional temporary supporting structure. The structural performance of the arch during construction was assessed using a discrete element modelling approach [5], and the cooperative sequencing was later theorised to setups with more than two robots to further improve the structural performance during assembly [6]. In the second phase of the project, the rest of the vault was built layer by layer using the central arch as a backbone structure [7, 8].

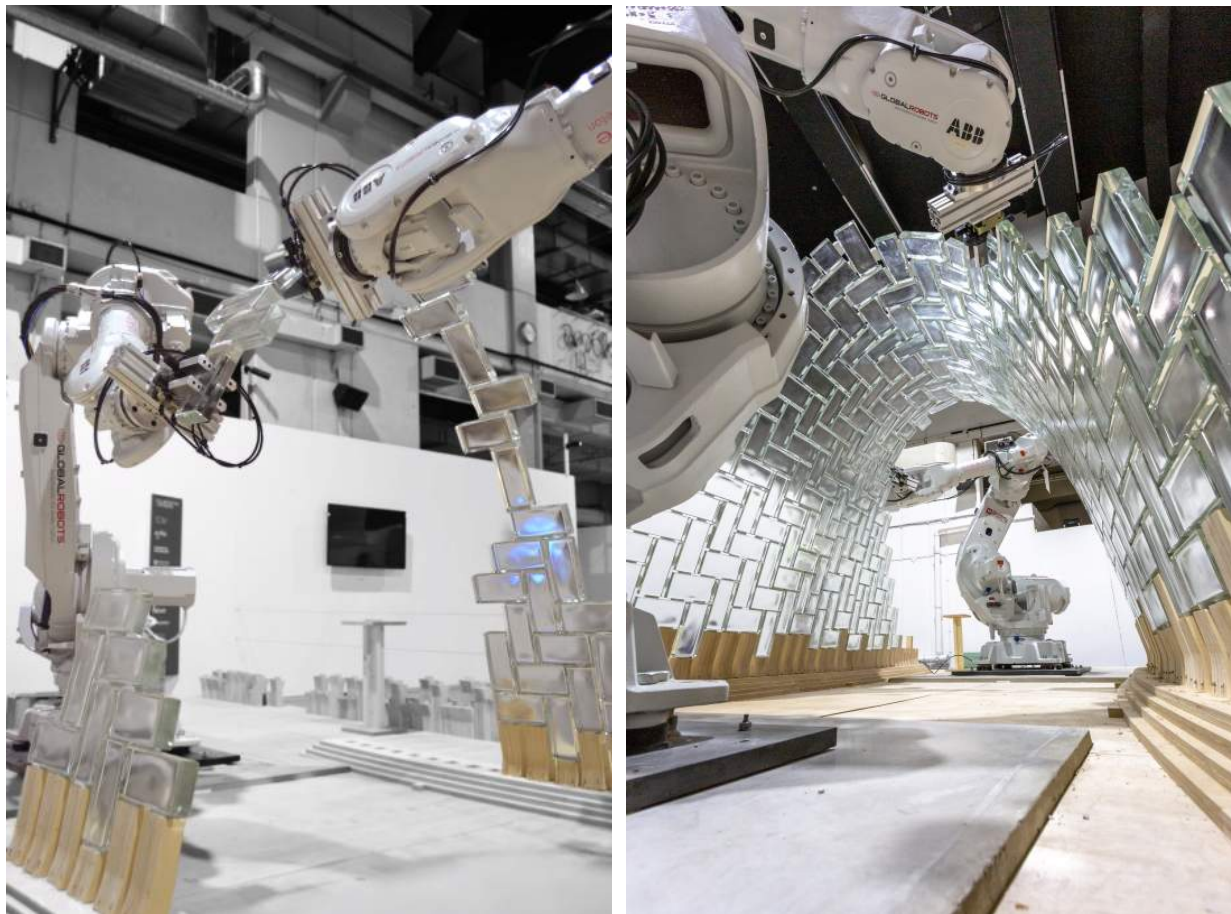


**Figure 7.2:** Scaffold-free cooperative robotic assembly of a masonry vault

Overall, this project demonstrated the first application of CRF for scaffold-free construction of spanning structures made from heavy materials (e.g., glass bricks). With respect to a circular economy, specifically the “slow” principle, the use of primary resources was reduced by both by eliminating temporary supporting structures and by minimizing the material necessary in the structure itself by enabling the construction of a structurally efficient but geometrically complex form that was designed to experience only compressive forces.

### **7.1.3 Rigidity Theory for the Design of Space Frame Structures that can be (Dis)Assembled without Scaffolding**

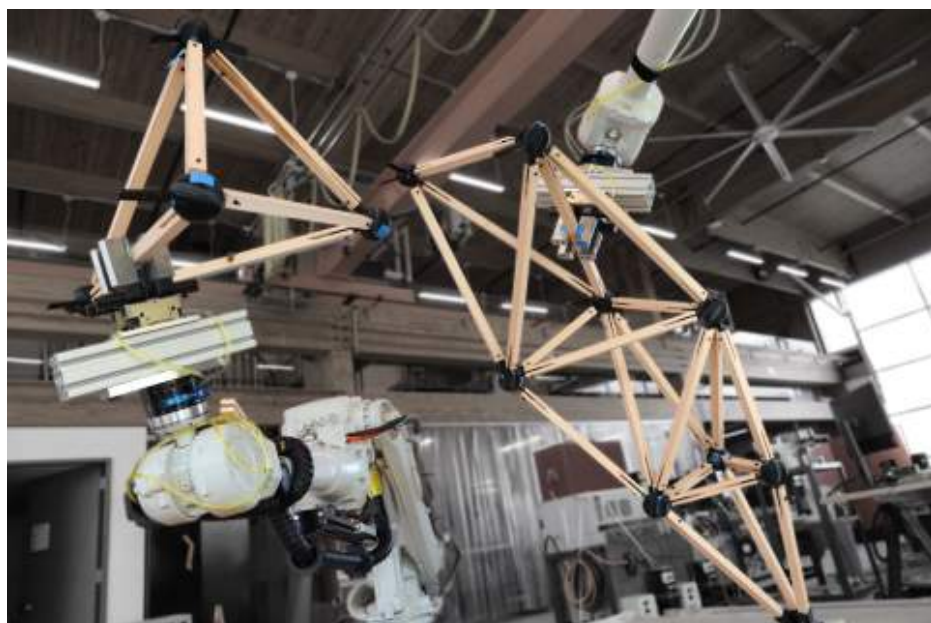
[Chapter 5](#) described the output from the Remote Robotic Assemblies workshop held at the 2021 Association for Computer Aided Design in Architecture (ACADIA) conference, where a timber space frame arch structure was first designed and then constructed using two cooperating robotic arms on linear tracks. This project was a demonstration of CRF applied to not just the assembly of the structure but extending its use for the first time to disassembly as well. Using a method based on rigidity theory, the space frame was designed explicitly to leverage cooperative robotic support sequencing to replace temporary supporting structure during both the construction and deconstruction phases [9]. The structure was first assembled element by element, where one passive robotic agent was always required to provide support to the partially assembled structure. Following this, the structure was disassembled cell by cell, taking advantage of the fact that it was designed explicitly as an assembly of locally rigid tetrahedral cells. These cells were sequentially supported, isolated, and then removed with one robot, while the other robot supported the partially disassembled structure ([fig. 7.3](#)). The disassembly process is an example of a collaborative-CRF (Co-CRF) process as the removal of individual elements to disconnect the rigid tetrahedral cells from the remaining structure was done in collaboration with a human.

Overall, this project demonstrated that CRF is a viable technology to reduce primary resource inputs in the form of scaffolding during both the assembly and disassembly of spanning space frame structures. With respect to a circular economy, this addresses the “slow” principle. In addition, extending the application of CRF to disassembly tasks highlighted the potential of including

considerations for disassembly at the outset of a design to better facilitate the reuse and recycling of building components at the end of a structure's life. This design for reversibility in a scaffold-free way addresses the "slow" principle as part of a circular economy.



**(a) Phase 1:** Assembling locally rigid cells by placing one element at a time while the remaining structure is supported.



**(b) Phase 2:** Isolating locally rigid cells in the scaffold-free cooperative robotic disassembly of a spanning timber space frame arch structure.

**Figure 7.3:** Scaffold-free (dis)assembly of a spanning timber space frame arch structure

### **7.1.4 Support Hierarchy Graphs for Planning the Scaffold-Free Dis-and-Reassembly of a Frame Structure with Cooperating Robots**

[Chapter 6](#) described the development of a graph-based cooperative robotic sequence planning approach and its physical robotic implementation as part of the ZeroWaste project. This project explored the idea of treating existing timber buildings as stores of valuable reusable material in the context of a circular economy [10, 11]. Rather than demolishing and disposing of a building at the end of its life, the goal was to leverage the use of a CRF setup to first gather data about an unknown existing structure and then use this information together with the robotic setup to disassemble and then reassemble the structure into new feasible configurations.

As the starting point, a pavilion-scale timber structure was built manually to act as a stand-in representing a generic unknown existing structure built according to standard stick framing construction practices. Next, 3D cameras were mounted on two robotic arms, which were then used to take several point cloud captures of the structure from various locations and angles. Using the accurate positional information queried from the robotic controller, the individual point cloud captures were transformed and then stitched together to create a complete spatial model of the existing structure. Creating this complete model was only possible when using multiple robots, as a single robot would not have the required reach and manoeuvrability to fully capture the structure. For an existing building, the exact geometry and spatial location of the structure is not known, thus the as-built geometric information gathered in this imaging process was necessary when later planning the RF sequences.

Next, scaffold-free robotic cooperative disassembly and reassembly sequences were calculated algorithmically using a support hierarchy graph representation of the structure. These sequences were specifically planned for execution with the three robotic arms available in the fabrication cell, two on linear tracks and one stationary, without requiring external temporary formwork. The physical RF process was split into four distinct phases, targeting different objectives with respect to the cooperative robotic sequencing and the degree of disassembly and reassembly ([fig. 7.4](#)). [Chapter 6](#) solely encompasses phases 1, 2, and 3, as outlined in the published research paper that is integrated into this dissertation. The final phase, while yielding an aesthetically captivating structure, was completed without the use of a cooperative robotic framework and therefore falls

outside the main research scope if this dissertation.

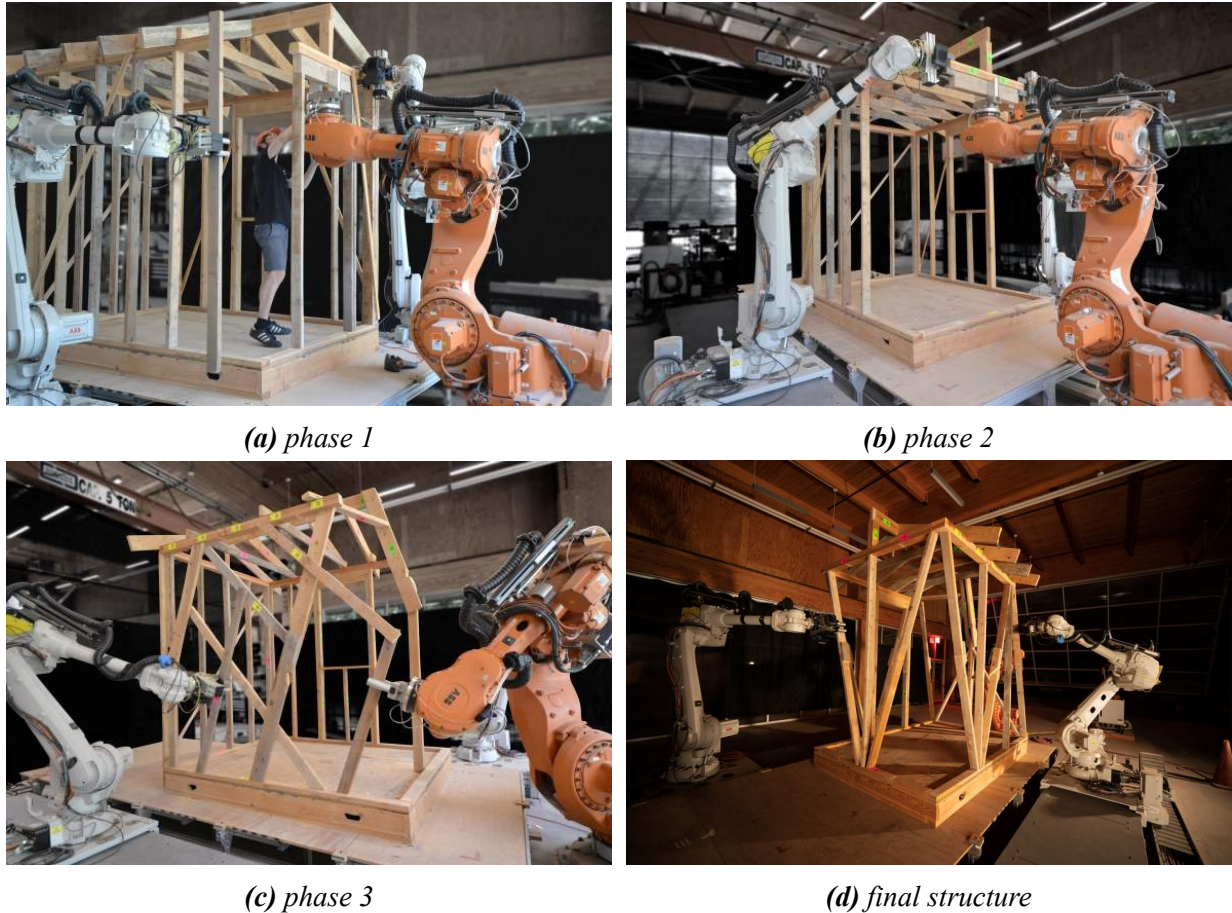


**Figure 7.4:** Snapshots from the different phases of the cooperative robotic disassembly and reassembly as part of the ZeroWaste project

Similarly to the project described in section 7.1.3, ZeroWaste demonstrated the use of a CRF setup in providing temporary support to a structure during disassembly, but further extended its use to perform scaffold-free reassembly and reuse of removed material. Improvements in construction efficiency were also demonstrated as the full fabrication process only required a single person working alongside the robots, whereas using non-robotic methods would typically require several workers to accomplish the same tasks. Overall, the successful use of CRF in the ZeroWaste project to assist in structural disassembly and reassembly tasks highlighted the potential of this technology to facilitate a more circular treatment of existing timber building stock through its reuse.

## 7.2 Recommendations for Future Research

The four robotic fabrication research projects outlined in this dissertation mark a significant advancement in showcasing innovative applications of scaffold-free cooperative robotic disassembly and reassembly processes for discrete element structures. At the same time, their completion also highlights several promising avenues for future research. While each chapter delves into project-specific limitations and potential research endeavors, this section aims to consolidate these discussions into broader categories that are broadly applicable across the research presented in the whole dissertation. Pursuing these future research directions promises to further improve the capabilities of cooperative robotic fabrication systems in the construction industry, thereby fostering more sustainable and efficient construction practices.

### 7.2.1 Human-Robot Collaboration

The research presented in this dissertation is primarily focused on cooperative robotic processes, wherein multiple robots collaborate to tackle tasks beyond the abilities of a single robot. While these processes exhibit remarkable potential, incorporating humans into the design and fabrication loop could significantly augment the utility and effectiveness of the overall setup. Despite various degrees of human involvement in realizing all the robotic fabrication demonstrator structures, such as material preparation, code execution, fabrication sequence planning, and data processing, only the research presented in [Chapter 3](#) showcased genuine human collaboration within a collaborative-cooperative robotic fabrication process, albeit at a limited structural scale.

Future research endeavors should center on refining fabrication processes to facilitate both cooperative sequencing among multiple robots while accounting for more direct human involvement in both the design and fabrication phases. This approach promises to unlock new avenues for digital and human collaboration, thereby fully harnessing the capabilities of robotic manipulators as indispensable design-fabrication tools. However, such collaboration between humans and robots requires further investigation into how to create a safe environment and workflow that would allow for both human-robot and robot-robot interactions to occur seamlessly.

## **7.2.2 Real-Time Control Through an Augmented/Virtual Reality Environment**

One notable limitation across all fabrication projects in this dissertation is the absence of real-time operation. In other words, users had to pre-plan fabrication processes, including robot sequencing and path planning, leading to a significant delay between planning and execution of fabrication tasks. While this approach is valid in many scenarios, it inherently introduces a time lag that can be prohibitive with respect to construction efficiency.

Future research should prioritize implementing cooperative robotic sequencing and control in a real-time environment. This could be achieved through autonomous robotic processes, where decisions regarding motion and execution are made based on predefined criteria, adapting in real-time to the evolving environment. Alternatively, a control method akin to current robotic usage could be employed just in a more efficient manner. Rather than users performing multiple offline steps before instructing the robots by executing blocks of code on a teach pendant, they could have direct connectivity to the robots and control them through wearable sensors.

For instance, users could wear augmented/virtual reality goggles coupled with gloves with motion capture targets. Through augmented/virtual reality, users could perceive the robot's work environment and manipulate objects using hand gestures, with the sensors on the gloves corresponding to the robot's motion. This approach allows users to execute simple actions ergonomically, translating digital manipulations into physical robot actions.

Moreover, this real-time control method could facilitate remote operation, eliminating the need for users and robots to be physically co-located. As long as the augmented reality environment mirrors the robot's operating space and there's a wireless link between the user's arm motion and the robot's action, remote operation becomes feasible.

## **7.2.3 Mixed Fixed/Mobile Robot Teams**

This research presented in this dissertation primarily focused on cooperative robotic fabrication within controlled laboratory settings. The robots utilized are typically fixed to the ground or operate on linear tracks. However, this approach encounters scalability issues, as the number of these larger fixed robots capable of operating simultaneously in a confined space is restricted.

Although fixed or linearly mobile robotic arms can be deployed on-site, as demonstrated in the LightVault project, their calibration and accuracy present significant challenges in active job site environments.

Nonetheless, this does not negate the potential role of such robotic setups on-site; rather, it underscores the necessity of enhancing flexibility by integrating mobile robots into the cooperative team. Future research should aim to broaden the field of cooperative robotic fabrication to incorporate mobile robots working alongside fixed robots. Despite mobile robots often having smaller payloads than fixed ones, their extended range, flexibility, and improved dexterity compensate for this limitation.

Therefore, a more resilient and adaptable robotic setup would integrate both fixed and mobile robots, possibly including human interaction as well. Each agent would undertake tasks suited to its capabilities. For instance, mobile robots could excel in tasks like data gathering and light material handling, while larger robots could handle long-duration tasks such as structural support, thereby enhancing the setup's overall flexibility and range of applications.

Integrating mobile robots with stationary robotic arms would streamline labor distribution and expand the setup's capabilities to manage larger and more varied construction scenarios. Moreover, mobile robots could supplant manual execution of tasks requiring fine motor skills typically performed by humans, such as fastener manipulation, thereby enhancing efficiency, precision, and the level of automation in the fabrication process.

#### **7.2.4 Incorporating Sensor Feedback in Design Process**

Future research will integrate feedback mechanisms, such as real-time 3D imaging of the structure during assembly or disassembly, to enhance the adaptability of the fabrication process to changing conditions, such as structural deformation due to self-weight. This approach will enable the fabrication process to directly adjust to unpredictable changes or deformations as they occur.

For example, in the ZeroWaste project, a current limitation arises from relying on pre-scanning the structure to generate a point cloud before initiating fabrication planning. However, the method lacks the ability to promptly and accurately update the point cloud model with changes

during fabrication, necessitating a complete re-scan for significant updates. Future research should prioritize developing processes that allow robots to dynamically collect information and update the as-built point cloud model while simultaneously performing fabrication tasks. This real-time feedback mechanism would enhance adaptability and accuracy in planning and executing fabrication processes, especially for complex and dynamically changing structures.

Additionally, employing a force-torque sensor mounted on the robot gripper could inform the placement of new components in locations that minimize total unbalanced force. These force-torque sensors, mounted on the robot tool flange, could also facilitate cooperative in situ non-destructive testing on structures, providing valuable data on their performance during assembly or disassembly, such as determining stiffness. This data can be used to design more material-efficient structures, assess overall structural performance during fabrication, and measure parameters like stiffness or degree of damage to a member. Each robot could effectively act as a 6-degree-of-freedom actuator capable of applying forces and moments to the structure at any location and orientation in space. By sequencing robots cooperatively, it becomes feasible to apply non-standard loading conditions, which would be challenging to evaluate in situ using conventional load testing methods, particularly for geometrically complex structures.

### **7.2.5 Path Planning and Structural Analysis Integration**

Another area for future research involves simplifying the manual steps needed to set up and process the results of path-planning and reachability feasibility assessments. Currently, users must manually select multiple locations in the digital environment representing the structure and robotic system to conduct a series of brute force path-planning and reachability checks at these locations. This preparation process is time-consuming and labor-intensive. Future research should explore automated methods for this process, potentially utilizing machine learning and computer vision techniques to automate point cloud processing for path-planning checks.

Similarly, implementing a more automated approach to creating the finite element model for assessing the progressive behavior of the structure during a robotic process would speed up structural feasibility assessments. For example, in the ZeroWaste project, users manually process the point cloud to construct the structural analysis model for each sequence, based on the centerline

locations of members.

Enhanced integration between structural results from finite element analysis and the robotic path planning process would enable the creation of a more informed optimization process for generating and selecting fabrication sequences. Establishing an automated workflow to select a fabrication sequence based on optimization criteria linked to structural performance during fabrication would lead to a faster and less manual sequence generation process across all the different applications described in this dissertation. For instance, if relying on a graph-based method, the could be formulated as an optimization problem by setting edge weights in the graph based on the structural loading or other structural criteria of interest. Then, the objective function for the problem could be formulated to minimize the cumulative value across the graph representing the structure during the entire fabrication process. Overall, better integration of finite element structural results, the robotic path planning process, and a graph representation used to suggest feasible robotic sequences would reduce the manual work required for planning a cooperative robotic fabrication process.

### **7.2.6 Applications to Continuous Material Systems**

The research chapters in this dissertation focused on the robotic fabrication of discrete element structural systems, such as space frames, masonry structures, and stick frame structures. Moving forward, research should explore employing cooperative robotic techniques for continuous material systems.

For instance, in 3D printing of concrete, current methods typically utilize a single robot or print-head to extrude material layer by layer, limiting the ability to create complex shapes with inclined or sloping geometry. An avenue for future exploration involves employing cooperative robotic methods to enable the construction of more intricate shapes. One approach could involve one robot performing the printing while another provides temporary support to inclined or sloping concrete layers. Additionally, the supporting robot could handle tasks like placing reinforcement bars or other structural elements within the 3D printed concrete structure, tasks that are currently either manual or not performed at all.

Another potential application lies in metallic additive manufacturing or continuous welding

processes. In this scenario, one robot would handle material placement while the other would perform inspection and monitoring of the material deposition. This setup enables real-time correction or adjustment of the process, ensuring quality and precision throughout fabrication.

### 7.2.7 Increased Payload and Work Area

One limitation of the research presented in this dissertation stems from the inherent physical constraints of the available robotic setup. While having access to three larger-scale robotic arms presents a unique opportunity for innovative research, certain limitations affect the scope of exploration. Specifically, two of the robots were confined to a linear travel of 3.9m on tracks spaced 3.45m apart, defining the reachable work area. Additionally, the third robot was fixed to the ground without a track, further restricting its reach and motion capabilities.

Ground-mounted robots inherently face limitations in their reach, especially in height, thereby constraining the cooperative build volume to a small area between the two tracked robots. This spatial restriction is depicted in [Figure 7.5](#), illustrating the limited cooperative reach zone formed by the two robots.

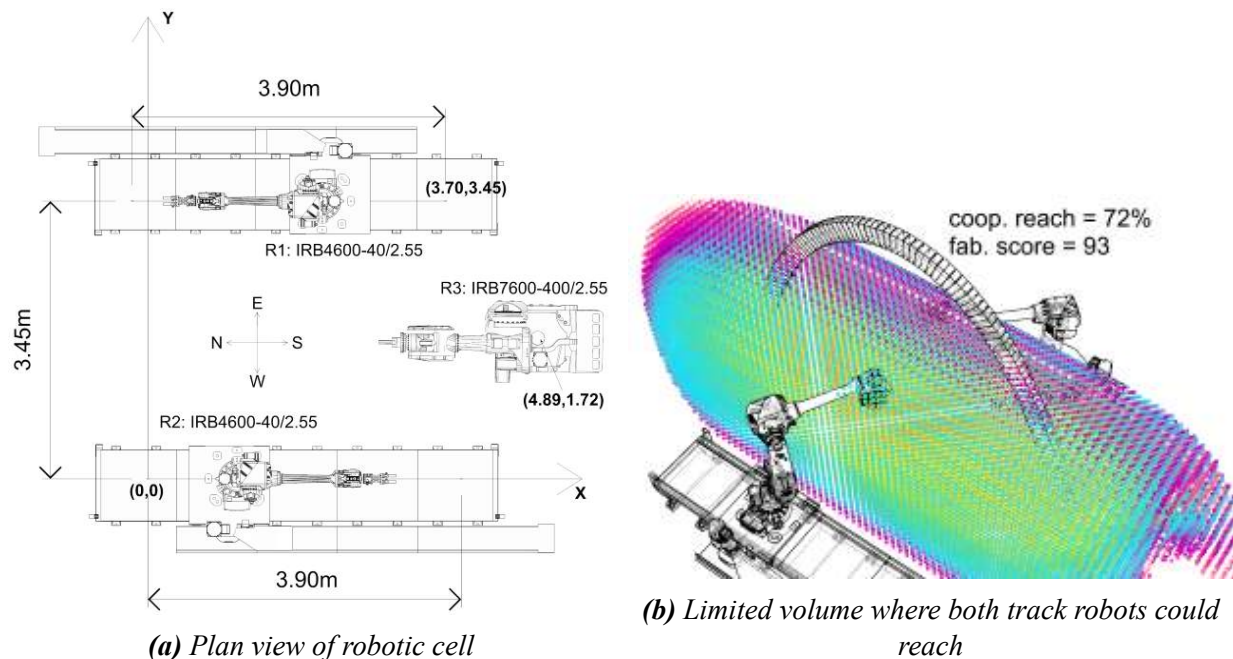


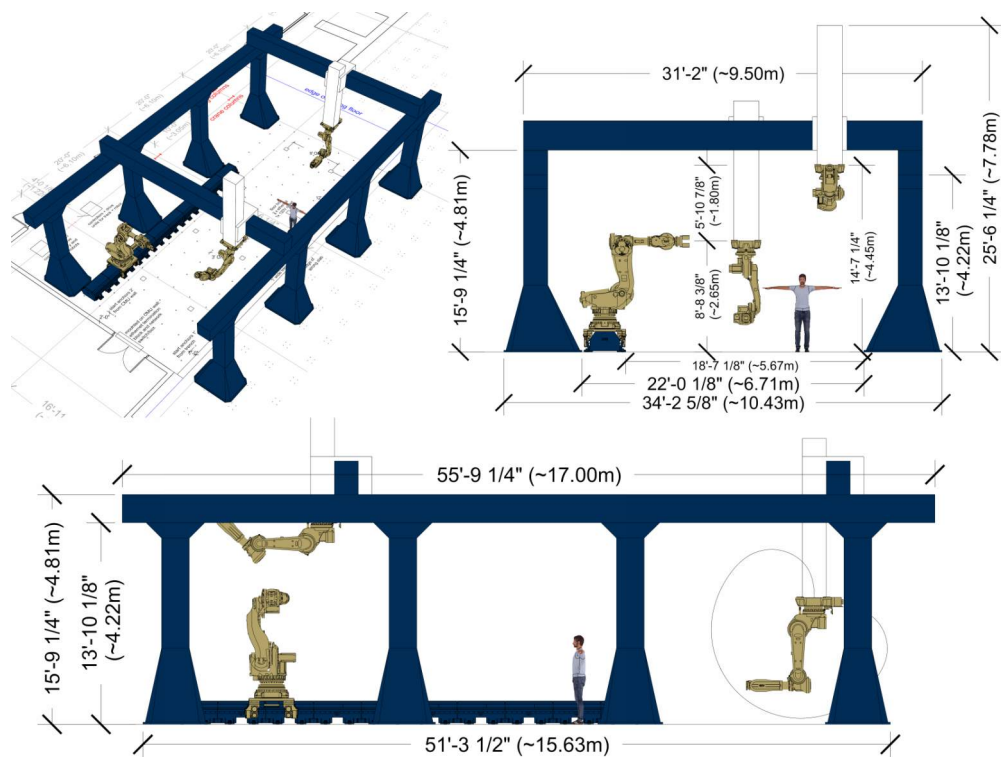
**Figure 7.5:** Robotic setup used throughout dissertation research

Moreover, the payload capacities of the robots serve as another limiting factor, impacting the size and scale of structural components that can be manipulated and supported during construction. While the two tracked robots had a payload limit of 40kg each, sufficient for handling lighter materials and tasks at reasonable scales, this limit remained a significant constraint. The third fixed robot had a payload capacity of 400kg; however, due to its limited reach without a track, it primarily served support functions and some restricted material handling tasks.

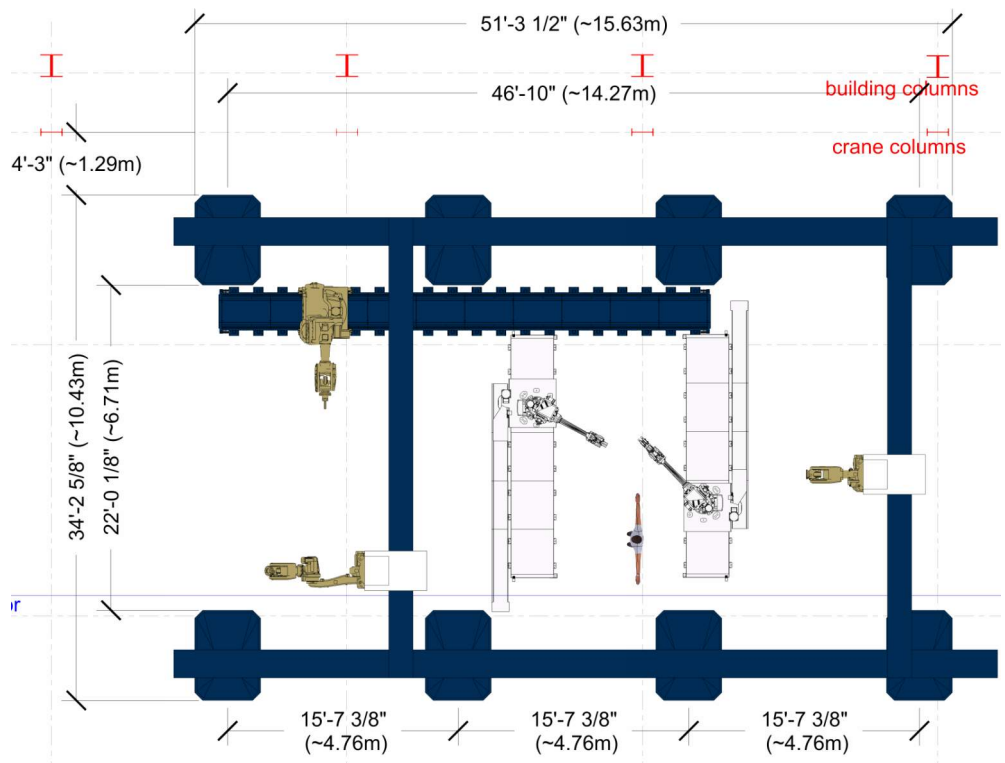
To address the physical limitations affecting the type and size of structures that can be constructed and disassembled robotically, future efforts should concentrate on establishing a more adaptable and versatile laboratory environment.

[Figure 7.6](#) depicts a novel research facility developed by the author for future research that features an overhead cartesian gantry system supporting two suspended robots, along with a heavy-payload robot mounted on a track. This setup is inspired by the Robotic Fabrication Lab (RFL) for the Institute of Technology in Architecture (ITA) on the Hoenggerberg Campus of ETH Zurich [12]. By suspending two robots from an overhead gantry capable of movement in the X, Y, and Z axes, complete reachability across a significantly larger work volume is achieved, resolving the previous issue of limited cooperative work zones. For the purpose of scale comparisons, the current robotic research setup utilized to construct the physical demonstrators described in this dissertation is shown inside the gantry work area.

The gantry provides a spacious working area measuring approximately 16.6 by 6.7 meters, with a height clearance of up to 4.2 meters. Furthermore, the suspended robots on the gantry's Z-axis boast significantly higher payload capacities compared to robots mounted on tracks in the current setup used by the author of this dissertation in the course of their research. With a payload capacity of 200kg each, these suspended robots can accommodate larger tools and manipulate more substantial structural elements, facilitating the completion of more intricate fabrication tasks.



*(a)* various views of the robotic gantry setup



*(b)* plan view of the gantry setup with the Princeton ECL setup in the middle for scale

**Figure 7.6:** Conceptual cooperative robotic gantry setup improving payload and reach.

### 7.3 General Conclusion

The global population is on a trajectory of rapid growth, with estimates projecting a population of 9.8 billion by 2050. This growth, accompanied by accelerating urbanization, emphasizes the urgent need for the architecture, engineering, and construction (AEC) industries to innovate and develop new technologies. These innovations are crucial for meeting the escalating infrastructure demands while simultaneously addressing the significant environmental impacts that stem from high energy consumption and CO<sub>2</sub> emissions. Robotic automation in the AEC industry has the potential to enable novel construction processes for geometrically complex structures. The research presented in this dissertation demonstrates the use of Cooperative Robotic Fabrication (CRF) setups, where multiple robots collaborate on construction tasks, for applications in the assembly, disassembly, and reuse of discrete element structures, developing and showcasing computational methods that coordinate multiple robotic arms to ensure structural stability without the need for external supports or scaffolding.

The dissertation begins with CRF applications focused solely on assembly and then extends to more complex tasks that involve structural disassembly and reuse. It introduces a bottom-up human-robot design framework where two cooperating robots aid in designing branching spatial structures in pseudo real-time, incorporating path-planning constraints in conjunction with human decision-making. Following this, the research showcases CRF for constructing geometrically intricate spanning masonry structures. In these scenarios, the structure is modeled as a lumped spring system, and robots are sequenced in a manner that ensures the stability of the central arch without external scaffolding. Next, the dissertation demonstrates a fabrication-informed approach for designing space frame structures, using rigidity theory and Henneberg planar graph assembly steps to build rigid space frames intended for scaffold-free assembly and disassembly. Finally, CRF is applied to the disassembly and reuse of an existing prototype structure, satisfying circular economy principles by minimizing material waste and facilitating reuse. This is achieved through a novel graph-based method that uses the concept of structural support hierarchy to isolate affected members within the structure and generate sequences for removing these members without destabilizing the remaining structure.

The research presented in this dissertation does not claim to solve all the challenges currently

facing the AEC industry. However, it provides a crucial step forward in promoting the adoption of novel automation techniques and technologies. Specifically, this dissertation illustrates how structures can be designed to leverage advanced robotic assembly and disassembly techniques more effectively. The research demonstrates the potential of multiple robots working cooperatively to enhance the construction of discrete element structures such as masonry vaults, space frames and timber structures. This cooperative multi-robotic approach can significantly reduce or eliminate the need for scaffolding and temporary supports during both assembly and disassembly phases, thus minimizing overall material usage and waste.

While this dissertation highlights the potential of robotic arms to transform construction processes, future work will aim to adapt the computational methods and cooperative robot sequencing developed here to a broader array of applications and structural typologies. Notably, the groundwork for this adaptation is already being laid, as the methods proposed in this dissertation are designed to be easily applied to other systems. This is an important contribution to the field.

Limitations due to small work volumes and payloads of the robotic setup for cooperative robotic processes were also a significant constraint experienced in all of the research conducted as part of this dissertation. Thus, for further innovation in the structural cooperative robotic research space to occur, larger and more flexible research apparatuses, such as a gantry and suspended robot setup with increased reach and payload, will be necessary at the institutional level. By continuing to innovate in automation technology, the AEC industry can progress towards more sustainable and efficient construction practices. These practices are essential to meeting the demands of a growing and urbanizing global population while continuously striving to limit their environmental impact.

## References

- [1] E. P. G. Bruun, I. Ting, S. Adriaenssens, S. Parascho, Human–robot collaboration: A fabrication framework for the sequential design and construction of unplanned spatial structures, *Digital Creativity* 31 (4) (2020) 320–336. doi:10.1080/14626268.2020.1845214.
- [2] S. Parascho, I. X. Han, A. Beghini, M. Miki, S. Walker, E. P. G. Bruun, S. Adriaenssens, LightVault: A design and robotic fabrication method for complex masonry structures, in: *Advances in Architectural Geometry 2020*, Presses des Ponts, Paris, France, 2021, pp. 350–375.  
URL <https://oar.princeton.edu/handle/88435/pr1s17ss4d>
- [3] S. Parascho, A. Gandia, A. Mirjan, F. Gramazio, M. Kohler, Cooperative fabrication of spatial metal structures, in: *Fabricate 2017: Rethinking Design and Construction*, UCL Press, London, 2017, pp. 24–29. doi:10.3929/ethz-b-000219566.
- [4] S. Parascho, T. Kohlhammer, S. Coros, F. Gramazio, M. Kohler, Computational design of robotically assembled spatial structures: A sequence based method for the generation and evaluation of structures fabricated with cooperating robots, in: *Advances in Architectural Geometry 2018*, Klein Publishing GmbH, Gothenburg, Sweden, 2018, pp. 112 – 139.  
URL <https://research.chalmers.se/en/publication/504188>
- [5] V. Paris, N. Lepore, E. P. G. Bruun, G. Ruscica, M. D. Piccioni, A. Beghini, S. Parascho, S. Adriaenssens, Robotic construction of a self-balancing glass masonry vault: DEM study of stability during construction stages, in: *Proceedings of the IASS Annual Symposium 2020/2021*, Surrey, 2021, pp. 314–325.  
URL <http://arks.princeton.edu/ark:/88435/pr12n4zh86>
- [6] E. P. G. Bruun, R. Pastrana, V. Paris, A. Beghini, A. Pizzigoni, S. Parascho, S. Adriaenssens, Three cooperative robotic fabrication methods for the scaffold-free construction of a masonry arch, *Automation in Construction* 129 (2021) 103803. doi:10.1016/j.autcon.2021.103803.

- [7] S. Parascho, I. X. Han, S. Walker, A. Beghini, E. P. G. Bruun, S. Adriaenssens, Robotic vault: A cooperative robotic assembly method for brick vault construction, *Construction Robotics* 4 (3) (2020) 117–126. doi:10.1007/s41693-020-00041-w.
- [8] I. X. Han, E. P. G. Bruun, S. Marsh, S. Adriaenssens, S. Parascho, From concept to construction: A transferable design and robotic fabrication method for a building-scale vault, in: *Proceedings of the 40th Annual Conference of the Association for Computer Aided Design in Architecture*, Online, 2020, pp. 614–623. doi:10.52842/conf.acadia.2020.1.614.
- [9] E. P. G. Bruun, S. Adriaenssens, S. Parascho, Structural rigidity theory applied to the scaffold-free (dis)assembly of space frames using cooperative robotics, *Automation in Construction* 141 (2022) 104405. doi:10.1016/j.autcon.2022.104405.
- [10] E. P. G. Bruun, S. Adriaenssens, E. Besler, S. Parascho, ZeroWaste: Towards Computing Cooperative Robotic Sequences for the Disassembly and Reuse of Timber Frame Structures, in: *Proceedings of the 42nd Annual Conference of the Association for Computer Aided Design in Architecture*, Philadelphia, USA, 2022, pp. 586–597.  
URL <http://arks.princeton.edu/ark:/88435/pr1wp9t657>
- [11] E. P. G. Bruun, S. Adriaenssens, E. Besler, S. Parascho, ZeroWaste: Disassembly and reuse of a timber frame structure using cooperating robots, *Construction Robotics*(Submitted) (2024).
- [12] Chair of Architecture and Digital Fabrication, Robotic Fabrication Lab (RFL) (2016).  
URL <https://systems.arch.ethz.ch/rfl/robotic-fabrication-lab>

# A

## Appendix for Chapter 4

## A.1 2-Robot Fabrication Sequence Analysis Results

**Table A.1:** Analysis results for the sequential method

Step	Type	# Bricks	<i>rob1</i>		<i>rob2</i>		<i>rob3</i>		<i>F<sub>rob1</sub></i>		<i>F<sub>rob2</sub></i>		<i>F<sub>rob3</sub></i>		<i>F<sub>sup</sub></i>		<i>M<sub>sup</sub></i>		<i>F<sub>min</sub></i>		<i>F<sub>max</sub></i>		<i>F<sub>avg</sub></i>		<i>T%<sup>1</sup></i>		<i>Δ<sub>max</sub></i>		<i>Δ<sub>avg</sub></i>		<i>Δ<sub>σ</sub><sup>2</sup></i>	
			b	n	b	n	b	n	N	N	N	N	N	N	N	N	N · m	N	N	N	N	N	[10 <sup>-3</sup> ] mm	[10 <sup>-3</sup> ] mm	[10 <sup>-3</sup> ] mm							
1	place	1	1	1	—	—	—	—	35.6	—	—	1.8	0.1	0.0	17.6	4.4	50.0	0.0	0.0	0.0	0.0	0.0	0.0	0.0	0.0	0.0	0.0	0.0	0.0	0.0		
2	place	2	1	1	2	2	—	—	36.6	38.3	—	2.9	0.5	0.0	17.6	2.5	71.4	0.1	0.0	0.0	0.0	0.0	0.0	0.0	0.0	0.0	0.0	0.0	0.0	0.0	0.0	
3	release	2	—	—	2	2	—	—	—	54.3	—	19.0	0.8	-17.5	17.6	0.1	71.4	0.1	0.0	0.0	0.0	0.0	0.0	0.0	0.0	0.0	0.0	0.0	0.0	0.0	0.0	
4	place	3	3	4	2	2	—	—	36.1	54.6	—	18.1	0.4	-17.6	17.6	0.0	50.0	0.1	0.0	0.0	0.0	0.0	0.0	0.0	0.0	0.0	0.0	0.0	0.0	0.0	0.0	
5	release	3	3	4	—	—	—	—	71.5	—	—	36.2	1.1	-35.4	35.1	-1.9	30.0	0.1	0.1	0.1	0.1	0.1	0.1	0.1	0.1	0.1	0.1	0.1	0.1	0.1	0.1	
6	place	4	3	4	4	7	—	—	73.4	35.2	—	35.9	0.8	-35.4	35.1	-0.1	46.2	0.2	0.1	0.1	0.1	0.1	0.1	0.1	0.1	0.1	0.1	0.1	0.1	0.1	0.1	
7	release	4	—	—	4	7	—	—	—	87.3	—	56.9	3.6	-54.6	68.3	1.5	53.8	0.4	0.3	0.3	0.2	0.2	0.2	0.2	0.2	0.2	0.2	0.2	0.2	0.2	0.2	
8	place	5	5	8	4	7	—	—	25.7	101.4	—	55.9	3.0	-54.2	68.6	0.7	43.8	0.4	0.2	0.2	0.1	0.1	0.1	0.1	0.1	0.1	0.1	0.1	0.1	0.1	0.1	
9	release	5	5	8	—	—	—	—	75.0	—	—	106.1	6.8	-103.9	36.9	-24.2	43.8	1.3	0.7	0.7	0.4	0.4	0.4	0.4	0.4	0.4	0.4	0.4	0.4	0.4	0.4	
10	place	6	5	8	6	11	—	—	76.9	54.5	—	85.2	5.4	-82.9	57.7	-6.6	47.4	0.9	0.4	0.4	0.3	0.3	0.3	0.3	0.3	0.3	0.3	0.3	0.3	0.3	0.3	
11	release	6	—	—	6	11	—	—	—	85.2	—	132.2	8.3	-129.9	45.5	-31.8	36.8	2.2	1.1	1.1	0.6	0.6	0.6	0.6	0.6	0.6	0.6	0.6	0.6	0.6	0.6	
12	place	7	7	13	6	11	—	—	78.0	68.5	—	107.9	8.8	-104.8	70.9	-6.1	59.1	2.0	0.9	0.9	0.6	0.6	0.6	0.6	0.6	0.6	0.6	0.6	0.6	0.6	0.6	
13	release	7	7	13	—	—	—	—	127.7	—	—	124.4	11.5	-120.3	105.4	-8.7	50.0	2.4	1.5	1.5	0.8	0.8	0.8	0.8	0.8	0.8	0.8	0.8	0.8	0.8	0.8	
14	place	8	7	13	8	15	—	—	168.8	56.5	—	114.7	7.5	-112.3	111.5	-2.6	48.0	1.4	0.7	0.7	0.5	0.5	0.5	0.5	0.5	0.5	0.5	0.5	0.5	0.5	0.5	
15	release	8	—	—	8	15	—	—	—	138.4	—	149.5	13.9	-145.3	97.7	-16.6	44.0	3.6	2.0	2.0	1.2	1.2	1.2	1.2	1.2	1.2	1.2	1.2	1.2	1.2	1.2	
16	place	9	9	16	8	15	—	—	58.6	186.2	—	138.1	10.0	-135.4	105.6	-8.6	50.0	2.3	1.2	1.2	0.9	0.9	0.9	0.9	0.9	0.9	0.9	0.9	0.9	0.9	0.9	
17	release	9	9	16	—	—	—	—	144.5	—	—	178.9	16.7	-174.8	101.1	-27.4	46.4	5.1	2.8	2.8	1.8	1.8	1.8	1.8	1.8	1.8	1.8	1.8	1.8	1.8		
18	place	10	9	16	10	19	—	—	187.7	44.5	—	161.7	12.1	-158.8	114.4	-13.7	48.4	3.2	1.6	1.6	1.2	1.2	1.2	1.2	1.2	1.2	1.2	1.2	1.2	1.2		
19	release	10	—	—	10	19	—	—	—	110.8	—	248.2	21.7	-244.8	72.2	-65.0	32.3	9.2	5.3	5.3	3.0	3.0	3.0	3.0	3.0	3.0	3.0	3.0	3.0	3.0	3.0	
20	place	11	11	20	10	19	—	—	—	46.0	180.3	—	232.0	19.8	-228.7	85.2	-48.1	35.3	8.1	4.3	4.3	2.7	2.7	2.7	2.7	2.7	2.7	2.7	2.7	2.7	2.7	2.7
21	release	11	11	20	—	—	—	—	—	86.6	—	—	311.7	21.5	-309.8	23.7	-103.8	26.5	12.8	6.9	6.9	3.9	3.9	3.9	3.9	3.9	3.9	3.9	3.9	3.9	3.9	3.9
22	place	12	11	20	12	23	—	—	—	79.0	46.4	—	307.3	21.5	-305.2	28.7	-92.1	24.3	11.5	6.1	6.1	4.0	4.0	4.0	4.0	4.0	4.0	4.0	4.0	4.0	4.0	
23	release	12	—	—	12	23	—	—	—	89.7	—	347.9	22.0	-346.5	11.4	-120.2	18.9	16.9	8.3	8.3	4.6	4.6	4.6	4.6	4.6	4.6	4.6	4.6	4.6	4.6	4.6	
24	place	13	13	25	12	23	—	—	34.6	119.1	—	352.6	17.9	-351.5	34.7	-117.6	17.5	12.8	6.4	3.9	3.9	3.9	3.9	3.9	3.9	3.9	3.9	3.9	3.9	3.9	3.9	
25	release	13	13	25	—	—	—	—	77.2	—	—	416.5	14.4	-416.2	0.8	-163.0	10.0	12.9	7.6	4.2	4.2	4.2	4.2	4.2	4.2	4.2	4.2	4.2	4.2	4.2	4.2	4.2
26	place	14	13	25	14	26	—	—	—	362.2	-203.2	—	346.4	16.8	-345.4	79.9	-102.3	16.3	10.7	5.6	3.8	3.8	3.8	3.8	3.8	3.8	3.8	3.8	3.8	3.8	3.8	3.8
27	release	14	—	—	14	26	—	—	—	96.7	—	436.5	10.7	-436.3	0.8	-169.4	11.6	12.2	7.0	4.0	4.0	4.0	4.0	4.0	4.0	4.0	4.0	4.0	4.0	4.0	4.0	
28	place	15	15	28	14	26	—	—	—	146.6	280.0	—	393.3	13.6	-392.8	38.2	-129.4	15.2	11.2	5.9	4.0	4.0	4.0	4.0	4.0	4.0	4.0	4.0	4.0	4.0	4.0	
29	release	15	15	28	—	—	—	—	119.9	—	—	448.9	7.7	-448.9	0.8	-171.1	10.9	11.3	6.5	3.8	3.8	3.8	3.8	3.8	3.8	3.8	3.8	3.8	3.8	3.8	3.8	
30	place	16	15	28	16	31	—	—	—	197.6	-52.0	—	418.3	10.9	-418.1	20.2	-140.8	16.3	11.1	5.8	4.0	4.0	4.0	4.0	4.0	4.0	4.0	4.0	4.0	4.0	4.0	
31	release	16	—	—	16	31	—	—	—	143.9	—	463.0	3.4	-463.0	0.8	-177.6	12.2	10.3	6.4	3.2	3.2	3.2	3.2	3.2	3.2	3.2	3.2	3.2	3.2	3.2	3.2	
32	place	17	17	33	16	31	—	—	—	31.1	171.4	—	454.7	4.8	-454.7	14.4	-162.1	15.4	10.5	6.0	3.5	3.5	3.5	3.5	3.5	3.5	3.5	3.5	3.5	3.5	3.5	
33	release	17	17	33	—	—	—	—	—	170.8	—	470.0	21.3	-470.0	0.8	-177.0	9.6	70.8	33.1	23.1	23.1	23.1	23.1	23.1	23.1	23.1	23.1	23.1	23.1	23.1	23.1	
34	place	18	17	33	18	35	—	—	—	123.1	93.1	—	465.0	2.8	-465.0	33.6	-165.7	14.5	10.2	6.0	3.4	3.4	3.4	3.4	3.4	3.4	3.4	3.4	3.4	3.4	3.4	
35	release	18	—	—	18	35	—	—	—	—	203.8	—	468.9	29.6	-468.9	0.8	-173.2	9.1	97.5	47.3	33.2	33.2	33.2	33.2	33.2	33.2	33.2	33.2	33.2	33.2	33.2	33.2
36	place	19	19	37	18	35	—	—	—	152.2	109.2	—	463.7	1.7	-463.7	44.9	-167.3	12.1	10.2	5.9	3.3	3.3	3.3	3.3	3.3	3.3	3.3	3.3	3.3	3.3	3.3	
37	release	19	19	37	—	—	—	—	—	236.3	—	—	471.3	1.1	-471.3	0.8	-176.8	12.1	10.9	6.6	3.3	3.3	3.3	3.3	3.3	3.3	3.3	3.3	3.3	3.3	3.3	
38	place	20	19	37	20	39	—	—	—	256.1	68.0	—	462.7	2.2	-462.7	3.5	-165.1	11.5	10.1	5.6	3.5	3.5	3.5	3.5	3.5	3.5	3.5	3.5	3.5	3.5		
39	release	20	—	—	20	39	—	—	—	269.9	—	—	471.5	2.8	-471.5	0.8	-176.0	9.8	12.5	7.4	3.9	3.9	3.9	3.9	3.9	3.9	3.9	3.9	3.9	3.9	3.9	
40	place	21	21	40	20	39	—	—																								

**Table A.2:** Analysis results for the cantilever method

Step	Type	# Bricks	rob1	rob2	rob3	F <sub>rob1</sub>	F <sub>rob2</sub>	F <sub>rob3</sub>	F <sub>sup</sub>	M <sub>sup</sub>	F <sub>min</sub>	F <sub>max</sub>	F <sub>avg</sub>	T% <sup>1</sup>	Δ <sub>max</sub>	Δ <sub>avg</sub>	Δσ <sup>2</sup>			
			b	n	b	n	b	n	N	N · m	N	N	N	[10 <sup>-3</sup> ] mm	[10 <sup>-3</sup> ] mm	[10 <sup>-3</sup> ] mm				
1	place	1	1	1	—	—	—	—	35.6	—	1.8	0.1	0.0	17.6	4.4	50.0	0.0			
2	place	2	1	1	2	2	—	—	36.6	38.3	—	2.9	0.5	0.0	17.6	2.5	71.4	0.1		
3	release	2	1	1	—	—	—	—	72.9	—	—	-10.0	0.7	-35.1	17.6	-7.5	57.1	0.3		
4	place	3	1	1	3	5	—	—	74.2	40.3	—	-3.3	0.8	-35.2	17.9	-3.3	80.0	0.2		
5	release	3	1	1	—	—	—	—	110.0	—	—	-10.2	0.5	-70.3	17.5	-19.3	40.0	0.5		
6	place	4	1	1	4	7	—	—	75.3	70.3	—	-5.7	0.3	-35.6	51.9	5.2	61.5	0.2		
7	release	4	—	—	4	7	—	—	—	87.3	—	56.9	3.6	-54.6	68.3	1.5	53.8	0.4		
8	place	5	5	8	4	7	—	—	25.7	101.4	—	55.9	3.0	-54.2	68.6	0.7	43.8	0.4		
9	release	—	—	—	4	7	—	—	—	124.0	—	55.8	2.9	-54.1	68.6	-2.9	43.8	0.4		
10	place	6	6	10	4	7	—	—	52.2	109.3	—	55.0	2.4	-53.8	68.8	1.4	47.4	0.3		
11	release	6	—	—	4	7	—	—	—	161.6	—	53.9	1.6	-69.2	69.1	-9.3	42.1	0.6		
12	place	7	7	13	4	7	—	—	68.6	129.4	—	54.6	2.0	-53.6	68.9	3.3	50.0	0.3		
13	release	7	7	13	—	—	—	—	127.7	—	124.4	11.5	-120.3	105.4	-8.7	50.0	2.4	1.5	0.8	
14	place	8	7	13	8	15	—	—	168.8	56.5	—	114.7	7.5	-112.3	111.5	-2.6	48.0	1.4	0.7	0.5
15	release	8	7	13	—	—	—	—	165.9	—	—	121.9	10.4	-118.2	107.0	-8.9	48.0	2.1	1.2	0.7
16	place	9	7	13	9	17	—	—	178.3	36.1	—	116.3	8.1	-113.6	110.4	-4.8	50.0	1.5	0.8	0.5
17	release	9	7	13	—	—	—	—	206.3	—	—	117.0	8.4	-114.2	110.0	-10.4	42.9	1.6	0.9	0.5
18	place	10	7	13	10	19	—	—	184.1	64.8	—	114.9	7.5	-112.5	111.3	-0.7	48.4	1.4	0.6	0.5
19	release	10	—	—	10	19	—	—	—	110.8	—	248.2	21.7	-244.8	72.2	-65.0	32.3	9.2	5.3	3.0
20	place	11	11	20	10	19	—	—	46.0	180.3	—	232.0	19.8	-228.7	85.2	-48.1	35.3	8.1	4.3	2.7
21	release	11	—	—	10	19	—	—	—	154.4	—	240.6	20.7	-237.2	78.4	-55.6	32.4	8.5	4.7	2.8
22	place	12	12	22	10	19	—	—	60.5	233.7	—	202.4	15.6	-199.5	108.8	-25.4	45.9	5.5	2.6	2.0
23	release	12	—	10	19	—	—	—	205.9	—	224.9	18.6	-221.8	90.8	-44.2	32.4	7.3	3.9	2.3	
24	place	13	13	25	10	19	—	—	58.9	230.5	—	204.1	15.9	-201.2	107.4	-22.4	47.5	5.6	2.5	2.0
25	release	13	13	25	—	—	—	—	77.2	—	416.5	14.4	-416.2	0.8	-163.0	10.0	12.9	7.6	4.2	
26	place	14	13	25	14	26	—	—	362.2	-203.2	—	346.4	16.8	-345.4	79.9	-102.3	16.3	10.7	5.6	3.8
27	release	14	13	25	—	—	—	—	112.9	—	405.9	14.8	-405.5	12.8	-144.2	11.6	12.9	7.1	4.1	
28	place	15	13	25	15	29	—	—	218.1	-40.4	—	365.3	16.6	-364.6	40.4	-106.8	19.6	11.5	5.9	4.0
29	release	15	13	25	—	—	—	—	161.7	—	386.4	15.5	-385.9	25.7	-121.4	17.4	11.8	6.4	3.9	
30	place	16	13	25	16	31	—	—	239.0	-21.4	—	354.6	16.6	-353.7	61.2	-89.9	28.6	10.9	5.2	4.0
31	release	16	—	—	16	31	—	—	—	143.9	—	463.0	3.4	-463.0	0.8	-177.6	12.2	10.3	6.4	3.2
32	place	17	17	33	16	31	—	—	-31.1	171.4	—	454.7	4.8	-454.7	14.4	-162.1	15.4	10.5	6.0	3.5
33	release	17	—	—	16	31	—	—	—	177.2	—	458.9	4.6	-458.9	29.6	-163.8	13.5	11.2	6.4	3.5
34	place	18	18	34	16	31	—	—	48.4	202.7	—	440.5	7.4	-440.5	24.2	-145.1	14.5	10.5	5.4	3.8
35	release	18	—	—	16	31	—	—	—	214.8	—	451.8	5.3	-451.8	59.3	-148.8	20.0	10.4	5.7	3.4
36	place	19	19	37	16	31	—	—	48.0	208.9	—	442.5	7.0	-442.5	41.2	-138.5	17.2	10.5	5.2	3.8
37	release	19	19	37	—	—	—	—	236.3	—	471.3	1.1	-471.3	0.8	-176.8	12.1	10.9	6.6	3.3	
38	place	20	19	37	20	39	—	—	256.1	68.0	—	462.7	2.2	-462.7	3.5	-163.8	11.5	10.1	5.6	3.5
39	release	20	19	37	—	—	—	—	271.0	—	469.6	3.0	-469.6	33.6	-166.2	13.1	13.2	7.4	4.1	
40	place	21	19	37	21	41	—	—	277.3	35.6	—	464.9	2.4	-464.9	35.1	-156.3	15.6	10.2	5.5	3.6
41	release	21	19	37	—	—	—	—	307.2	—	466.7	1.0	-466.7	67.3	-154.9	17.2	10.5	5.8	3.4	
42	place	22	19	37	22	43	—	—	279.3	64.9	—	463.5	2.3	-463.4	36.2	-150.0	17.9	10.1	5.2	3.7
43	release	22	—	—	22	43	—	—	—	338.1	—	472.6	2.0	-472.6	0.8	-182.8	10.4	11.3	6.8	3.4
44	place	23	23	44	22	43	—	—	26.0	349.5	—	471.3	1.3	-471.3	10.5	-174.2	12.9	10.6	6.2	3.5
45	release	23	—	—	22	43	—	—	—	373.4	—	471.7	3.7	-471.7	34.8	-173.6	12.9	15.9	8.5	4.8
46	place	24	24	46	22	43	—	—	52.1	358.3	—	469.5	1.4	-469.4	17.8	-166.5	13.7	10.6	5.7	3.7
47	release	24	—	—	22	43	—	—	—	409.3	—	470.3	0.9	-470.2	69.6	-164.0	16.4	11.1	6.0	3.6
48	place	25	25	49	22	43	—	—	69.4	375.5	—	469.5	0.5	-469.5	35.2	-158.5	15.6	10.6	5.4	3.8
49	release	25	—	—	—	—	—	—	—	—	—	0.7	-471.9	0.8	-204.7	10.4	11.9	7.4	3.6	

— = same in cantilever and sequential

<sup>1</sup> % of total edges in the analysis model that are in tension

<sup>2</sup> standard deviation of all nodal displacements

## A.2 Optimized Three Robot Method Analysis Results

**Table A.3:** Analysis results for the three-robot sequence

Step	Type	# Bricks	rob1			rob2			rob3			$F_{rob1}$	$F_{rob2}$	$F_{rob3}$	$F_{sup}$	$M_{sup}$	$F_{min}$	$F_{max}$	$F_{avg}$	$T^1\%$	$\Delta_{max}$	$\Delta_{avg}$	$\Delta_{\sigma}^2$
			b	n	b	n	b	n	N	N	N	$N \cdot m$	N	N	N	N	[10 <sup>-3</sup> ] mm	[10 <sup>-3</sup> ] mm	[10 <sup>-3</sup> ] mm				
1	place	1	1	1	—	—	—	—	35.6	—	—	1.8	0.1	0	17.6	4.4	50	0	0	0	0		
2	place	2	1	1	2	2	—	—	36.6	38.3	—	2.9	0.5	0	17.6	2.5	71.4	0.1	0	0	0		
3	place	3	1	1	2	2	3	4	35.8	37.4	36.4	1.7	0.1	-0.2	17.6	1.7	40	0.1	0	0	0		
4	release	3	—	—	2	2	3	4	—	54.6	36.1	18.1	0.4	-17.6	17.6	0	50	0.1	0	0	0		
5	place	4	4	7	2	2	3	4	35.5	54.1	36.7	18.1	0.4	-17.6	17.6	1.3	53.8	0.1	0	0	0		
6	release	4	4	7	—	—	3	4	35.2	—	73.4	35.9	0.8	-35.4	35.1	-0.1	46.2	0.2	0.1	0.1	0.1		
7	reposition	4	4	7	2	2	3	4	35.5	54.1	36.7	18.1	0.4	-17.6	17.6	1.3	53.8	0.1	0	0	0		
8	release	4	4	7	2	2	—	—	52.9	73.7	—	17.9	0.4	-17.9	34.6	2.6	61.5	0.1	0	0	0		
9	place	5	4	7	2	2	5	8	64.3	72.9	25.7	18	0.4	-17.8	34.6	1.3	56.3	0.1	0	0	0		
10	release	5	—	—	2	2	5	8	—	112.2	52.6	17.9	1.3	-55.3	17.6	-6.9	43.8	0.4	0.2	0.2	0.2		
11	reposition	5	4	6	2	2	5	8	65	71.2	26.4	18.1	0.5	-27	17.6	-2.6	50	0.1	0	0	0		
12	release	5	4	6	—	—	5	8	100.8	—	26.6	53.6	1.3	-53.1	52.2	-4.8	37.5	0.3	0.1	0.1	0.1		
13	place	6	4	6	6	11	5	8	98.1	30.6	34.7	53.8	1.4	-53.1	52.2	-4	36.8	0.3	0.1	0.1	0.1		
14	release	6	4	6	6	11	—	—	128.9	35.4	—	53	1.5	-54.3	52.4	-8.3	36.8	0.5	0.2	0.1	0.1		
15	reposition	6	4	6	6	11	5	8	98.1	30.6	34.7	53.8	1.4	-53.1	52.2	-4	36.8	0.3	0.1	0.1	0.1		
16	release	6	—	—	6	11	5	8	—	54.5	76.9	85.2	5.4	-82.9	57.7	-6.6	47.4	0.9	0.4	0.3	0.3		
17	place	7	7	13	6	11	5	8	47.7	57	70.7	82.9	4.4	-81.2	59.2	-2	54.5	0.7	0.3	0.3	0.3		
18	release	7	7	13	—	—	5	8	83.3	—	76.6	94.4	8	-91.6	62.8	-3.5	54.5	1.7	0.8	0.5	0.5		
19	reposition	7	7	13	4	6	5	8	58.2	110.4	31.9	53.1	1	-52.8	52.4	-1.9	45.5	0.5	0.2	0.1	0.1		
20	release	7	7	13	4	6	—	—	67.8	131.3	—	53	0.7	-54.7	52.4	-2.6	45.5	0.4	0.2	0.1	0.1		
21	place	8	7	13	4	6	8	15	76.8	128.4	34.1	53.3	1.2	-53.4	52.3	-2	44	0.3	0.1	0.1	0.1		
22	release	8	—	—	4	6	8	15	—	151	84.5	52.6	0.7	-73.6	52.6	-4.5	48	0.5	0.2	0.2	0.2		

= optimized support location

1 % of total edges in the analysis model that are in tension

2 standard deviation of all nodal displacements

23	reposition	8	3 4 4 6 8 15	70.1	104.5	84.6	35.7	0.9	-73.4	46.4	-3.8	44	0.5	0.2	0.2
24	release	8	3 4 - - 8 15	155.5	-	98.7	34.8	0.9	-77.7	59.6	-4.5	48	1.1	0.4	0.4
25	place	9	3 4 9 17 8 15	152.5	25.5	118	34.8	0.4	-75.8	61	-3.6	50	1	0.3	0.3
26	release	9	3 4 9 17 - -	212.7	79.6	-	35.1	4.6	-135	35.9	-25.4	46.4	4.1	1.3	1.1
27	reposition	9	3 4 9 17 4 6	75.6	70.9	162.2	35.5	3.7	-124.9	35.2	-19.2	35.7	3.3	0.8	0.8
28	release	9	- - 9 17 4 6	-	69.6	204.1	51.9	4	-126.5	53	-20.4	35.7	3.4	0.9	0.8
29	place	10	10 19 9 17 4 6	52.9	57.8	199	51.7	3	-118.7	53.1	-13.7	48.4	2.7	0.8	0.7
30	release	10	10 19 - - 4 6	85.9	-	224.9	51.7	2.3	-142.5	53.7	-19.9	38.7	2.7	1.2	1
31	reposition	10	10 19 6 11 4 6	76.4	75.1	160.2	52.2	3.2	-82.8	52.8	-12.6	41.9	2.7	0.7	0.7
32	release	10	10 19 6 11 - -	93	131.5	-	137.2	11	-134.8	64.8	-19.3	41.9	4.6	1.7	1.1
33	place	11	10 19 6 11 11 20	129.3	141.8	53.4	126.6	8.6	-124.7	64.8	-13.5	38.2	3.1	1.2	0.8
34	release	11	- - 6 11 11 20	-	176	74.7	147.4	8.3	-145.4	29.5	-37.1	26.5	3.7	1.7	1
35	reposition	11	5 8 6 11 11 20	116.9	129.5	68	85.7	3.4	-109.3	55.3	-20.5	38.2	2.6	0.9	0.7
36	release	11	5 8 - - 11 20	174.9	-	81.3	143.4	15.7	-140.4	28.8	-42.8	32.4	11.1	3.8	2.7
37	place	12	5 8 12 23 11 20	184.8	52.5	80.9	127	9.6	-124.9	38.6	-31.7	35.1	5.1	2	1.5
38	release	12	5 8 12 23 - -	209.6	85.4	-	143.5	9.4	-164.9	26.4	-50.2	21.6	5	2.5	1.6
39	reposition	12	5 8 12 23 11 20	184.8	52.5	80.9	127	9.6	-124.9	38.6	-31.7	35.1	5.1	2	1.5
40	release	12	- - 12 23 11 20	-	46.4	79	307.3	21.5	-305.2	28.7	-92.1	24.3	11.5	6.1	4
41	place	13	13 25 12 23 11 20	-62.8	106.2	126.3	262	18.2	-259.8	67.2	-53.3	40	8.4	4	3.1
42	release	13	13 25 - - 11 20	28.8	-	125.8	-	19.3	-323.4	16.6	-101	15	11.9	5.9	3.6
43	reposition	13	13 25 6 11 11 20	43.9	188	96.7	142.3	6.3	-140.8	33.5	-31.9	30	4	1.6	1.1
44	release	13	13 25 6 11 - -	69.9	229.4	-	189.9	13.5	-200.8	31.4	-79.2	12.5	8.9	4	2.7
45	place	14	13 25 6 11 14 26	267.9	207.4	-130.3	156.6	9.3	-154.5	50.8	-42.7	25.6	5.4	2.1	1.5
46	release	14	- - 6 11 14 26	-	239.9	91.3	203.9	14.8	-226.6	34.3	-91.2	11.6	11.3	4.8	3.2
47	reposition	14	8 14 6 11 14 26	170.4	149.6	82	118.3	4.8	-148.3	57.7	-38.6	25.6	3.7	1.3	1
48	release	14	8 14 - - 14 26	209.8	-	81.1	226.3	16.3	-224.1	18.2	-69.4	18.6	8.7	4	2.1
49	place	15	8 14 15 29 14 26	219.4	-68.6	146.8	199.5	13.4	-197.5	63.9	-48.1	21.7	5.2	2.5	1.5
50	release	15	8 14 15 29 - -	254.1	104.4	-	198.7	12.5	-196.8	44.7	-62.8	21.7	4.5	2.8	1.2
51	reposition	15	8 14 15 29 15 28	241.9	87.9	54	207.4	13.7	-205.5	36.4	-64.9	19.6	5.2	2.8	1.5
52	release	15	- - 15 29 15 28	-	7	115.7	448.9	7.7	-448.8	0.8	-171.1	8.7	11.2	6.5	3.8

= optimized support location

1 % of total edges in the analysis model that are in tension

2 standard deviation of all nodal displacements

53	place	16	16 31 15 29	15 28	-52	11	186.6	418.3	10.9	-418.1	20.1	-140.8	14.3	11.1	5.8	4
54	release	16	16 31 - -	15 28	-52	-	197.6	418.3	10.9	-418.1	20.2	-140.8	16.3	11.1	5.8	4
55	reposition	16	16 31 15 29	15 28	-52	11	186.6	418.3	10.9	-418.1	20.1	-140.8	14.3	11.1	5.8	4
56	release	16	16 31 15 29	- -	93	94.9	-	440	7.8	-439.9	31.2	-159.1	12.2	10.8	6.1	3.7
57	place	17	16 31 15 29	17 33	113.7	115.6	61.2	435	8.3	-434.9	20.1	-146.9	15.4	10.7	5.7	3.8
58	release	17	- - 15 29	17 33	-	126.3	69	438.6	7.9	-438.6	17.9	-147.7	11.5	10.7	5.8	3.7
59	reposition	17	16 31 15 29	17 33	113.7	115.6	61.2	435	8.3	-434.9	20.1	-146.9	15.4	10.7	5.7	3.8
60	release	17	16 31 - -	17 33	171.4	-	-31.1	454.7	4.8	-454.7	14.4	-162.1	15.4	10.5	6	3.5
61	place	18	16 31 18 35	17 33	206.7	30.5	-36	440.4	7.3	-440.3	19.5	-145.1	16.4	10.5	5.4	3.8
62	release	18	16 31 18 35	- -	200.9	31.2	-	445.9	6.8	-445.9	34.8	-147.5	18.2	10.6	5.6	3.7
63	reposition	18	16 31 18 35	17 32	221.5	22.8	-85.1	439.2	7.5	-439.2	15.8	-144.5	14.5	10.5	5.3	3.8
64	release	18	- - 18 35	17 32	-	27.8	194.4	459.8	4.3	-459.8	12.1	-161.7	14.5	10.4	5.9	3.5
65	place	19	19 37 18 35	17 32	31.4	20.3	203.1	451.9	5.1	-451.9	13	-149.3	15.5	10.2	5.3	3.7
66	release	19	19 37 - -	17 32	40.7	-	212.3	451.9	5.1	-451.9	22.7	-149.3	13.8	10.2	5.3	3.7
67	reposition	19	19 37 15 29	17 32	45.9	107.7	113.9	433	8.5	-432.9	21	-132.2	13.8	10.7	5.1	3.9
68	release	19	19 37 15 29	- -	139.6	128.7	-	431.6	8.6	-431.5	16.9	-138.3	12.1	10.7	5.2	3.8
69	place	20	19 37 15 29	20 39	139.8	129.7	35.4	432.8	8.5	-432.7	18.4	-131.3	11.5	10.7	5	3.8
70	release	20	- - 15 29	20 39	-	139.6	162.9	431.4	8.6	-431.3	18.2	-133.8	9.8	10.7	5.1	3.7
71	reposition	20	17 33 15 29	20 39	89.9	132.3	83.1	429.5	9.2	-429.4	24.1	-123.3	16.4	10.9	4.9	4
72	release	20	17 33 - -	20 39	129.1	-	155.9	457.9	4	-457.9	31.3	-155.2	11.5	10.2	5.5	3.5
73	place	21	17 33 21 41	20 39	136.5	43.3	178.2	456.5	4	-456.5	39.3	-146.7	14.1	10.4	5.2	3.7
74	release	21	17 33 21 41	- -	201.3	114.7	-	456.5	4.2	-456.5	20.5	-141.4	15.6	12.8	6.3	3.9
75	reposition	21	17 33 21 41	15 29	124.4	72.3	144	428.1	9.4	-428	61.8	-112	18.8	11.1	4.8	3.9
76	release	21	- - 21 41	15 29	-	154.1	194.4	428.4	10	-428.2	40.7	-121	17.2	12.1	6.7	3.4
77	place	22	22 43 21 41	15 29	126.4	107.2	149.7	427	9	-426.9	20.2	-128	10.4	10.7	5	3.5
78	release	22	22 43 - -	15 29	227	-	148.2	426.8	9.1	-426.6	10.9	-132.8	10.4	10.9	5.2	3.4
79	reposition	22	22 43 18 35	15 29	153.4	96.2	129.6	430.8	8.8	-430.7	31.1	-125.5	9	11	5.1	3.6
80	release	22	22 43 18 35	- -	188.2	161.5	-	460.6	2.9	-460.6	22.5	-154.2	10.4	11.4	5.7	3.7
81	place	23	22 43 18 35	23 44	215.6	174.5	57.3	459.7	3.3	-459.7	33.4	-145.7	12.9	11.3	5.3	3.8
82	release	23	- - 18 35	23 44	-	243	141.8	457.8	6.2	-457.8	27.1	-137.7	15.7	17	8.2	5

= optimized support location

1 % of total edges in the analysis model that are in tension

2 standard deviation of all nodal displacements

83	reposition	23	14 27 18 35 23 44	164.4	154.5	108.9	409	12.1	-408.7	62.2	-94.1	24.3	12.1	4.9	3.7
84	release	23	14 27 - - 23 44	213.5	-	225.3	401.6	15.6	-401.2	52	-108.8	22.9	19.6	9.7	4.7
85	place	24	14 27 24 47 23 44	165.5	113.9	196.7	404.2	12.4	-403.9	36.9	-118.6	13.7	11.4	5.3	3.3
86	release	24	14 27 24 47 - -	224.6	257.2	-	385.6	16.2	-385.1	33	-103.2	20.5	27.9	12.9	7.4
87	reposition	24	14 27 24 47 17 33	151.8	150.5	175.6	416.8	12.4	-416.6	87.7	-96	23.3	12	6	3.4
88	release	24	- - 24 47 17 33	-	170	254.1	452.4	7.5	-452.4	63.8	-125.6	21.9	21.9	10.2	5.8
89	place	25	25 49 24 47 17 33	191.8	115.5	199.1	455.7	4.3	-455.7	82.4	-136.3	14.3	13.4	5.8	4.1
90	release	25	25 49 - - 17 33	270.1	-	200.4	455.4	4.3	-455.4	30	-140	16.9	13.5	5.9	3.9

= optimized support location

1 % of total edges in the analysis model that are in tension

2 standard deviation of all nodal displacements

# B

## Appendix for Chapter 5

### B.1 Space Frame Arch Design and Assembly

This appendix presents additional information for the space frame arch structure that was designed in [Section 5.4.5](#) and the cooperative robotic sequence that was used to assemble the structure as discussed in [Section 5.6.1](#).

[Table B.1](#) summarizes the results from each iteration of the design process, showing the new edges connecting each new vertex to the existing graph and the calculated mapping of this vertex to  $\mathbb{R}^3$ . [Table B.2](#) summarizes the cooperative robotic fabrication sequence that was used to build the resulting space frame arch. This table shows the member #, its corresponding edges in the graph representation, and the specific robot (either R1 or R2) that was used to place the member. Each new node is added through one of the following feasible 3-member placement sequences using both robots: R1-R2-R1, R1-R2-R2, R2-R1-R2, or R2-R1-R1. Note that the first 6 members comprise a complete tetrahedral that was added manually as a base to initialize the construction, and are therefore not associated with a robotic placement.

**Table B.1:** Vertex mapping to  $\mathbb{R}^3$  and graph connectivity at each aggregation phase ( $G'$ ) following an iteration of the design process.

$v$	node	added edges
	$n : v \rightarrow \mathbb{R}^3$	$(u, v) \in G'(E)$
0	(-0.639, 1.730, 0.000)	-
1	(-0.529, 1.646, 0.670)	{(0, 1)}
2	(-0.385, 1.927, 0.576)	{(0, 2), (1, 2)}
3	(-0.211, 1.558, 0.546)	{(0, 3), (1, 3), (2, 3)}
4	(-0.177, 2.015, 1.117)	{(1, 4), (2, 4), (3, 4)}
5	(-0.188, 1.568, 1.307)	{(1, 5), (3, 5), (4, 5)}
6	(0.181, 1.390, 1.058)	{(3, 6), (4, 6), (5, 6)}
7	(0.512, 2.065, 1.539)	{(4, 7), (5, 7), (6, 7)}
8	(0.512, 1.413, 1.793)	{(5, 8), (6, 8), (7, 8)}
9	(0.914, 1.754, 1.394)	{(6, 9), (7, 9), (8, 9)}
10	(1.431, 1.885, 1.655)	{(7, 10), (8, 10), (9, 10)}
11	(1.487, 1.237, 1.274)	{(8, 11), (9, 11), (10, 11)}
12	(1.431, 2.050, 1.107)	{(9, 12), (10, 12), (11, 12)}
13	(1.854, 1.710, 0.812)	{(10, 13), (11, 13), (12, 13)}
14	(2.211, 2.024, 0.957)	{(10, 14), (12, 14), (13, 14)}
15	(2.189, 1.444, 0.925)	{(10, 15), (13, 15), (14, 15)}
16	(2.397, 1.725, 0.000)	{(13, 16), (14, 16), (15, 16)}

**Table B.2:** Cooperative robotic assembly sequence for the space frame arch.

member #	edge ( $u, v$ )	robot #
0	(0, 1)	-
1	(0, 2)	-
2	(0, 3)	-
3	(2, 3)	-
4	(1, 3)	-
5	(1, 2)	-
6	(1, 4)	R2
7	(2, 4)	R1
8	(3, 4)	R2
9	(1, 5)	R2
10	(4, 5)	R1
11	(3, 5)	R2
12	(3, 6)	R2
13	(4, 6)	R1
14	(5, 6)	R2
15	(5, 7)	R2
16	(6, 7)	R1
17	(4, 7)	R1
18	(6, 8)	R2
19	(7, 8)	R1
20	(5, 8)	R1
21	(7, 9)	R1
22	(6, 9)	R2
23	(8, 9)	R2
24	(9, 10)	R2
25	(7, 10)	R1
26	(8, 10)	R2
27	(9, 11)	R1
28	(8, 11)	R2
29	(10, 11)	R2
30	(10, 12)	R1
31	(11, 12)	R2
32	(9, 12)	R1
33	(12, 13)	R1
34	(10, 13)	R2
35	(11, 13)	R2
36	(10, 14)	R1
37	(13, 14)	R2
38	(12, 14)	R1
39	(10, 15)	R2
40	(14, 15)	R1
41	(13, 15)	R2
42	(13, 16)	R2
43	(14, 16)	R1
44	(15, 16)	R2

## B.2 Axial Strain Energy in Disassembly

This appendix presents all the strain energy data that was generated in the process of determining what members to robotically support in each of the four disassembly phases for the space frame arch. The sequence of rigid cells to remove and support was planned in [Section 5.5.5](#) with results of the physical implementation of the disassembly sequence shown in [Section 5.6.2](#).

Each table summarizes the average axial strain energy ( $10^{-9} \text{ kN} \cdot \text{m}$ ) per member in the structure, for each disassembly step in a specific disassembly phase, for every possible combination of supported members. There are 7 distinct disassembly steps in a typical phase (i.e., 7 entries per table cell). These 7 steps corresponds to: first supporting the structure with two robots, and then manually removing the 6 intermediate members,  $E_{remove}$ , one-by-one. The structure is analyzed, and the average strain energy is recorded after the simulation of each of these 7 steps.

There are 36 unique combinations of members for the two robots (R1 and R2) to support in each phase because there are 6 potential members to support in either of the chosen rigid cells,  $C_{remove}$  and  $C_{support}$ . The horizontal and vertical axes of each table show the member #, and corresponding graph edge, representing a potential member to support in each cell. The combination of support members representing the lowest average axial strain over all 7 steps is highlighted in the table for each phase. These members were then chosen to be supported in the physical implementation of the disassembly sequence shown in [Section 5.6.2](#). The final phase only requires one robot supporting the structure and the removal of 3 members connecting the final cell to the foundation, hence there are only 4 steps and 6 unique support combinations possible.

**Table B.3:** Average axial strain energy ( $10^{-9} \text{ kN} \cdot \text{m}$ ) in disassembly phase 1.

R2 \ R1	24 (9, 10)	27 (9, 11)	29 (10, 11)	30 (10, 12)	31 (11, 12)	32 (9, 12)
39 (13,15)	7.89	8.40	9.20	9.41	8.98	9.46
	8.05	8.48	9.55	9.62	9.15	9.54
	8.23	9.91	9.77	9.84	9.33	11.80
	8.36	10.57	10.16	10.03	9.50	12.03
	8.54	11.89	11.63	10.27	9.73	12.32
	8.65	12.19	11.93	11.55	9.98	12.68
	38.64	12.50	12.23	22.81	10.23	16.01
40 (13,14)	7.86	8.09	9.09	9.74	8.94	9.30
	8.04	8.35	9.30	9.96	9.10	9.48
	8.22	9.47	9.52	10.19	9.29	11.88
	8.40	10.57	10.17	10.43	9.51	12.16
	8.58	11.89	11.64	10.69	9.74	12.46
	8.63	12.16	11.90	11.53	9.95	12.65
	38.61	12.47	12.21	22.78	10.21	15.98
41 (14,15)	8.06	8.70	9.11	9.53	8.95	11.34
	8.24	9.55	9.32	9.74	9.10	11.80
	8.54	10.16	9.59	10.04	9.23	13.44
	8.70	11.06	10.56	10.27	9.45	13.76
	8.98	11.84	11.58	10.56	9.68	14.27
	9.29	12.13	11.87	13.21	9.93	13.95
	38.60	12.46	12.19	22.77	10.20	15.97
42 (13,16)	8.08	8.60	9.49	10.13	9.12	9.57
	8.24	8.64	9.84	10.40	9.28	9.67
	8.43	10.26	10.07	10.64	9.47	12.18
	8.56	10.75	10.35	11.13	9.69	13.08
	8.74	12.08	11.82	11.40	9.92	13.40
	8.80	12.33	12.07	11.70	10.12	12.82
	38.78	12.65	12.38	22.95	10.38	16.16
43 (15,16)	8.31	10.14	9.44	9.77	9.39	11.89
	8.46	11.62	9.77	9.97	9.46	12.01
	8.79	12.93	10.08	10.28	9.59	13.68
	8.99	12.84	12.21	10.49	9.98	14.85
	9.25	12.77	12.52	10.97	10.62	15.29
	9.62	13.09	12.83	15.47	10.88	14.50
	38.74	12.60	12.34	22.91	10.34	16.11
44 (14,16)	8.66	8.86	9.34	10.23	9.29	12.74
	8.86	9.71	9.55	10.46	9.44	13.36
	9.14	10.35	9.81	10.81	9.56	15.78
	9.36	11.22	10.72	11.07	9.79	16.15
	9.55	12.16	11.90	11.38	10.00	16.99
	65.77	12.49	12.23	33.63	10.29	22.28
	38.75	12.61	12.35	22.92	10.35	16.12

**Table B.4:** Average axial strain energy ( $10^{-9} \text{ kN} \cdot \text{m}$ ) in disassembly phase 2.

R2 \ R1	14 (5, 6)	15 (5, 7)	16 (6, 7)	18 (6, 8)	19 (7, 8)	20 (5, 8)
24 (9,10)	4.68	5.46	6.63	5.70	7.67	3.85
	3.30	2.91	4.93	4.87	6.89	2.95
	3.48	2.86	5.04	5.02	7.11	3.05
	3.31	2.96	5.21	5.25	7.35	3.00
	7.99	3.99	5.33	5.43	7.60	3.11
	7.95	4.14	5.52	37.53	7.88	5.70
	8.25	4.22	5.73	38.92	10.07	13.09
27 (9,11)	9.86	7.22	8.94	8.25	10.32	6.57
	10.17	8.38	9.73	8.51	10.65	6.78
	219.87	184.75	186.93	256.24	189.00	219.19
	2.84	2.49	4.73	4.78	6.88	2.53
	7.50	3.51	4.85	4.94	7.12	2.62
	7.45	3.63	5.02	37.03	7.37	5.19
	7.72	3.70	5.20	38.40	9.55	12.56
29 (10,11)	5.68	3.37	5.20	4.98	6.59	3.48
	5.76	4.69	5.57	5.14	6.80	3.58
	18.24	6.88	6.25	5.31	7.02	3.70
	17.05	7.11	6.45	6.02	7.25	3.68
	23.99	10.93	11.93	34.71	20.78	22.16
	24.69	25.90	22.26	54.27	57.00	31.22
	8.02	3.99	5.50	38.70	9.84	12.86
30 (10,12)	4.75	4.32	5.81	5.43	7.13	3.98
	5.09	4.05	5.57	6.13	7.18	5.60
	5.94	4.15	5.62	6.33	7.41	5.78
	5.85	4.29	5.81	23.18	7.66	15.27
	9.21	4.69	5.88	24.19	8.10	15.50
	8.93	6.27	6.51	38.52	8.36	23.91
	8.69	4.66	6.17	39.37	10.51	13.53
31 (11,12)	4.39	3.29	5.10	5.01	6.46	3.72
	4.47	3.86	5.23	5.17	6.66	3.84
	5.45	4.10	5.25	5.31	6.86	3.96
	5.31	5.16	5.57	6.03	7.12	4.98
	8.41	5.28	5.60	6.51	7.50	5.77
	8.14	5.33	5.71	37.72	7.78	22.96
	7.97	3.94	5.45	38.65	9.79	12.81
32 (9,12)	8.70	8.02	9.80	12.68	11.07	8.24
	7.84	6.95	9.25	12.41	10.80	7.83
	8.59	7.35	9.53	13.34	11.60	8.57
	3.09	2.74	4.98	5.03	7.13	2.78
	7.76	3.76	5.10	5.20	7.37	2.88
	7.71	3.90	5.29	37.30	7.64	5.46
	8.00	3.97	5.48	38.68	9.82	12.84

**Table B.5:** Average axial strain energy ( $10^{-9} \text{ kN} \cdot \text{m}$ ) in disassembly phase 3.

R2 \ R1	3 (2, 3)	4 (1, 3)	5 (1, 2)	6 (1, 4)	7 (2, 4)	8 (3, 4)
14 (5,6)	7.00	7.11	6.63	5.68	6.29	5.92
	1.73	1.92	1.84	1.62	2.27	1.88
	1.84	2.03	2.22	1.71	2.39	1.98
	2.24	3.39	2.48	1.80	2.52	2.09
	2.37	3.59	2.69	1.90	2.56	2.21
	2.50	3.81	2.85	2.02	2.64	2.48
	2.67	4.06	3.38	2.22	15.01	2.64
15 (5,7)	2.53	2.73	3.54	3.33	3.38	2.65
	2.61	2.79	3.65	3.50	3.55	2.79
	2.75	2.94	5.02	3.94	3.85	2.89
	3.19	4.34	5.26	4.16	4.06	3.05
	1.53	2.75	1.85	1.07	1.73	1.38
	1.62	2.92	1.96	1.13	1.75	1.59
	1.72	3.11	2.43	1.27	14.06	1.69
16 (6,7)	1.66	2.04	1.98	1.27	2.45	1.52
	1.66	2.00	2.04	1.33	2.57	1.59
	1.65	1.96	2.25	1.40	2.71	1.67
	1.79	2.93	2.27	1.48	3.00	1.79
	1.90	3.10	2.59	1.61	2.99	1.90
	1.97	3.28	3.30	1.90	23.31	1.95
	2.32	3.71	3.02	1.87	14.66	2.29
18 (6,8)	4.56	5.36	5.01	2.11	3.30	2.35
	4.56	6.13	4.97	1.90	3.13	2.14
	4.75	7.71	4.97	2.00	3.29	2.25
	16.96	17.96	22.42	20.30	34.22	17.15
	17.96	19.01	26.97	23.57	35.91	18.15
	18.79	20.09	33.16	27.80	142.06	18.76
	2.34	3.73	3.05	1.89	14.68	2.31
19 (7,8)	1.87	2.00	3.46	2.59	5.81	1.92
	1.93	2.03	3.80	2.72	6.10	2.01
	1.82	1.89	4.09	2.72	7.40	2.11
	2.13	3.25	4.23	2.87	8.03	2.17
	2.12	3.30	4.69	2.96	8.13	2.17
	2.13	3.44	5.72	3.48	60.95	2.11
	1.35	2.74	2.05	0.90	13.69	1.32
20 (5,8)	6.97	7.24	8.60	4.34	4.68	4.25
	7.64	7.56	9.92	3.70	4.08	3.64
	27.25	27.44	29.36	30.86	33.28	27.39
	29.05	30.21	31.61	32.58	35.13	28.91
	2.42	3.64	2.74	1.96	2.61	2.26
	2.56	3.86	2.91	2.08	2.70	2.53
	2.73	4.12	3.43	2.28	15.07	2.70

**Table B.6:** Average axial strain energy ( $10^{-9} \text{ kN} \cdot \text{m}$ ) in disassembly phase 4.

R1	3 (2, 3)	4 (1, 3)	5 (1, 2)	6 (1, 4)	7 (2, 4)	8 (3, 4)
-	1.31	3.73	2.59	0.66	21.98	1.36
	1.57	4.20	2.91	0.74	31.44	39.18
	1.79	0.88	3.32	0.93	35.93	0.96
	2.09	1.02	1.49	1.13	1.88	1.12

# C

## Appendix for Chapter 6

## C.1 Code for Topological Support Hierarchy

### C.1.1 breadth-first search subgraph calculation functions

---

Calculate subgraphs for individual user-specified active members

---

```
1: function calc_subg(G, rm_memb)
2:   nodes_queue  $\leftarrow$  [rm_memb]
3:   nodes_checked  $\leftarrow$  []
4:
5:   while nodes_queue is not empty do
6:     n_check  $\leftarrow$  nodes_queue.pop(0)
7:     node_type  $\leftarrow$  _check_node_type(G, n_check, rm_memb)
8:     if node_type in [“remove”, “normal”, “normal_1side_fixed”] then
9:       nodes_queue, nodes_checked  $\leftarrow$  _find_adjacent_nodes(G, n_check, nodes_queue, nodes_checked)
10:      end if
11:      nodes_checked.append(n_check)
12:      node_draw_settings(G, [n_check], node_type)
13:   end while
14:
15:   return G.subgraph(nodes_checked)
16: end function

1: function _check_node_type(G, n_check, rm_memb)
2:   in_degree  $\leftarrow$  G.in_degree(n_check)
3:   out_degree  $\leftarrow$  G.out_degree(n_check)
4:   fixed_sides_count  $\leftarrow$  _count_fixed_sides(G, n_check)
5:
6:   if n_check in rm_memb and in_degree == 0 then
7:     node_type  $\leftarrow$  “remove_start”
8:   else if n_check in rm_memb then
9:     node_type  $\leftarrow$  “remove”
10:   else if in_degree == 0 then
11:     node_type  $\leftarrow$  “start”
12:   else if out_degree == 0 then
13:     node_type  $\leftarrow$  “end.foundation”
14:   else if fixed_sides_count == 2 then
15:     node_type  $\leftarrow$  “end_2sides_fixed”
16:   else if fixed_sides_count == 1 then
17:     if _check_if_fixed_exists_multi(G, n_check, rm_memb) then
18:       node_type  $\leftarrow$  “danger_1side_fixed”
19:     else if not any(G.has_edge(n_check, m) for m in rm_memb) then
20:       node_type  $\leftarrow$  “danger_1side_fixed”
21:     else
22:       node_type  $\leftarrow$  “normal_1side_fixed”
23:     end if
24:   else
25:     node_type  $\leftarrow$  “normal”
26:   end if
27:
28:   return node_type
29: end function
```

---

### C.1.2 fixed member check functions

---

Check if any members with a fixed connection are fully removed

---

```

1: function fxd_nodes_cut(G, K)
2:   fxd_n_cut_rmv  $\leftarrow$  set()
3:   for n in K.nodes() do
4:     fully_removed  $\leftarrow$  (K.in_degree(n) + K.out_degree(n)) == (G.in_degree(n) + G.out_degree(n))
5:     if fully_removed then
6:       in_edges, out_edges  $\leftarrow$  set(K.in_edges(n)), set(K.out_edges(n))
7:       fixed_edges  $\leftarrow$  in_edges.intersection([(v, u) for u, v in out_edges])
8:       if fixed_edges is not empty then
9:         fxd_n_cut_rmv.update(v for u, v in fixed_edges)
10:      end if
11:    end if
12:   end for
13:   return list(fxd_n_cut_rmv)
14: end function
```

---



---

Check support conditions of any fixed members in a subgraph

---

```

1: function fxd_nodes_support(G, K, rm_membs, fxd_n_cut_rmv)
2:   fxd_n_check  $\leftarrow$  []
3:   for n_check in K.nodes() do
4:     node_type  $\leftarrow$  _check_node_type(G,n_check,rm_membs)
5:     if node_type in ["end_2sides_fixed", "danger_1side_fixed"] then
6:       fxd_n_check.append(n_check)
7:     end if
8:   end for
9:   n_safe_fix1, n_safe_fix2, n_notsafe  $\leftarrow$  _check_connected(G, K, fxd_n_cut_rmv, fxd_n_check)
10: end function
11: function _check_connected(G, K, fxd_n_cut_rmv, fxd_n_check)
12:   n_safe_fix1, n_safe_fix2, n_notsafe  $\leftarrow$  [],[],[]
13:   for n in fxd_n_check do
14:     e_G,e_K  $\leftarrow$  list(G.out_edges(n)),list(K.out_edges(n))
15:     num_supports, flag  $\leftarrow$  (len(e_G) - len(e_K)), False
16:     for (u,v) in e_K do
17:       if _check_if_fixed_exists(G, u, v) then
18:         if u  $\notin$  fxd_n_cut_rmv and v  $\notin$  fxd_n_cut_rmv then
19:           num_supports,flag  $\leftarrow$  num_supports+1, True
20:         end if
21:       end if
22:     end for
23:     if num_supports < 2 then
24:       n_notsafe.append(n)
25:     else if _count_fixed_sides(G, n) == 2 and flag then
26:       n_safe_fix2.append(n)
27:     else if _count_fixed_sides(G, n) == 2 then
28:       n_safe_fix1.append(n)
29:     else if _count_fixed_sides(G, n) == 1 then
30:       n_safe_fix1.append(n)
31:     end if
32:   end for
33:   return n_safe_fix1, n_safe_fix2, n_notsafe
34: end function
```

---

### C.1.3 disassembly sequence functions

---

Select any members for a free robot to grip as support

---

```
1: function set_n_to_rob_support(K)
2:   select ← yes/no
3:   if select then
4:     n ← selected members that will be supported in the next step
5:     node_draw_settings(K, n, "rob_sprt")
6:   end if
7: end function
```

---

---

Find and select active members in the current subgraph for this step of the sequence

---

```
1: function find_n_active(K, n_type)
2:   if any n_type in K.nodes() then
3:     n_active ← n_type in K.nodes()
4:   else
5:     n_active ← []
6:   end if
7:   return n_active
8: end function

1: function select_n_active(n1,n2)
2:   n_rob_sprt ← n2
3:   number_of_free_robs ← number_of_total_robs - number_of_robs_supporting
4:   for rob in number_of_free_robs do
5:     n_rmv ← choose n in n1 to remove
6:     n_rob_sprt ← choose additional n in n1 to support
7:   end for
8:   node_draw_settings(K, n_rmv, "start")
9:   node_draw_settings(K, n_rob_sprt, "rob_sprt")
10:  return n_rmv,n_rob_sprt
11: end function
```

---

---

Relabel subgraph with new potential start nodes after the current step is executed

---

```
1: function new_subg_relabel(K, rms)
2:   K_new ← _relabel_from_connectivity(K,rms)
3:   K_new ← _relabel_from_rob_support(K_new)
4:   K_new ← _relabel_from_fixed_supports(K_new)
5:   K_new ← _relabel_from_end_conditions(K_new)
6:   return K_new
7: end function
```

---

## C.2 Fabrication Photos

### C.2.1 Phase 1

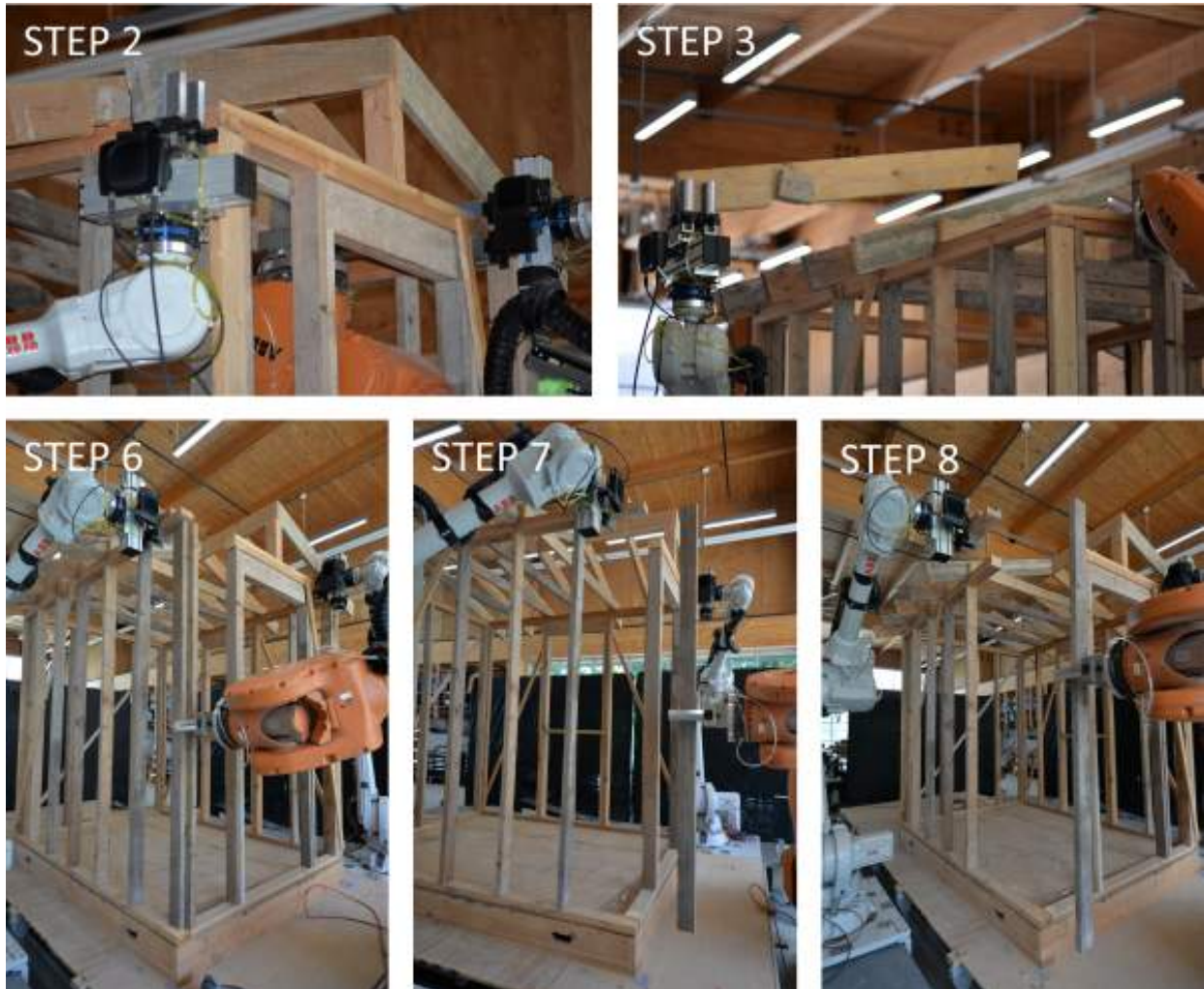


*Figure C.1: Phase 1 fabrication photos*

### C.2.2 Phase 2

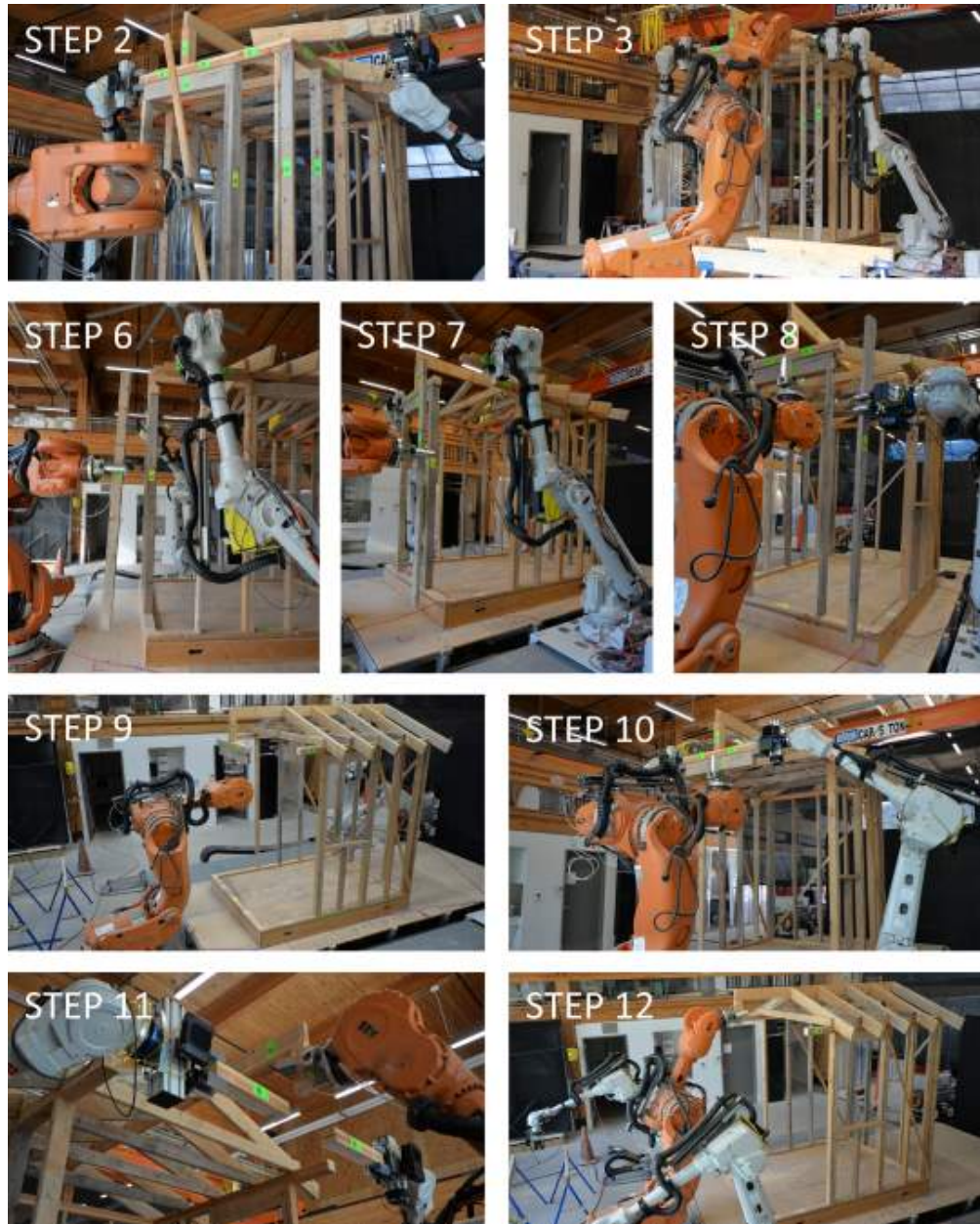


**Figure C.2:** Phase 2 fabrication photos (disassembly)

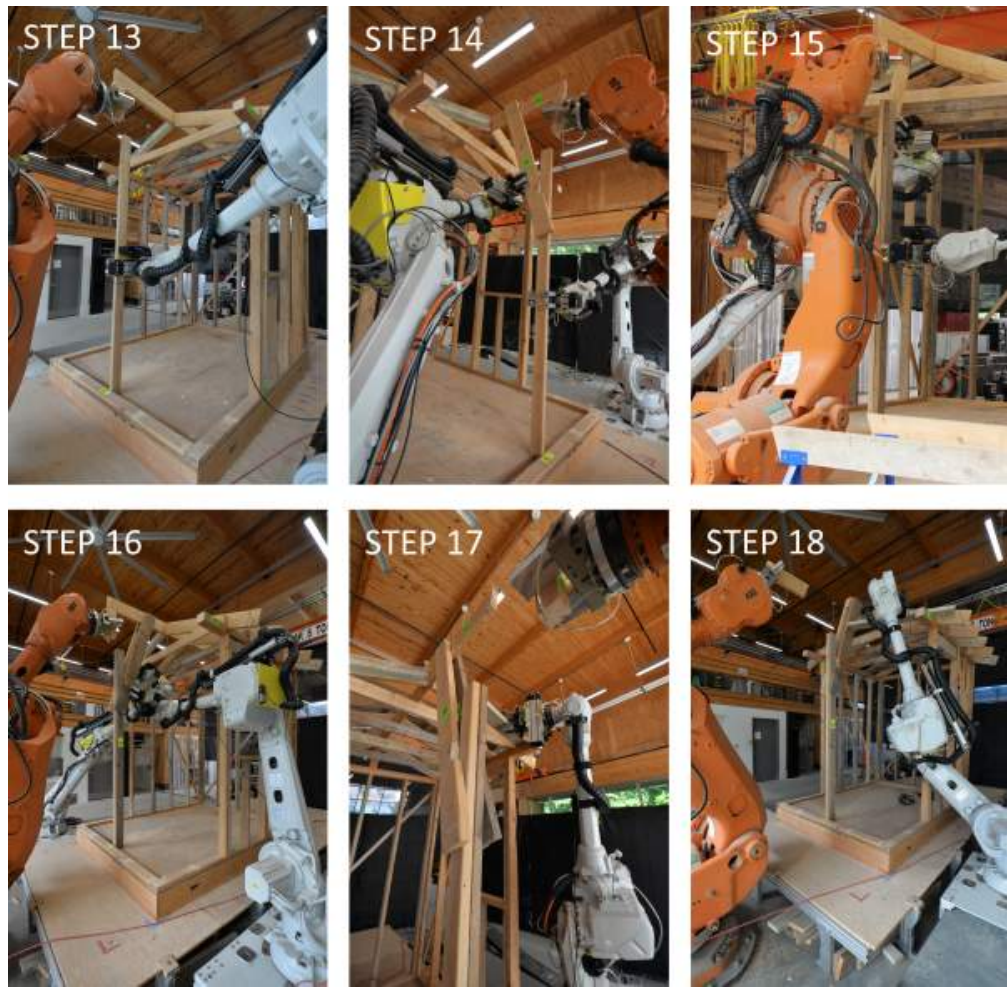


**Figure C.3:** Phase 2 fabrication photos (reassembly)

### C.2.3 Phase 3

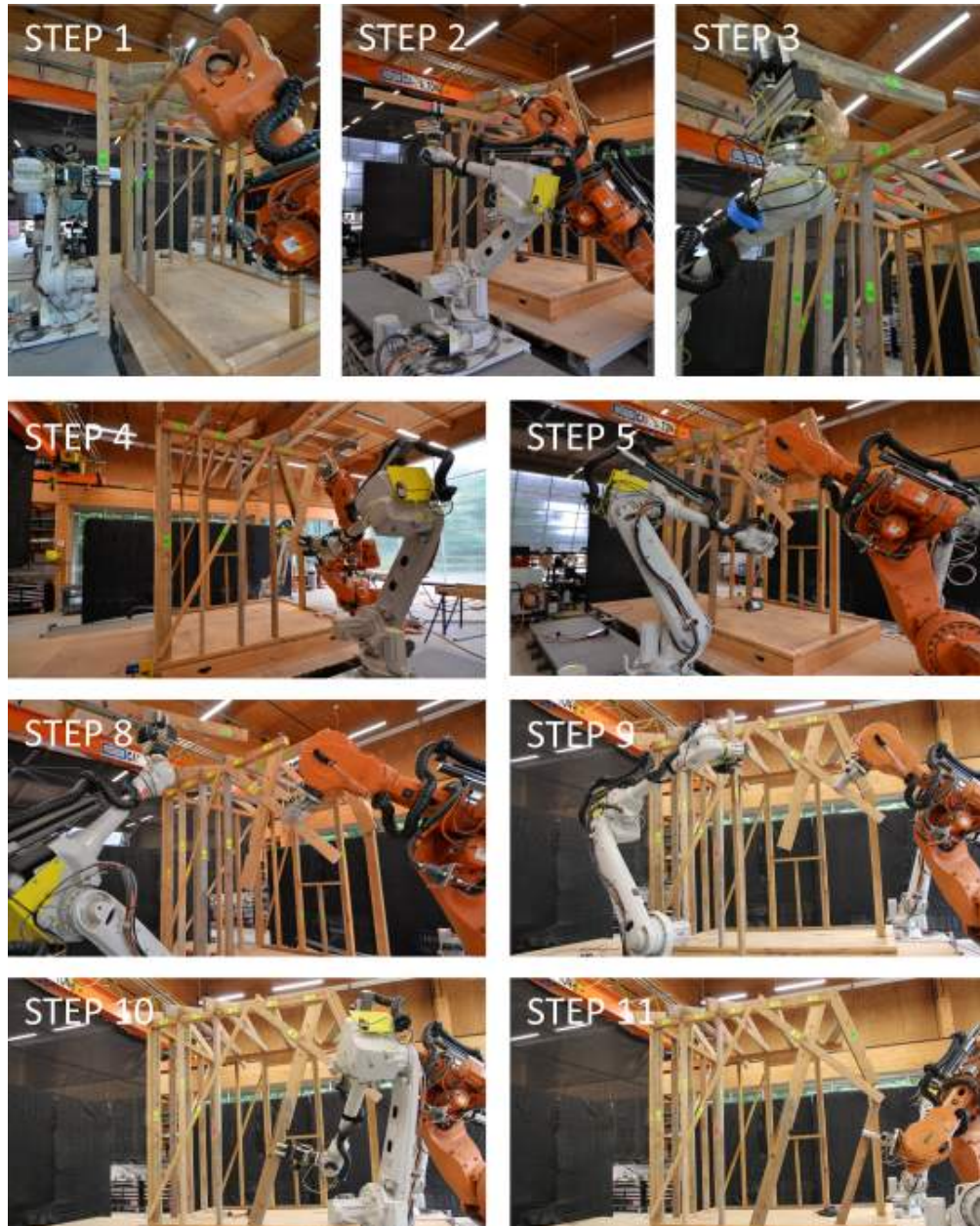


*Figure C.4: Phase 3 first half of disassembly/reassembly photos*

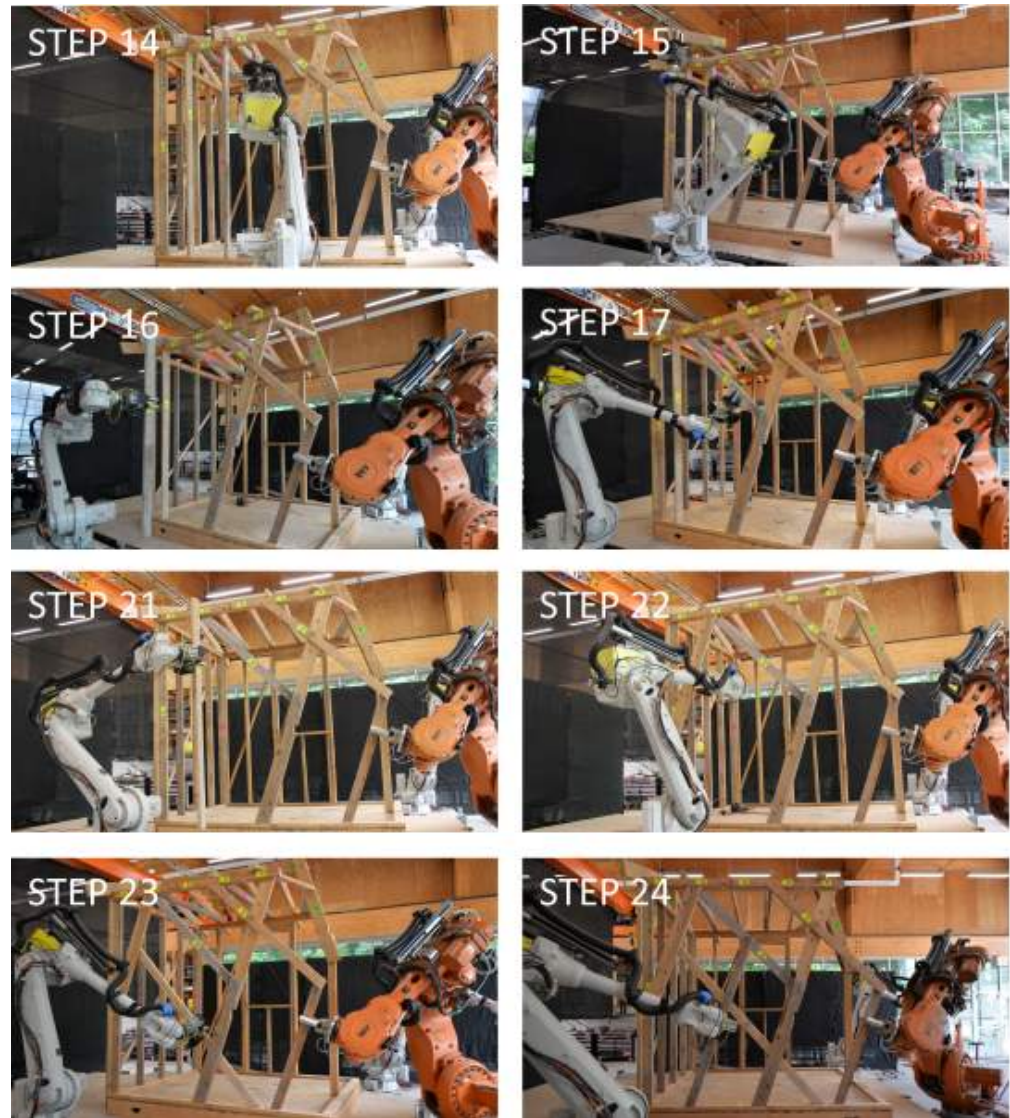


**Figure C.5:** Phase 3 second half of disassembly/reassembly photos